ÇUKUROVA UNIVERSITY
INSTITUTE OF NATURAL AND APPLIED SCIENCES

PhD THESIS

Muhammet Nasıf KURU

NUMERICAL CALCULATION OF HEAT TRANSFER AND PRESSURE DROP IN AXIALLY FINNED IN-LINE AND STAGGERED TUBE BANK HEAT EXCHANGERS

DEPARTMENT OF MECHANICAL ENGINEERING

ADANA-2019

ÇUKUROVA UNIVERSITY
INSTITUTE OF NATURAL AND APPLIED SCIENCES

NUMERICAL CALCULATION OF HEAT TRANSFER AND PRESSURE DROP IN AXIALLY FINNED IN-LINE AND STAGGERED TUBE BANK HEAT EXCHANGERS

Muhammet Nasıf KURU

PhD THESIS

DEPARTMENT OF MECHANICAL ENGINEERING

We certify that the thesis titled above was reviewed and approved for the award of the degree of the Philosophy of Doctorate by the board of jury on 30/10/2019.

…….....	……	……..……..…
Prof. Dr. Alper YILMAZ	Prof. Dr. Hakan YAVUZ	Assoc. Prof. Dr. Arif ÖZBEK
SUPERVISOR	MEMBER	MEMBER
……...……	……..….	
Assoc. Prof. Dr. Önder KAŞKA	Assoc. Prof. Dr. Ertaç HÜRDOĞAN	
MEMBER	MEMBER	

PhD Thesis is written at the Department of Mechanical Engineering of Institute of Natural and Applied Sciences of Çukurova University
Registration Number:

Prof. Dr. Mustafa GÖK
Director
Institute of Natural and Applied Sciences

Note: The usage of the presented specific declarations, tables, figures, and photographs either in this thesis or in any other reference without citation is subject to "The law of Arts and Intellectual Products" number of 5846 of Turkish Republic.

ABSTRACT

PhD THESIS

NUMERICAL CALCULATION OF HEAT TRANSFER AND PRESSURE DROP IN AXIALLY FINNED IN-LINE AND STAGGERED TUBE BANK HEAT EXCHANGERS

Muhammet Nasıf KURU

ÇUKUROVA UNIVERSITY
INSTITUTE OF NATURAL AND APPLIED SCIENCES
DEPARTMENT OF MECHANICAL ENGINEERING

Supervisor : Prof. Dr. Alper YILMAZ
Year: 2019, Pages: 192
Jury : Prof. Dr. Alper YILMAZ
Prof. Dr. Hakan YAVUZ
Assoc. Prof. Dr. Arif ÖZBEK
Assoc. Prof. Dr. Önder KAŞKA
Assoc. Prof. Dr. Ertaç HÜRDOĞAN

Numerical prediction and optimization of fluid flow and heat transfer characteristics of tube bank heat exchangers with axial fins are investigated in this work. Finite volume method is used for solving the governing differential equations numerically. Moreover, Multi-objective Genetic Algorithm II (MOGA-II) is selected to find optimum designs for the optimization study. Unfinned in-line and staggered tube bank configurations are selected from existing studies in literature and validation studies are carried out.

Firstly, the effect of axial finning for four different axial and transversal pitch ratios are investigated for in-line and staggered tube banks. Then, numerical optimization of heat and fluid flow over in-line and staggered tube banks for both unfinned and axially finned cases are presented. Optimization problem has two goals which are maximization of total heat transfer from tube bank and minimization of tube bank volume for the given mass flow rate, allowable pressure drop and tube bank effectiveness. As a result, axial fins improve heat transfer for both in-line and staggered tube banks, and volume can be decreased for staggered arrangements.

Key Words : Numerical optimization, in-line and staggered tube banks, heat transfer, pressure loss, axially finned tubes

ÖZ

DOKTORA TEZİ

EKSENEL KANATLI DÜZGÜN VE KAYDIRILMIŞ SIRALI BORU DEMETİ ISI DEĞİŞTİRGEÇLERİNDE ISI GEÇİŞİ VE BASINÇ DÜŞÜMÜNÜN SAYISAL HESAPLAMASI

Muhammet Nasıf KURU

ÇUKUROVA ÜNİVERSİTESİ
FEN BİLİMLERİ ENSTİTÜSÜ
MAKİNA MÜHENDİSLİĞİ ANABİLİM DALI

Danışman : Prof. Dr. Alper YILMAZ
Yıl: 2019, Sayfa: 192
Jüri : Prof. Dr. Alper YILMAZ
Prof. Dr. Hakan YAVUZ
Doç. Dr. Arif ÖZBEK
Doç. Dr. Önder KAŞKA
Doç. Dr. Ertaç HÜRDOĞAN

Bu çalışmada eksenel kanatlı boru demeti ısı değiştiricileri üzerindeki akış ve ısı transferi karakteristiklerinin sayısal tahmini ve eniyilemesi incelenmiştir. Sonlu hacim yöntemi, ana diferansiyel denklemleri sayısal olarak çözmek için kullanılmıştır. Ayrıca, bu eniyileme çalışmasında, Çok Amaçlı Genetik Algoritması II (MOGA-II) en uygun tasarımları bulmak için seçilmiştir. Kanatsız düzgün ve kaydırılmış sıralı boru demeti literatürde var olan çalışmalardan seçilerek doğrulamaları yapılmıştır.

İlk olarak, dört farklı eksenel ve boyuna aralık oranlarında, düzgün ve kaydırılmış sıralı boru demetinde eksenel kanatın etkileri incelenmiştir. Daha sonra, kanatsız ve eksenel kanatlı, düzgün ve kaydırılmış sıralı boru demeti üzerinde ısı ve akışın sayısal eniyilemesi sunulmuştur. Eniyileme probleminin iki amacı vardır; verilen kütle akısı, izin verilebilir basınç düşümü ve boru demeti verimi için boru demetinin toplam ısı geçişinin arttırılması ve toplam hacminin azaltılmasıdır. Sonuçta, eksenel kanatlar ısı transferini düzgün ve kaydırılmış sıralı boru demetleri için geliştirir ve hacim kaydırılmış sıralı diziliş kullanılarak küçültülebilir.

Anahtar Kelimeler : Sayısal eniyileme, düzgün ve kaydırılmış sıralı boru demeti, ısı geçişi, basınç kaybı, eksenel kanatlı borular

EXTENDED ABSTRACT

Numerical simulation and optimization of heat and fluid flow over in-line and staggered tube bank heat exchangers are investigated for both unfinned and axially finned cases in this work. Present study has two aims: (1) investigation of axial fin effects on different axial and transversal pitch ratios and comparison of obtained results with unfinned cases, (2) optimization of unfinned and axially finned tube banks for the given mass flow rate, allowable pressure drop and tube bank effectiveness where objective functions are maximization of total heat transfer over tube bank and minimization of tube bank volume.

In the first part of present study, heat transfer and pressure loss computations over in-line and staggered tube banks are carried out for four different axial and transversal pitch ratios including unfinned and axially finned cases; namely, $s_L^* = 3$ and $s_T^* = 1.5$, $s_L^* = 3$ and $s_T^* = 2$, $s_L^* = 5$ and $s_T^* = 1.5$, $s_L^* = 5$ and $s_T^* = 2$. Two different values of Prandtl numbers are used (0.7, 7) for prescribed mass flow rates.

Tube bank is assumed to be at constant inlet and wall temperatures; while the flow is assumed to be steady state, turbulent, incompressible and periodic fully developed. Finite volume method is used for solving the conservation equations numerically. In order to ensure reliability of numerical model, unfinned in-line and staggered tube bank configurations are firstly simulated and compared with results from existing studies. It is shown that the results are in accordance with the experimental studies obtained previously in literature.

Moreover, velocity streamlines and temperature contours along the flow field are given. Effects of axial (s_L^*) and transversal (s_T^*) pitch ratios and fin lengths on the average Nusselt number and friction factor are also presented on graphical and tabular forms.

It is found that adding axial fins to in-line and staggered tube banks result in heat transfer increment for the increase in fin length. While Reynolds number increases, friction factor decreases which is the expected situation.

For axially finned in-line tube banks, for a prescribed Reynolds number, increasing s_T^* from 1.5 to 2 contribute very little to the total heat transfer, but finning decreases friction factor. At Re = 1500 and Pr = 0.7, 2D-Finned case of $s_L^* = 5$ and $s_T^* = 2$ shows 34.50% $\overline{Nu}$ increment as compared to D-Finned case of $s_L^* = 3$ and $s_T^* = 2$. But f is increased from 0.30 to 0.32, so 3.55% f increment is observed for Re = 1500.

Furthermore, for $s_L^* = 5$, $s_T^* = 2$ and Pr = 7, D-Finned case leads to average Nusselt number ($\overline{Nu}^+$) enhancement of 68.08% with respect to unfinned case at Re = 1500, also 2D-Finned case has average Nusselt number ($\overline{Nu}^{+,D}$) enhancement of 102.92% with respect to unfinned case. Compared with the 127% and 254% of surface area increase, one can see that 58% and 40.5% of these values are arrived. However, friction factor is decreased (f^+) 18.72% for D-Finned case with respect to unfinned case while for 2D-Finned case 27.16% decrement (f_D^+) is observed as compared to unfinned case at Re = 1500.

For axially finned staggered tube banks, increasing s_T^* from 1.5 to 2.0 for studied cases does not cause a big change in average Nusselt numbers for both Prandtl values of 0.7 and 7. However, the values of f decrease with the use of $s_T^* = 2$. Almost the same heat transfer is obtained with a lower pressure drop at $s_T^* = 2$. The only disadvantage is that the heat exchanger size is larger for $s_T^* = 2$. Increasing s_T^* from 1.5 to 2.0 for all studied cases, average Nusselt number decreases only for 2D-Finned case of $s_L^* = 3$ where Re = 1500 and Pr = 0.7. However, f values decrease with the use of $s_T^* = 2$. Obtained heat transfer values are almost same with a lower pressure drop for $s_T^* = 2$, but heat exchanger has greater size.

Moreover, for D-Finned case of $s_L^* = 5,\ s_T^* = 2$ and Pr = 7 leads to 76.81% enhancement in average Nusselt number ($\overline{Nu}^+$) as compared to unfinned case at Re = 1500, besides 2D-Finned case has 157.85% increment in average Nusselt number ($\overline{Nu}^{+,D}$) with respect to unfinned case. 60.5% and 62.1% of heat transfer increment values are obtained where 127% and 254% are surface area increment values. Friction factor decreases (f^+) 15.24% for D-Finned case to unfinned case while for 2D-Finned case 10.31% decrement (f_D^+) is obtained as compared to unfinned case at Re = 1500.

In the second part of present study, numerical optimization of heat and fluid flow over in-line and staggered tube banks are investigated for both unfinned and axially finned cases. Optimization problems have two goals which are maximization of total heat transfer and minimization of volume of tube bank for the given mass flow rate, allowable pressure drop and tube bank effectiveness.

Present optimization study has same assumptions outlined in Yilmaz and Yilmaz's (2016) and Yilmaz et al.'s (2017) studies. Using their equations, it is possible to design optimum in-line and staggered tube bank heat exchangers. So, obtained numerical results are compared with their studies.

Similar to first part of this work, fluid flow is steady state, incompressible, turbulent and periodic fully developed in the tube bank. Furthermore, inlet and wall temperatures are constant. Finite volume code is used for numerical computations. Multi-objective Genetic Algorithm II (MOGA-II) is used to control optimization problem. Moreover, optimum designs are given on tabular forms and variations of total heat transfer with total volume, effects of transversal and longitudinal pitches on objective functions are presented graphically.

The optimization problem with fully developed periodic flow assumption for the given differential equations and boundary conditions is solved numerically in this study. A number of commercial codes were used to obtain maximum heat transfer and minimum volume of tube bank. Parametric geometry is modeled with

Ansys Design Modeler. The present computational domains are generated with Ansys Mesher using quadrilateral mesh elements. Heat transfer and pressure drop in in-line and staggered tube banks are computed by using Ansys Fluent software which is based on finite volume numerical scheme. Multi-objective design optimization software Modefrontier was used to control optimization problem. Optimization problems are studied on a computer with an Intel I7 CPU 4720 GHz processor and 16 GB Ram on Microsoft Windows 10 operating system.

Optimization studies are carried out for both unfinned and axially finned cases of in-line and staggered tube banks and comparisons of optimum designs are discussed detailly. Heat transfer and pressure drop calculations are studied for Prandtl number of 0.71. Fixed mass flow rate over the tube bank is $\dot{m}_N = 0.5\ kg/s$ and allowable pressure drop is $\Delta p_{allow} = 100\ Pa$. Constant inlet temperature $T_i = 443.15\ K$ and constant wall temperature $T_w = 383.15\ K$ are assigned to tube bank. Tube diameter is $D = 10\ mm$. Tube bank effectiveness is $\eta = 0.75$.

As a result of optimization studies, optimum axially finned in-line tube bank has higher volume with respect to unfinned in-line tube bank for the given optimization problem. So, it can be concluded that axial fins are not suitable if the goal is to obtain minimum volume of tube bank and maximum heat transfer from tube bank. Similarly, axial fins result in 42.70% decrement in volume of staggered tube bank with respect to unfinned case while heat transfer values are approximately equal with maximum obtainable heat transfer rate for the given optimization problem. Thus, volume of tube bank is minimized using axially finned staggered tube banks.

For future works, it is recommended to use parallel algorithms for optimization studies to reduce computation times. Parallel algorithms can not be used with Modefrontier, so MOGA-II algorithm can be written in a programming language and the written code can be enabled for parallel programming. Morover, it

is clear from numerical calculations that staggered tube banks with axial fins are very effective, so it can be validated with experimental studies in future.

ACKNOWLEDGEMENTS

Firstly, I would like to thank my advisor, Prof. Dr. Alper YILMAZ for his technical support, guidance and contributions during my thesis. I sincerely acknowledge Research Assistant Dr. Mehmet Tahir ERDİNÇ for his help, comments and valuable advises throughout this work. Finally, I'm grateful for assistance of Research Assistant Arif Emre AKTAŞ.

I would like to thank my family who are the main people behind my every accomplishment.

CONTENTS **PAGE**

ABSTRACT…….....I
ÖZ……...II
EXTENDED ABSTRACT……III
ACKNOWLEDGEMENT……..……..IX
CONTENTS……..……...…….X
LIST of TABLES……..…….....XIV
LIST of FIGURES……...……..…..XVIII
NOMENCLATURE……..……...…...XXVI
1. INTRODUCTION……...1
2. LITERATURE SURVEY……...…….....…….....7
2.1. Circular Tube Banks.……...…….…….....7
2.2. Different Shaped Tube Banks……13
2.2.1. Elliptical / Oval Shaped Tube Banks…….13
2.2.2. Cam Shaped Tube Banks……...14
2.2.3. Wing Shaped Tube Banks……16
2.2.4. Flat Tube Banks……17
2.3. Extended Surfaces (Fins)……...…19
2.3.1. Axially Finned Tube Banks……..19
2.3.2. Plain / Wavy / Elliptical / Corrugated / Oval Finned Tube Banks……..22
2.3.3. Different Type of Finned Tube Banks……...26
2.4. Periodic Flow Studies……27
2.5. Optimum Tube Banks……28
3. OBJECTIVES and OUTLINE……...……....33
4. MATERIALS and METHODS……...35
4.1. Solution Methods for Conservation Equations……..35
4.2. Turbulence Models……36

4.2.1. The Standard k-ε Model……..……..……37
4.2.2. The RNG k-ε Model……...……..……...…38
4.2.3. The Realizable k-ε Model……..……...…38
4.3. Physical Model……..39
4.4. Definition of Parameters……....43
4.5. Periodic Flow Formulations...……...46
4.6. Optimization Problem Formulation……48
4.6.1. Heat Transfer……....49
4.6.2. Volume……50
4.6.3. Effectiveness…...……51
4.7. Methods of Yilmaz and Yilmaz (2016) and Yilmaz et al. (2017)……52
4.7.1. Method of Yilmaz and Yilmaz (2016) (In-line Arrangement)…….52
4.7.2. Method of Yilmaz et al. (2017) (Staggered Arrangement)……..54
4.8. Boundary Conditions……....57
4.9. Computational Details……...59
4.10. Mesh Independence……62
5. RESULTS……65
5.1. Unfinned and Axially Finned In-line Tube Banks Studies....……65
5.1.1. Validation of Unfinned In-line Tube Bank.……..65
5.1.2. Results and Discussions of Unfinned and Axially Finned In-line Tube Banks.....67
5.1.3. Comparison of Studied Cases for In-line Tube Banks.....……..…82
5.2. Unfinned and Axially Finned Staggered Tube Banks Studies.……..85
5.2.1. Validation of Unfinned Staggered Tube Bank.....……..85
5.2.2. Results and Discussions of Unfinned and Axially Finned Staggered Tube Banks…….....……87
5.2.3. Comparison of Studied Cases for Staggered Tube Banks..……101
5.3. Comparison of Studied Cases (Table 5.1 and Table 5.6) for both In-line

and Staggered Arrangements……..…104
5.4. Optimization of Axially Finned Tube Banks……..…111
5.4.1. Unfinned and Axially Finned In-line Tube Banks
Optimization Studies……112
5.4.1.1 Optimization Results of Unfinned In-line Tube Banks…....112
5.4.1.2 Optimization Results of Axially Finned In-line
Tube Banks……..126
5.4.2. Unfinned and Axially Finned Staggered Tube Banks
Optimization Studies……....134
5.4.2.1 Optimization Results of Unfinned Staggered
Tube Banks……..134
5.4.2.2 Optimization Results of Axially Finned Staggered
Tube Banks……..…147
6. CONCLUSIONS and FUTURE WORK……...……157
REFERENCES……....163
CURRICULUM VITAE……..173
APPENDIX……..175

LIST OF TABLES **PAGE**

Table 4.1. Boundary conditions for solution domains 59

Table 5.1. s_L^* and s_T^* values of present unfinned and axially finned in-line tube bank studies 68

Table 5.2a. Calculated values of $\overline{Nu}$ for unfinned and D-Finned in-line tube banks where $s_L^* = 3, s_T^* = 1.5$ 70

Table 5.2b. Calculated values of f for unfinned and D-Finned in-line tube banks where $s_L^* = 3,\ s_T^* = 1.5$ 71

Table 5.3a. Calculated values of $\overline{Nu}$ for unfinned and D-Finned in-line tube banks where $s_L^* = 3,\ s_T^* = 2$ 74

Table 5.3b. Calculated values of f for unfinned and D-Finned in-line tube banks where $s_L^* = 3, s_T^* = 2$ 75

Table 5.4a. Calculated values of $\overline{Nu}$ for unfinned, D-Finned and 2D-Finned in-line tube banks where $s_L^* = 5,\ s_T^* = 1.5$ 78

Table 5.4b. Calculated values of f for unfinned, D-Finned and 2D-Finned in-line tube banks where $s_L^* = 5,\ s_T^* = 1.5$ 79

Table 5.5a. Calculated values of $\overline{Nu}$ for unfinned, D-Finned and 2D-Finned in-line tube banks where $s_L^* = 5,\ s_T^* = 2$ 80

Table 5.5b. Calculated values of f for unfinned, D-Finned and 2D-Finned in-line tube banks where $s_L^* = 5,\ s_T^* = 2$ 80

Table 5.6. s_L^* and s_T^* values of present unfinned and axially finned staggered tube bank studies 88

Table 5.7a. Calculated values of $\overline{Nu}$ for unfinned, D-Finned and 2D-Finned staggered tube banks where $s_L^* = 3,\ s_T^* = 1.5$.....90

Table 5.7b. Calculated values of f for unfinned, D-Finned and 2D-Finned staggered tube banks where $s_L^* = 3,\ s_T^* = 1.5$ 91

Table 5.8a. Calculated values of $\overline{Nu}$ for unfinned, D-Finned and 2D-Finned staggered tube banks where $s_L^* = 3,\ s_T^* = 2$ 94
Table 5.8b. Calculated values of f for unfinned, D-Finned and 2D-Finned staggered tube banks where $s_L^* = 3,\ s_T^* = 2$ 95
Table 5.9a. Calculated values of $\overline{Nu}$ for unfinned, D-Finned and 2D-Finned staggered tube banks where $s_L^* = 5,\ s_T^* = 1.5$ 98
Table 5.9b. Calculated values of f for unfinned, D-Finned and 2D-Finned staggered tube banks where $s_L^* = 5,\ s_T^* = 1.5$.....98
Table 5.10a. Calculated values of $\overline{Nu}$ for unfinned, D-Finned and 2D-Finned staggered tube banks where $s_L^* = 5,\ s_T^* = 2$ 99
Table 5.10b. Calculated values of f for unfinned, D-Finned and 2D-Finned staggered tube banks where $s_L^* = 5,\ s_T^* = 2$ 99
Table 5.11. Yilmaz and Yilmaz's (2016) optimum design results for the optimization problem given in equation 5.5.....115
Table 5.12. Pareto designs for unfinned in-line tube bank optimization study.....116
Table 5.13. Pareto Designs for axially finned in-line tube bank optimization study 130
Table 5.14. Yilmaz et al.'s (2017) optimum design results for the optimization problem given in equation 5.7.....135
Table 5.15. Pareto designs for unfinned staggered tube bank optimization study 136
Table 5.16. Pareto designs for axially finned staggered tube bank optimization study 150
Table A.1a. C_1 and m constants in equation A.2 for in-line tube banks where $N_L \geq 10$, Grimison (1937).....178
Table A.1b. C_1 and m constants in equation A.2 for staggered tube banks where $N_L \geq 10$, Grimison (1937).....179

Table A.2a. Correction factor C_2 in equation A.4 for in-line tube banks where $N_L < 10$, Kays and London (1964)……...…..179

Table A.2b. Correction factor C_2 in equation A.4 for staggered tube banks where $N_L < 10$, Kays and London (1964)……..…..179

Table A.3a. Average Nusselt Numbers, $\overline{Nu}$ for in-line tube banks where $N_L > 16$, Zukauskas (1972)…….…..181

Table A.3b. Average Nusselt Numbers, $\overline{Nu}$ for staggered tube banks where $N_L > 16$, Zukauskas (1972)…….…..181

Table A.4a. Correction factor C_2 in equation A.10 for in-line tube banks where $Re \geq 1000$ and $N_L \leq 16$, Zukauskas (1972)……..182

Table A.4b. Correction factor C_2 in equation A.10 for staggered tube banks where $Re \geq 1000$ and $N_L \leq 16$, Zukauskas (1972)……..182

LIST OF FIGURES **PAGE**

Figure 1.1. General tube bank heat exchanger in cross flow.....1
Figure 1.2. Tube bank with (a) an in-line arrangement (b) a staggered arrangement (Beale, 1993)……..……..2
Figure 1.3. (a) Circular (b) spiral (c) axial (d) plate (e) wavy finned type tube banks……..…4
Figure 1.4. Basic vortex generators (He et al., 2013)…….……..5
Figure 2.1. (a) Single tube (b) Single tube row (c) Staggered tube bank (Buyruk, 1999)…….....…....10
Figure 2.2. Staggered tube bank configurations (Rahmani et al., 2005)……....12
Figure 2.3. Elliptic tube details studied by Talaat and Gomaa (2009)…..… ……14
Figure 2.4. In-line cam shaped tube bank (Lavasani et al., 2014)……..……15
Figure 2.5. Geometrical models studied by Horvat et al. (2005)…….....17
Figure 2.6. In-line flat tube bank (Haitham et al., 2005)…….....……18
Figure 2.7. Staggered tube bank with axial (a) front (b) back (c) front and back fins (Sparrow and Kang, 1985)……19
Figure 2.8. Flow patterns for different cases of elliptic tubes at Re = 4.8 x 10^3, NOF = No fin, BF = Back Fin, FF = Front Fin, FBF = Both Front and Back Fins (Ibrahim and Moawed, 2009)……..……20
Figure 2.9. Wing-shaped cross-sectional tube with axial fin (Sayed Ahmet et al., 2016)……...….21
Figure 2.10. Temperature contour for staggered tube bank with splitter plate (Re = 5500) (Mangrulkar et al., 2017)……..……22
Figure 2.11. Four different inlet air angles (Du et al., 2014)…….....……24
Figure 2.12. Plain finned in-line tube bank heat exchanger with rectangular winglet pair (RWP) (Chu et al., 2009)……..…....25
Figure 2.13. Circular pin finned tube of tube bank (Tian et al., 2015)…….……26

Figure 2.14. Solution domain of Grannis and Sparrow (1991)…….....27
Figure 2.15. (a) Solution domain, (b) front and (c) top view of elliptic tube bank with wavy fins (Damavandi et al., 2017)…….……32
Figure 4.1. Axially finned in-line tube bank heat exchanger of length L, height H and width B……..……40
Figure 4.2. Axially finned staggered tube bank heat exchanger of length L, height H and width B…….....……...……....40
Figure 4.3. Solution domain for in-line (a) unfinned tube bank (b) D-Finned tube bank of $s_L^* = 5$ and $s_T^* = 1.5$……42
Figure 4.4. Solution domain for staggered (a) unfinned tube bank (b) D-Finned tube bank of $s_L^* = 3$ and $s_T^* = 1.5$……...……..…..43
Figure 4.5. Boundaries for D-Finned study of $s_L^* = 5$ and $s_T^* = 1.5$ (in-line arrangement)…….…….. ..…..58
Figure 4.6. Boundaries for D-Finned study of $s_L^* = 3$ and $s_T^* = 1.5$ (staggered arrangement)……..……..……..…..58
Figure 4.7. In-line tube bank solution domain for unfinned study of $s_L^* = 3$ and $s_T^* = 1.5$…… …....60
Figure 4.8. (a) Solution domain of axially finned staggered tube bank (b) mesh around the tube for D-Finned study of $s_L^* = 3$ and $s_T^* = 1.5$…… …....60
Figure 4.9. Optimization workflow ……..……61
Figure 4.10. The mesh independence study for in-line tube banks…….....…....63
Figure 4.11. The mesh independence study for staggered tube banks.....63
Figure 5.1. Comparison of $\overline{Nu}$ values with empirical studies of Zukauskas (1972), Gnielinski (2010) and Yilmaz and Yilmaz (2016) for $Pr = 0.7$, $s_L^* = 1.5$, $s_T^* = 1.5$…….....66

Figure 5.2. Comparison of f values with empirical studies of Zukauskas (1972), Gaddis (2010), Yilmaz and Yilmaz (2016) for $s_L^* = 1.5$, $s_T^* = 1.5$.....67
Figure 5.3. Variation of $\overline{Nu}$ number with Re number for unfinned and D-Finned tube banks for $s_L^* = 3,\ s_T^* = 1.5$.....70
Figure 5.4. Variation of f with Re number for unfinned and D-Finned tube banks for $s_L^* = 3,\ s_T^* = 1.5$.....71
Figure 5.5. Temperature contours for unfinned and D-Finned in-line tube banks for Pr = 0.7, $s_L^* = 3,\ s_T^* = 1.5$.....72
Figure 5.6. Temperature contours for unfinned and D-Finned in-line tube banks for Pr = 7, $s_L^* = 3,\ s_T^* = 1.5$.....72
Figure 5.7. Velocity streamlines for unfinned and D-Finned in-line tube banks for $s_L^* = 3,\ s_T^* = 1.5$ 73
Figure 5.8. Variation of $\overline{Nu}$ number with Re number for unfinned and D-Finned tube banks for $s_L^* = 3,\ s_T^* = 2$.....75
Figure 5.9. Variation of f with Re number for unfinned and D-Finned tube banks for $s_L^* = 3,\ s_T^* = 2$ 76
Figure 5.10. Variation of $\overline{Nu}$ with Re number for unfinned, D-Finned and 2D-Finned tube banks for $s_L^* = 5,\ s_T^* = 1.5$.....77
Figure 5.11. Variation of f with Re number for unfinned, D-Finned and 2D-Finned tube banks for $s_L^* = 5,\ s_T^* = 1.5$.....78
Figure 5.12. $\overline{Nu}$ for unfinned, D-Finned and 2D-Finned tube banks, where $s_L^* = 5,\ s_T^* = 2$ 81
Figure 5.13. f for unfinned, D-Finned and 2D-Finned tube banks, where $s_L^* = 5,\ s_T^* = 2$.....82
Figure 5.14. $\overline{Nu}$ vs. s_T^* values for studied cases where $Re = 1500$ and $Pr = 0.7$.....83

Figure 5.15. $\overline{Nu}$ vs. s_T^* values for studied cases where $Re = 1500$ and $Pr = 7$.....84
Figure 5.16. f vs. s_T^* values for studied cases where $Re = 1500$.....85
Figure 5.17. Comparison of $\overline{Nu}$ values with experimental studies of Zukauskas (1972), Gnielinski (2010) and Yilmaz et al. (2017) for $Pr = 0.7$, $s_L^* = \sqrt{3}/2\, s_T^*$, $s_T^* = 1.5$ 86
Figure 5.18. Comparison of f values with Zukauskas's (1972) and Gaddis's (2010) experimental studies for $s_L^* = \sqrt{3}/2\, s_T^*$, $s_T^* = 1.5$.....87
Figure 5.19. Variation of $\overline{Nu}$ number with Re number for unfinned, D-Finned and 2D-Finned tube banks for $s_L^* = 3$, $s_T^* = 1.5$.....90
Figure 5.20. Variation of f with Re number for unfinned, D-Finned and 2D-Finned tube banks for $s_L^* = 3$, $s_T^* = 1.5$.....91
Figure 5.21. Temperature contours for unfinned, D-Finned and 2D-Finned staggered tube banks for Pr = 0.7, Re = 1500, $s_L^* = 3$, $s_L^* = 1.5$.....92
Figure 5.22. Velocity streamlines for unfinned, D-Finned and 2D-Finned staggered tube banks for Re = 1500, $s_L^* = 3$, $s_T^* = 1.5$.....93
Figure 5.23. Variation of $\overline{Nu}$ number with Re number for unfinned, D-Finned and 2D-Finned tube banks for $s_L^* = 3$, $s_T^* = 2$.....95
Figure 5.24. Variation of f with Re number for unfinned, D-Finned and 2D-Finned tube banks for $s_L^* = 3$, $s_T^* = 2$.....96
Figure 5.25. Variation of $\overline{Nu}$ number with Re number for unfinned, D-Finned and 2D-Finned tube banks for $s_L^* = 5$, $s_T^* = 1.5$.....97
Figure 5.26. Variation of f with Re number for unfinned, D-Finned and 2D-Finned tube banks for $s_L^* = 5$, $s_T^* = 1.5$.....97
Figure 5.27. Variation of $\overline{Nu}$ number with Re number for unfinned, D-Finned and 2D-Finned tube banks for $s_L^* = 5$, $s_T^* = 2$.....100

Figure 5.28. Variation of f with Re number for unfinned, D-Finned and 2D-Finned tube banks for $s_L^* = 5,\ s_T^* = 2$.....100
Figure 5.29. $\overline{Nu}$ vs. s_T^* values for studied cases where $Re = 1500$ and $Pr = 0.7$ 102
Figure 5.30. $\overline{Nu}$ vs. s_T^* values for studied cases where $Re = 1500$ and $Pr = 7$.....103
Figure 5.31. f vs. s_T^* values for studied cases where $Re = 1500$..... 104
Figure 5.32. $\overline{Nu}$ / f values comparison for the studied cases (tables 5.1, 5.6) for both in-line and staggered arrangements where $Pr = 0.7$.....107
Figure 5.33. $\overline{Nu}$ where $Pr = 0.7$ and f comparisons for the studied cases (tables 5.1, 5.6) for both in-line and staggered arrangements.....108
Figure 5.34. $\overline{Nu}$ / f values comparison for the studied cases (tables 5.1, 5.6) for both in-line and staggered arrangements where $Pr = 7$.....109
Figure 5.35. $\overline{Nu}$ where $Pr = 7$ and f comparisons for the studied cases (tables 5.1, 5.6) for both in-line and staggered arrangements.....110
Figure 5.36. Optimization workflow for unfinned in-line tube bank.....114
Figure 5.37. Variation of total heat transfer $\dot{Q}_N$ with total volume V_N for all designs of unfinned in-line tube bank.....122
Figure 5.38. Variation of total heat transfer $\dot{Q}_N$ with transversal pitch s_T for all designs of unfinned in-line tube bank.....123
Figure 5.39. Variation of total heat transfer $\dot{Q}_N$ with longitudinal pitch s_L for all designs of unfinned in-line tube bank.....124
Figure 5.40. Variation of total volume V_N with transversal pitch s_T for all designs of in-line tube bank.....125
Figure 5.41. Variation of total volume V_N with longitudinal pitch s_L for all designs of in-line tube bank.....125
Figure 5.42. Optimization workflow for axially finned in-line tube bank.....127

Figure 5.43. Variation of total heat transfer $\dot{Q}_N$ with total volume V_N for pareto designs of unfinned and axially finned in-line tube banks.....129
Figure 5.44. Variation of total heat transfer $\dot{Q}_N$ with total volume V_N for all designs of unfinned staggered tube bank.....143
Figure 5.45. Variation of total heat transfer $\dot{Q}_N$ with transversal pitch s_T for all designs of unfinned staggered tube bank.....144
Figure 5.46. Variation of total heat transfer $\dot{Q}_N$ with longitudinal pitch s_L for all designs of unfinned staggered tube bank.....145
Figure 5.47. Variation of total volume V_N with transversal pitch s_T for all designs of unfinned staggered tube bank.....146
Figure 5.48. Variation of total volume V_N with longitudinal pitch s_L for all designs of unfinned staggered tube bank.....147
Figure 5.49. Variation of total heat transfer $\dot{Q}_N$ with total volume V_N for all designs of axially finned staggered tube bank.....152
Figure 5.50. Variation of total heat transfer $\dot{Q}_N$ with transversal pitch s_T for all designs of axially finned staggered tube bank.....153
Figure 5.51. Variation of total heat transfer $\dot{Q}_N$ with longitudinal pitch s_L for all designs of axially finned staggered tube bank.....154
Figure 5.52. Variation of total volume V_N with transversal pitch s_T for all designs of axially finned staggered tube bank.....155
Figure 5.53. Variation of total volume V_N with longitudinal pitch s_L for all designs of axially finned staggered tube bank.....155
Figure A.1. Correction factor C_2 for the number of tube rows from tube banks, Zukauskas (1972) 183
Figure A.2. Friction factor f and correction factor χ for in-line tube banks, Zukauskas (1972) 188

Figure A.3. Friction factor f and correction factor χ for staggered tube banks, Zukauskas (1972) 188

NOMENCLATURE

A	area (m^2)
A_{half}	inlet periodic area of half of the tube (m^2), eqn. 4.21
A_N	cross-sectional area of tube bank in the flow direction at inlet (m^2), eqn. 4.19
B	tube bank width (m)
c_p	fluid specific heat (kJ/kg)
D	tube diameter (m)
d^*	dimensionless diameter, defined in eqns. 4.53 and 4.64 by Yilmaz and Yilmaz (2016) and Yilmaz et al. (2017), respectively
ΔT	temperature difference (K), eqn. 4.52
f	dimensionless friction factor, eqn. 4.29
f^+	friction factor increment with respect to unfinned case (%)
f_D^+	friction factor increment with respect to D-Finned case (%)
F	surface area (m^2)
F^*	surface ratio, eqn. 5.2
F_N	total surface area of the tube bank (m^2), eqn. 4.43
G_k	generation of turbulence kinetic energy (Pa/s), eqn. 4.8
$\bar{h}_{half}$	mean heat transfer coefficient of half the tube ($W/(m^2.K)$), eqn. 4.38
$\bar{h}_N$	mean heat transfer coefficient of tube bank ($W/(m^2.K)$), eqn. 4.40
H	tube bank height (m), eqn. 4.49
k	turbulence kinetic energy (m^2/s^2)
L	tube bank length (m), eqn. 4.48
L_f	fin length, given in terms of tube diameter (D)
$\overline{Nu}$	average Nusselt number, eqn. 4.24
$\overline{Nu}^+$	average Nusselt number increment with respect to unfinned case (%)

$\overline{\mathrm{Nu}}^{+,D}$	average Nusselt number increment with respect to D-Finned case (%)
$\dot{m}_N$	mass flow rate over tube bank (kg/s), eqn. 4.18
$\dot{m}_{half}$	mass flow rate over half of the tube (kg/s)
N	number of tubes in the tube bank, eqn. 4.44
N_L	number of tubes in the longitudinal direction
N_T	number of tubes in the transversal direction
p	pressure (Pa)
$\widetilde{P}$	periodic pressure (Pa)
Pr	Prandtl number, eqn. 4.14
Pr_t	turbulent Prandtl number
$q^{"}$	heat flux (W/m^2)
q_1	term defined in eqns. 4.60 and 4.73 by Yilmaz and Yilmaz (2016) and Yilmaz et al. (2017), respectively
q_2	term defined in eqns. 4.61 and 4.74 by Yilmaz and Yilmaz (2016) and Yilmaz et al. (2017), respectively
$\dot{q}_{V,o}$	optimum volumetric heat flow, defined in eqns. 4.62 and 4.76 by Yilmaz and Yilmaz (2016) and Yilmaz et al. (2017), respectively
$\dot{q}^*_{V,o}$	optimum dimensionless volumetric heat flow, defined in eqns. 4.59 and 4.70 by Yilmaz and Yilmaz (2016) and Yilmaz et al. (2017), respectively
$\dot{Q}_N$	total heat transfer from tube bank (W), eqns. 4.41 and 4.42
$\dot{Q}_{max}$	maximum obtainable heat transfer over tube bank (W), eqn. 4.51
Re	Reynolds number, eqn. 4.13
s_L	pitch in longitudinal/axial direction (mm)
s_T	pitch in transversal direction (mm)
s_D	pitch between rows in the flow direction (mm)
s^*_o	optimum dimensionless pitch, defined in eqn. 4.55 by Yilmaz and Yilmaz (2016)

s_L^* longitudinal/axial pitch ratio, eqn. 4.23

s_T^* transversal pitch ratio, eqn. 4.22

$s_{L,o}^*$ optimum dimensionless longitudinal pitch ratio, defined in eqn. 4.69 by Yilmaz et al. (2017)

$s_{T,o}^*$ optimum dimensionless transversal pitch ratio, defined in eqn. 4.66 by Yilmaz et al. (2017)

t fin thickness (mm)

T temperature (K)

$\overline{T}$ average temperature (K)

u velocity in x direction (m/s)

u_p pressure velocity, defined in eqns. 4.53 and 4.64 by Yilmaz and Yilmaz (2016) and Yilmaz et al. (2017), respectively

U_∞ inlet velocity of tube bank (m/s)

U_{max} average velocity in the minimum cross-sectional area of tube bank (m/s), eqn. 4.14

v velocity in y direction (m/s)

V_N volume of tube bank (m^3), eqn. 4.47

x x coordinate

y y coordinate

y_1 term defined in eqns. 4.56 and 4.67 by Yilmaz and Yilmaz (2016) and Yilmaz et al. (2017) respectively

y_2 term defined in eqns. 4.57 and 4.68 by Yilmaz and Yilmaz (2016) and Yilmaz et al. (2017) respectively

Greek Symbols

β pressure gradient (Pa/m), eqn. 4.31

Δp_N pressure drop over tube bank (Pa), eqn. 4.29

Δp_{allow} allowable pressure drop over tube bank (Pa)

ε energy dissipation rate (m^2/s^3)

υ kinematic viscosity (m^2/s)

θ dimensionless temperature, eqn. 4.33

ρ density (kg/m^3)

μ dynamic viscosity ($Pa.s$)

μ_t turbulent viscosity ($Pa.s$), eqn. 4.5

μ_{eff} effective turbulent viscosity ($Pa.s$), eqn. 4.4

α_k inverse effective Prandtl number of k

α_ε inverse effective Prandtl number of ε

η tube bank effectiveness, eqn. 4.50

η_o optimum tube bank effectiveness, defined in eqns. 4.54 and 4.65 by Yilmaz and Yilmaz (2016) and Yilmaz et al. (2017) respectively

δ term defined in eqns. 4.53 and 4.64 by Yilmaz and Yilmaz (2016) and Yilmaz et al. (2017) respectively

χ correction factor, eqn. A.28

Subscripts

allow allowable

eff effective

f film

half half of the tube

i inlet

L longitudinal

lm logarithmic mean

max maximum

N number of tubes

o outlet

t	turbulent
T	transversal
w	wall

Abbreviations

CFD	Computational Fluid Dynamics
DOE	Design of Experiment
MOGA-II	Multi-objective Genetic Algorithm II
RNG	Renormalization Group

1. INTRODUCTION

Tube bank heat exchangers are widely used to exchange heat between two fluids in many industrial heat transfer applications such as refrigeration, power generation, HVAC, cooling of electronic chips, aerospace and automotive industries. Generally, one fluid flows over the tube bank and the other fluid which has different temperature passes through tubes in the tube bank. Two fluids are usually orthogonal each other and the flow appear similar to cross flow. Tube banks are sub-component of shell and tube heat exchangers. Schematic view of a general tube bank heat exchanger is demonstrated in figure 1.1.

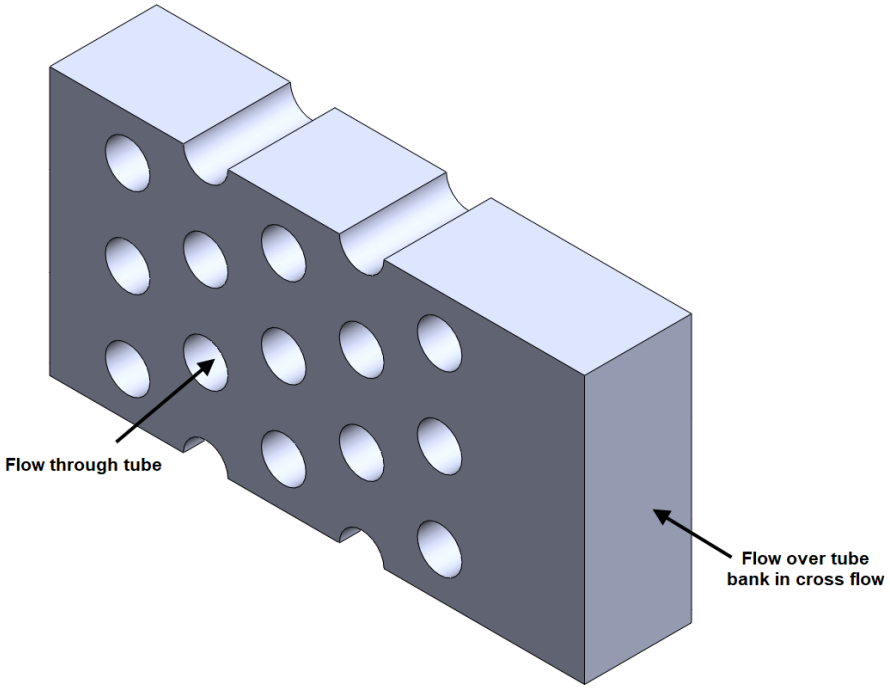
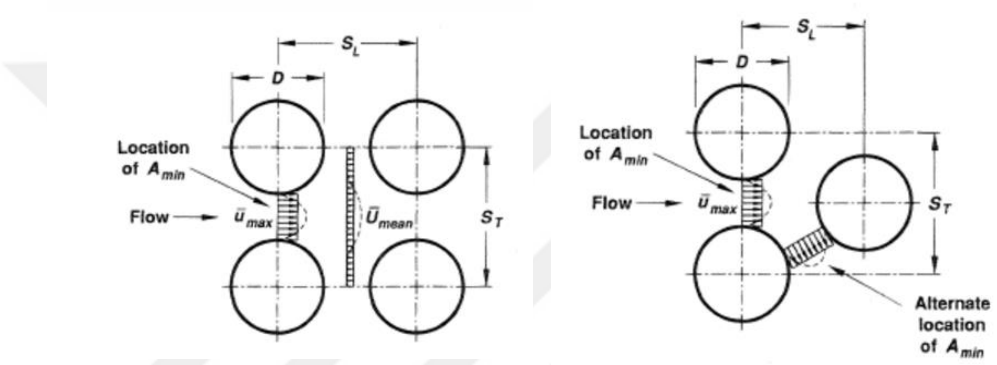


Figure 1.1. General tube bank heat exchanger in cross flow

Tube bank heat exchangers are simple and effective therefore, they are preferred for many works. Gas-gas, liquid-liquid and gas-liquid type heat transfer can be used within tube banks. In general, liquid flows in the tubes and gas flows outside of the tubes. As it is shown in figure 1.2, in-line and staggered arrangements can be applied within tube banks. Both circular and non-circular type of tube cross-section geometries can be used in the tube banks, but circular cross-section geometries are used frequently because they can be manufactured easily.



(a) (b)

Figure 1.2. Tube bank with (a) an in-line arrangement (b) a staggered arrangement (Beale, 1993)

Heat and fluid flow details of tube bank heat exchangers must be understood well to improve their thermal performances. Tube configuration significantly effects the variation of heat and fluid flow over the tube bank. First tubes in the rows of the tube bank has similar flow characteristics to a single tube in cross flow for both in-line and staggered arrangements. Therefore, heat transfer coefficients of first tubes and a single tube approximately equal to each other whereas inner tubes of the tube bank are affected by neighbouring tubes which result in heat transfer coefficient increment. Zukauskas (1972), Aiba et al. (1982), Murray and Fitpatrick (1988) observed that third tubes in the rows of the tube bank have highest heat transfer rate

as compared to other tubes. Poskas and Survilo (1983) indicated that heat transfer from fourth or fifth tube becomes constant.

Moreover, both unfinned and finned type of tube banks are commonly used. Heat transfer surface is extended with fins which leads to increase in the heat transfer rate. Since the thermal conductivity of gases have less values than liquids, gas side thermal resistance of the flow decreases because of extended surfaces. More common finned tubes are illustrated in figure 1.3, including circular, spiral, axial, plate and wavy fins.

Thermal performance of the tube bank is substantially affected by vortex formation, boundary layer separation and wake which is encountered in the downstream of the tube. Vortex formation and wake must be kept down to improve heat transfer over the tube bank, so different shaped tubes (cam, elliptical, oval, i.e.), fins (axial, radial, i.e.) are commonly used for this purpose.

Furhermore, vortex generators are widely used to obtain higher heat transfer value, lighter weight and lower cost. Four basic vortex generators including delta and rectangular wings, delta and rectangular winglets which enables better fluid mixing and distributes boundary layer are depicted in figure 1.4 (He et al., 2013). Vortex generators can be used inside and outside of the tubes or ducts i.e. Akcayoglu and Nazli (2018) carried out numerical study using delta-winglet type vortex generators in triangular ducts to enhance heat transfer.

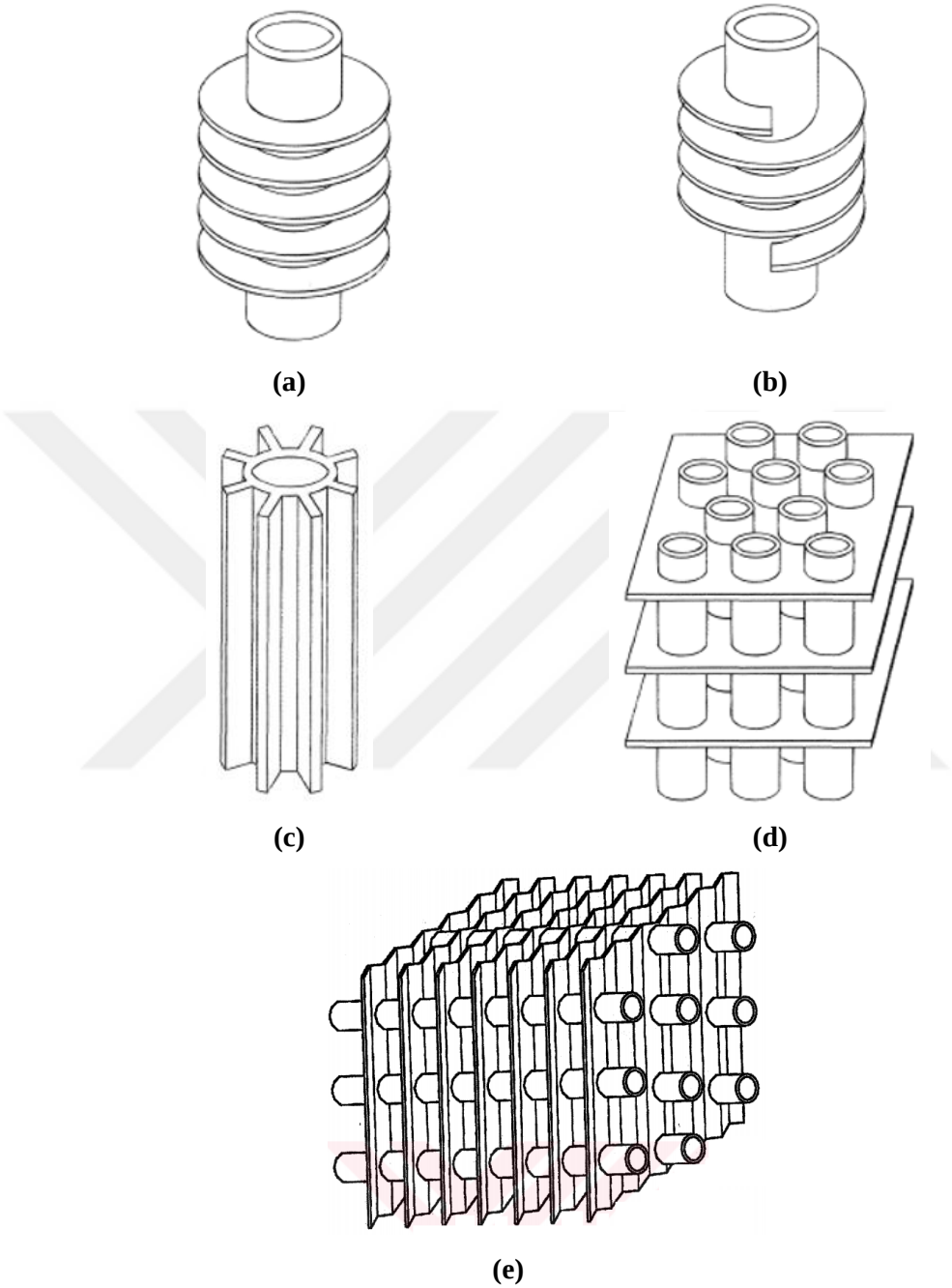


Figure 1.3. (a) Circular (b) spiral (c) axial (d) plate (e) wavy finned type tube banks

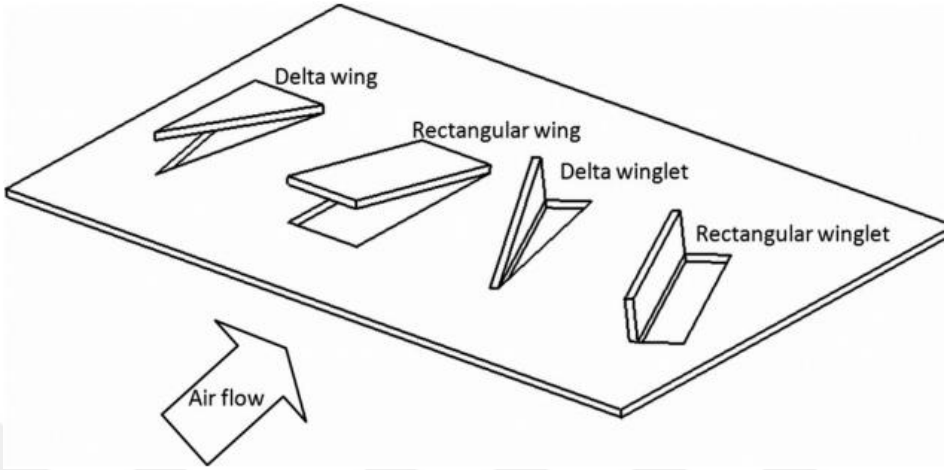


Figure 1.4. Basic vortex generators (He et al., 2013)

In the next chapter, literature review of tube banks in cross flow are investigated in detail. In the third chapter, objective and outline of this thesis is presented. In the following chapter, numerical calculation procedures are explained, and results are given in the fifth chapter. Finally, obtained results are discussed and recommendations are given for future studies. In appendix, the most common tube bank correlations and experimental data are presented.

2. LITERATURE SURVEY

There are lots of studies about flow and heat transfer in in-line and staggered tube banks. A lot of researchers investigated the usage of different geometries such as circular, elliptic, cam and wing profiles within the tube banks to obtain higher heat transfer rates and lower pressure drop values. The most effective method to enhance heat transfer and pressure drop from tube banks is the usage of extended surfaces (fins). In the followings, literature review of mentioned tube banks are given detailly.

2.1. Circular Tube Banks

In the early part of 20^{th} century, tube banks are investigated experimentally by many researchers. Firstly, Hilpert (1933) and Grimison (1937) supplied empirical correlations for the determination of average Nusselt number in circular tube banks. Bergelin et al. (1950, 1952) summarized circular tube bank studies in the range of low and medium Reynolds numbers.

Zukauskas (1972) supplied results for fluid flow and heat transfer for circular tube banks for in-line and staggered arrangements. He also gave the influence of pitches on graphical and tabular forms in the range of Prandtl number from 0.7 to 500 and Reynolds number from 1 to 2×10^6. Moreover, Zukauskas (1988) publishes extensive review of heat and fluid flow over in-line and staggered tube banks for a variety of dimensionless pitches.

The Engineering Sciences Data Unit (ESDU) (1973, 1980) gave empirical correlations from several researchers works for heat transfer and pressure drop computations. Numerical calculations of local heat transfer were given by Fujii and Fujii (1984), Dhaubhadel et al. (1987), Wung and Chen (1989), Beale (1992) for tube banks including a great number of pitches, Prandtl and Reynolds numbers.

Buyruk (1999) performed an experimental study of heat transfer and fluid flow from one tube (figure 2.1a), from single tube row (figure 2.1b) and from staggered tube bank in cross flow (figure 2.1c). In the first part of his study, local Nusselt number variation over staggered tube bank is examined where transversal (s_T) and longitudinal pitches (s_L) are 1.5 x 1.5 and 1.5 x 1.25 while Reynolds number is 4.8 x 10^4. Staggered tube bank experiments show that increasing longitudinal pitch 1.25 to 1.5 does not lead to a significant increment in the average Nusselt number. In the second part of his study, blockage of a single tube where blockage is defined as $B = D/W$ and transversal pitch (s_T) for a single tube row is examined. Blockage ratio is in the range of 0.131 to 0.843 where Reynolds number lies between 7960 and 47770. Local Nusselt numbers and pressure coefficients are fairly different where blockage ratio is varied from 0.668 to 0.843 whereas the blockage ratio is less than 0.5, it is not considerably varied both local Nusselt numbers and pressure loss coefficients.

Wilson and Bassiouny (2000) present a mathematical method to calculate heat transfer and pressure drop using finite volume method for laminar and turbulent flow regime of air in in-line and staggered tube banks. For in-line tube bank, highest average Nusselt number values are obtained when s_L is nearly 3, increasing s_L result in a pressure drop increment which is not recommended. For staggered tube bank, for the values of s_L greater than 1.5, there is not significant enhancement on pressure drop and average Nusselt number. They found that for the lower values of s_L, staggered tube banks perform better compared to in-line tube banks.

Buyruk (2002) studied numerically heat transfer from two tandem cylinders, from in-line and staggered tube banks using finite element method in cross-flow of air. For two tandem cylinders study, longitudinal pitch (s_L) take the values of 1.13, 2, 3 and 6 where Reynolds number equals to 400. Higher values are obtained in the first cylinder while lower values are obtained for the second cylinder. $s_L = 1.13$ has

lower heat transfer values as compared to other longitudinal pitches. He also studied in-line and staggered tube banks where $s_L = s_T = 2$ and Reynolds number varies from 80 to 200. He concluded that increasing Reynolds number causes an increment in the heat transfer for both in-line and staggered tube banks.

Mandhani et al. (2002) carried out a numerical study to obtain heat and fluid flow characteristics of tube bundle under steady state and incompressible flow assumptions. Single cylinder in the tube bank is chosen for computational studies and finite difference method is used for numerical calculations. Reynolds number lies between 1 to 500, porosity is in the range of 0.4 - 0.99 (porosity has two limits, porosity = 1 corresponds to flow over a single cylinder and porosity = 0 shows zero flow state) and two Prandtl numbers of 0.71 and 7.7 are studied. Local Nusselt number variation is affected by the values of Reynolds numbers, porosity and Prandtl numbers. They concluded that increasing Reynolds number and Prandtl number have a positive effect on average Nusselt number whereas increasing porosity has negative effect on average Nusselt number.

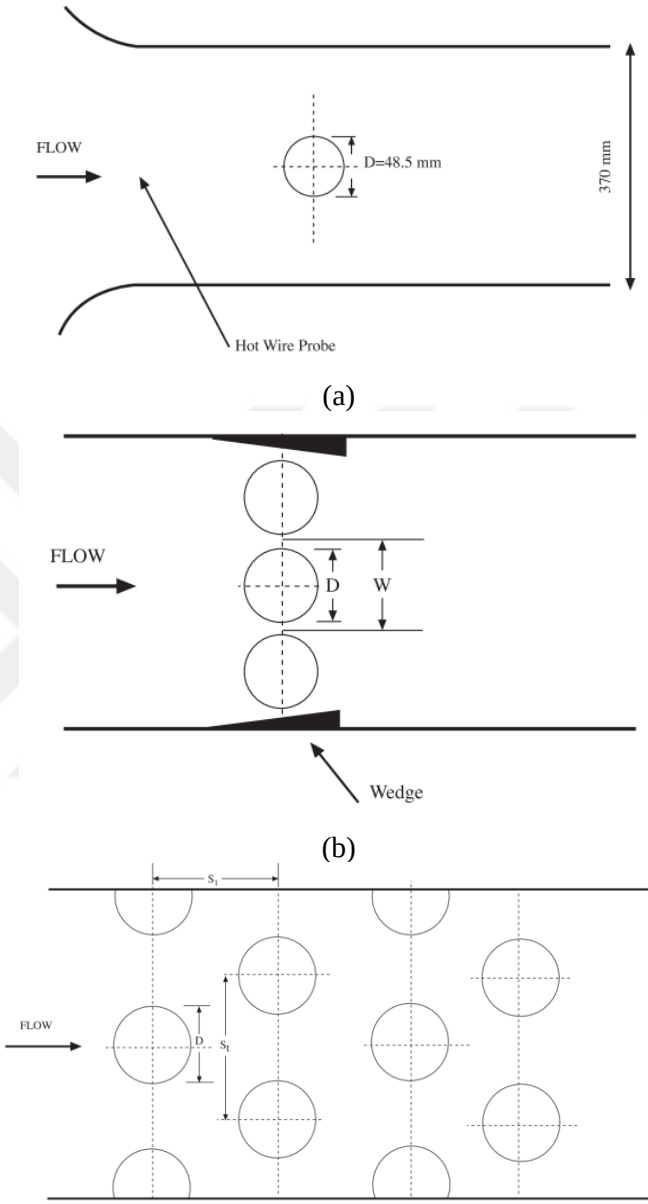


Figure 2.1. (a) Single tube (b) Single tube row (c) Staggered tube bank (Buyruk, 1999)

El-Shaboury and Ormiston (2005) use finite volume method to investigate heat transfer and pressure drop analysis for in-line tube banks in steady, laminar, two-dimensional cross-flow. The in-line tube bank under consideration consists of five tubes in the flow direction. Combinations of longitudinal and transversal pitch ratios of 1.25, 1.5 and 2.0 are presented for both square and non-square arrangements. Reynolds numbers are 100 and 300 while Prandtl number is 0.71. They showed that average Nusselt number from the first tube has higher value as compared to other tubes and a periodic flow is observed after the third tube in the in-line tube bank for the studied Reynolds numbers. Increasing transversal pitch ratio result in friction factor decrement. If transversal pitch is kept constant and longitudinal pitch is decreased, friction factor slightly reduces. Average Nusselt number of five in-line tube bank increases using low values of transversal pitch and higher values of longitudinal pitch. Finally, they presented new equations for average friction factor correction in non-square in-line tube banks.

Rahmani et al. (2005) performed a numerical study of heat transfer and pressure loss of staggered tube banks for two-dimensional, steady, laminar and incompressible cross-flow. A finite volume analysis was carried out to solve continuity, momentum and energy equations. Ten tubes in the flow direction is investigated and Reynolds numbers are 100, 300 and 500. Heat and fluid flow analysis are done for dimensionless diameter pitch ratios of 1.33, 1.6 and 2 for ES (equal spacing), ET (equilateral triangle) and RS (rotated square) arrangements (figure 2.2). They reported that first tube has higher average Nusselt number as compared to with other tubes for all studied arrangements (ES, ET and RS). Moreover, average Nusselt number of ten tubes increases with the decrement in Reynolds number or dimensionless diameter pitch ratio. Also, friction factor increases for the dimensionless lower values of diameter pitch ratio and ET arrangement has the maximum friction factor while RS arrangement has the

minimum friction factor value where dimensionless diameter pitch ratio equals to 1.33.

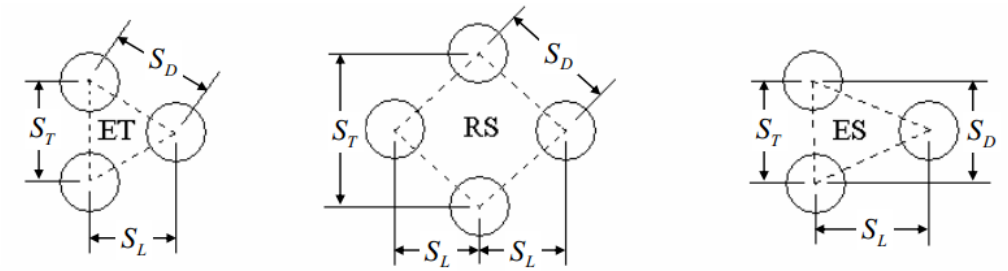


Figure 2.2. Staggered tube bank configurations (Rahmani et al., 2005)

Khan et al. (2006) derived new equations for heat transfer calculations from in-line and staggered tube banks analytically. Steady, laminar, fully developed flow is assumed while constant temperature is assigned to tube walls. They found that heat transfer increases extremely with the decrement in longitudinal pitch and slightly with the increment in transversal pitch for both arrangements. Moreover, staggered tube banks have higher heat transfer values as compared to in-line tube banks for the same pitch ratios.

Gnielinski (2010) presented complete equations for heat transfer coefficient calculation in broad range of pitch ratios for in-line and staggered tube banks. Gaddis (2010) presented equations for the estimation of pressure drop for in-line and staggered tube banks.

Jeong et al. (2011) carried out experimental and numerical studies to investigate heat transfer characteristics of staggered tube banks. Average heat transfer coefficient can be calculated in two ways: (1) using the difference between the bulk fluid temperature and the average surface temperature of the tubes (surface temperature method) (2) log mean temperature difference (LMTD) method between two working fluids. Tube diameter is 1.5 mm and Reynolds number varies from 3000 to 7000. They concluded in their work that average heat transfer coefficient has

22.6% lower value for LMTD method as compared to surface temperature method and the difference of two methods must be considered for convenient heat exchanger design.

Tahseen et al. (2013) presented numerical heat transfer calculation of staggered tube banks in cross-flow under the assumption of two-dimensional, incompressible, steady state, laminar flow. Finite volume method is used to obtain average Nusselt numbers and constant heat flux imposed on the tubes. Transversal pitch ratios of 1.25, 1.5 and 2.0 are studied, Reynolds number is in the range of 25 to 250, and Prandtl number is considered as 0.71. The results show that with the increment in transversal pitch ratio, higher values of average Nusselt number can be obtained.

The average Nusselt number correlations supplied by Zukauskas (1972) have large discontinuities and differences. Therefore, Yilmaz and Yilmaz (2016) and Yilmaz et al. (2017) derived equations based on Zukauskas's (1972) empirical data for in-line and staggered arrangements.

2.2. Different Shaped Tube Banks

2.2.1. Elliptical / Oval Shaped Tube Banks

The first study for flow over elliptical tube bank is carried out by Joyner and Palmer (1943). Using elliptical tubes in tube banks, higher heat transfer values can be obtained with lower pressure drop values, more geometrical parameters are applicable with elliptical tubes as compared to circular ones (Khan et al., 2005).

Talaat and Gomaa (2009) carried out numerical and experimental study of heat and fluid flow through elliptic tube bundle in cross-flow and staggered arrangement. Reynolds number varied from 5600 to 40000, angle of attack ranges from 0 to 150 (α from figure 2.3), minor to major axis ratios (a/b in figure 2.3) are 0.25, 0.33, 0.5 and 1. Turbulent flow is considered while making calculations. The

maximum heat transfer is obtained at α = 90, also minimum heat transfer is occurred at α = 0. They concluded in their work that staggered elliptic tube bank heat exchanger shows better thermal performance where Reynolds number, axis ratio and angle of attack have lower values.

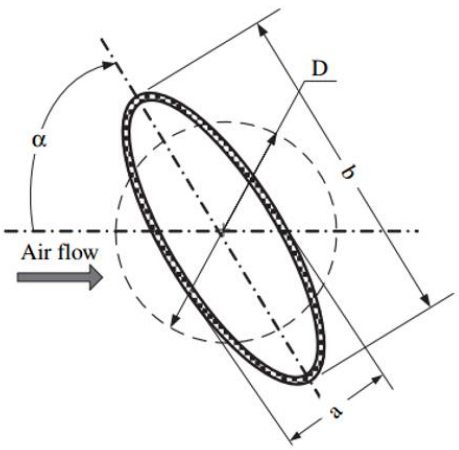


Figure 2.3. Elliptic tube details studied by Talaat and Gomaa (2009)

2.2.2. Cam Shaped Tube Banks

Lavasani et al. (2014) perform heat transfer calculations from in-line cam shaped tube banks experimentally (figure 2.4). Two longitudinal pitch ratios 1.5 and 2 are studied and Reynolds number ranges from 27000 to 42500. Increasing longitudinal pitch 1.5 to 2 result in 7-14% heat transfer enhancement for the studied Reynolds numbers. Moreover, thermal hydraulic performance of cam shaped tube is approximately six times greater than circular tube for the same equivalent diameter. Friction factor decreased using cam shaped tube bank as compared to circular tube bank. They reported that tube bank size is minimized using cam shaped tubes instead circular ones.

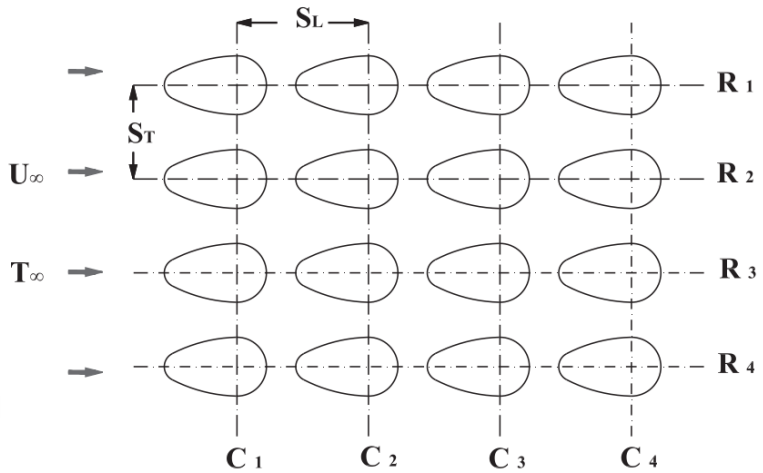


Figure 2.4. In-line cam shaped tube bank (Lavasani et al., 2014)

Moreover, Lavasani and Bayat (2016) investigated heat and fluid flow of nanofluid over circular and cam shaped tube banks numerically. Reynolds number varies from 100 to 400 while Al_2O_3 nano particle is added to pure water with volume fraction of 1-7%. Both in-line and staggered arrangements are studied under the assumptions of steady, laminar, incompressible two-dimensional flow. Constant temperature was assigned to tube walls. For the studied Reynolds numbers and volume fractions, friction factor of cam shaped tube bank is lower than circular ones about 68-71% and 68-74% for in-line and staggered arrangements, respectively. However, nanofluid increases friction factor for both circular and cam shaped tube banks. Average Nusselt number values are maximum when nanofluid has volume fraction of 7% for both circular and cam shaped tube banks. The authors concluded that using nanofluids over cam shaped tube banks in cross-flow lead to heat transfer increment and friction factor decrement which is the efficient method for conservation of energy.

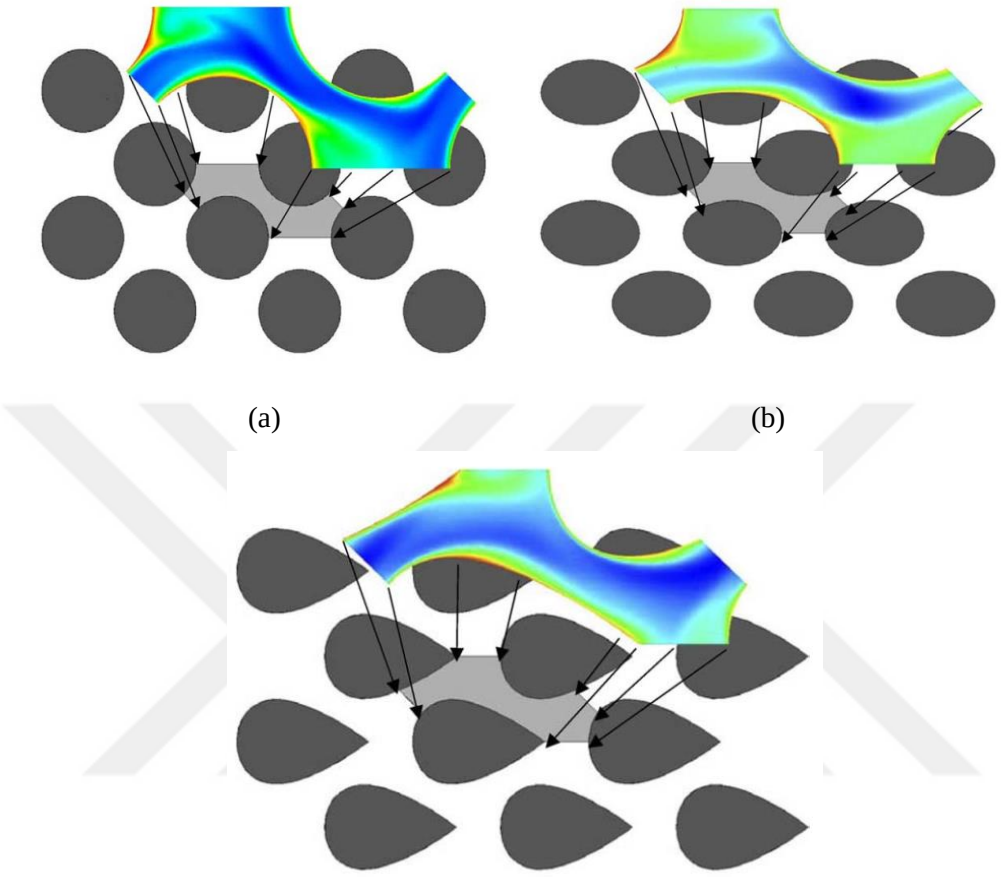
Mangrulkar et al. (2017) carried out a numerical study to investigate heat transfer and friction factor behavior of in-line cam shaped tube bank in cross-flow

which was formerly studied experimentally by Lavasani et al. (2014). Two longitudinal pitch ratios 1.5 and 2 were studied and Reynolds number lies between 11500 to 42500. They found that transversal pitch did not affect the temperature distribution along the tube bank and temperature gradients have higher values till Reynolds number of 20000. Heat transfer enhancement was observed after the first column of tube bank and average Nusselt number of tube bank reaches maximum for the longitudinal pitch ratio of 2 and Reynolds number of 42500. Furthermore, increasing longitudinal pitch ratio 1.5 to 2.0 increases vortex formation so it leads to increment in friction factor. They concluded that cam shaped tube bank performs better as compared to circular tube bank, but Reynolds number should be less than 30000 because of the difficulties in the manufacturing stage.

2.2.3. Wing Shaped Tube Banks

Horvat et al. (2005) presented transient numerical analysis of heat and fluid flow (in turbulent region) over tube banks which have circular, elliptic and wing shaped profiles (figure 2.5). Stanton number and drag coefficient correlations are given as a function of Reynolds number and hydraulic diameter. Generally, Stanton numbers and drag coefficients increase with the decrement in Reynolds number for any hydraulic diameter. They concluded that Stanton numbers and drag coefficients are higher for circular tubes as compared to elliptic and wing shaped tubes.

Sayed Ahmet et al. (2014) studied heat and fluid flow over staggered wing shaped tubes in cross flow, numerically and experimentally. Angle of attack (θ) varies from 0^{o} to 330^{o} while Reynolds number is between 1800 and 9700. They concluded that wing shaped tube bank performs better as compared to circular and elliptic tube banks.



(a) (b)

(c)

Figure 2.5. Geometrical models studied by Horvat et al. (2005)

2.2.4. Flat Tube Banks

Haitham et al. (2005) studied laminar, two dimensional, steady state, incompressible flow over flat tube banks for both in-line and staggered arrangements, numerically (figure 2.6). Finite volume method is applied using Fortran code to obtain heat transfer and pressure drop of flat tube banks. Flat tube bank studies are done for various configurations including Reynolds and Prandtl

numbers, height ratio (H/Da) and length ratio (L/Da). Ten flat tubes in the flow direction is considered for both in-line and staggered flat tube banks. Reynolds number varies from 25 to 400 and two different Prandtl numbers of 0.7 and 7 are studied. They reported that periodic fully developed flow is observed after the fourth flat tube. Average Nusselt number has significantly higher values for Pr = 7 as compared to Pr = 0.7. For lower values of height ratio (H/Da) and higher values of length ratio (L/Da) better thermal performance in in-line configuration for the studied Reynolds numbers except Re = 25 is observed (Da is diameter of circular tube, Db is longitudinal tube diameter). Staggered configuration has greater heat transfer values with respect to in-line configuration. They concluded that equivalent circular tubes show better heat transfer rates as compared to flat tubes, but flat tubes indicate lower pressure loss values than equivalent circular tubes, as a result overall thermal performance is preferable for flat tubes.

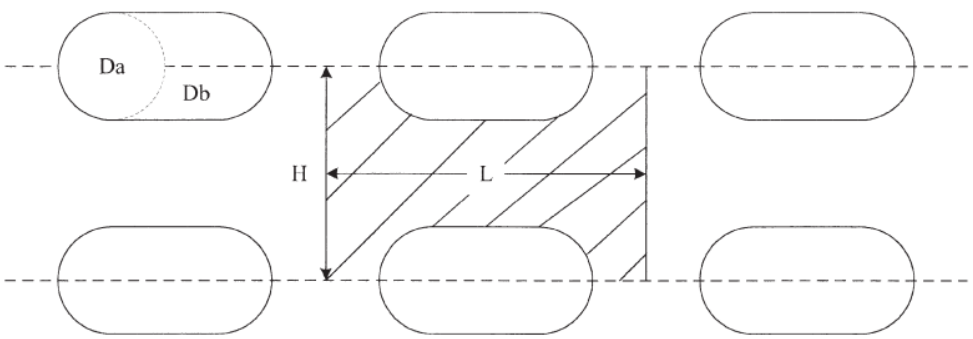


Figure 2.6. In-line flat tube bank (Haitham et al., 2005)

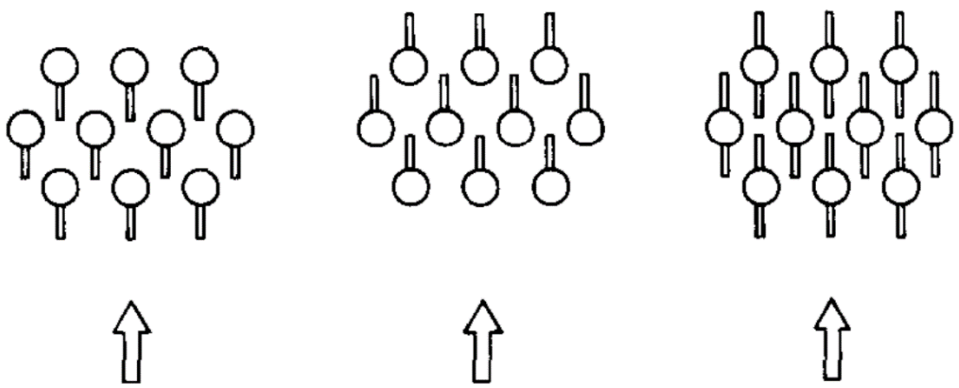
Abdel-Rehim (2012) investigated heat and fluid flow over in-line flat tube bank numerically under steady, laminar, two dimensional, incompressible flow conditions. Finite volume based commercial code Fluent is used for the calculations. A variety of parameters that effect heat and fluid flow over flat tubes are studied including Reynolds numbers between the range of 50-400, length ratios (L/D) of 2.5,

2, 1.5, 1.0, 0.5 and 0.0 where Prandtl number is 0.71. He concluded that increment in the length ratio does not significantly affect heat transfer and pressure drop except L/D = 0 which corresponds to a circular tube.

2.3. Extended Surfaces (Fins)

2.3.1. Axially Finned Tube Banks

Sparrow and Kang (1985) carried out an experimental study of axially finned staggered tube banks (figure 2.7). Fin tip shape, fin thickness and fin positions (front, rear, front and rear of tube) were investigated for Reynolds numbers between 1000 to 8000. As a result, they found that axial finning of staggered tube banks lead to notable heat transfer enhancement.



(a) (b) (c)

Figure 2.7. Staggered tube bank with axial (a) front (b) back (c) front and back fins (Sparrow and Kang, 1985)

Faghri and Rao (1987) investigated the effect of axial finning on the heat and fluid flow of an in-line tube bank numerically. They assume laminar, incompressible, steady state, periodic fully developed flow to solve continuity, momentum and energy equations. Reynolds number varies from 1 to 1000 where pitch ratios are $s_L^* = 2.4$ and $s_T^* = 1.5$. They found that axially finned in-line tube

banks do not significantly increase the heat transfer as compared to unfinned in-line tube bank. This result differs from Sparrow and Kang's (1985) conclusion who stated that axial finning lead to notable increment in heat transfer. It is probably the reason that Faghri and Rao (1987) carried out their studies with laminar flow assumption.

Ibrahim and Moawed (2009) studied heat transfer and entropy generation of individual axially finned elliptic tubes in cross-flow, experimentally (figure 2.8). Axial fins are replaced at the front, rear and both front and rear of elliptic tubes. Working fluid is air in cross flow and Reynolds number varies from 4.75 x 10^3 to 3.96 x 10^4. Maximum average Nusselt number values are obtained using both front and back fins (FBF) while friction factor is higher as compared to front fin (FF), back fin (BF) and NOF (No Fin) cases.

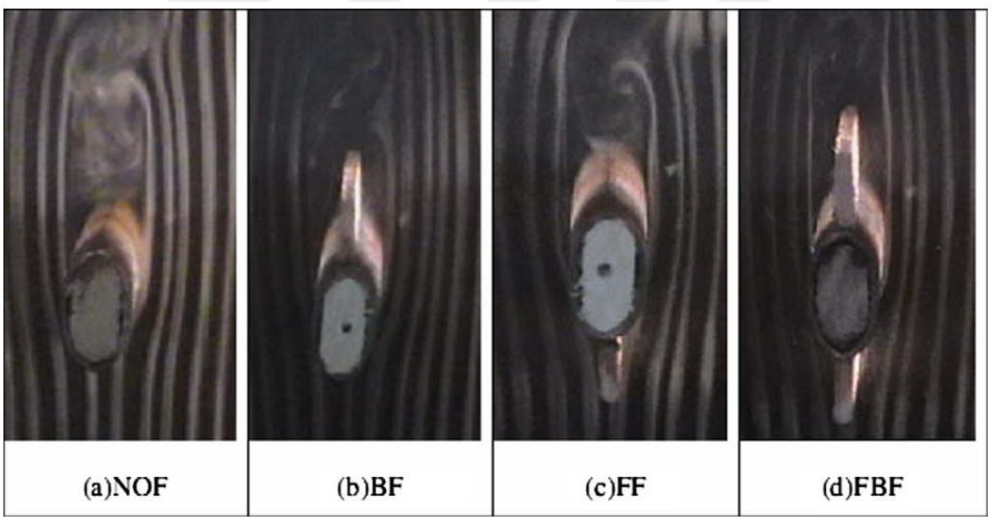


Figure 2.8. Flow patterns for different cases of elliptic tubes at Re = 4.8 x 10^3, NOF = No fin, BF = Back Fin, FF = Front Fin, FBF = Both Front and Back Fins (Ibrahim and Moawed, 2009)

Sayed Ahmet et al. (2016) performed numerical study on wing shaped cross-sectional tube bank with axial fins at downstream side at staggered arrangement in

cross flow (figure 2.9). Steady, incompressible, turbulent, two-dimensional flow is assumed while tested fluid is air and Reynolds number lies between 1.8 x 10^3 and 9.7 x 10^3. Fluent commercial program is used for finite volume analysis to obtain heat transfer, effectiveness and entropy generation for staggered wing shaped tube banks. Fin height (h_f) is between 2 mm and 12 mm, fin thickness (δ) changes in the range of 1.5 mm to 3.5 mm. Fin usage increases average Nusselt number 11% to 36% for the studied fin heights of 2 mm to 12 mm respectively as compared to unfinned case. They reported that staggered wing shaped tube bank performs best where fin height (h_f) equals to 6 mm and average Nusselt number is not affected from fin thickness (δ) variation.

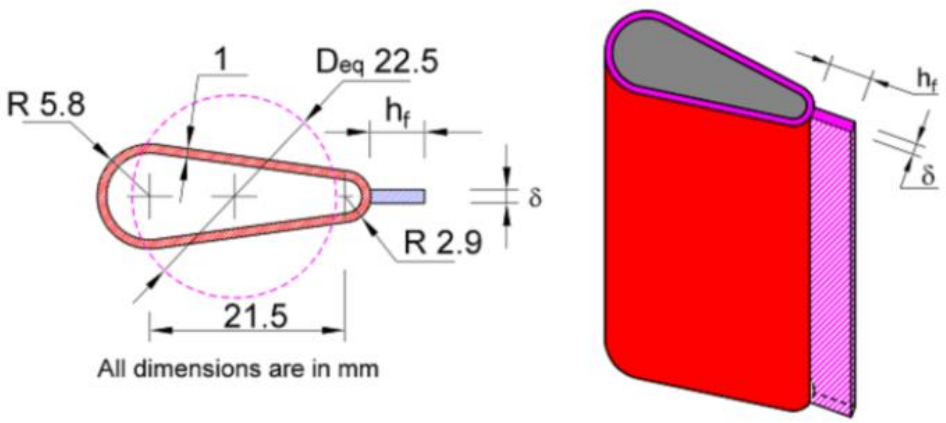


Figure 2.9. Wing shaped cross-sectional tube with axial fin (Sayed Ahmet et al., 2016)

Mangrulkar et al. (2017) investigated experimental and numerical study of splitter plate attachment in the rear of tubes in staggered tube bank (figure 2.10) where Reynolds number ranges from 5500 to 14500. Pitch ratios s_L/D and s_T/D are 1.75 and 2 respectively, ratio of splitter plate length to tube diameter (L/D) is 1.

Using splitter plate in staggered tube bank, heat transfer increases while pressure drop decreases with respect to bare cylinder usage in staggered tube bank. They concluded that overall thermal performance was enhanced up to 82% using splitter plate at Reynolds number of 5500.

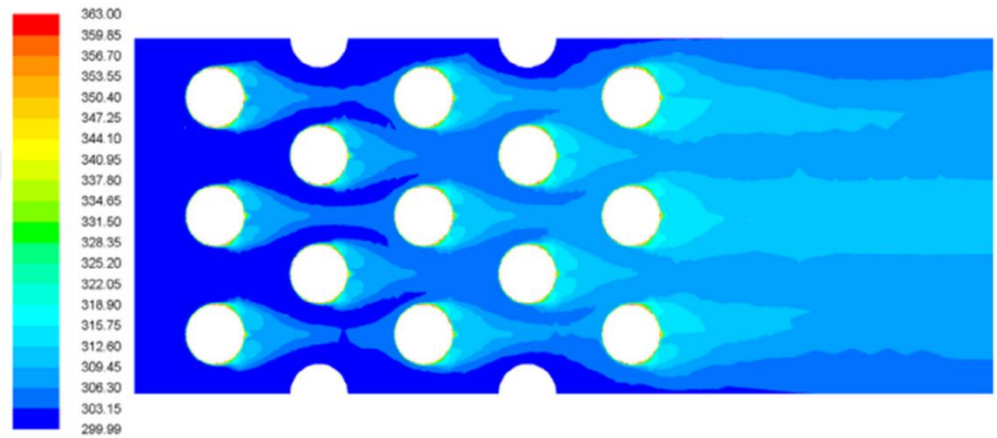


Figure 2.10. Temperature contour for staggered tube bank with splitter plate (Re = 5500) (Mangrulkar et al., 2017)

2.3.2. Plain / Wavy / Elliptical / Corrugated / Oval Finned Tube Banks

Goldstein and Sparrow (1976) used naphthalene sublimation technique to measure heat transfer coefficients of wavy finned tube heat exchanger. Reynolds number varies from 135 to 1200. They concluded that average heat transfer coefficient is 45% higher than plain finned tube heat exchanger where Reynolds number equals to 1000.

Rocha et al. (1997) performed two dimensional (2-D) numerical heat transfer analysis over elliptical and circular plain finned heat exchangers. Using elliptical tubes, fin efficiency is gained up to 18% as compared to circular tubes. In the previous studies, Brauer (1964) and Bordalo and Saboya (1995) stated that elliptical tubes reduce pressure loss up to 25% with respect to circular ones. So, Rocha et al.

(1997) combined their studies with previous studies and reported that elliptic arrangement shows considerably better overall performance as compared to circular arrangement.

Wang et al. (1997) carried out an experimental study on wavy finned tube heat exchangers to investigate heat transfer and pressure drop characteristics and obtained results are compared with plain finned tube heat exchangers. Reynolds number ranges from 400 to 8000. They stated that wavy finned tube heat exchangers have up to 70% increment while friction factor increment was observed up to 140% as compared to plain ones.

Akkoca (2004) investigated plain and wavy finned heat exchangers under laminar and turbulent flow regimes. Fin spacing, tube row number, tube arrangement (in-line or staggered), fin configuration (wavy, plain) and Reynolds number were found to be very important for the design process. Fin spacing and Reynolds number have positive effects on heat transfer coefficient. Staggered arrangement has higher heat transfer and pressure drop as compared to in-line arrangement. The author stated that optimum designs of heat exchanger satisfy these conditions: (1) non-dimensional fin spacing (= fin spacing / tube diameter) is in the range of 0.20 and 0.30, (2) wavy fin configuration usage, (3) staggered arrangement.

Chu et al. (2009) studied heat transfer and fluid flow of plain finned tube bank heat exchanger with rectangular winglet pair (RWP) numerically (figure 2.12). Three-dimensional numerical study is carried out using Fluent program. Reynolds number ranges from 500 to 800. Using rectangular winglet pair heat transfer is increased up to 131% for the studied Reynolds numbers and configurations but pressure drop increases too. They reported that rectangular winglet pairs in staggered arrangement perform better heat transfer while increasing pressure drop as compared to in-line arrangement.

Du et al. (2014) investigated heat transfer and pressure drop over oval finned

tube banks experimentally. Inlet air angle varies from 30 to 90 degrees as it is shown in figure 2.11, Reynolds number ranges from 1300 to 13000. Comparisons of different cases are made with same mass flow rate and identical pressure drop over oval finned tube bank. Under the identical mass flow rate, oval finned tube bank performs best where inlet air angle equals to 45 degrees. However, air inlet angle of 60 degree shows better performance for identical pressure drop as compared to other cases. Zhang et al. (2014) and Kim et al. (2013) studied oval shaped finned tube banks also.

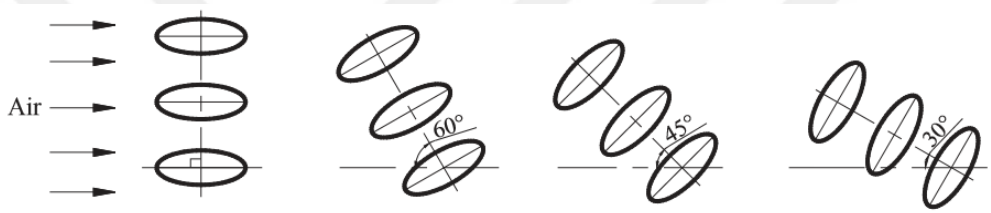


Figure 2.11. Four different inlet air angles (Du et al., 2014)

Moreover, Tahseen et al. (2015) presented detailed research about plain plate finned tube banks. Tang et al. (2009) investigated fin and tube heat exchangers for different fin shapes experimentally and numerically.

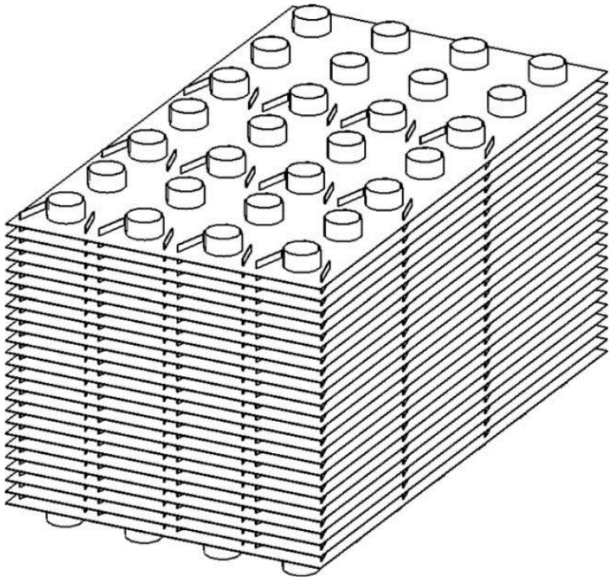


Figure 2.12. Plain finned in-line tube bank heat exchanger with rectangular winglet pair (RWP) (Chu et al., 2009)

Gholami et al. (2017) conducted numerical study of fluid and heat flow over corrugated fins with oval tube banks where Reynolds number is in the range of 200 and 900. Four oval shaped tubes with in-line arrangement were investigated for one and three corrugated fins. Corrugated fins are replaced in the radial direction. It is found that hot and cold fluids were mixed well with the usage of corrugated fins so obtained heat transfer was enhanced in the wake region. Moreover, oval tubes lead to delay of separation point as compared to circular ones which causes pressure drop decrement. They stated that using corrugated fins with oval tubes, average Nusselt number can be enhanced up to 20% while pressure drop was decreased up to 19% as compared to plain fins with circular tubes.

2.3.3. Different Type of Finned Tube Banks

Tian et al. (2015) investigated heat and fluid flow over staggered pin finned tube bank in cross flow numerically (figure 2.13). Three-dimensional, turbulent, incompressible, steady state flow with constant thermo-physical properties are assumed and seven tube rows are selected for numerical calculations using finite volume-based software, Ansys Fluent. Reynolds number varies from 954 to 3.81 x 10^4. They concluded that fin height, fin diameter and fin number have positive impact whereas transversal pitch and fin axial pitch have negative impact on thermal performance. Moreover, longitudinal pitch and tube bank configuration (in-line, staggered) does not significantly affect thermal performance.

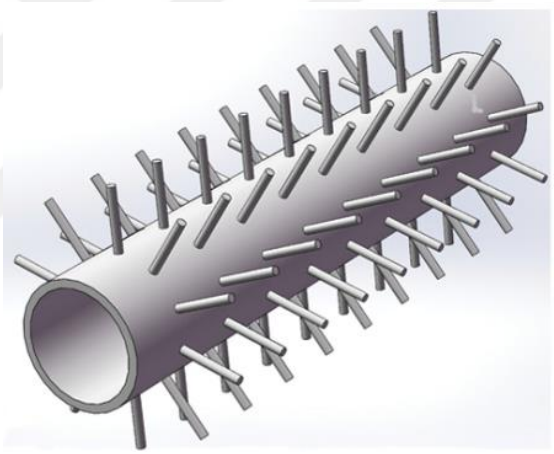


Figure 2.13. Circular pin finned tube of tube bank (Tian et al., 2015)

Jin et al. (2013) carried out heat transfer and pressure drop computations numerically on H-type fins in the tube bank. Spirally corrugated tubes are investigated by Li et al. (2012), Rainieri et al. (2012a, 2012b) and Jin et al. (2017).

2.4. Periodic Flow Studies

Numerical computations of conservation equations with periodic fully developed flow assumption are studied by some researchers. Firstly, Patankar et al. (1977) presented periodic fully developed flow concepts for ducts under constant heat flux and constant wall temperature boundary conditions. He stated that cross-section of duct remains same along the longitudinal direction so heat and fluid flow analysis can be done for a part of duct without considering entrance region effect on the solutions and it represents all of the duct.

Grannis and Sparrow (1991) study heat transfer and fluid flow over diamond shaped pin fin arrays placed in heat exchanger, numerically (figure 2.14). Two-dimensional, periodic fully developed flow is assumed, and finite element method is used for numerical calculations.

Beale and Spalding (1998) studied tube bank heat exchangers with periodic fully developed and laminar flow assumptions in cross flow. Comprehensive results for in-line square, rotated square and equilateral triangle type tube banks are presented. Faghri and Rao (1987), Beale (2008) carried out their investigations under periodic fully developed flow assumption.

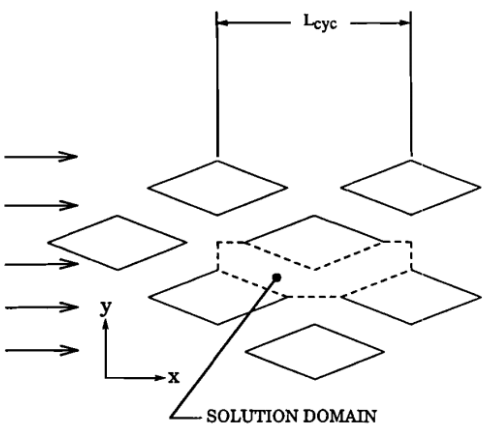


Figure 2.14. Solution domain of Grannis and Sparrow (1991)

Igci and Arici (2016) study periodic fully developed fluid and heat flow in a duct numerically where fluid flows in the stream-wise direction. Finite volume code written in FORTRAN was used to solve governing equations under steady state, turbulent, incompressible fluid flow assumptions. Four different low Reynolds number k-ε turbulence models are tested and compared with the existing experimental study from literature. They concluded that all the models gave higher local Nusselt Numbers to the experimental study because low Reynolds number models produced higher turbulence in the near wall region which result in higher local Nusselt number calculation.

2.5. Optimum Tube Banks

In the recent decade, the optimization of tube banks has been investigated by many researchers, due to optimum design demand and performance improvement of tube bank heat exchangers. The cost of energy increases and material usage leads to higher weight, so it is important to enhance heat transfer with low cost of energy and material. Yilmaz and Yilmaz (2016) and Yilmaz et al. (2017) reported that for optimum design of tube bank heat exchangers, it is important to obtain maximum heat transfer with minimum volume of tube bank for the given mass flow rate, allowable pressure drop and tube bank effectiveness. Moreover, Jayavel and Tiwari (2009), Aiba et al. (1982) stated that heat exchanger design must have two goals: (1) maximizing heat transfer, (2) minimizing pressure drop, so optimum design can be found using these goals.

Different objectives and constraints are used to obtain optimal designs of heat exchangers, i.e. Yilmaz (2009) and Shi et al. (2015) used entropy generation as an objective; Yilmaz et al. (2000), Yilmaz (2008), Khan et al. (2016) and Rashidi et al. (2015) employed pressure drop as a constraint; Bejan et al. (1995), Fowler et al. (1997) and Stanescu et al. (1996) used volume as a constraint.

Matos et al. (2001) carried out an optimization and heat transfer study using unfinned circular and elliptic tubes in staggered arrangement numerically. Heat transfer calculations are performed on two-dimensional (2-D) circular and elliptic tubes and then optimization study was conducted to obtain maximum total heat transfer rate for fixed volume in staggered arrangements. The Reynolds number varies from 300 to 800. They stated that heat transfer was increased up to 13% using optimal elliptical arrangement as compared to optimal circular arrangement.

Matos et al. (2004) perform a three-dimensional (3-D) optimization of finned circular and elliptic tubes in staggered arrangement, numerically and experimentally. The results were obtained for Reynolds numbers of 852 and 1065 in the laminar flow regime. Heat transfer is increased up to 19% in optimal elliptical arrangement as compared to optimal circular arrangement. 32% material mass reduction is observed using optimal elliptic tubes with respect to optimal circular ones.

Ranut et al. (2014) presented multi objective optimization of tube banks having cross-flow including three objective functions: (1) maximizing heat transfer in the outer of the tube bank, (2) minimizing pressure drop in the inner and (3) outer of the tube bank. Optimization studies are done with Modefrontier program while numerical calculations of fluid and heat flow are carried out with Ansys Cfx under steady, laminar and three-dimensional flow assumptions and as a boundary condition, constant temperature was assigned to tubes. In the optimization process, two genetic algorithms Non-dominated Sorting Genetic Algorithm (NSGA-II) and Fast Multi-objective Genetic Algorithm (FMOGA-II) are employed and comparisons of genetic algorithms are demonstrated. They found that FMOGA-II reduced the computation time of optimization study. Both non-periodic and periodic solution domains are modeled, however the authors suggested to use periodic solution domains due to significant reduction in the computation time.

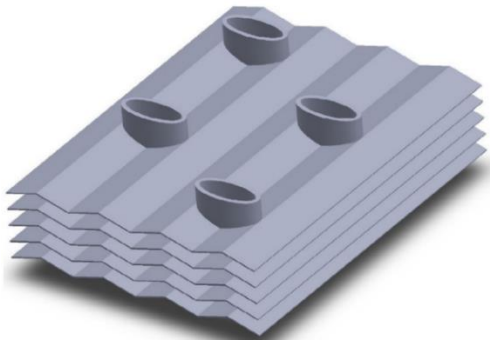
Gharbi et al. (2015) carried out a numerical optimization study to investigate heat transfer and fluid flow over circular, elliptic and wing shaped tube banks where heat transfer surfaces of three geometries are equal. Finite volume method is used, two-dimensional, steady, incompressible, turbulent flow is assumed while air is taken as a working fluid. Heat transfer and pressure drop performance for all shapes are evaluated using total entropy generation and the best configuration must be obtained with least entropy generation. Reynolds number is in the range of 5×10^3 and 2.4×10^4 , pitch ratios are $s_L^* = 1.03$ and $s_T^* = 2.07$. They concluded that elliptical and wing shaped geometries have smaller wake regions as compared to circular geometries, so they reduce pressure drop. Moreover, best configuration is not clear for all geometries, but the circular geometry is the worst for Reynolds number higher than 1.5×10^4 and the elliptic geometry is the best for Reynolds number higher than 2.3×10^5.

Yilmaz and Yilmaz (2016) carried out an optimization study based on tube bank effectiveness for in-line tube banks. For optimum in-line tube bank dimensioning (pitch lengths, tube numbers, height, length and width of tube bank), new equations are derived so it is possible to obtain minimum volume of tube bank for the given mass flow rate, allowable pressure drop and effectiveness. Dimensionless numbers are used to derive optimum in-line tube bank heat exchanger. For heat transfer calculations, Gnielinski's (2010) and Zukauksas's (1972) empirical correlations are used while Gaddis's (2010) and Zukauskas's (1972) empirical studies are used for pressure drop computations.

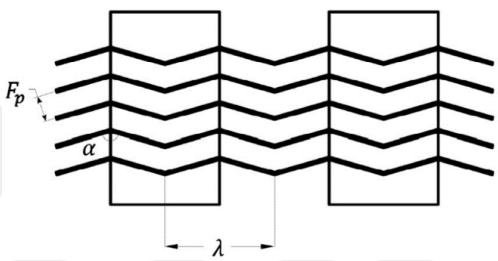
Similar study of Yilmaz and Yilmaz (2016) is carried out by Yilmaz et al. (2017) to design optimum staggered tube banks. They derived new equations using dimensionless numbers to get minimum volume of staggered tube bank for a given mass flow rate, prescribed pressure loss and effectiveness. Gnielinski's (2010) and Zukauskas's (1972) empirical correlations are used for heat transfer computations,

Gaddis's (2010) and Zukauskas's (1972) empirical studies are used for pressure drop calculations.

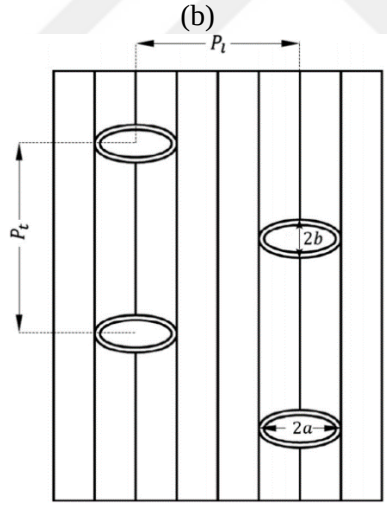
Damavandi et al. (2017) performed multi-objective optimization of elliptic tube banks with wavy fins (figure 2.15a) in staggered arrangement to obtain maximum heat transfer and minimum pressure drop using Computational Fluid Dynamics (CFD) and Non-Dominated Sorting Genetic Algorithm II (NSGA-II). In the optimization study, colburn factor (j) and friction factor (f) are the objective functions. Four design parameters were considered in the optimization study such as semi minor axis of tube bank (b), transverse tube pitch (P_t), wavy angle of fin (α), and pitch between fins (F_p) as shown in figures 2.15b and 2.15c. Moreover, constant values are assigned to wavelength of fin (λ), semi-major axis of tube bank (a), longitudinal tube pitch (P_l). Three dimensional, steady, turbulent and incompressible flow of air is modeled. Reynolds number of the study equals to 2000. After the investigation of optimum designs, it is found that a little reducing heat transfer result in significant decrement in pressure drop. Moreover, wavy fins are found to be more effective by the reason of better fluid mixing.



(a)



(b)



(c)

Figure 2.15. (a) Solution domain, (b) front and (c) top view of elliptic tube bank with wavy fins (Damavandi et al., 2017)

3. OBJECTIVES and OUTLINE

There is not any comprehensive investigation in the literature for axially finned tube banks, so the present study has two goals: (1) To investigate the effect of axial finning for different axial and transversal pitch ratios for both in-line and staggered arrangements, (2) Numerical optimization of heat and fluid flow over axially finned tube banks for both in-line and staggered arrangements. Maximization of total heat transfer from tube bank and minimization of tube bank volume are the goals of optimization problem for the given mass flow rate, allowable pressure drop and tube bank effectiveness which was formerly studied by Yilmaz and Yilmaz (2016) and Yilmaz et al. (2017).

Tube banks are assumed to be at constant wall temperature; while the flow is assumed to be steady state, turbulent, incompressible and periodic fully developed. Two equation k-ε model with enhanced wall treatment is chosen for the simulation of turbulent flow.

The heat and fluid flow over tube banks with fully developed periodic flow assumption for the given differential equations and boundary conditions is solved numerically in this study. Parametric geometry is modeled with Ansys Design Modeler. The present computational domains are generated with Ansys Mesher using quadrilateral mesh elements. Heat transfer and pressure drop in tube banks are computed by using Ansys Fluent software which is based on finite volume numerical scheme. Multi-objective design optimization software Modefrontier is chosen to solve optimization problem.

So as to confirm numerical studies' reliability, both in-line and staggered unfinned tube bank configurations are validated with experimental studies in literature.

Two goals of present study are given below:

(1) Heat transfer and pressure loss computations are carried out for four different axial and transversal pitch ratios which are $s_L^* = 3$ and $s_T^* = 1.5$, $s_L^* = 3$ and $s_T^* = 2$, $s_L^* = 5$ and $s_T^* = 1.5$, $s_L^* = 5$ and $s_T^* = 2$, especially the influence of fin lengths are compared with the unfinned cases. Reynolds number values lie in between 400 and 1500 while two Prandtl numbers 0.7 and 7 are studied with prescribed mass flow rates. Furthermore, velocity streamlines and temperature contours throughout tube banks are illustrated. Influences of axial (s_L^*) and transversal pitch (s_T^*) ratios and fin lengths on the average Nusselt number and friction factor are also shown graphically and tabulated.

(2) Optimization of unfinned and axially finned tube banks are studied and compared each other in detail. Heat transfer and pressure drop calculations are studied for $Pr = 0.71$ and a fixed mass flow rate of $\dot{m}_N = 0.5\ kg/s$ where allowable pressure drop is $\Delta p_{allow} = 100$ Pa. A constant inlet temperature $T_i = 443.15$ K and a constant wall temperature $T_w = 383.15$ K are used. Tube diameter and tube bank effectiveness are $D = 10$ mm and $\eta = 0.75$ respectively.

The given goals are carried out for both in-line and staggered arrangements, comparisons of the studied cases are detailly discussed in Results section.

4. MATERIALS and METHODS

Experimental studies on tube bank heat exchangers consume time and cost, so numerical methods increasingly take a place to develop new tube banks. In contrast to experimental works, it is possible to design optimum tube banks with numerical calculations. Numerical heat and fluid flow studies are done with Computational Fluid Dynamics (CFD) software Ansys Fluent which uses finite volume method for solving the conservation equations. Moreover, optimization studies are carried out with optimization software Modefrontier.

4.1. Solution Methods for Conservation Equations

The heat and fluid flow in the tube banks is determined by conservation of mass, momentum and energy equations under the assumption of steady state, two-dimensional, single phase and incompressible turbulent flow with constant thermo-physical properties. These conservation equations in the Cartesian coordinates are given as follows (Mangrulkar et al. (2017), Ansys Fluent Manual):

$$\frac{\partial}{\partial x}(\rho u) + \frac{\partial}{\partial y}(\rho v) = 0 \tag{4.1}$$

$$\frac{\partial}{\partial x}(\rho u u) + \frac{\partial}{\partial y}(\rho u v) = -\frac{\partial p}{\partial x} + 2\frac{\partial}{\partial x}\left(\mu_{eff}\frac{\partial u}{\partial x}\right) + \frac{\partial}{\partial y}\left[\mu_{eff}\left(\frac{\partial u}{\partial y} + \frac{\partial v}{\partial x}\right)\right] \tag{4.2a}$$

$$\frac{\partial}{\partial x}(\rho uv) + \frac{\partial}{\partial y}(\rho vv) = -\frac{\partial p}{\partial y} + \frac{\partial}{\partial x}\left[\mu_{eff}\left(\frac{\partial u}{\partial y} + \frac{\partial v}{\partial x}\right)\right] + 2\frac{\partial}{\partial y}\left(\mu_{eff}\frac{\partial v}{\partial y}\right) \quad (4.2b)$$

$$\frac{\partial}{\partial x}(\rho uT) + \frac{\partial}{\partial y}(\rho vT) = \frac{\partial}{\partial x}\left[\left(\frac{\mu}{Pr} + \frac{\mu_t}{Pr_t}\right)\frac{\partial T}{\partial x}\right] + \frac{\partial}{\partial y}\left[\left(\frac{\mu}{Pr} + \frac{\mu_t}{Pr_t}\right)\frac{\partial T}{\partial y}\right] \quad (4.3)$$

μ_{eff} shows the effective turbulent viscosity and it is given as;

$$\mu_{eff} = \mu + \mu_t \quad (4.4)$$

μ_t indicates the turbulent (or eddy) viscosity,

$$\mu_t = \rho C_\mu \frac{k^2}{\varepsilon} \quad (4.5)$$

The Navier-Stokes equations describe the fluid flow accurately. For complex problems of fluid flow, it costs too much and consumes time to solve momentum equations, Jaw and Chen (1996). Two methods were presented to overcome these obstacles: (1) Reynolds Averaged Navier Stokes (RANS) method, (2) Large Eddy Simulation (LES) method. The RANS method solves equations for the mean flow quantities.

4.2. Turbulence Models

For the turbulent flow simulation, the k-ε models which consist of standard k-ε, Renormalization Group (RNG) k-ε and realizable k-ε are used in this study due to closer results to experimental data. Moreover, the RNG k-ε turbulence model with

enhanced wall treatment shows good agreement with the experimental studies, so this model is chosen in this study.

The k-ε models are the two equation RANS based turbulence models and commonly used in engineering applications. The transport equations of standard, RNG and realizable k-ε models have similar forms for turbulence kinetic energy (k) and energy dissipation rate (ε). The basic differences are given as follows:

(1) Turbulent viscosity, μ_t calculation

(2) Generation of turbulence kinetic energy, G_k in the energy dissipation rate (ε) equation

4.2.1. The Standard k-ε Model

The standard k-ε model is valid for fully turbulent flows.

$$\frac{\partial}{\partial x}(\rho k u) + \frac{\partial}{\partial y}(\rho k v) = \frac{\partial}{\partial x}\left[\left(\mu + \frac{\mu_t}{\sigma_k}\right)\frac{\partial k}{\partial x}\right] + \frac{\partial}{\partial y}\left[\left(\mu + \frac{\mu_t}{\sigma_k}\right)\frac{\partial k}{\partial y}\right] + G_k - \rho\varepsilon \tag{4.6}$$

$$\frac{\partial}{\partial x}(\rho \varepsilon u) + \frac{\partial}{\partial y}(\rho \varepsilon v) = \frac{\partial}{\partial x}\left[\left(\mu + \frac{\mu_t}{\sigma_\varepsilon}\right)\frac{\partial \varepsilon}{\partial x}\right] + \frac{\partial}{\partial y}\left[\left(\mu + \frac{\mu_t}{\sigma_\varepsilon}\right)\frac{\partial \varepsilon}{\partial y}\right] + C_{1\varepsilon}\frac{\varepsilon}{k}G_k - C_{2\varepsilon}\,\rho\,\frac{\varepsilon^2}{k} \tag{4.7}$$

G_k indicates the generation of turbulence kinetic energy and it is given below:

$$G_k = -\mu_t \left[2\left(\frac{\partial u}{\partial x}\right)^2 + 2\left(\frac{\partial v}{\partial y}\right)^2 + \left(\frac{\partial u}{\partial y} + \frac{\partial v}{\partial x}\right)^2 \right] \tag{4.8}$$

The model constants are $C_{1\varepsilon} = 1.44$, $C_{2\varepsilon} = 1.92$, $C_\mu = 0.09$, $\sigma_k = 1.0$, $\sigma_\varepsilon = 1.3$ (Ansys Fluent Manual).

4.2.2. The RNG k-ε Model

k and ε differential equations in the steady state can be written in the following forms:

$$\frac{\partial}{\partial x}(\rho k u) + \frac{\partial}{\partial y}(\rho k v) = \frac{\partial}{\partial x}\left(\alpha_k \mu_{eff} \frac{\partial k}{\partial x}\right) + \frac{\partial}{\partial y}\left(\alpha_k \mu_{eff} \frac{\partial k}{\partial y}\right) + G_k - \rho\varepsilon \tag{4.9}$$

$$\frac{\partial}{\partial x}(\rho \varepsilon u) + \frac{\partial}{\partial y}(\rho \varepsilon v) = \frac{\partial}{\partial x}\left[\left(\mu + \frac{\mu_t}{\sigma_\varepsilon}\right)\frac{\partial \varepsilon}{\partial x}\right] + \frac{\partial}{\partial y}\left[\left(\mu + \frac{\mu_t}{\sigma_\varepsilon}\right)\frac{\partial \varepsilon}{\partial y}\right] + C_{1\varepsilon}\frac{\varepsilon}{k}G_k - C_{2\varepsilon}\,\rho\,\frac{\varepsilon^2}{k} \tag{4.10}$$

The inverse effective Prandtl numbers of k and ε are denoted as α_k and α_ε respectively. C_μ is 0.0845 (Ansys Fluent Manual). The model constants $C_{1\varepsilon}$ and $C_{2\varepsilon}$ equal to 1.42 and 1.68 respectively which are derived using the RNG theory (Ansys Fluent Manual).

4.2.3. The Realizable k-ε Model

The realizable k-ε model equations are given as below:

$$\frac{\partial}{\partial x}(\rho k u) + \frac{\partial}{\partial y}(\rho k v) = \frac{\partial}{\partial x}\left[\left(\mu + \frac{\mu_t}{\sigma_k}\right)\frac{\partial k}{\partial x}\right] + \frac{\partial}{\partial y}\left[\left(\mu + \frac{\mu_t}{\sigma_k}\right)\frac{\partial k}{\partial y}\right] + G_k - \rho\varepsilon \tag{4.11}$$

$$\frac{\partial}{\partial x}(\rho \varepsilon u) + \frac{\partial}{\partial y}(\rho \varepsilon v) = \frac{\partial}{\partial x}\left[\left(\mu + \frac{\mu_t}{\sigma_\varepsilon}\right)\frac{\partial \varepsilon}{\partial x}\right] + \frac{\partial}{\partial y}\left[\left(\mu + \frac{\mu_t}{\sigma_\varepsilon}\right)\frac{\partial \varepsilon}{\partial y}\right] - \rho\, C_2 \frac{\varepsilon^2}{k + \sqrt{v\varepsilon}} \tag{4.12}$$

The model constants are $C_\mu = 0.09$, $C_2 = 1.9$, $\sigma_k = 1.0$, $\sigma_\varepsilon = 1.2$ (Ansys Fluent Manual).

4.3. Physical Model

An axially finned in-line tube bank is illustrated in figure 4.1. Axially finned in-line tube bank is comprised of N tubes which are independent from each other. Number of tubes in the longitudinal and transversal directions are N_L and N_T, respectively. Fluid with mass flow rate $\dot{m}_N$ enters the tube bank with inlet temperature T_i and leaves it with outlet temperature T_o. U_∞ is the velocity of the fluid before entering the tube bank. Constant wall (T_w) and inlet (T_i) temperatures are assumed.

As seen in figure 4.1, the pitches in longitudinal and transversal directions are s_L and s_T, respectively. Tube bank heat exchanger length and height are denoted as L and H, respectively. B is the tube bank width and D is denoted for tube diameter.

Fin length and thickness are denoted as L_f and t, respectively. Similarly, an axially finned staggered tube bank is illustrated in figure 4.2.

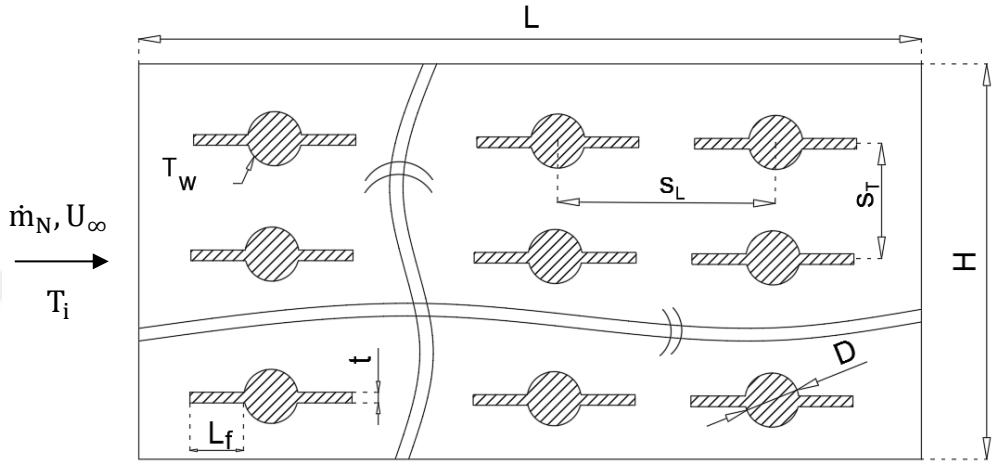


Figure 4.1. Axially finned in-line tube bank heat exchanger of length L, height H and width B

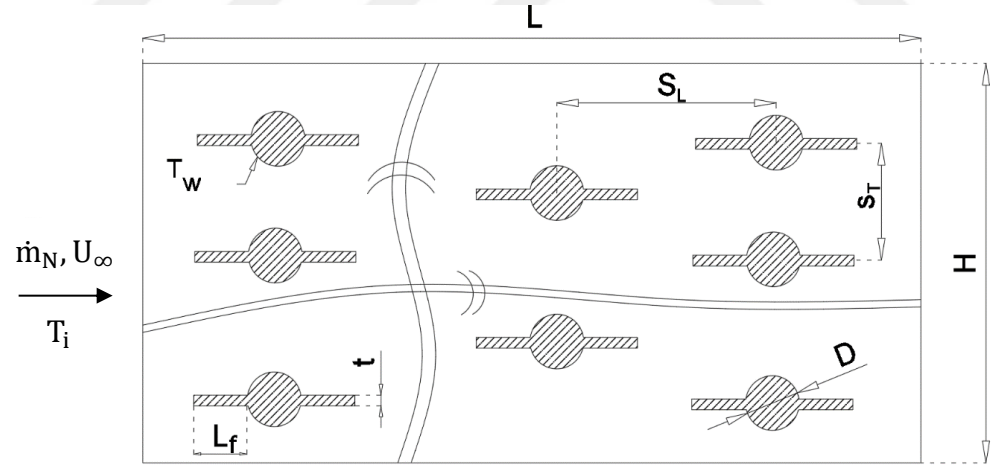


Figure 4.2. Axially finned staggered tube bank heat exchanger of length L, height H and width B

Numerical calculations of fluid and heat flow in tube banks still increases solution time in spite of high speed computing ability. In order to reduce computation time to solve governing equations, simplification of tube bank models must be done. The geometry of axially finned in-line and staggered tube banks and the expected solutions have a periodically repeating form. The geometries are constant along the flow direction, so it leads to periodic fully developed flow. Therefore, periodic flow is assumed while making the calculations to simplify the numerical model.

The computational domains are modeled as a cylinder for in-line tube bank and two cylinders for staggered tube bank with the assumption of periodic fully developed flow. Note that for staggered arrangement, two cylinders are chosen for solution domains to show better fluid and heat flow. Due to the symmetricity of cylinders, numerical results are obtained around the halves of the cylinders as shown in figures 4.3 and 4.4.

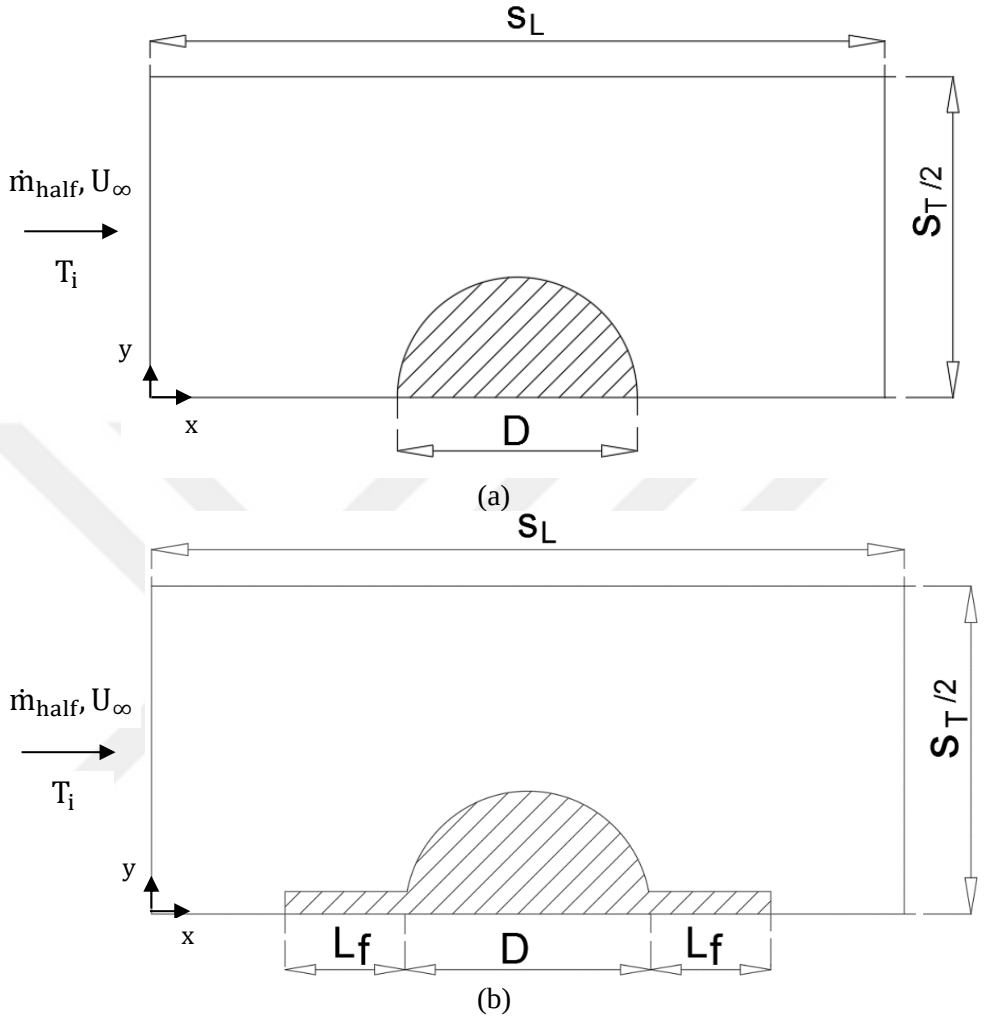


Figure 4.3. Solution domain for in-line (a) unfinned tube bank (b) D-Finned tube bank of $s_L^* = 5$ and $s_T^* = 1.5$

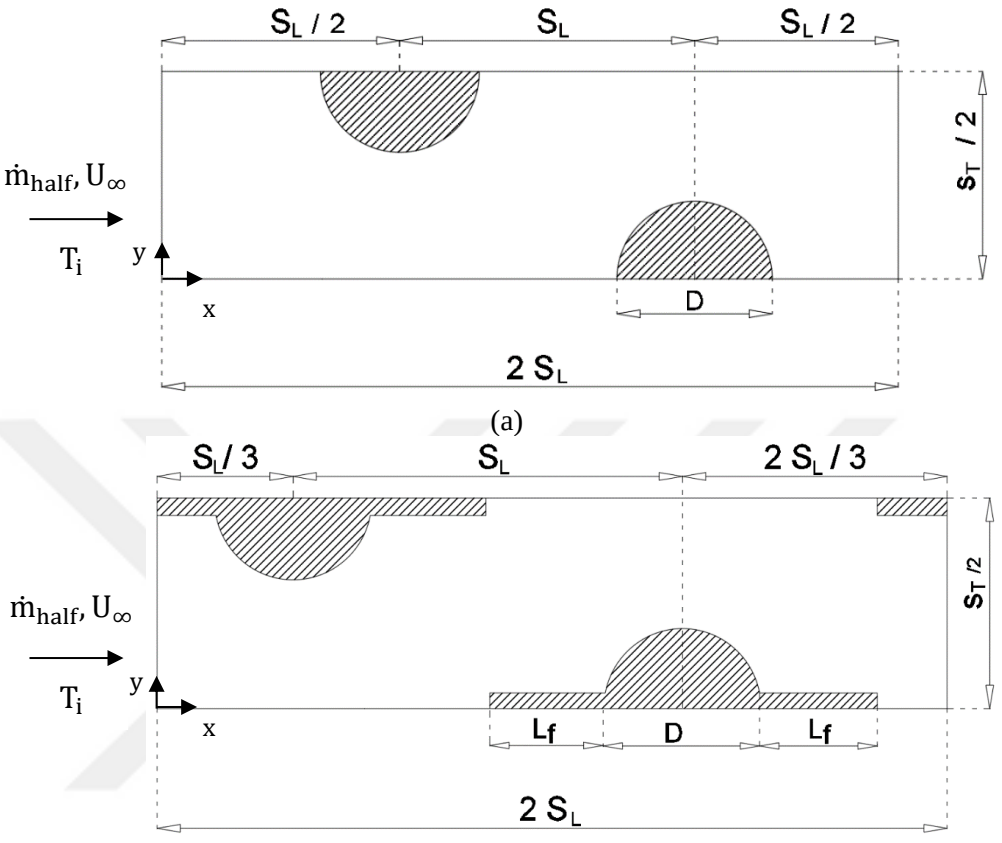


Figure 4.4. Solution domain for staggered (a) unfinned tube bank (b) D-Finned tube bank of $s_L^* = 3$ and $s_T^* = 1.5$

4.4. Definition of Parameters

Reynolds number Re is calculated by average velocity in the minimum cross-sectional area of tube bank, which is the maximum average velocity U_{max} :

$$Re = \frac{U_{max}\ D}{\upsilon} \tag{4.13}$$

Prandtl number Pr is given as;

$$Pr = \frac{\mu\, c_p}{k} \tag{4.14}$$

For in-line tube banks, the minimum cross section is formed between the tubes perpendicular to the cross flow;

$$U_{max} = \frac{s_T}{s_T - D} U_\infty \tag{4.15}$$

For staggered tube banks, the maximum average velocity U_{max} can be calculated from:

$$s_D < \frac{s_T + D}{2} \quad : \quad U_{max} = \frac{s_T}{2(s_D - D)} U_\infty \tag{4.16a}$$

$$s_D \geq \frac{s_T + D}{2} \quad : \quad U_{max} = \frac{s_T}{s_T - D} U_\infty \tag{4.16b}$$

where

$$s_D = \left[s_L^2 + \left(\frac{s_T}{2}\right)^2 \right]^{1/2} \tag{4.17}$$

Fluid enters the tube bank with mass flow rate of $\dot{m}_N$ and it is defined as:

$$\dot{m}_N = \rho\, U_\infty\, A_N \tag{4.18}$$

where A_N is the cross-sectional area of tube bank in the flow direction at inlet (figures 4.1 and 4.2):

$$A_N = B\,H \tag{4.19}$$

For a given mass flow rate of tube bank $\dot{m}_N$, U_∞ can be calculated using equations 4.18 and 4.19. Mass flow rate from half of the tube $\dot{m}_{half}$ is calculated as follows:

$$\dot{m}_{half} = \rho\, U_\infty\, A_{half} \tag{4.20}$$

where A_{half} is the cross-sectional area of half of the tube in the flow direction at inlet (figures 4.3 and 4.4):

$$A_{half} = B\,\frac{s_T}{2} \tag{4.21}$$

Transversal pitch ratio s_T^* and axial pitch ratio s_L^* are defined as follows:

$$s_T^* = \frac{s_T}{D} \tag{4.22}$$

$$s_L^* = \frac{s_L}{D} \tag{4.23}$$

Average Nusselt number and mean heat transfer coefficient are written as;

$$\overline{Nu} = \frac{\bar{h}\,D}{k} \tag{4.24}$$

$$\bar{h} = \frac{q''}{\Delta T_{lm}} \tag{4.25}$$

where $q^{"}$ is heat flow transferred from the wall into the fluid and, ΔT_{lm} is the logarithmic mean temperature difference:

$$\Delta T_{lm} = \frac{(T_w - T_i) - (T_w - T_o)}{\ln \frac{T_w - T_i}{T_w - T_o}} \tag{4.26}$$

4.5. Periodic Flow Formulations

For the periodic fully developed flow over the tube bank, velocity components must be same in the periodic boundaries where the periodic length equals to s_L (figures 4.3 and 4.4) and it is given as follows:

$$u(x, y) = u(x + s_L, y) \tag{4.27}$$

$$v(x, y) = v(x + s_L, y) \tag{4.28}$$

Across the tube bank, pressure drop Δp_N is determined by;

$$\Delta p_N = f\, N_L \frac{\rho\, U_{max}^2}{2} \tag{4.29}$$

The pressure drop Δp_N between solution domains is periodic;

$$\frac{\Delta p_N}{N_L} = p(x, y) - p(x + s_L, y) = p(x + s_L, y) - p(x + 2s_L, y) = \cdots \tag{4.30}$$

We also define a pressure gradient β as follows:

$$\beta = \frac{\Delta p_N}{L} = \frac{\Delta p_N}{N_L \, s_L} \tag{4.31}$$

and it is possible to express pressure in the following form:

$$p(x, y) = -\beta x + \widetilde{P}(x, y) \tag{4.32}$$

where $\widetilde{P}(x, y)$ is the periodic pressure and βx is the linearly varying and non-periodic term of pressure (Patankar et al., 1977). βs_L represents the pressure drop over periodic solution domain where L is the periodic solution domain length.

For constant wall temperature boundary condition, temperature of fluid approaches to the wall temperature through the tube bank. Moreover, the fluid temperature behaves periodically if it can be scaled as (Patankar et al., 1977):

$$\theta(x, y) = \frac{T(x, y) - T_w}{\overline{T}(x, y) - T_w} \tag{4.33}$$

$$\theta(x + s_L, y) = \frac{T(x + s_L, y) - T_w}{\overline{T}(x + s_L, y) - T_w} \tag{4.34}$$

Equation 4.35 is the periodic generalization of equations 4.33 and 4.34 which is in the periodic form through the tube bank.

$$\theta(x, y) = \theta(x + s_L, y) = \theta(x + 2s_L, y) = \cdots \tag{4.35}$$

The bulk temperature is defined as:

$$\overline{T}(x,y) = \frac{\int_A T\rho\, u\, dA}{\int_A \rho\, u\, dA} \quad , \quad \overline{T}(x+s_L,y) = \frac{\int_A T\,\rho\, u\, dA}{\int_A \rho\, u\, dA} \tag{4.36}$$

4.6. Optimization Problem Formulation

Two objective functions are defined in the optimization problem: (1) maximize total heat transfer from tube bank, $\dot{Q}_N$ (2) minimize tube bank volume, V_N. Furthermore, one constraint must be satisfied: $\dot{Q}_N$ is equal or lower than maximum obtainable heat transfer over tube bank, $\dot{Q}_{max}$. A multi-objective design optimization problem for present study is given as:

Objective Function	Maximize $\dot{Q}_N$, Minimize V_N	(4.37)
Constraints	$\dot{Q}_N \leq \eta \dot{Q}_{max}$	
Optimization Variables	s_L , s_T , N_L , N_T , B, t	
Given Data	$\dot{m}_N$, Δp_{allow}, T_i , T_w , η, D	

With periodic fully developed flow assumption, computations are carried out for half of one tube for in-line arrangement and halves of two tubes for staggered arrangement and generalized to whole tube bank which consists of N tubes. Ansys Fluent software has two options for periodic flow calculation of solution domain: $\dot{m}_{half}$ or β can be specified. In the optimization studies, β which can be computed from equation 4.31 is used. So, it is possible to obtain heat transfer ($\dot{Q}_N$) from tube bank for the given allowable pressure drop (Δp_N).

In order to obtain optimum dimensions of tube bank, we must formulate total heat transfer ($\dot{Q}_N$) and volume (V_N) for the whole tube bank which has N tubes. In the followings, the definitions of physical quantities are given.

4.6.1. Heat Transfer

Heat flux from half of the tube q''_{half} is calculated using Ansys Fluent software under periodic fully developed flow assumption and then mean heat transfer coefficient from half of the tube $\bar{h}_{half}$ is computed as follows:

$$\bar{h}_{half} = \frac{q''_{half}}{\Delta T_{lm,half}} \tag{4.38}$$

where $\Delta T_{lm,half}$ is logarithmic mean temperature difference of half of the tube and it is given as follows:

$$\Delta T_{lm,half} = \frac{(T_w - \overline{T}(x,y)) - (T_w - \overline{T}(x+s_L,y))}{\ln \frac{T_w - \overline{T}(x,y)}{T_w - \overline{T}(x+s_L,y)}} \tag{4.39}$$

Because of the periodic fully developed flow assumption, mean heat transfer coefficient of half of s_T ($\bar{h}_{half}$) also represents the mean heat transfer coefficient of whole tube bank ($\bar{h}_N$). So, we can write;

$$\bar{h}_N = \bar{h}_{half} \tag{4.40}$$

Heat transfer from whole tube bank $\dot{Q}_N$ can be written as:

$$\dot{Q}_N = \dot{m}_N \, c_p \, (T_o - T_i) \tag{4.41}$$

$$\dot{Q}_N = \bar{h}_N \, F_N \, \Delta T_{lm,N} \tag{4.42}$$

Here, c_p is fluid specific heat and F_N is the total surface area of whole tube bank and given as:

$$F_N = N \pi D B \tag{4.43}$$

Here, number of tubes N in the tube bank is determined using the following formulation:

$$N = N_L N_T \tag{4.44}$$

$\Delta T_{lm,N}$ is logarithmic temperature difference from whole tube bank:

$$\Delta T_{lm,N} = \frac{(T_w - T_i) - (T_w - T_o)}{\ln \frac{T_w - T_i}{T_w - T_o}} \tag{4.45}$$

Inlet-outlet temperature difference can be determined using the equations 4.41, 4.42 and 4.45 as follows:

$$T_o - T_i = (T_w - T_i) \left[1 - \exp\left(-\frac{\bar{h}_N F_N}{\dot{m}_N c_p}\right)\right] \tag{4.46}$$

$\dot{Q}_N$ can be calculated using equations 4.41 and 4.46.

4.6.2 Volume

Here, V_N is the volume of whole tube bank:

$$V_N = L B H \tag{4.47}$$

where L is

$$L = N_L \, s_L \tag{4.48}$$

and H equals to

$$H = N_T \, s_T \tag{4.49}$$

4.6.3 Effectiveness

We define the effectiveness of tube bank η as:

$$\eta = \frac{\dot{Q}_N}{\dot{Q}_{max}} \tag{4.50}$$

where $\dot{Q}_N$ is the heat transferred from tube bank and $\dot{Q}_{max}$ is maximum obtainable heat transfer if tube bank is infinitely long. Maximum obtainable heat transfer $\dot{Q}_{max}$ is determined from:

$$\dot{Q}_{max} = \dot{m}_N \, c_p \, \Delta T \tag{4.51}$$

where

$$\Delta T = T_w - T_i \tag{4.52}$$

Economical and practical effectiveness of tube bank can be between 60% and 80% (Yilmaz and Yilmaz, 2016).

4.7. Methods of Yilmaz and Yilmaz (2016) and Yilmaz et al. (2017)

Present optimization study has same assumptions given in Yilmaz and Yilmaz's (2016) and Yilmaz et al.'s (2017) studies. Using Yilmaz and Yilmaz's (2016) equations, it can be designed unfinned optimum in-line tube bank heat exchangers. Similarly, Yilmaz et al.'s (2017) equations lead to obtain unfinned optimum staggered tube banks. So, numerical calculation results of present computations are compared with their studies.

4.7.1. Method of Yilmaz and Yilmaz (2016) (In-line Arrangement)

Mass flow rate $\dot{m}_N$, allowable pressure drop Δp_{allow} , optimum tube bank effectiveness η_o , inlet and wall temperatures T_i , T_w are specified for in-line tube bank, minimum tube diameter D is chosen then dimensionless diameter d^* is calculated as:

$$d^* = \frac{D}{\delta} \quad : \quad \delta = \frac{\upsilon}{u_p} \quad : \quad u_p = \sqrt{\frac{2\,\Delta p_{allow}}{\rho}} \tag{4.53}$$

where u_p is the pressure velocity. Optimum tube bank effectiveness η_o is also given as:

$$\eta_o = \frac{1}{1 + \frac{0.39\,d^{*0.3}}{N_L}} \tag{4.54}$$

Using d^* and η_o, number of tubes in the longitudinal direction N_L can be determined by equation 4.54. Optimum dimensionless pitch s_o^* is determined from

$$s_o^* = 1 + \left(\frac{0.23^5 + y_1^5}{1 + \frac{0.23^5 + y_1^5}{y_2^5}} \right)^{0.2} \tag{4.55}$$

where

$$y_1 = \left(0.07 + \frac{3.45}{d^{*0.44}} \right) N_L^{0.54} \tag{4.56}$$

$$y_2 = 1.48 + \frac{66}{d^{*0.68}} \tag{4.57}$$

Moreover, optimum dimensionless pitch s_o^* equals to optimum transversal and longitudinal pitches.

$$s_o^* = s_L^* = s_T^* \tag{4.58}$$

Optimum dimensionless volumetric heat flow $\dot{q}_{V,o}^*$ can be calculated using the equations below:

$$\dot{q}_{V,o}^* = \frac{q_2}{\left[1 + \left(\frac{q_2}{q_1} \right)^{4/3} \right]^{3/4}} \tag{4.59}$$

$$q_1 = \frac{0.36}{d^{*1.31} N_L^{1/3}} \tag{4.60}$$

$$q_2 = \frac{0.57}{d^* \, N_L^{1.5}} \tag{4.61}$$

Using $\dot{q}^*_{V,o}$, optimum volumetric heat flow $\dot{q}_{V,o}$ is calculated from

$$\dot{q}_{V,o} = \frac{\dot{q}^*_{V,o} \, \rho \, c_p \, u_p \, (T_w - T_i)}{\delta} \tag{4.62}$$

The volume of tube bank is given as:

$$V_N = \frac{\dot{m}_N \, c_p \, (T_w - T_i) \, \eta_o}{\dot{q}_{V,o}} \tag{4.63}$$

Length of tube bank L is obtained from $L = N_L \, s_L$. Subsequently, cross-sectional area of N tubes A_N can be calculated using $A_N = \frac{V_N}{L}$. Tube bank width B is chosen freely and height H can be calculated from $H = \frac{A_N}{B}$. Then, number of tubes in transversal direction N_T is determined using $H = N_T \, s_T$. N_T is selected, B and H of the tube bank is corrected. The optimum dimensions of in-line tube bank are obtained.

Optimum dimensioning equations are valid for $Pr = 0.71$, $2 \leq N_L \leq 40$ and $500 \leq d^* \leq 50.000$ (Yilmaz and Yilmaz, 2016).

4.7.2 Method of Yilmaz et al. (2017) (Staggered Arrangement)

Mass flow rate $\dot{m}_N$, allowable pressure drop Δp_{allow} , optimum tube bank effectiveness η_o , inlet and wall temperatures T_i , T_w are selected for staggered tube bank, minimum tube diameter D is preferred then dimensionless diameter d^* is computed as:

$$d^* = \frac{D}{\delta} \quad : \quad \delta = \frac{\upsilon}{u_p} \quad : \quad u_p = \sqrt{\frac{2\,\Delta p_{allow}}{\rho}} \tag{4.64}$$

where u_p is the pressure velocity. Optimum tube bank effectiveness η_o is

$$\eta_o = \frac{1}{1 + \dfrac{0.035\, d^{*0.54}(1 + 3680/d^*)^{0.27}}{N_L^{1.38}}} \tag{4.65}$$

Number of tubes in the longitudinal direction N_L can be calculated by equation (4.65) using d^* and η_o. Optimum dimensionless transversal pitch $s^*_{T,o}$ is obtained from

$$s^*_{T,o} = 1.29 + \frac{26.8}{d^{*0.78}} + \frac{y_2}{[1 + (y_2/y_1)^{2/3}]^{3/2}} \tag{4.66}$$

where

$$y_1 = 0.142\, \frac{N_L^{2.35}}{d^{*0.4}} \tag{4.67}$$

$$y_2 = 1 + \frac{400}{d^*\,[1 + d^*/6240]^{1/2}} \tag{4.68}$$

Besides, optimum dimensionless longitudinal pitch $s^*_{L,o}$ is

$$s^*_{L,o} = \frac{\sqrt{3}}{2}\, s^*_{T,o} \tag{4.69}$$

Optimum dimensionless volumetric heat flow $\dot{q}^{*}_{V,o}$ can be computed using following equations:

$$\dot{q}^{*}_{V,o} = \frac{m}{d^{*n}} \tag{4.70}$$

$$n = 1.03 + 0.62 \exp[-0.175\ (N_L + 4)] \tag{4.71}$$

$$m = b\ q_1 + (1 - b)\ q_2 \tag{4.72}$$

$$q_1 = \frac{350000}{N_L^{1.32}} \tag{4.73}$$

$$q_2 = \frac{295000}{N_L^{1.51}} \tag{4.74}$$

$$b = \frac{1}{1 + (N_L / 7)^4} \tag{4.75}$$

Optimum volumetric heat flow $\dot{q}_{V,o}$ is computed as below:

$$\dot{q}_{V,o} = \frac{\dot{q}^{*}_{V,o}\ \rho\ c_p\ u_p\ (T_w - T_i)}{\delta\ 10^6} \tag{4.76}$$

The tube bank volume is given as:

$$V_N = \frac{\dot{m}_N\ c_p\ (T_w - T_i)\ \eta_o}{\dot{q}_{V,o}} \tag{4.77}$$

Length of tube bank L is $L = 2\,N_L\,s_L$. Afterward, cross-sectional area of N tubes A_N can be computed from $A_N = \frac{V_N}{L}$. Tube bank width B is selected arbitrary and height H is $H = \frac{A_N}{B}$. Later, number of tubes in transversal direction N_T is calculated using $H = N_T\,s_T$. N_T is chosen, B and H of the tube bank is modified. The staggered tube bank's optimum dimensions are attained.

Optimum dimensioning equations are applicable for $Pr = 0.71$, $2 \leq N_L \leq 20$ and $500 \leq d^* \leq 50.000$. Moreover, tube diameter must be in the range of 10 mm and 50 mm while optimum tube bank effectiveness has to be between 50% and 90% (Yilmaz et al., 2017).

4.8. Boundary Conditions

The solution domain boundaries of in-line tube bank are shown in figure 4.5 for D-Finned case of $s_L^* = 5$ and $s_T^* = 1.5$. Also, D-Finned case of $s_L^* = 3$ and $s_T^* = 1.5$'s solution domain boundaries are presented in figure 4.6 for staggered tube bank. Boundaries are given in table 4.1.

1-2, 7-8, 9-10 and 1-2, 7-8, 11-12 are the symmetry lines of in-line and staggered arrangements respectively and flow does not pass from these boundaries. As stated in table 4.1, the gradient of x component of velocity ($\partial u(x,y)/\partial y$), y component of velocity ($v(x,y)$) and the gradient of temperature ($\partial T(x,y)/\partial y$) are set to zero for the lines of symmetry.

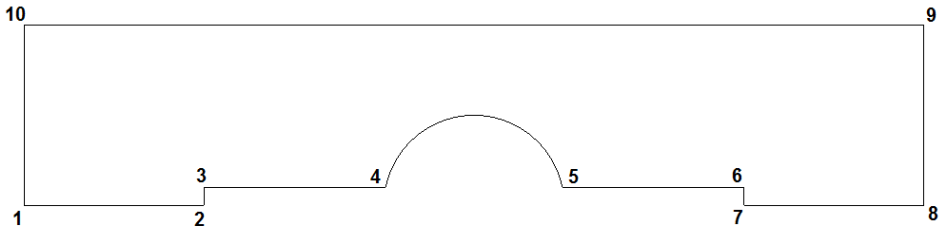


Figure 4.5. Boundaries for D-Finned study of $s_L^* = 5$ and $s_T^* = 1.5$ (In-line Arrangement)

Inlet and outlet lines are the lines of periodic boundaries where velocity components $u(x, y)$ and $v(x, y)$ and dimensionless temperatures $\theta(x, y)$ are equal to each other. Inlet temperature is constant and different from the cylinder and fin surface temperatures.

The cylinder and fin surface lines are defined as wall boundary conditions which have no slip condition so that the velocity components $u(x, y)$ and $v(x, y)$ and dimensionless temperatures $\theta(x, y)$ are equal to zero. A constant wall temperature is assigned to cylinder and fin surfaces.

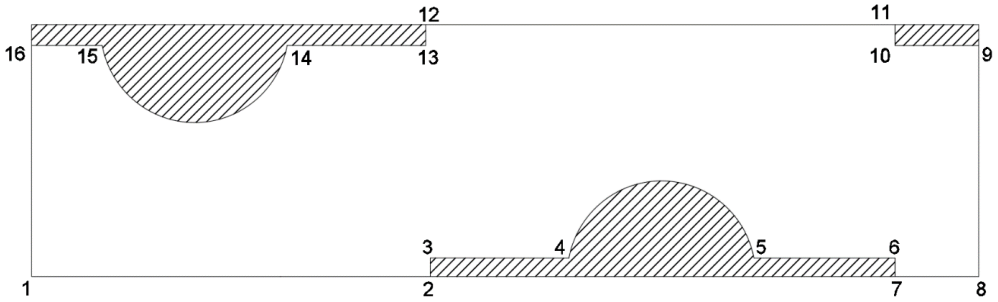


Figure 4.6. Boundaries for D-Finned study of $s_L^* = 3$ and $s_T^* = 1.5$ (Staggered Arrangement)

Table 4.1. Boundary conditions for solution domains

Boundaries		Type	u	v	T
In-line	Staggered				
1-2 7-8 9-10	1-2 7-8 11-12	Symmetric	$\frac{\partial u(x,y)}{\partial y} = 0$	$v(x,y) = 0$	$\frac{\partial T(x,y)}{\partial y} = 0$
2-3 3-4 4-5 5-6 6-7	2-3 3-4 4-5 5-6 6-7 9-10 10-11 12-13 13-14 14-15 15-16	Wall	$u(x,y) = 0$	$v(x,y) = 0$	$\theta(x,y) = 0$
1-10 8-9	1-16 8-9	Periodic Flow	$u(x,y) = u(x + s_L, y)$	$v(x,y) = v(x + s_L, y)$	$\theta(x,y) = \theta(x + s_L, y)$

4.9. Computational Details

The above explained model with the given differential equations and boundary conditions is solved numerically. Heat and fluid flow computations in two-dimensional axially finned in-line and staggered tube banks in cross-flow is carried out using commercial CFD software Ansys Fluent. Parametric geometry is modeled with Ansys Design Modeler. The present solution domains are produced with quadrilateral mesh elements with Ansys Mesher as shown in figures 4.7 and 4.8. The present numerical study utilizes second-order accuracy for momentum, energy and turbulence equations. For convergence criteria, energy residual is less than 10^{-9} and the other quality residuals are less than 10^{-6}.

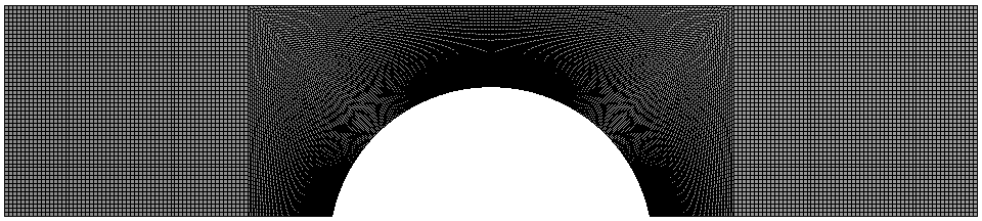
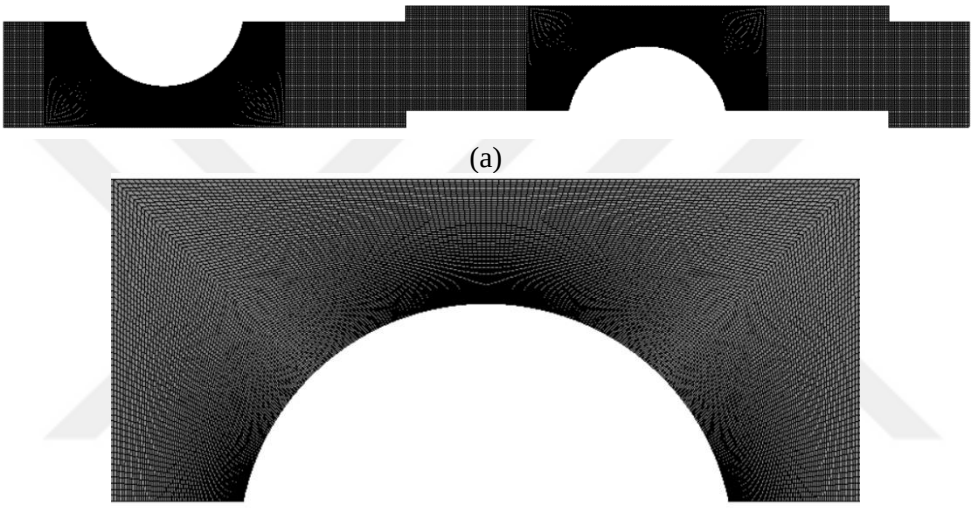


Figure 4.7. In-line tube bank solution domain for unfinned study of $s_L^* = 3$ and $s_T^* = 1.5$



(a)

(b)

Figure 4.8. (a) Solution domain of axially finned staggered tube bank (b) mesh around the tube for D-Finned study of $s_L^* = 3$ and $s_T^* = 1.5$

Modefrontier commercial optimization driver is chosen to obtain optimum designs. Furthermore, Modefrontier enables coupling with Ansys Fluent software.

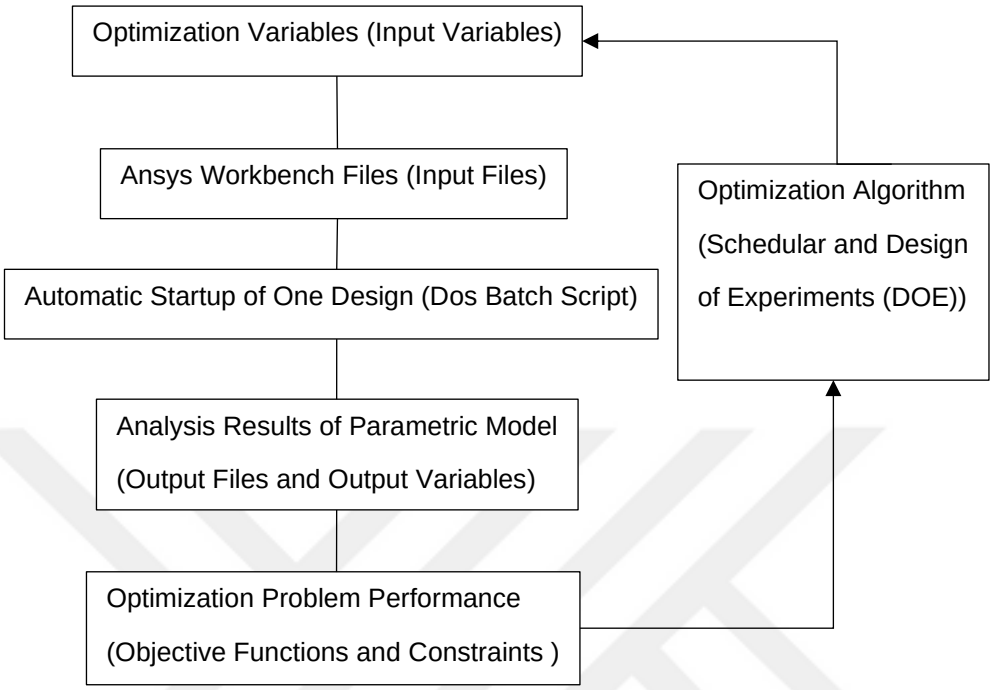


Figure 4.9. Optimization workflow

The periodic solution domain of tube bank configuration is modeled parametrically using Ansys Software and linked to the optimization driver Modefrontier. The optimization workflow given in figure 4.9 integrates parametric model and optimization algorithm so different designs of tube bank configurations can be obtained for the given optimization study.

Firstly, input variables of optimization study are defined and then parametric model is given in input files which was created with Ansys software and contains input variables. Batch script executes one design automatically for the given tube bank configuration. The response of parametric model simulation are linked to output files and output variables. This process continues until the optimization algorithm reaches optimum values.

Before the optimization algorithm try to find optimum solutions of the given optimization problem, initial designs which are called Design of Experiments

(DOEs) must be stated. DOEs provide baseline designs so they are used as starting point of the optimization problem. The optimization algorithm used in this study is Multi-objective Genetic Algorithm II (MOGA-II). Initial population for the MOGA-II is composed with DOEs. MOGA-II searches new solutions under three criteria: (1) best designs selection (2) new generation with cross-over (3) randomly selected design (mutation).

4.10. Mesh Independence

The mesh independency study is essential for the validity and accuracy of computations. The mesh independence is studied and is illustrated in figures 4.10 and 4.11 taking unfinned validation studies as an example. In order to obtain mesh independent solution, four meshes were selected for an identical Reynolds number.

In figures 4.10 and 4.11, variation of average Nusselt numbers ($\overline{\mathrm{Nu}}$) with mesh sizes for $\mathrm{Re} = 1500$ is presented for both in-line and staggered arrangements. For in-line tube banks, the difference in $\overline{\mathrm{Nu}}$ between the last two meshes are around 0.10% and fourth mesh is regarded as grid independent solution in which 90000 elements are used. For staggered tube banks, the difference in $\overline{\mathrm{Nu}}$ among the last two meshes are nearly 0.13% and fourth mesh is accepted as grid independent solution where 168000 elements are used. Numerical results also reveal that this mesh study provides mesh independent solutions for other cases.

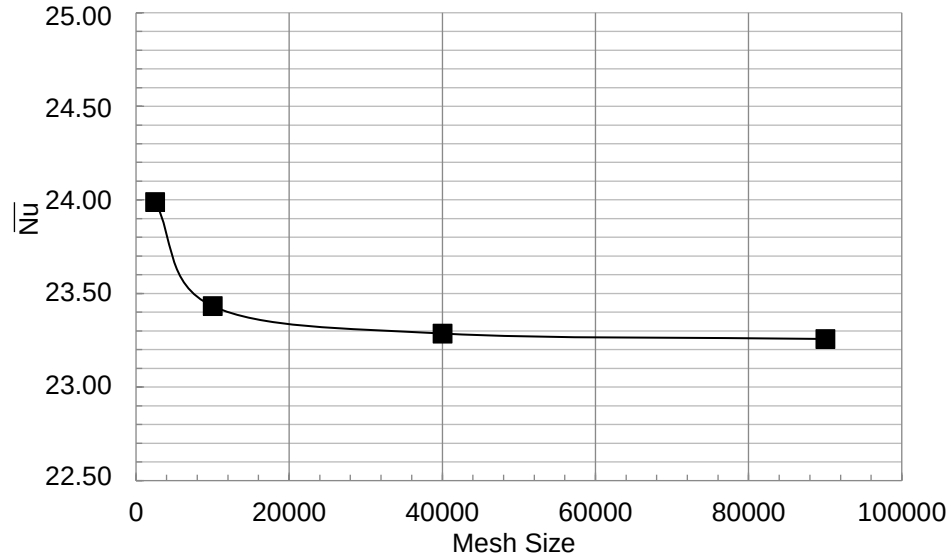


Figure 4.10. The mesh independence study for in-line tube banks

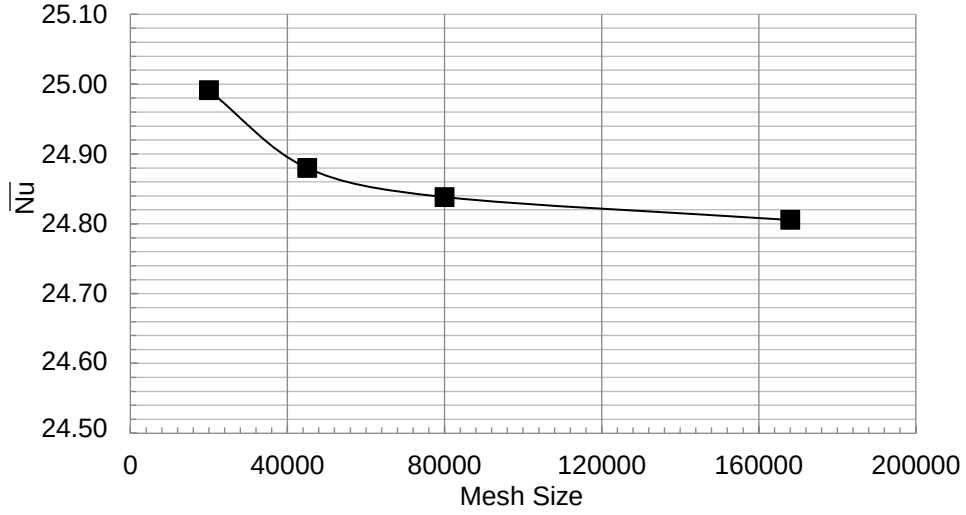


Figure 4.11. The mesh independence study for staggered tube banks

5. RESULTS

This chapter deals with computation results of heat and fluid flow over unfinned and axially finned in-line and staggered tube banks. Firstly, heat transfer and pressure loss calculations over unfinned and axially finned tube banks for both in-line and staggered arrangements including different axial and transversal pitch ratios, Reynolds numbers, fin lengths and Prandtl numbers are studied in sections 5.1, 5.2 and 5.3. Afterwards, optimization of unfinned and axially finned in-line and staggered tube banks are carried out for the given mass flow rate, allowable pressure drop and tube bank effectiveness in section 5.4.

5.1. Unfinned and Axially Finned In-line Tube Banks Studies

5.1.1. Validation of Unfinned In-line Tube Bank

Since there is no other studies to compare with described study, numerical calculations for heat transfer and pressure loss of unfinned in-line tube banks are compared with existing studies. The computations for heat transfer and pressure loss are performed for an unfinned in-line tube bank to make comparisons with the experimental studies in literature (Zukauskas (1972), Gnielinski (2010), Gaddis (2010), Yilmaz and Yilmaz (2016)). The axial and transversal pitch ratios have the following values

$$s_L^* = 1.5 \, , \, s_T^* = 1.5 \tag{5.1}$$

Reynolds number ranges between 400 and 1500. Numerical calculations for heat transfer and pressure loss are undertaken for Prandtl number 0.7.

In figures 5.1 and 5.2, present studies for both laminar and turbulent flows and the other studies in literature are demonstrated for average Nusselt numbers ($\overline{Nu}$) and friction factors (f), respectively. It is observed from figures 5.1 and 5.2 that RNG

k–ε model with enhanced wall treatment studies are in good agreement with the empirical studies of Zukauskas (1972), Gnielinski (2010), Gaddis (2010) and Yilmaz and Yilmaz (2016) while laminar studies are not compatible. So, it is reasonable to assume turbulent flow for the studied Reynolds numbers.

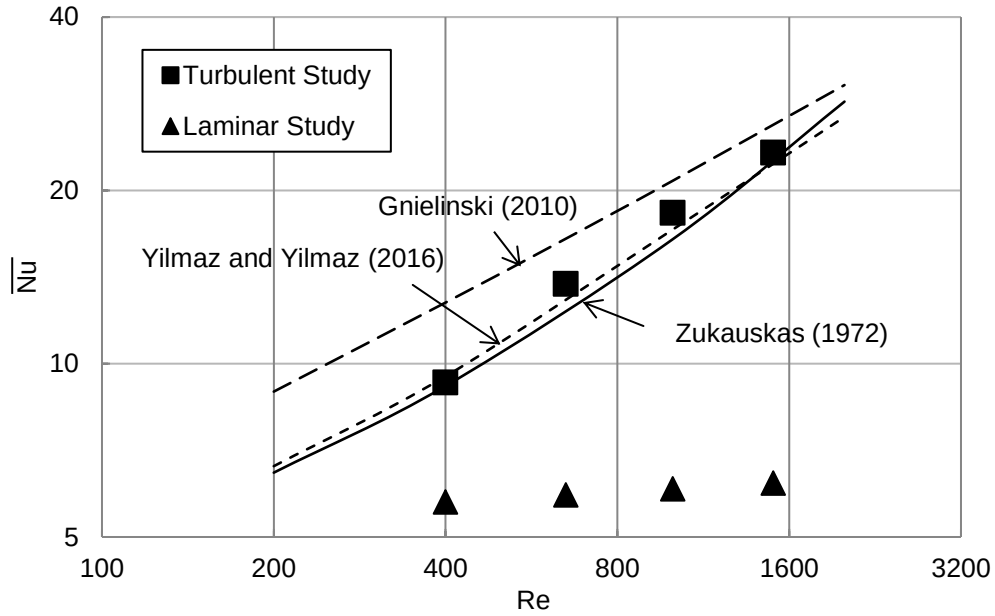


Figure 5.1. Comparison of $\overline{\mathrm{Nu}}$ values with empirical studies of Zukauskas (1972), Gnielinski (2010) and Yilmaz and Yilmaz (2016) for $\mathrm{Pr} = 0.7$, $s_L^* = 1.5$, $s_T^* = 1.5$

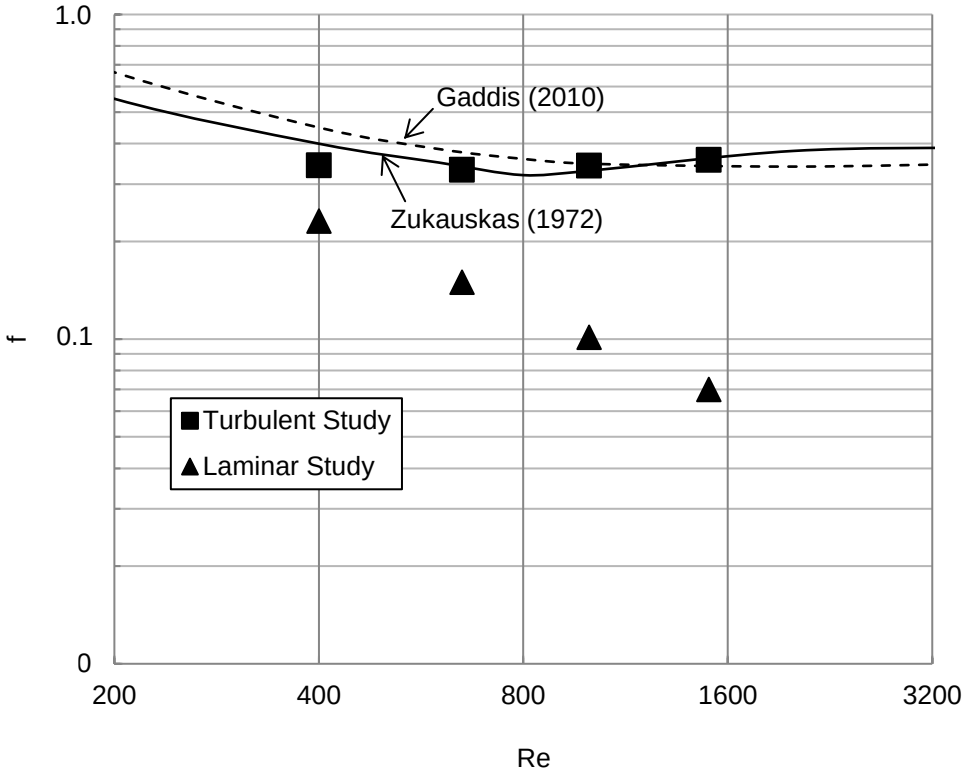


Figure 5.2. Comparison of f values with empirical studies of Zukauskas (1972), Gaddis (2010), Yilmaz and Yilmaz (2016) for $s_L^* = 1.5$, $s_T^* = 1.5$

5.1.2 Results and Discussions of Unfinned and Axially Finned In-line Tube Banks

In this section, heat transfer and pressure loss characteristics in in-line tube banks for unfinned and axially finned cases at cross-flow are presented for Reynolds numbers in the range of 400-1500. Four different s_L^* and s_T^* values are chosen for this study and given in table 5.1. Here, D-Finned represents fin length of D mm and 2D-Finned represents fin length of 2D mm at the front and rear of the tube. The surface ratio

$$F^* = \frac{F_{finned}}{F_{unfinned}} \tag{5.2}$$

is defined to describe the increase of surface area which are defined as $F^*_{D-Finned} = 2.27$ and $F^*_{2D-Finned} = 3.54$. In table 5.1, case (a) and (b) includes unfinned and D-Finned studies, whereas case (c) and (d) includes unfinned, D-Finned and 2D-Finned studies. In all cases, fin thickness is 4 mm.

Table 5.1. s_L^* and s_T^* values of present unfinned and axially finned in-line tube bank studies

Case	s_L^*	s_T^*	Unfinned	D-Finned	2D-Finned
a	3	1.5	X	X	-
b	3	2.0	X	X	-
c	5	1.5	X	X	X
d	5	2.0	X	X	X

The effect of axial finning on $\overline{Nu}$ for the cases a, b, c and d stated in table 5.1 are graphically presented in figures 5.3, 5.8, 5.10 and 5.12 which show plots of the variation of average Nusselt number with Reynolds number for Prandtl numbers of 0.7 and 7. Plots of friction factors variations with Reynolds number are demonstrated in figures 5.4, 5.9, 5.11 and 5.13 for the unfinned and axially finned cases. The calculated results for f and $\overline{Nu}$ are listed in tables 5.2-5.5.

Moreover, increment ratios for friction factor (f^+, f_D^+) and average Nusselt number ($\overline{Nu}^+, \overline{Nu}^{+,D}$) are given in these tables. The average Nusselt number $\overline{Nu}$ values for axially finned in-line tube banks are calculated based on the area of an unfinned in-line tube bank. Figure 5.5 and 5.6 show temperature contours for Prandtl numbers of 0.7 and 7, respectively whereas figure 5.7 show velocity streamlines where $s_L^* = 3$, $s_T^* = 1.5$. Comparison of studied cases a, b, c and d are shown in

figures 5.14 and 5.15 for average Nusselt number variation with pitch ratios at Re = 1500. Also, figure 5.16 presents the variation of friction factor with pitch ratios at Re = 1500. In the followings, different cases a-d are discussed.

Case (a) : $s_L^* = 3,\ s_T^* = 1.5$

Heat transfer computation results in figure 5.3 show that average Nusselt number as a result of axial finning increases for both Prandtl numbers 0.7 and 7. Moreover, average Nusselt number indicates major change at high Reynolds numbers. For $s_L^* = 3,\ s_T^* = 1.5$, unfinned results (table 5.2a) are obtained and then D mm length fin is added to the tube. For both $Pr = 0.7$ and $Pr = 7$, heat transfer is maximum for D mm fin length at Re = 1500. At Re = 1500, using D mm length fin causes 45.96% and 56.80% increment in average Nusselt number ($\overline{Nu}^+$) for $Pr = 0.7$ and $Pr = 7$, respectively. These values are less than 127% of the surface area increase because of the finning. Axial finning causes friction factor decrease as can be seen from figure 5.4. For Re = 400, D-Finned case has 23.73% decrement in friction factor (f^+). As Reynolds number increases, friction factor decreases which is expectable.

It is observed from Table 5.2b that D-Finned case has lower friction factor, because vortex formation is weaker compared to the unfinned cases.

Table 5.2a. Calculated values of $\overline{Nu}$ for unfinned and D-Finned in-line tube banks where $s_L^* = 3, s_T^* = 1.5$

Pr	Re	$\overline{Nu}$	$\overline{Nu}$	$\overline{Nu}^+$ (%)
		Unfinned	D-Finned	
0.7	400	10.68	14.03	31.30
	650	13.61	18.52	36.09
	1000	16.94	23.86	40.82
	1500	20.91	30.53	45.96
7	400	23.59	32.53	37.86
	650	30.62	43.74	42.83
	1000	38.60	57.68	49.40
	1500	48.11	75.43	56.80

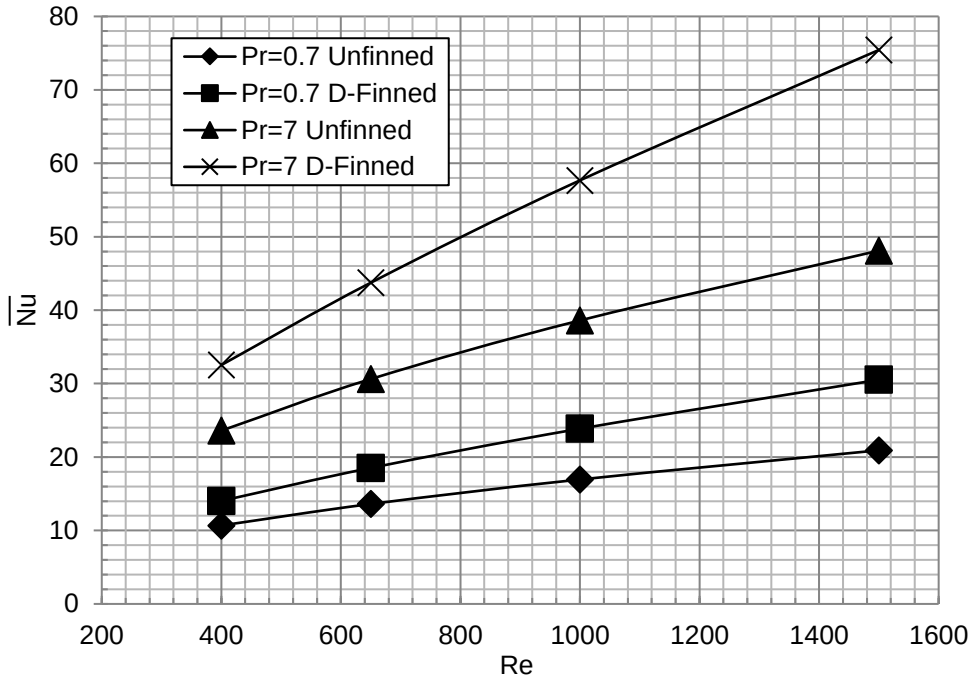


Figure 5.3. Variation of $\overline{Nu}$ number with Re number for unfinned and D-Finned tube banks for $s_L^* = 3,\ s_T^* = 1.5$

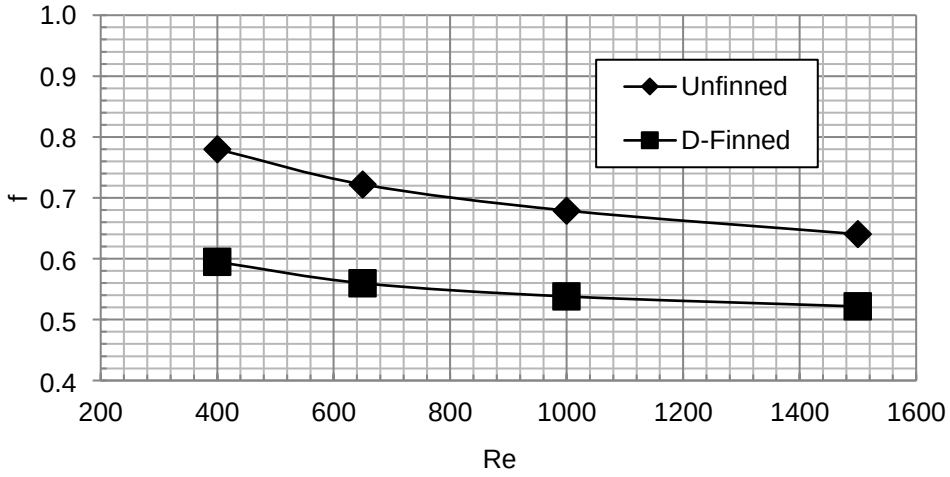


Figure 5.4. Variation of f with Re number for unfinned and D-Finned tube banks for $s_L^* = 3,\ s_T^* = 1.5$

Table 5.2b. Calculated values of f for unfinned and D-Finned in-line tube banks where $s_L^* = 3,\ s_T^* = 1.5$

Re	f	f	f^+ (%)
	Unfinned	D-Finned	
400	0.78	0.60	-23.73
650	0.72	0.56	-22.48
1000	0.68	0.54	-20.77
1500	0.64	0.52	-18.54

Figures 5.5 and 5.6 depict temperature contours for Prandtl numbers of 0.7 and 7, respectively. It is seen in figures 5.5 and 5.6 that axial fins form thermal boundary layer across the flow domain, so it leads to increase in temperature gradient. For Re = 1500, thermal boundary layer thickness is thinner than at Re = 400, so heat transfer rate is higher for increasing Reynolds numbers.

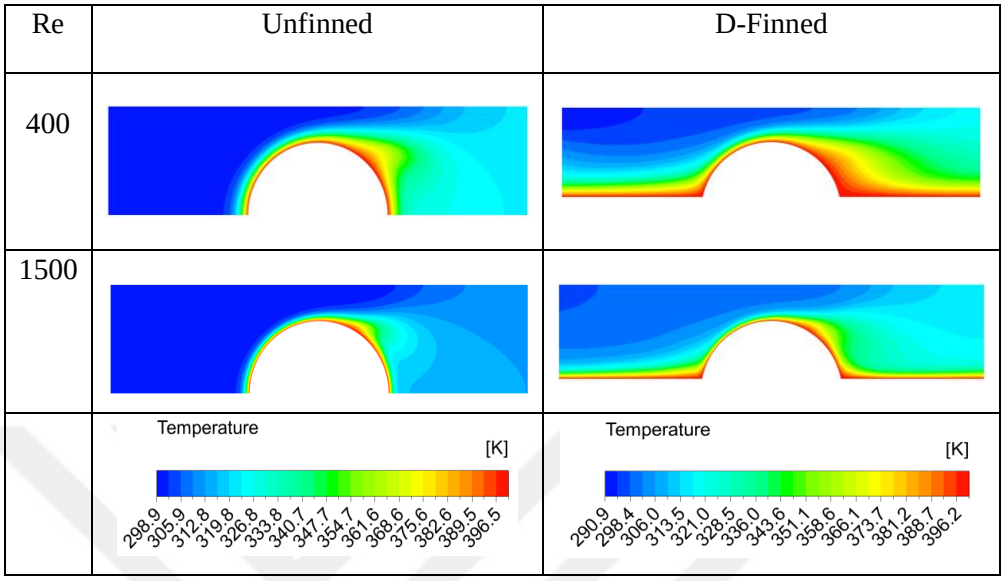


Figure 5.5. Temperature contours for unfinned and D-Finned in-line tube banks for Pr = 0.7, $s_L^* = 3, s_T^* = 1.5$

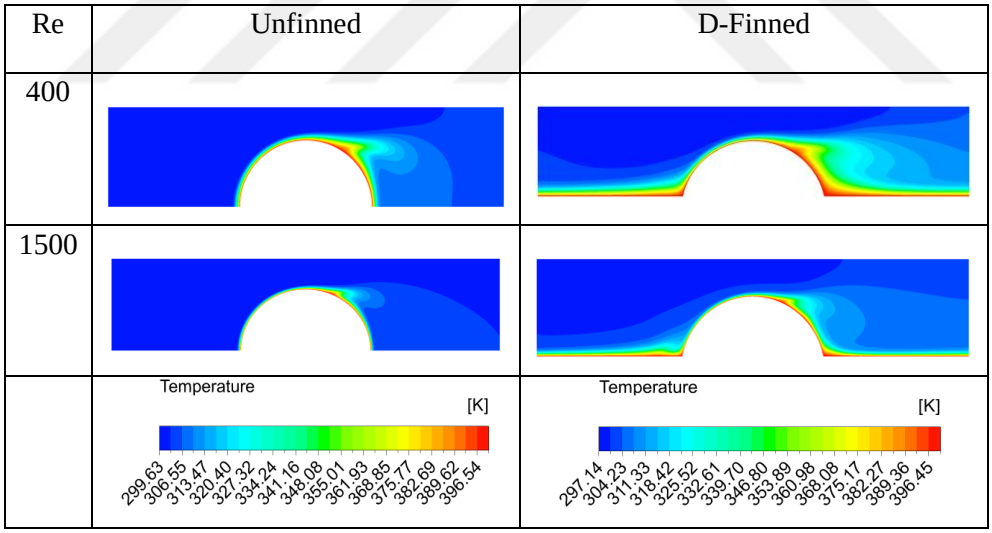


Figure 5.6. Temperature contours for unfinned and D-Finned in-line tube banks for Pr = 7, $s_L^* = 3, s_T^* = 1.5$

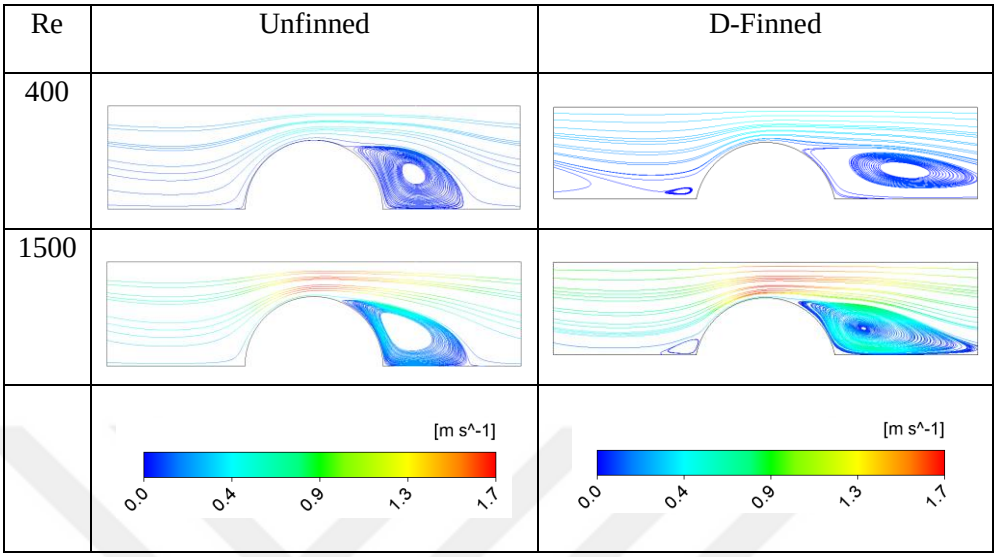


Figure 5.7. Velocity streamlines for unfinned and D-Finned in-line tube banks for $s_L^* = 3,\ s_T^* = 1.5$

The temperature distribution for unfinned and D-Finned tube banks are represented by the temperature contours. Maximum temperature 400K corresponds to cylinder wall temperature which is assigned as wall boundary condition in table 4.1. The temperature gradient for the computational domains in figures 5.5 and 5.6 increases with the increment in the Re number which shows better heat transfer at higher Re values. Figure 5.7 show velocity streamlines where $\mathrm{Re} = 400$ and $\mathrm{Re} = 1500$ for the unfinned and D-Finned in-line tube banks (Case a). From figure 5.7, when Re values increase, higher heat transfer values from cylinder surfaces both in unfinned and D-Finned studies are observed and it is clear that the increment in Re number causes higher turbulence so that the heat transfer enhancement is higher at the higher Re values.

Moreover, it is seen from studies axial fins lead to decrement in friction factors. These results are compatible for the conclusion reached by Mangrulkar et al. (2017), who observed that axial fins serve as obstacles to avoid bulk mixing and

interaction of heat is achieved along axial fins so friction factor reduces with fin usage.

Case (b) : $s_L^* = 3,\ s_T^* = 2$

Similarly, figure 5.8 shows the variation of $\overline{Nu}$ with Re values for Prandtl numbers of 0.7 and 7 and figure 5.9 shows the variation of f with Re values. Axial finning leads to increment in $\overline{Nu}$ number while a decrement in friction factor f. For $s_L^* = 3,\ s_T^* = 2$, unfinned and D-Finned computations are shown in tables 5.3a and 5.3b. For Pr = 7, 59.71% enhancement in average Nusselt number ($\overline{Nu}^+$) is obtained with respect to unfinned case at Re = 1500 for D-Finned case. This value is less than 127% of surface increasing value. Friction factor is 24.91% (f^+) lower than unfinned case. D-Finned case has lower friction factor for all studied Reynolds numbers.

Table 5.3a.Calculated values of $\overline{Nu}$ for unfinned and D-Finned in-line tube banks where $s_L^* = 3,\ s_T^* = 2$

Pr	Re	$\overline{Nu}$	$\overline{Nu}$	$\overline{Nu}^+$ (%)
		Unfinned	D-Finned	
0.7	400	9.78	11.69	19.55
	650	12.87	16.48	28.05
	1000	16.09	22.13	37.52
	1500	19.80	29.02	46.52
7	400	22.77	30.27	32.95
	650	30.13	42.16	39.93
	1000	37.86	56.82	50.07
	1500	46.85	74.82	59.71

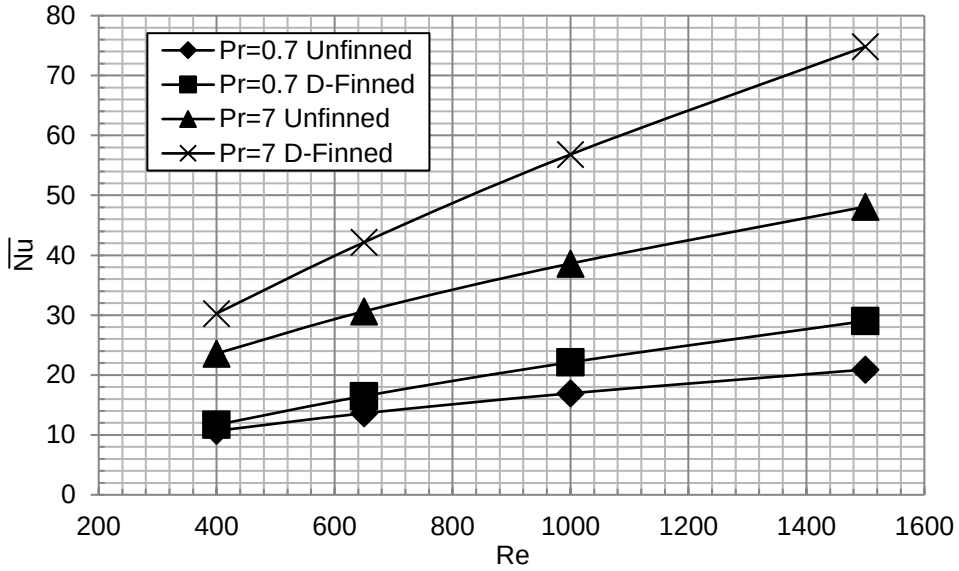


Figure 5.8. Variation of $\overline{Nu}$ number with Re number for unfinned and D-Finned tube banks for $s_L^* = 3,\ s_T^* = 2$

Table 5.3b. Calculated values of f for unfinned and D-Finned in-line tube banks where $s_L^* = 3,\ s_T^* = 2$

Re	f	f	f^+ (%)
	Unfinned	D-Finned	
400	0.50	0.30	-39.76
650	0.49	0.31	-37.02
1000	0.45	0.31	-31.45
1500	0.41	0.31	-24.91

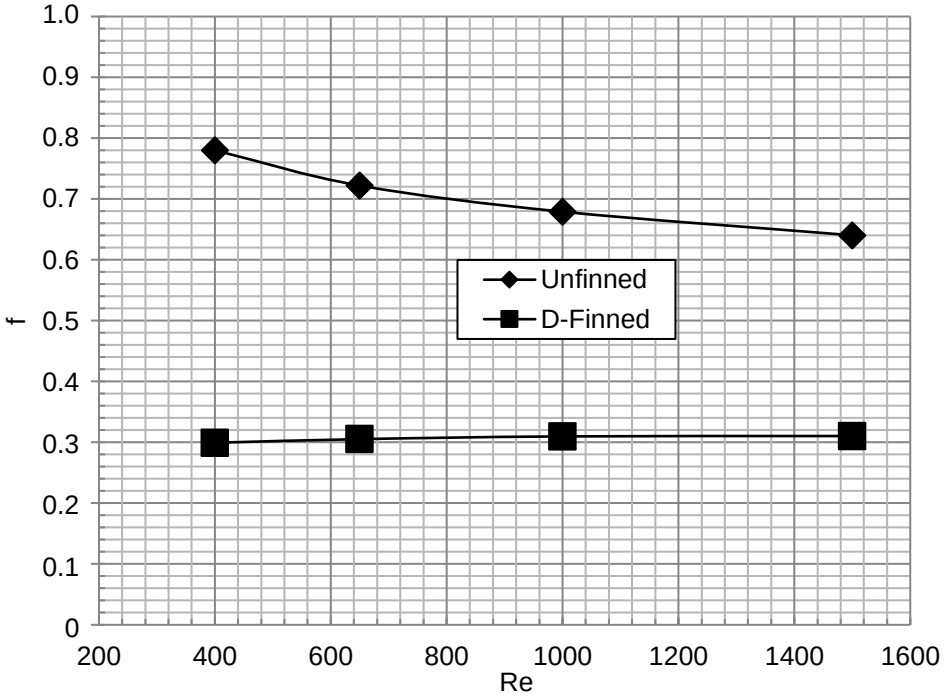


Figure 5.9. Variation of f with Re number for unfinned and D-Finned tube banks for $s_L^* = 3,\ s_T^* = 2$

Case (c) : $s_L^* = 5,\ s_T^* = 1.5$

Figure 5.10 demonstrates the variation of $\overline{Nu}$ with Re number for Prandtl numbers 0.7 and 7 while figure 5.11 shows variation of f with Re number. For $s_L^* = 5,\ s_T^* = 1.5$, unfinned, D-Finned and 2D-Finned computations are shown in tables 5.4a and 5.4b. For Pr = 0.7, D-Finned case leads to average Nusselt number ($\overline{Nu}^+$) enhancement of 55.90% while 2D-Finned case has an average Nusselt number ($\overline{Nu}^{+,D}$) enhancement of 93.42% with respect to unfinned case at Re = 1500. Another thing that should be emphasized here is 2D-Finned case has an average Nusselt number ($\overline{Nu}^{+,D}$) enhancement of 24.07% with respect to D-Finned case. Surface area increase for 2D-Finned tube is 254%. That means that using 2D-Finned tube, heat transfer is increased 36.8% of the maximum obtainable increase of surface area.

Friction factor either decreases while fin length is increased from D-Finned to 2D-Finned.

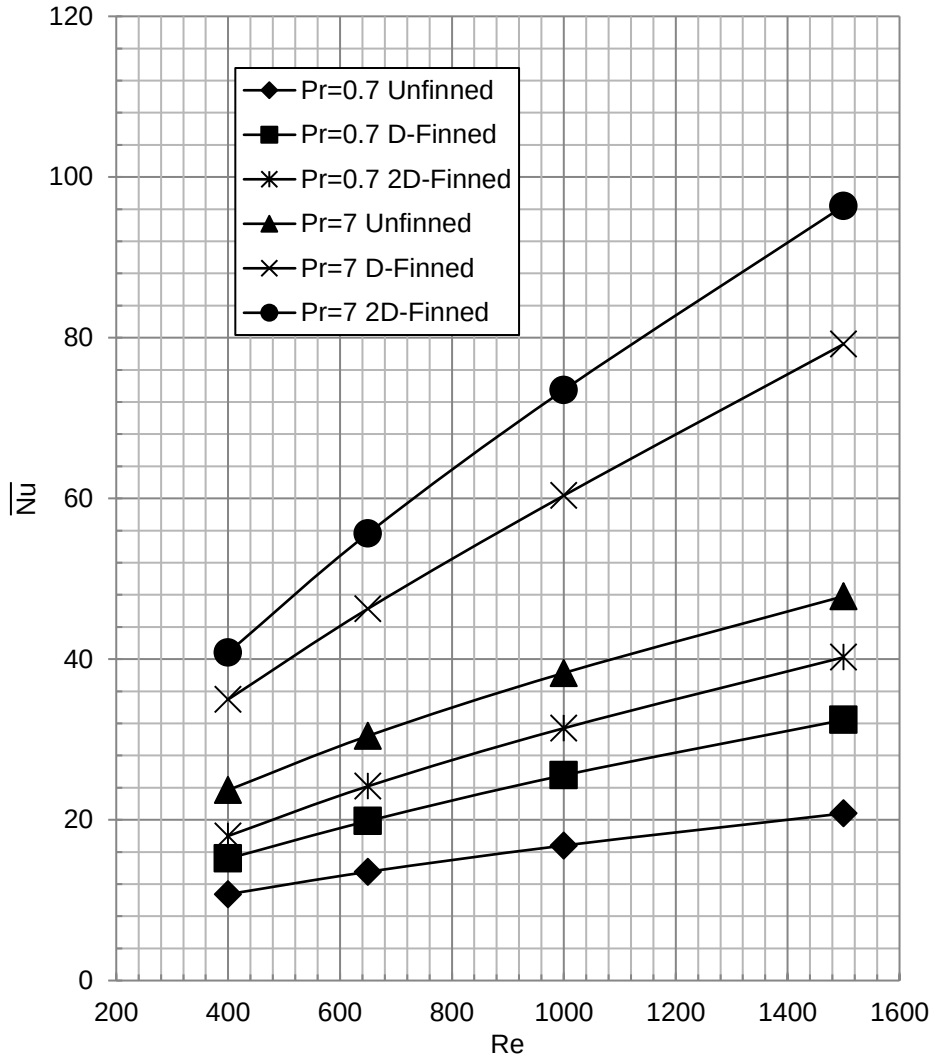


Figure 5.10. Variation of $\overline{Nu}$ with Re number for unfinned, D-Finned and 2D-Finned tube banks for $s_L^* = 5,\ s_T^* = 1.5$

Table 5.4a.Calculated values of $\overline{Nu}$ for unfinned, D-Finned and 2D-Finned in-line tube banks where $s_L^* = 5,\ s_T^* = 1.5$

Pr	Re	$\overline{Nu}$	$\overline{Nu}$	$\overline{Nu}^{+}$ (%)	$\overline{Nu}$	$\overline{Nu}^{+}$ (%)	$\overline{Nu}^{+,D}$ (%)
		Unfinned	D-Finned		2D-Finned		
0.7	400	10.74	15.18	41.30	17.99	67.48	18.53
	650	10.53	19.85	46.72	24.18	78.71	21.80
	1000	16.80	25.55	52.06	31.40	86.90	22.91
	1500	20.80	32.43	55.90	40.23	93.42	24.07
7	400	23.70	34.98	47.58	40.81	72.17	16.66
	650	30.45	46.28	51.99	55.64	82.76	20.25
	1000	38.28	60.36	57.70	73.49	92.01	21.76
	1500	47.82	79.21	65.62	96.39	101.55	21.69

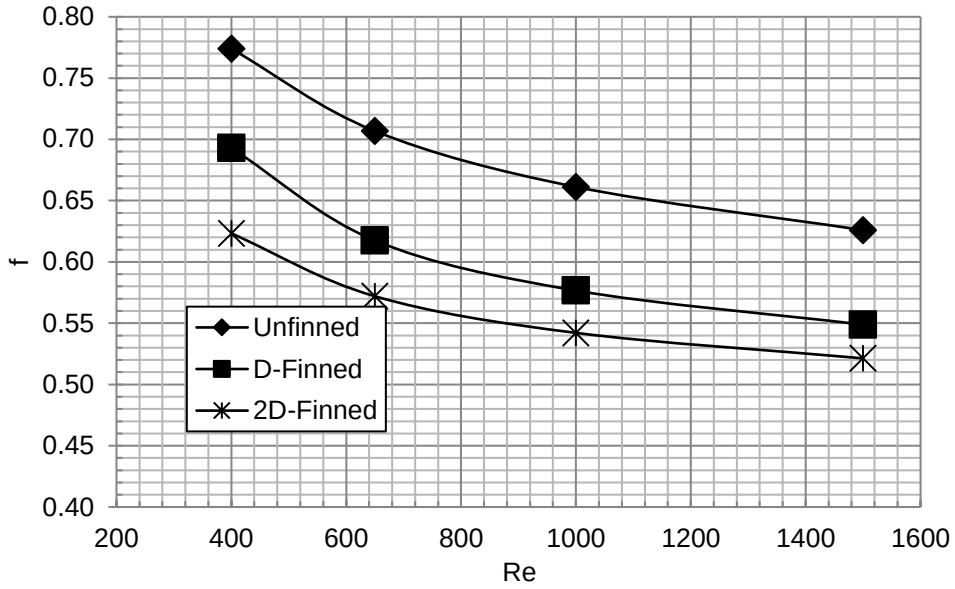


Figure 5.11. Variation of f with Re number for unfinned, D-Finned and 2D-Finned tube banks for $s_L^* = 5,\ s_T^* = 1.5$

Table 5.4b. Calculated values of f for unfinned, D-Finned and 2D-Finned in-line tube banks where $s_L^* = 5,\ s_T^* = 1.5$

Re	f	f	f^+ (%)	f	f^+ (%)	f_D^+ (%)
	Unfinned	D-Finned		2D-Finned		
400	0.77	0.69	-10.46	0.62	-19.44	-10.03
650	0.71	0.62	-12.64	0.57	-19.04	-7.33
1000	0.66	0.58	-12.79	0.54	-17.99	-5.97
1500	0.63	0.55	-12.32	0.52	-16.70	-5.00

Case (d) : $s_L^* = 5,\ s_T^* = 2$

Variation of $\overline{Nu}$ with Re number for Prandtl numbers 0.7 and 7 is demonstrated in figure 5.12 and figure 5.13 shows the variation of f with Re number. For $s_L^* = 5,\ s_T^* = 2$, unfinned, D-Finned and 2D-Finned computations are shown in tables 5.5a and 5.5b. For Pr = 7, D-Finned case leads to 68.08% enhancement in average Nusselt number ($\overline{Nu}^+$) as compared to unfinned case at Re = 1500, also 2D-Finned case has 102.92% enhancement in average Nusselt number ($\overline{Nu}^{+,D}$) as compared to unfinned case. Compared with the 127% and 254% of surface area increase one can see that 58% and 40.5% of these values are arrived. However, friction factor is decreased (f^+) 18.72% for D-Finned case with respect to unfinned case while for 2D-Finned case 27.16% decrement (f_D^+) is observed to unfinned case at Re = 1500.

Table 5.5a. Calculated values of $\overline{Nu}$ for unfinned, D-Finned and 2D-Finned in-line tube banks where $s_L^* = 5,\ s_T^* = 2$

Pr	Re	$\overline{Nu}$	$\overline{Nu}$	$\overline{Nu}^{+}$ (%)	$\overline{Nu}$	$\overline{Nu}^{+}$ (%)	$\overline{Nu}^{+,D}$ (%)
		Unfinned	D-Finned		2D-Finned		
0.7	400	10.40	13.94	34.02	15.61	50.05	11.97
	650	13.39	18.94	41.50	22.04	64.63	16.34
	1000	16.79	24.97	48.74	29.66	76.69	18.79
	1500	20.86	32.16	54.14	39.02	87.05	21.35
7	400	23.85	34.24	43.56	38.86	62.92	13.49
	650	30.98	46.39	49.72	54.66	76.43	17.84
	1000	39.12	62.09	58.74	74.22	89.75	19.54
	1500	48.92	82.22	68.08	99.27	102.92	20.73

Table 5.5b. Calculated values of f for unfinned, D-Finned and 2D-Finned in-line tube banks where $s_L^* = 5,\ s_T^* = 2$

Re	f	f	f^{+} (%)	f	f^{+} (%)	f_D^{+} (%)
	Unfinned	D-Finned		2D-Finned		
400	0.52	0.42	-20.68	0.34	-36.45	-19.50
650	0.50	0.39	-21.72	0.33	-34.04	-15.73
1000	0.47	0.37	-20.36	0.32	-30.77	-13.07
1500	0.44	0.36	-18.72	0.32	-27.16	-10.38

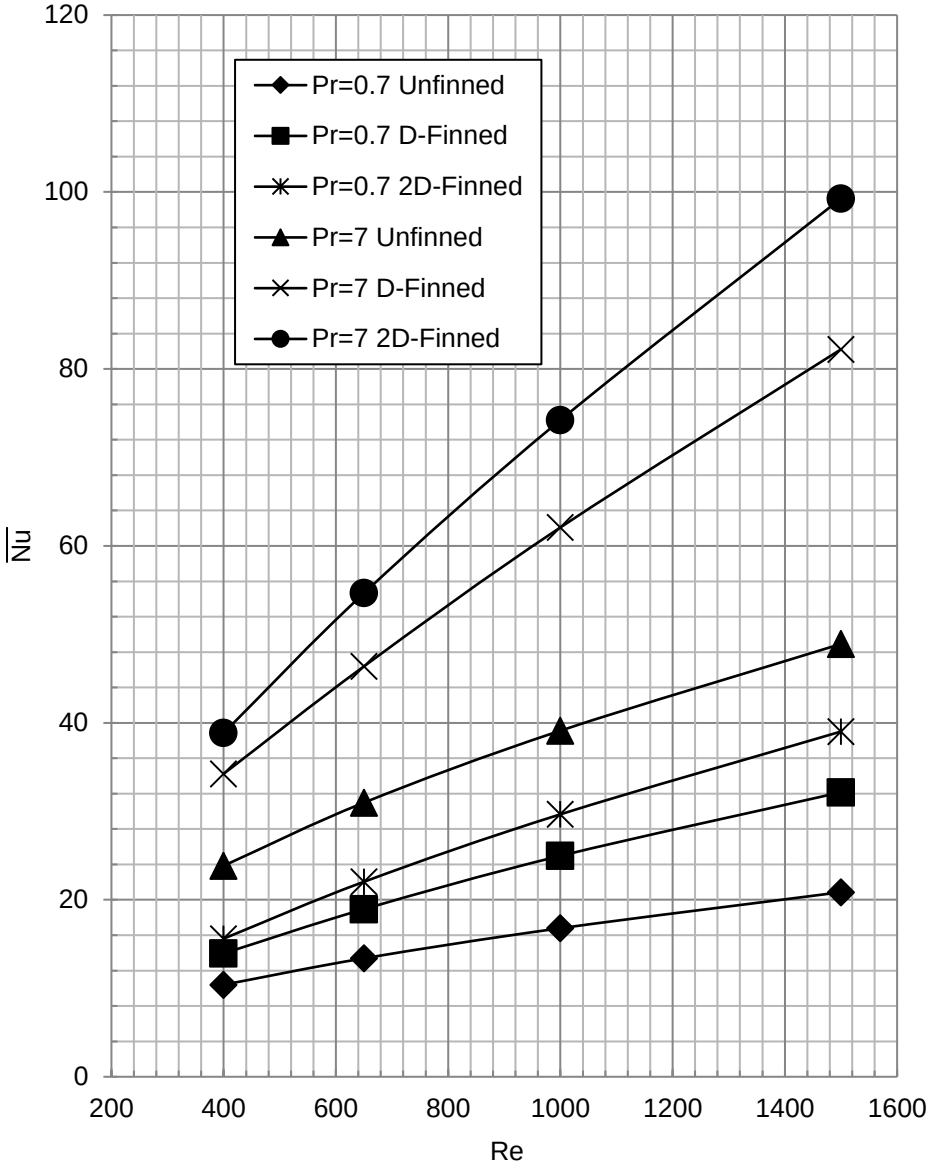


Figure 5.12. $\overline{Nu}$ for unfinned, D-Finned and 2D-Finned tube banks, where $s_L^* = 5$, $s_T^* = 2$

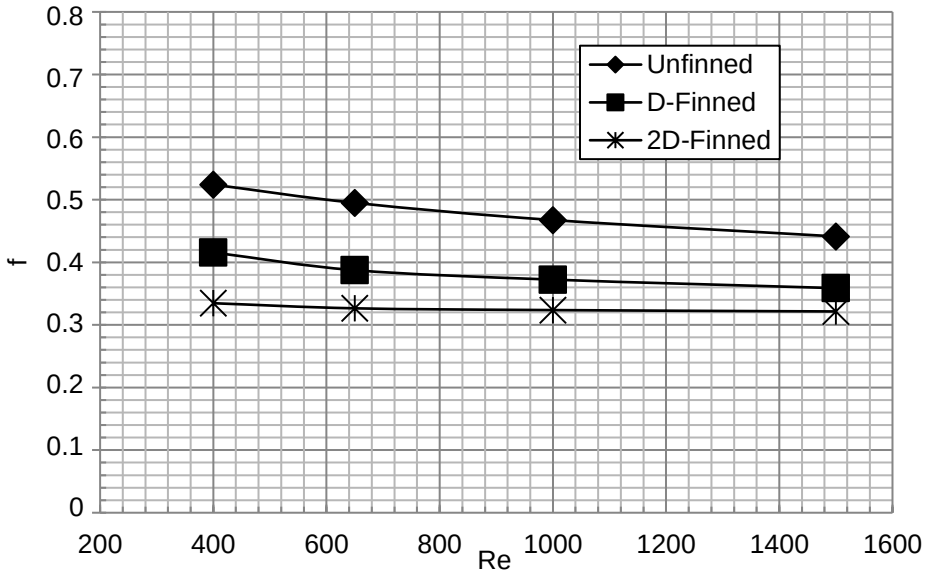


Figure 5.13. f for unfinned, D-Finned and 2D-Finned tube banks, where $s_L^* = 5$, $s_T^* = 2$

5.1.3. Comparison of Studied Cases for In-line Tube Banks

Increasing s_T^* from 1.5 to 2.0 for studied cases does not cause a big change in average Nusselt numbers for both Prandtl values of 0.7 and 7. However, the values of f decrease with the use of $s_T^* = 2$. Almost the same heat transfer is obtained with a lower pressure loss at $s_T^* = 2$. The only disadvantage is that the heat exchanger size is larger for $s_T^* = 2$.

Maximum heat transfer values are observed with axial finning. Figures 5.14 and 5.15 show comparison of $\overline{Nu}$ numbers as a function of s_T^* values for studied cases at $Re = 1500$ for $Pr = 0.7$ and $Pr = 7$, respectively. On the other hand, figure 5.16 shows comparison of f values as a function of s_T^* values for studied cases at Re = 1500.

For Pr = 0.7 and $Re = 1500$, $\overline{Nu}$ is 29.02 for D-Finned case of $s_L^* = 3$ and $s_T^* = 2$ while f equals to 0.31. s_T^* is kept constant when s_L^* is increased to 5 for the same Pr and Re numbers. For D-Finned case, $\overline{Nu}$ is 32.16 and f equals to 0.36.

Increasing s_L^* from 3 to 5 does not significantly increase heat transfer. But for 2D-Finned case of $s_L^* = 5$ and $s_T^* = 2$, $\overline{Nu}$ is 39.02 and f is 0.32. So, 34.50% $\overline{Nu}$ increment is obtained as compared to D-Finned case of $s_L^* = 3$ and $s_T^* = 2$. But f is increased from 0.30 to 0.32, so 3.55% f increment is observed for $Re = 1500$.

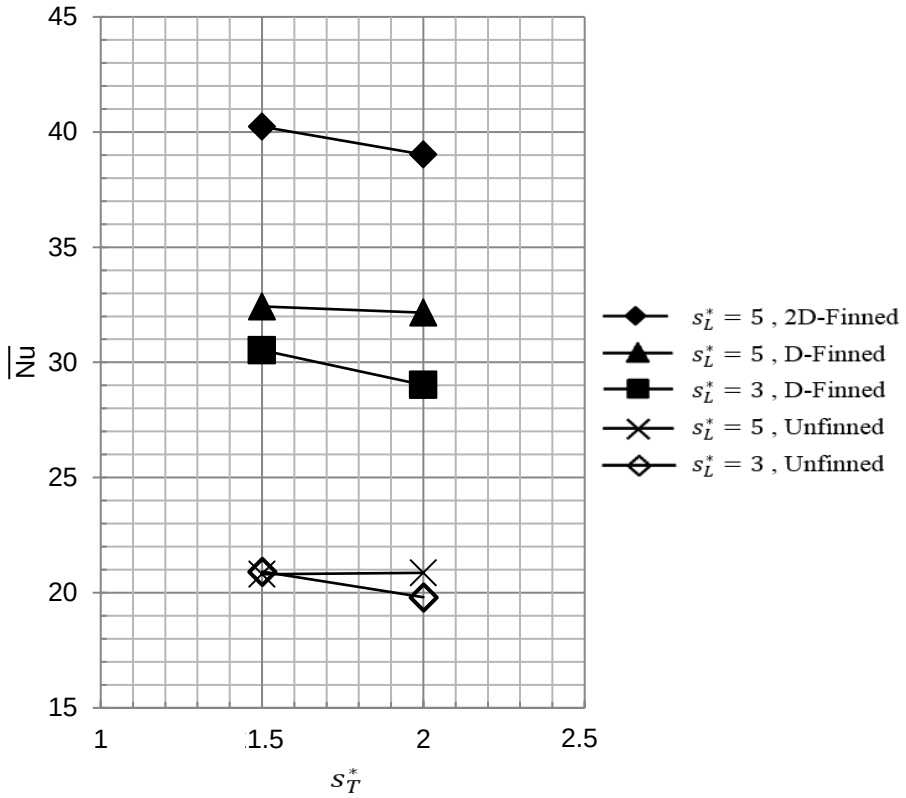


Figure 5.14. $\overline{Nu}$ vs. s_T^* values for studied cases where $Re = 1500$ and $Pr = 0.7$

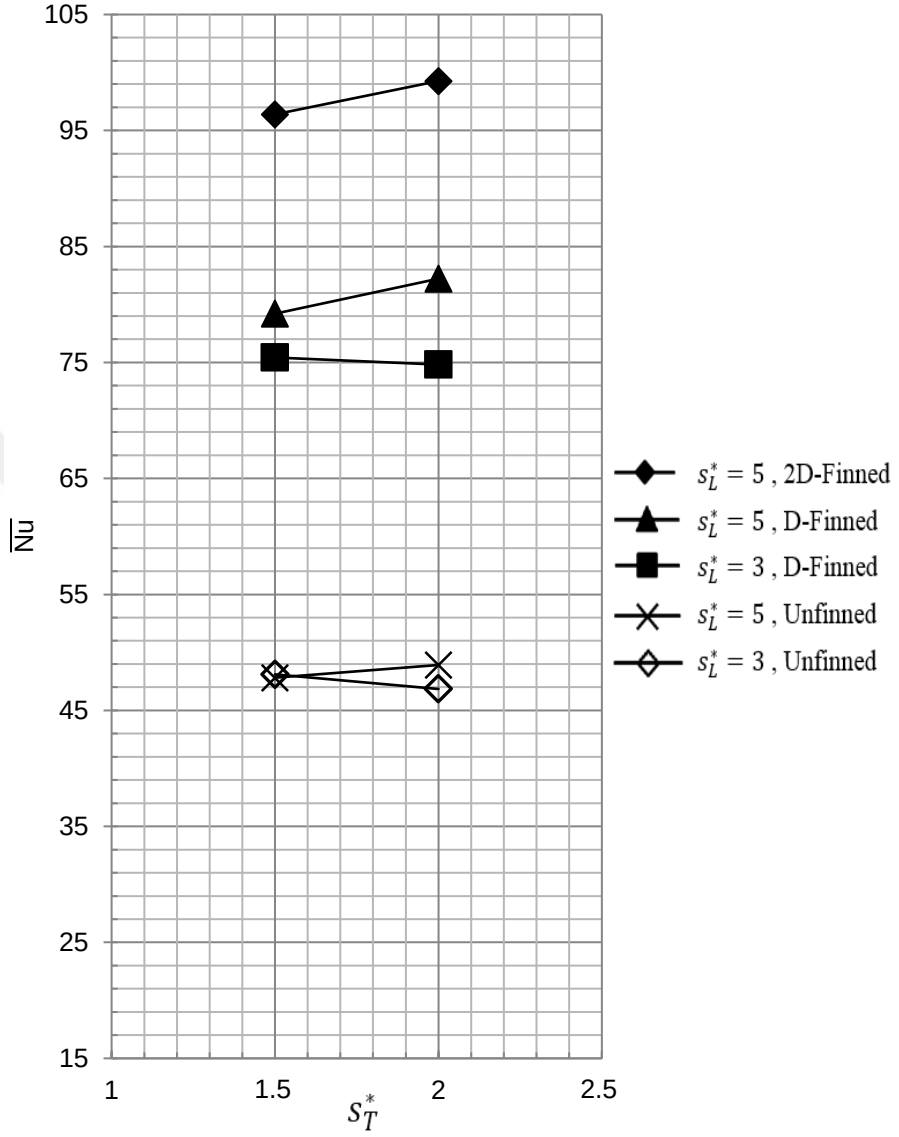


Figure 5.15. $\overline{Nu}$ vs. s_T^* values for studied cases where Re = 1500 and Pr = 7

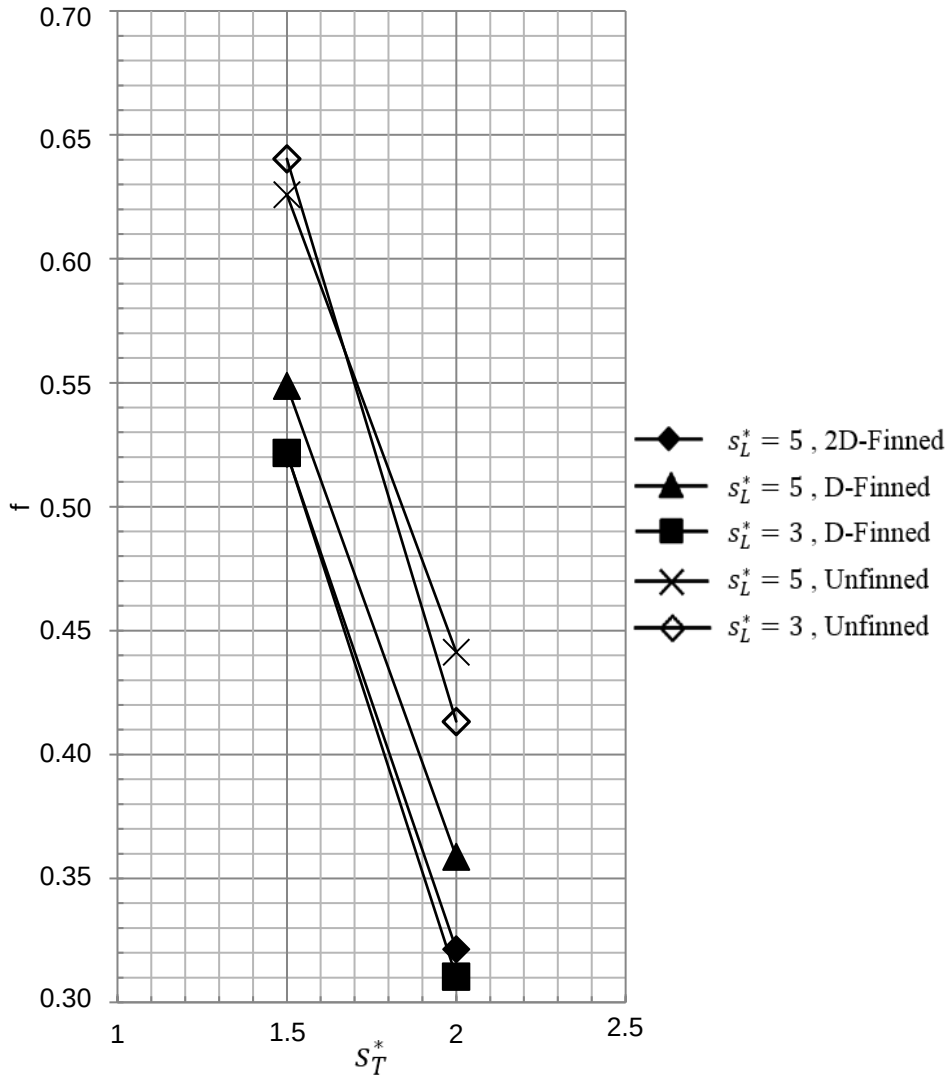


Figure 5.16. f vs. s_T^* values for studied cases where Re = 1500

5.2. Unfinned and Axially Finned Staggered Tube Banks Studies

5.2.1. Validation of Unfinned Staggered Tube Bank

Similarly, there is not any validation study for axially finned staggered tube banks, so numerical computations of an unfinned staggered tube bank are compared

with the experimental studies in literature (Zukauskas (1972), Gnielinski (2010), Gaddis (2010), Yilmaz et al. (2017)). The axial and transversal pitch ratios are given as follows:

$$s_L^* = \frac{\sqrt{3}}{2}\, s_T^*, \quad s_T^* = 1.5 \tag{5.3}$$

Heat transfer and pressure drop calculations are carried out for $Pr = 0.7$ and Reynolds number varies between 400 and 1500.

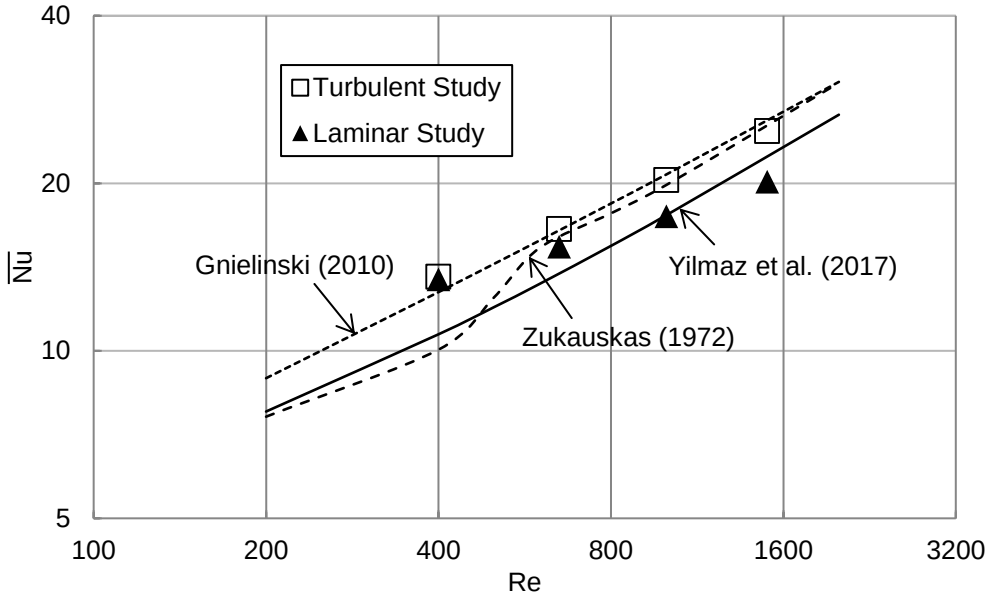


Figure 5.17. Comparison of $\overline{Nu}$ values with experimental studies of Zukauskas (1972), Gnielinski (2010) and Yilmaz et al. (2017) for $Pr = 0.7$, $s_L^* = \frac{\sqrt{3}}{2}\, s_T^*$, $s_T^* = 1.5$

Figures 5.17 and 5.18 show the plot of the average Nusselt numbers and friction factors with respect to Reynolds numbers for present study of unfinned staggered tube bank for both laminar and turbulent flows, respectively. RNG k–ε

model with enhanced wall treatment turbulence model agrees well with the experimental studies of Zukauskas (1972), Gnielinski (2010), Gaddis (2010) and Yilmaz et al. (2017). Therefore, similar to in-line tube bank studies, turbulent flow is assumed for the calculations.

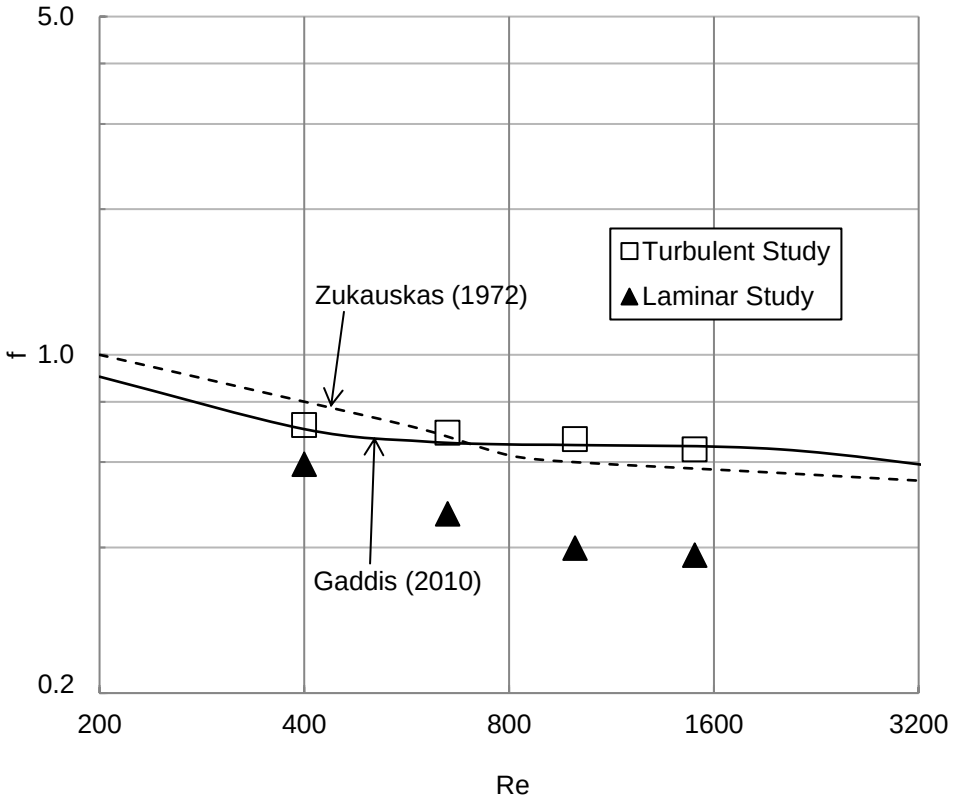


Figure 5.18. Comparison of f values with Zukauskas's (1972) and Gaddis's (2010) experimental studies for $s_L^* = \frac{\sqrt{3}}{2}\, s_T^*$, $s_T^* = 1.5$

5.2.2. Results and Discussions of Unfinned and Axially Finned Staggered Tube Banks

Heat transfer and pressure drop calculations for unfinned and axially finned staggered tube banks are studied for Reynolds numbers ranging from 400 to 1500

and Prandtl numbers of 0.7 and 7. In this section, four different s_L^* and s_T^* values are used and tabulated in table 5.6. Similarly, D-Finned and 2D-Finned are used to represent D mm and 2D mm fin lengths at the front and rear of the tube, respectively. The surface ratios for axially finned staggered tube banks, $F^*_{D-Finned} = 2.27$ and $F^*_{2D-Finned} = 3.54$ can be determined. In table 5.6, cases (a), (b), (c) and (d) comprises unfinned, D-Finned and 2D-Finned studies. Fin thickness equals to 4 mm for all cases.

Table 5.6. s_L^* and s_T^* values of present unfinned and axially finned staggered tube bank studies

Case	s_L^*	s_T^*	Unfinned	D-Finned	2D-Finned
a	3	1.5	X	X	X
b	3	2.0	X	X	X
c	5	1.5	X	X	X
d	5	2.0	X	X	X

Figures 5.19, 5.23, 5.25, 5.27 demonstrate the variation of average Nusselt number vs. Reynolds number for the cases a, b, c and d given in table 5.6 where Prandtl numbers equal to 0.7 and 7. Graphical representation of friction factors vs. Reynolds number variation are presented in figures 5.20, 5.24, 5.26, 5.28 for the unfinned and axially finned cases.

The results for $\overline{Nu}$ and f are tabulated in tables 5.7-5.10. Also, increment ratios for friction factor (f^+, f_D^+) and average Nusselt number ($\overline{Nu}^+, \overline{Nu}^{+,D}$) are listed. The area of an unfinned staggered tube bank is used to calculate the average Nusselt number $\overline{Nu}$ values for axially finned staggered tube banks.

Figure 5.21 demonstrates temperature contours where Prandtl number equals to 0.7 and velocity streamlines where Re = 1500 and $s_L^* = 3$, $s_T^* = 1.5$ are presented graphically in figure 5.22. Cases a, b, c and d given in table 5.6 are

compared in figures 5.29 and 5.30 for the variation of average Nusselt number versus pitch ratios at Re = 1500. In addition, friction factor versus pitch ratios variation at Re = 1500 are shown in figure 5.31. Hereinafter, studied cases are assessed.

Case (a) : $s_L^* = 3,\ s_T^* = 1.5$

It can be seen from figure 5.19 that axial finning of staggered tube banks increases average Nusselt number for both Prandtl numbers 0.7 and 7. Furthermore, significant improvement at high Reynolds numbers are achieved in terms of average Nusselt number. For $s_L^* = 3,\ s_T^* = 1.5$, unfinned, D-Finned and 2D-Finned results are listed in table 5.7a. Obtained heat transfer values are maximum for 2D-Finned cases for both $Pr = 0.7$ and $Pr = 7$. 2D-Finned case lead to 199.05% and 200.77% increment in average Nusselt number ($\overline{Nu}^+$) as compared to unfinned case at Re = 1500 for $Pr = 0.7$ and $Pr = 7$, respectively. These values are under 254% of the surface area increase by the reason of axial finning. Besides, 2D-Finned case enhances average Nusselt number ($\overline{Nu}^+$) 67.95% and 53.30% as compared to D-Finned case at Re = 1500 for $Pr = 0.7$ and $Pr = 7$, respectively.

It is observed from figure 5.20 that friction factor decreases for D-Finned case and increases for 2D-Finned case with respect to unfinned case. For Re = 400, D-Finned case leads to 11.78% decrement as compared to unfinned case and 2D-Finned case results in 42.32% increment with respect to D-Finned case. For the increasing values of Reynolds number, friction factor decreases. It is seen from table 5.7b that friction factor values are lower for D-Finned case and higher for 2D-Finned case as compared to unfinned case.

Table 5.7a.Calculated values of $\overline{Nu}$ for unfinned, D-Finned and 2D-Finned staggered tube banks where $s_L^* = 3,\ s_T^* = 1.5$

Pr	Re	$\overline{Nu}$	$\overline{Nu}$	$\overline{Nu}^+$ (%)	$\overline{Nu}$	$\overline{Nu}^+$ (%)	$\overline{Nu}^{+,D}$ (%)
		Unfinned	D-Finned		2D-Finned		
0.7	400	11.04	17.85	61.71	31.38	184.31	75.81
	650	13.93	23.73	70.40	39.97	187.03	68.44
	1000	17.41	30.57	75.62	51.21	194.19	67.51
	1500	21.72	38.67	78.05	64.95	199.05	67.95
7	400	24.27	40.30	66.07	52.65	116.98	30.66
	650	31.24	56.87	82.00	85.05	172.22	49.57
	1000	39.54	75.06	89.82	115.50	192.09	53.88
	1500	49.81	97.73	96.20	149.81	200.77	53.30

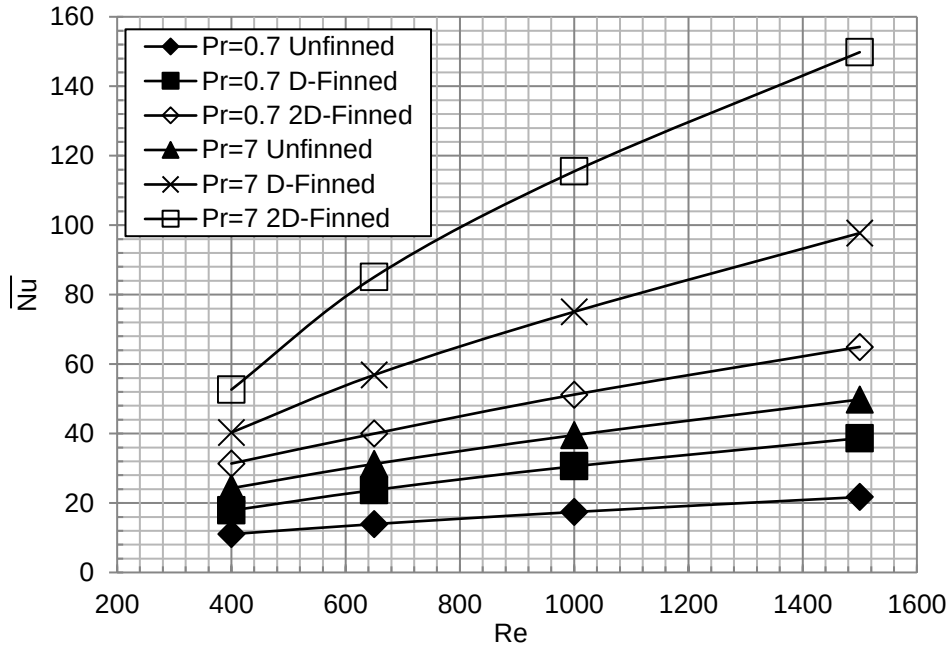


Figure 5.19. Variation of $\overline{Nu}$ number with Re number for unfinned, D-Finned and 2D-Finned tube banks for $s_L^* = 3, s_T^* = 1.5$

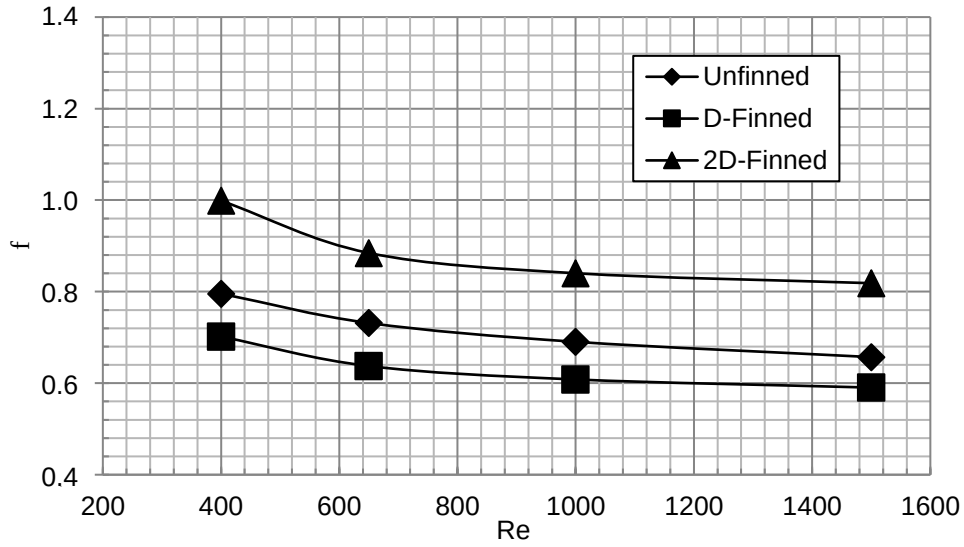


Figure 5.20. Variation of f with Re number for unfinned, D-Finned and 2D-Finned tube banks for $s_L^* = 3, s_T^* = 1.5$

Table 5.7b. Calculated values of f for unfinned, D-Finned and 2D-Finned staggered tube banks where $s_L^* = 3,\ s_T^* = 1.5$

Re	f	f	f^+ (%)	f	f^+ (%)	f_D^+ (%)
	Unfinned	D-Finned		2D-Finned		
400	0.80	0.70	-11.78	1.00	25.55	42.32
650	0.73	0.64	-12.86	0.88	20.91	38.75
1000	0.69	0.61	-11.91	0.84	21.71	38.17
1500	0.66	0.59	-10.14	0.82	24.58	38.63

Figure 5.21 demonstrates a plot of temperature contours for Prandtl number of 0.7 and figure 5.22 illustrates velocity streamlines where $\mathrm{Re} = 1500$ for the unfinned, D-Finned and 2D-Finned staggered tube banks (Case a). Axial fins increase temperature across the flow domain as can be seen from figure 5.21. Temperature gradient is higher for 2D-Finned cases as compared to unfinned and D-Finned cases, thus increment in fin length leads to obtain higher heat transfer.

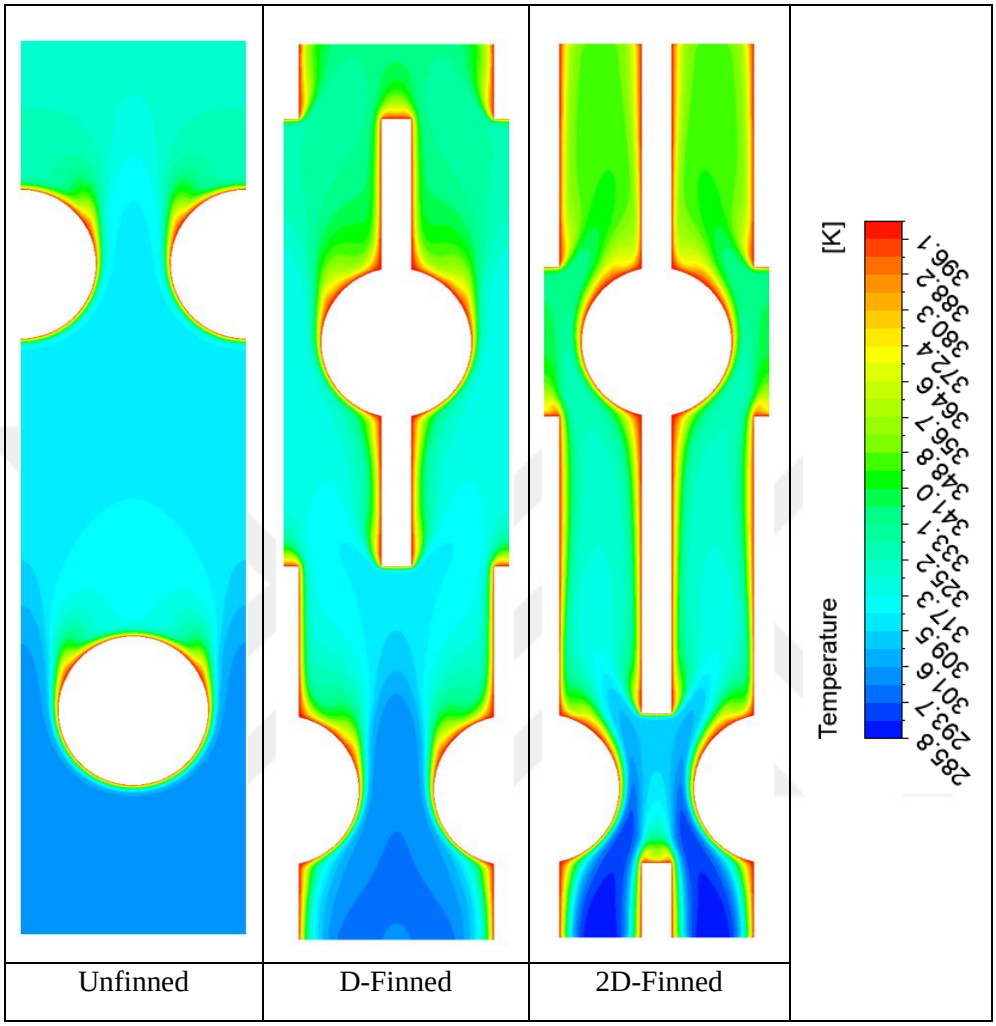
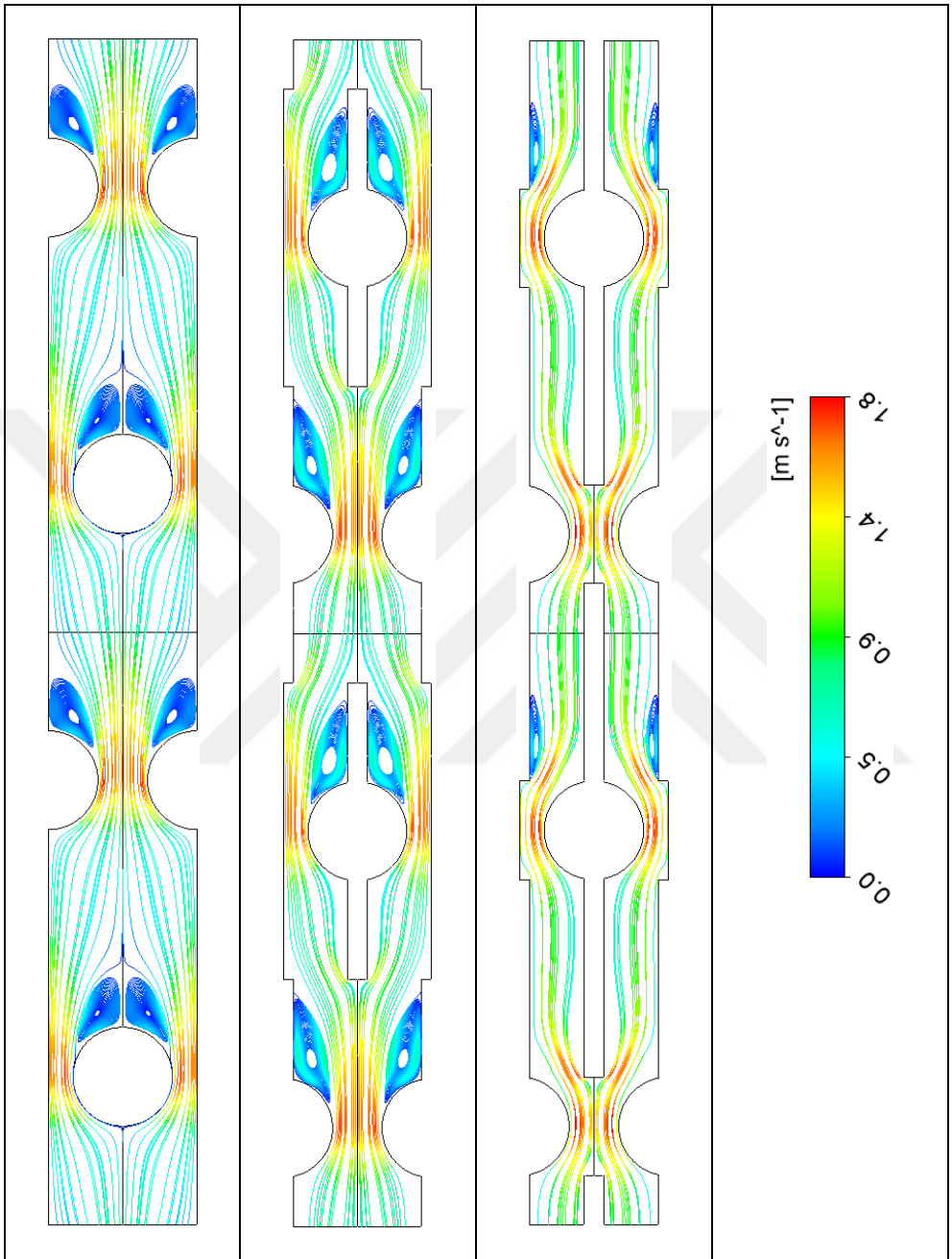


Figure 5.21. Temperature contours for unfinned, D-Finned and 2D-Finned staggered tube banks for Pr = 0.7, Re = 1500, $s_L^* = 3,\ s_T^* = 1.5$

Temperature value is maximum 400K for cylinder and fin surfaces where wall boundary condition is assigned. It is observed from figure 5.21 that heat transfer is higher for D-Finned and 2D-Finned cases.



Unfinned	D-Finned	2D-Finned	

Figure 5.22. Velocity streamlines for unfinned, D-Finned and 2D-Finned staggered tube banks for Re = 1500, $s_L^* = 3$, $s_T^* = 1.5$

Case (b) : $s_L^* = 3,\ s_T^* = 2$

In a similar way, the variation of $\overline{Nu}$ with Re values for Prandtl numbers 0.7 and 7 is plotted in figure 5.23. Figure 5.24 demonstrates the variation of f with Re values. D-Finned and 2D-Finned cases have higher $\overline{Nu}$ number values with respect to unfinned case due to axial finning. Furthermore, friction factor f decreases for D-Finned case and increases for 2D-Finned case with respect to unfinned case. Unfinned, D-Finned and 2D-Finned calculations are given in tables 5.8a and 5.8b for $s_L^* = 3,\ s_T^* = 2$. For Pr = 7 and 2D-Finned case, average Nusselt number ($\overline{Nu}^+$) is enhanced up to 190.33% as compared to unfinned case which is less than 254% of surface increasing value. Also, friction factor of 2D-Finned case is higher than D-Finned and unfinned cases for the same Reynolds number.

Table 5.8a. Calculated values of $\overline{Nu}$ for unfinned, D-Finned and 2D-Finned staggered tube banks where $s_L^* = 3,\ s_T^* = 2$

Pr	Re	$\overline{Nu}$	$\overline{Nu}$	$\overline{Nu}^+$ (%)	$\overline{Nu}$	$\overline{Nu}^+$ (%)	$\overline{Nu}^{+,D}$ (%)
		Unfinned	D-Finned		2D-Finned		
0.7	400	11.14	16.91	51.74	27.05	142.71	59.95
	650	14.27	23.24	62.86	36.41	155.19	56.69
	1000	18.11	31.09	71.64	48.11	165.57	54.72
	1500	22.85	40.33	76.47	62.70	174.37	55.48
7	400	25.15	39.49	57.02	59.35	135.99	50.29
	650	32.65	57.79	77.01	85.47	161.81	47.91
	1000	41.74	78.96	89.18	116.17	178.32	47.12
	1500	52.95	104.45	97.26	153.73	190.33	47.18

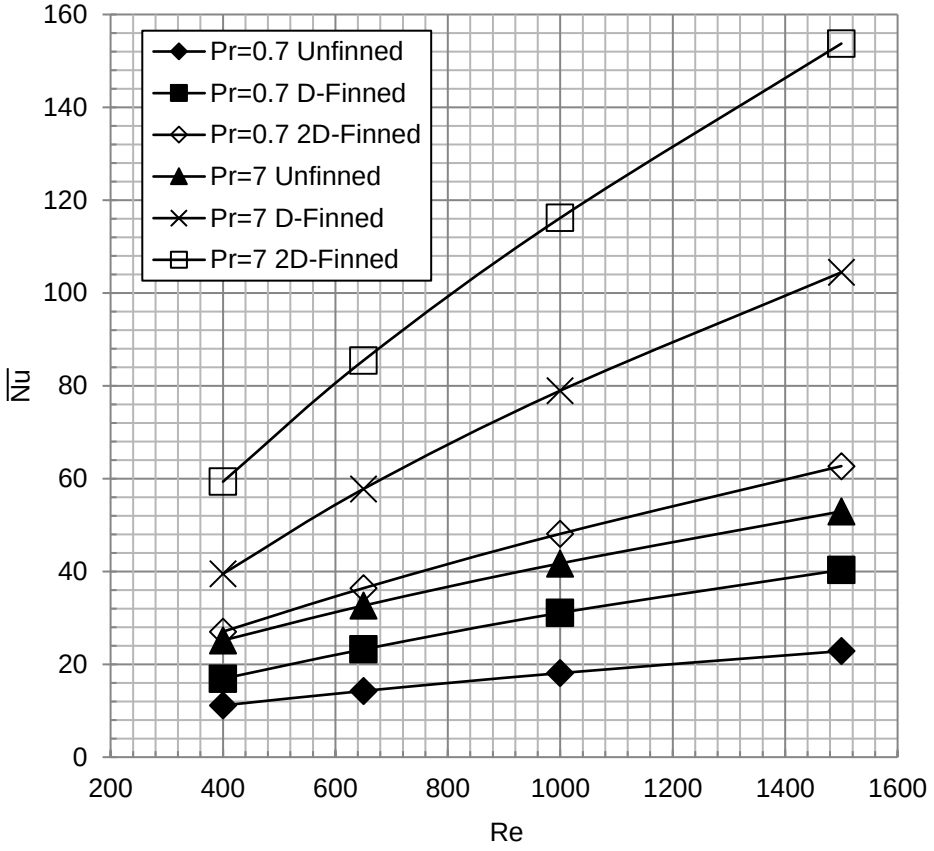


Figure 5.23. Variation of $\overline{Nu}$ number with Re number for unfinned, D-Finned and 2D-Finned tube banks for $s_L^* = 3,\ s_T^* = 2$

Table 5.8b. Calculated values of f for unfinned, D-Finned and 2D-Finned staggered tube banks where $s_L^* = 3,\ s_T^* = 2$

Re	f	f	f^+ (%)	f	f^+ (%)	f_D^+ (%)
	Unfinned	D-Finned		2D-Finned		
400	0.56	0.42	-24.73	0.67	19.23	58.40
650	0.54	0.41	-24.23	0.63	17.49	55.05
1000	0.51	0.41	-20.64	0.62	20.03	51.24
1500	0.49	0.41	-16.02	0.61	25.49	49.43

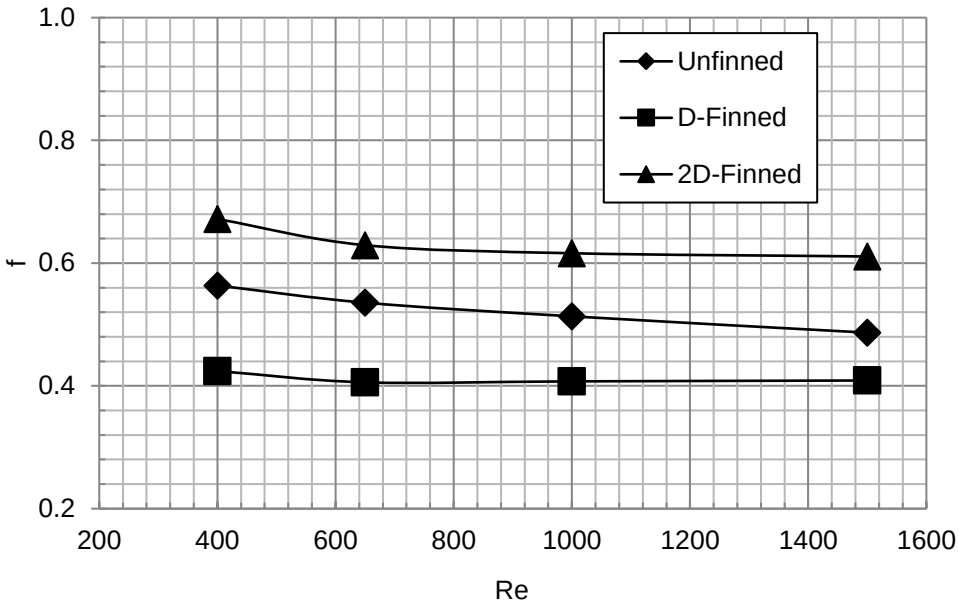


Figure 5.24. Variation of f with Re number for unfinned, D-Finned and 2D-Finned tube banks for $s_L^* = 3,\ s_T^* = 2$

Case (c) : $s_L^* = 5,\ s_T^* = 1.5$

Figure 5.25 indicates $\overline{Nu}$ vs. Re number variation for both Prandtl numbers of 0.7 and 7 whereas figure 5.26 illustrates variation of f with Re number. For $s_L^* = 5,\ s_T^* = 1.5$, unfinned, D-Finned and 2D-Finned calculations are tabulated in tables 5.9a and 5.9b. For Pr = 0.7, D-Finned case has 58.19% enhancement in average Nusselt number ($\overline{Nu}^+$) and 2D-Finned case enhances average Nusselt number ($\overline{Nu}^{+,D}$) to 133.27% according to unfinned case at Re=1500. 2D-Finned case increases average Nusselt number ($\overline{Nu}^{+,D}$) to 47.46% as compared to D-Finned case. As it is stated before, 254% of surface area increment can be achieved using 2D-Finned tube. 2D-Finned tube, heat transfer is increased 52.5% of the maximum surface area increment (133.27 / 254 = 52.5). In addition, friction factor increases for 2D-Finned case as compared to D-Finned case (Table 5.9b).

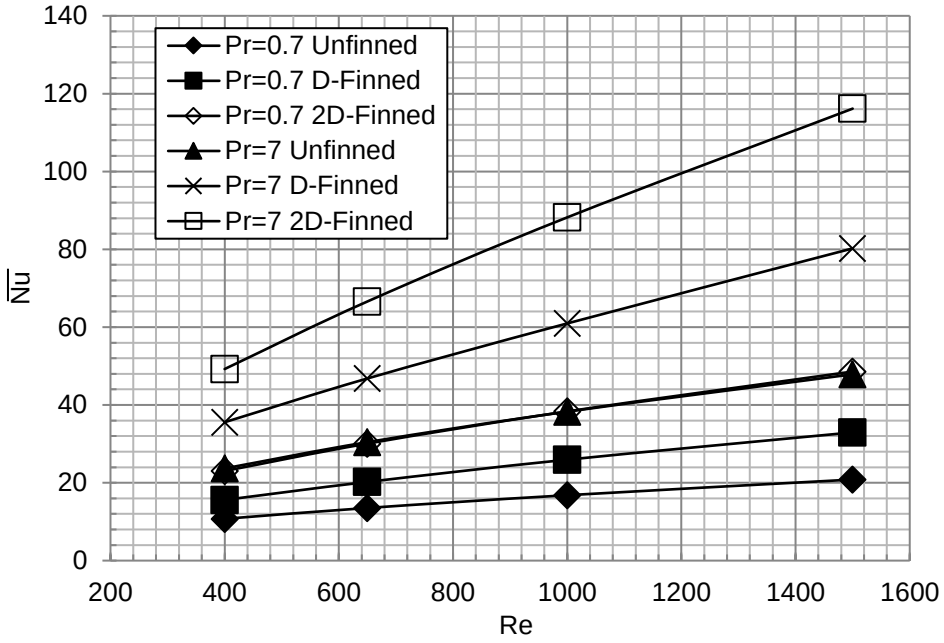


Figure 5.25. Variation of $\overline{Nu}$ number with Re number for unfinned, D-Finned and 2D-Finned tube banks for $s_L^* = 5,\ s_T^* = 1.5$

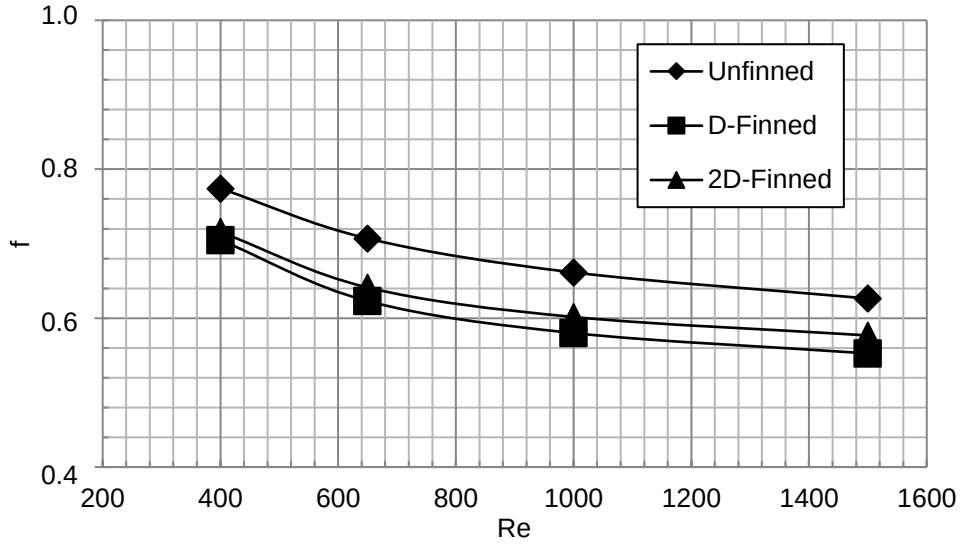


Figure 5.26. Variation of f with Re number for unfinned, D-Finned and 2D-Finned tube banks for $s_L^* = 5,\ s_T^* = 1.5$

Table 5.9a. Calculated values of $\overline{Nu}$ for unfinned, D-Finned and 2D-Finned staggered tube banks where $s_L^* = 5,\ s_T^* = 1.5$

Pr	Re	$\overline{Nu}$	$\overline{Nu}$	$\overline{Nu}^+$ (%)	$\overline{Nu}$	$\overline{Nu}^+$ (%)	$\overline{Nu}^{+,D}$ (%)
		Unfinned	D-Finned		2D-Finned		
0.7	400	10.74	15.60	45.21	23.04	114.46	47.69
	650	13.53	20.22	49.44	30.06	122.17	48.67
	1000	16.81	25.93	54.31	38.34	128.12	47.83
	1500	20.83	32.95	58.19	48.59	133.27	47.46
7	400	23.70	35.57	50.10	49.23	107.77	38.42
	650	30.44	46.81	53.77	66.59	118.76	42.27
	1000	38.28	60.95	59.21	88.20	130.40	44.72
	1500	47.88	80.23	67.58	116.15	142.60	44.77

Table 5.9b. Calculated values of f for unfinned, D-Finned and 2D-Finned staggered tube banks where $s_L^* = 5,\ s_T^* = 1.5$

Re	f	f	f^+ (%)	f	f^+ (%)	f_D^+ (%)
	Unfinned	D-Finned		2D-Finned		
400	0.77	0.70	-8.95	0.72	-7.55	1.54
650	0.71	0.62	-11.88	0.64	-9.30	2.93
1000	0.66	0.58	-12.31	0.60	-9.05	3.73
1500	0.63	0.55	-11.78	0.58	-7.92	4.37

Case (d) : $s_L^* = 5,\ s_T^* = 2$

Variation of $\overline{Nu}$ vs Re number for both Prandtl numbers of 0.7 and 7 is plotted in figure 5.27. Figure 5.28 demonstrates f versus Re number variation. For $s_L^* = 5,\ s_T^* = 2$, unfinned, D-Finned and 2D-Finned calculations are given in tables 5.10a and 5.10b. For Pr = 7, D-Finned case has 76.81% enhancement in average Nusselt number ($\overline{Nu}^+$) as compared to unfinned case at Re = 1500, besides 2D-

Finned case enhances average Nusselt number ($\overline{Nu}^{+,D}$) to 157.85% when compared to unfinned case. 60.5% and 62.1% of heat transfer increment values are obtained where 127% and 254% are surface area increment values.

On the other hand, friction factor has a decrement of 15.24% (f^{+}) for D-Finned case as compared to unfinned case and for 2D-Finned case, friction factor decreases 10.31% (f_D^{+}) to unfinned case at Re = 1500.

Table 5.10a. Calculated values of $\overline{Nu}$ for unfinned, D-Finned and 2D-Finned staggered tube banks where $s_L^* = 5,\ s_T^* = 2$

Pr	Re	$\overline{Nu}$	$\overline{Nu}$	$\overline{Nu}^{+}$ (%)	$\overline{Nu}$	$\overline{Nu}^{+}$ (%)	$\overline{Nu}^{+,D}$ (%)
		Unfinned	D-Finned		2D-Finned		
0.7	400	10.45	15.34	46.75	22.55	115.79	47.05
	650	13.48	20.23	50.07	29.93	122.00	47.93
	1000	17.06	26.46	55.06	39.02	128.65	47.46
	1500	21.50	34.47	60.32	50.71	135.85	47.11
7	400	23.93	36.41	52.10	50.22	109.82	37.94
	650	31.17	48.80	56.59	69.56	123.19	42.53
	1000	39.67	65.86	66.02	95.47	140.65	44.96
	1500	50.25	88.84	76.81	129.57	157.85	45.83

Table 5.10b. Calculated values of f for unfinned, D-Finned and 2D-Finned staggered tube banks where $s_L^* = 5,\ s_T^* = 2$

Re	f	f	f^{+} (%)	f	f^{+} (%)	f_D^{+} (%)
	Unfinned	D-Finned		2D-Finned		
400	0.53	0.47	-10.50	0.46	-12.41	-2.13
650	0.50	0.42	-15.41	0.43	-14.00	1.67
1000	0.48	0.40	-16.16	0.41	-12.75	4.06
1500	0.45	0.39	-15.24	0.41	-10.31	5.81

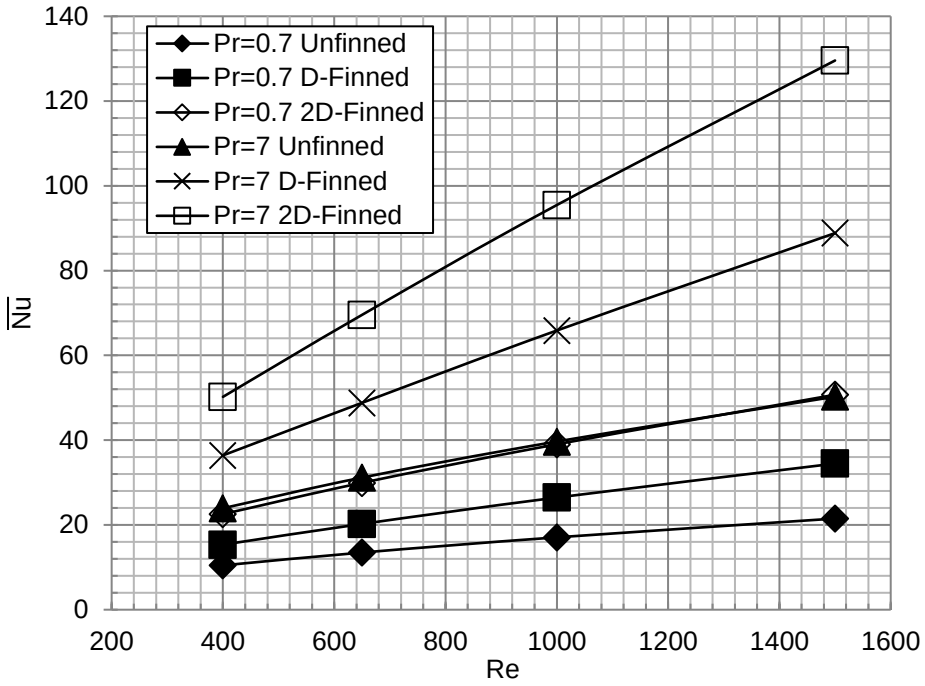


Figure 5.27. Variation of $\overline{\mathrm{Nu}}$ number with Re number for unfinned, D-Finned and 2D-Finned tube banks for $s_L^* = 5,\ s_T^* = 2$

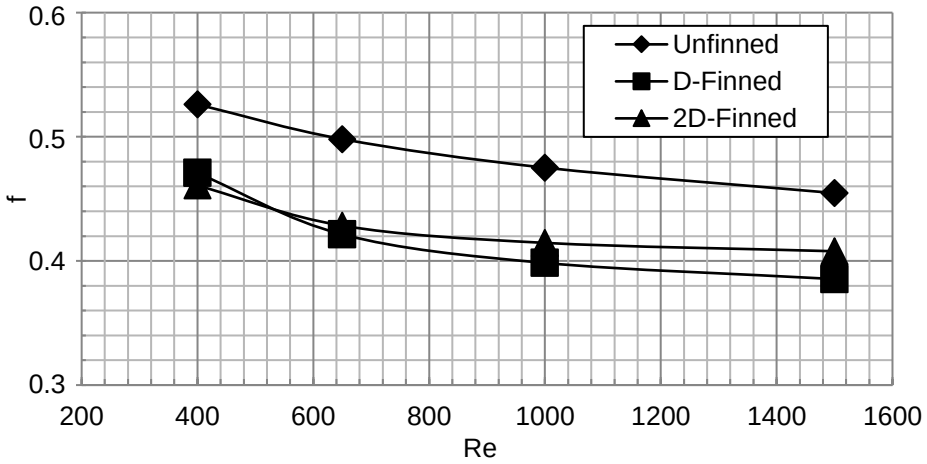


Figure 5.28. Variation of f with Re number for unfinned, D-Finned and 2D-Finned tube banks for $s_L^* = 5,\ s_T^* = 2$

5.2.3 Comparison of Studied Cases for Staggered Tube Banks

When s_T^* is increased from 1.5 to 2.0, average Nusselt number decreases only for 2D-Finned case of $s_L^* = 3$ where Re = 1500 and Pr = 0.7. Nevertheless, f values decrease with the use of $s_T^* = 2$ for all studied cases. Obtained heat transfer values are nearly same with a lower pressure drop at $s_T^* = 2$, but the drawback is that heat exchanger has larger size. Heat transfer is enhanced with the usage of axial fins. Figures 5.29 and 5.30 demonstrate $\overline{Nu}$ numbers versus s_T^* values for Pr = 0.7 and 7, respectively at Re = 1500 while figure 5.31 exhibits f vs. s_T^* values at Re = 1500.

For 2D-Finned case of $s_L^* = 3$ and $s_T^* = 1.5$, $\overline{Nu}$ is 64.95 for Pr = 0.7 and Re = 1500, while f equals to 0.82 at Re = 1500. When s_T^* is increased from 1.5 to 2.0 and s_L^* is unchanged (2D-Finned case of $s_L^* = 3$ and $s_T^* = 2$) for the identical Pr and Re numbers, $\overline{Nu}$ equals to 62.70 and f is 0.61. So, it can be concluded that heat transfer and friction factor decrease 3.5% and 25.61%, respectively. Similarly, $\overline{Nu}$ equals to 149.81 for Pr = 7 and f is 0.82 at Re = 1500 for 2D-Finned case of $s_L^* = 3$ and $s_T^* = 1.5$. Only if s_T^* is increased from 1.5 to 2, $\overline{Nu}$ is 153.73 and f equals to 0.6. It shows that s_T^* increment does not significantly augment heat transfer (2.6% increment). Additionally, f decreases from 0.82 to 0.61, so 25.61% f decrement is obtained.

For 2D-Finned case of $s_L^* = 3$ and $s_T^* = 1.5$, $\overline{Nu}$ is 64.95 for Pr = 0.7 and f is 0.82 at Re = 1500. If s_T^* remains constant and s_L^* is increased from 3 to 5 (2D-Finned case of $s_L^* = 5$ and $s_T^* = 1.5$) for the same Pr and Re numbers, it is observed that heat transfer and friction factor have 25.19% and 29.27% decrements, respectively.

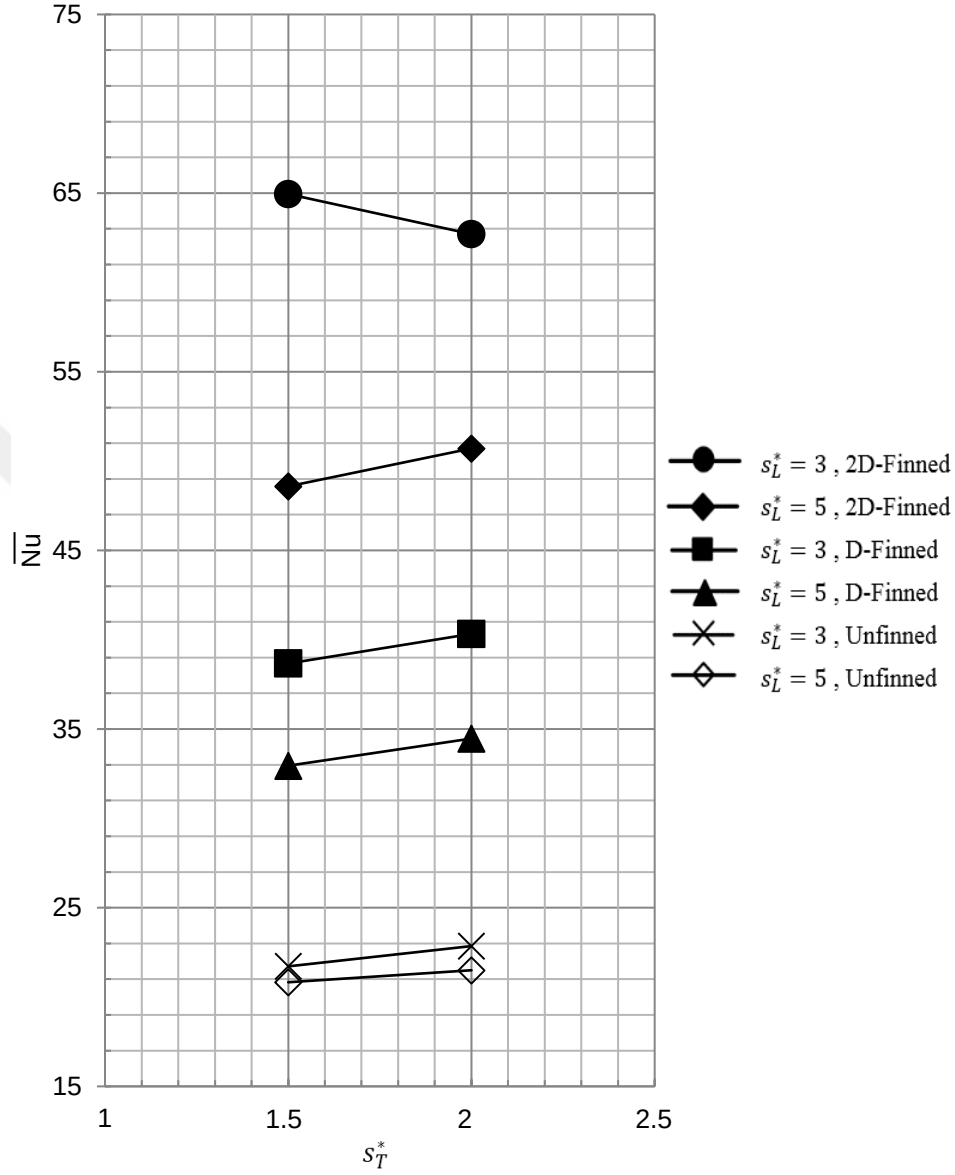


Figure 5.29. $\overline{Nu}$ vs. s_T^* values for studied cases where $Re = 1500$ and $Pr = 0.7$

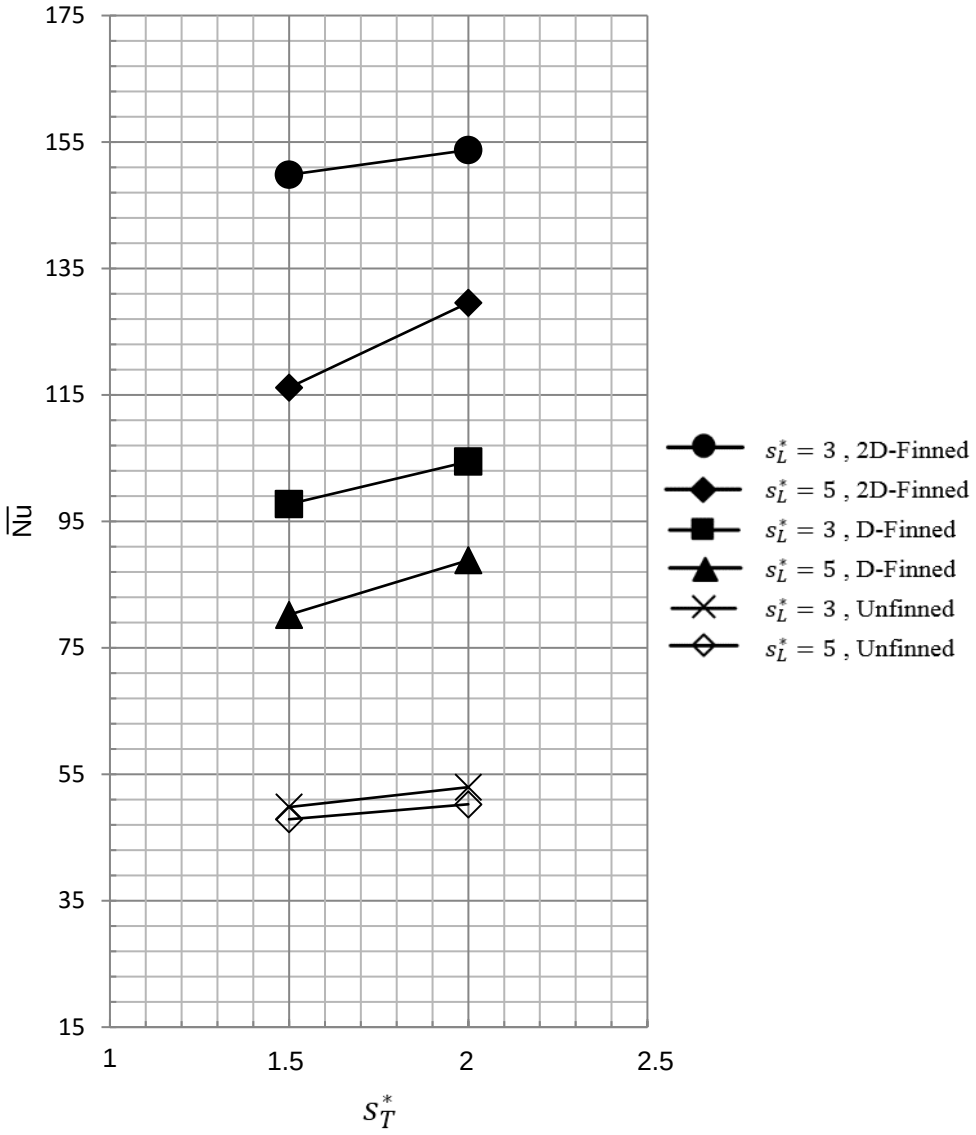


Figure 5.30. $\overline{Nu}$ vs. s_T^* values for studied cases where $Re = 1500$ and $Pr = 7$

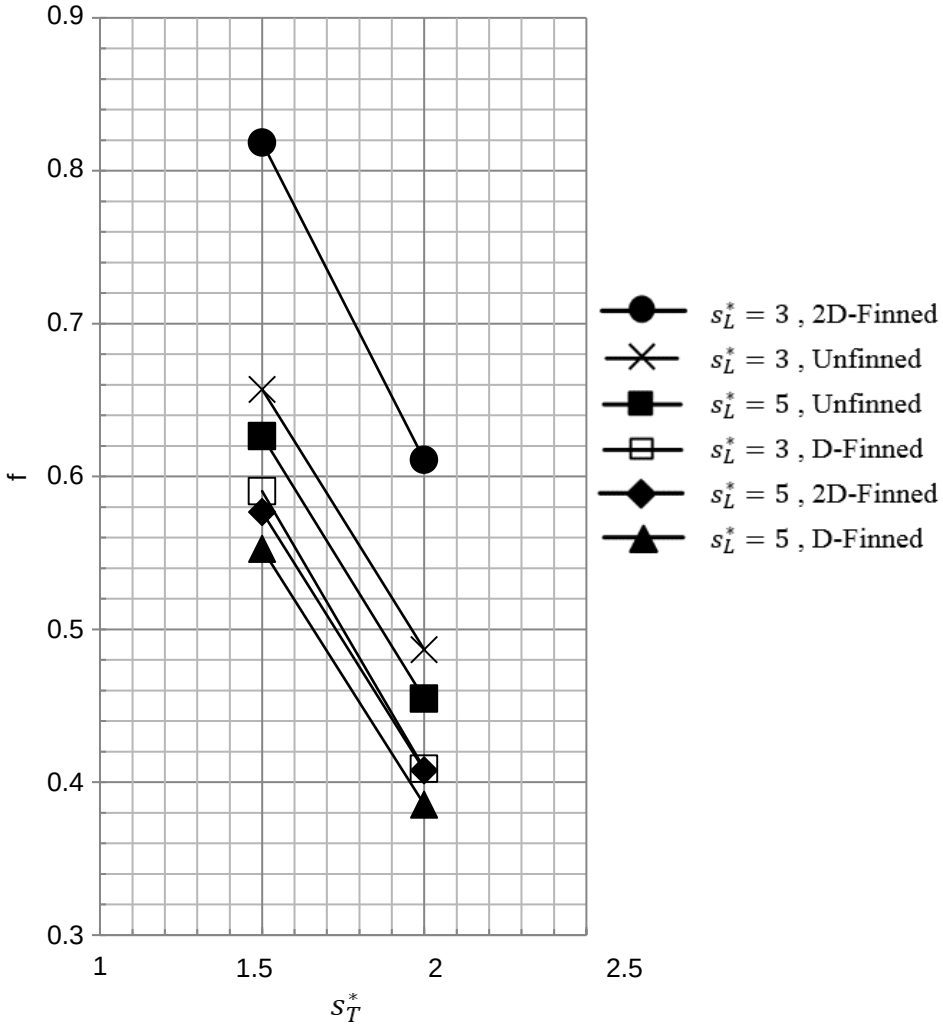


Figure 5.31. f vs. s_T^* values for studied cases where Re = 1500

5.3. Comparison of Studied Cases (Table 5.1 and Table 5.6) for Both In-line and Staggered Arrangements

In the sections 5.1 and 5.2, heat and fluid flow over in-line and staggered tube banks for unfinned and axially finned cases are studied where Reynolds numbers lie between 400-1500. Four different s_L^* and s_T^* values are chosen for both

in-line and staggered arrangements and given in tables 5.1 and 5.6. Staggered arrangement has 2D-Finned cases for $s_L^* = 3,\ s_T^* = 1.5$ and $s_L^* = 3,\ s_T^* = 2$ while 2D-Finned could not be possible for the given pitch ratios of in-line tube banks (2D-Finned case is only applicable for in-line arrangement where $s_L^* = 5$).

The thermal performance for the studied cases (tables 5.1 and 5.6) are presented graphically in terms of $\overline{Nu}$ / f for both in-line and staggered arrangements at Re = 1500. Figures 5.32 and 5.34 show the variation of $\overline{Nu}$ / f values for $Pr = 0.7$ and $Pr = 7$, respectively. $\overline{Nu}$ for $Pr = 0.7$ and f comparisons are also illustrated in figure 5.33 while $\overline{Nu}$ for $Pr = 7$ and f comparisons are shown in figure 5.35. In the followings, comparisons of different cases are given:

- Thermal performance $\overline{Nu}$ / f computation results in figures 5.32 and 5.34 show that as a result of axial finning $\overline{Nu}$ / f increases for both Prandtl numbers 0.7 and 7.
- 2D-Finned studies of $s_L^* = 5,\ s_T^* = 2$ show the best thermal performance for both in-line and staggered arrangements, whereas staggered arrangement has better than in-line arrangement. It should be noted that 2D-Finned case of $s_L^* = 3,\ s_T^* = 1.5$ for the staggered arrangement has the maximum $\overline{Nu}$ for $Pr = 0.7$ because heat transfer is better dispersed for the studied cases . Moreover, $\overline{Nu}$ is maximum for 2D-Finned case of $s_L^* = 3,\ s_T^* = 2$ where $Pr = 7$.
- For staggered arrangement, increasing s_L^* from 3 to 5 for 2D-Finned studied cases cause a big change in thermal performance $\overline{Nu}$ / f for both Prandtl values of 0.7 and 7. The main reason of that is the values of f decrease with the use of $s_L^* = 5$. The only disadvantage is that the heat exchanger size is larger for $s_L^* = 5$.
- For both in-line and staggered arrangements, increasing s_T^* from 1.5 to 2 for studied cases increase thermal performance $\overline{Nu}$ / f for Prandtl

numbers of 0.7 and 7. The reason is that values of f increase with the usage of $s_T^* = 1.5$.

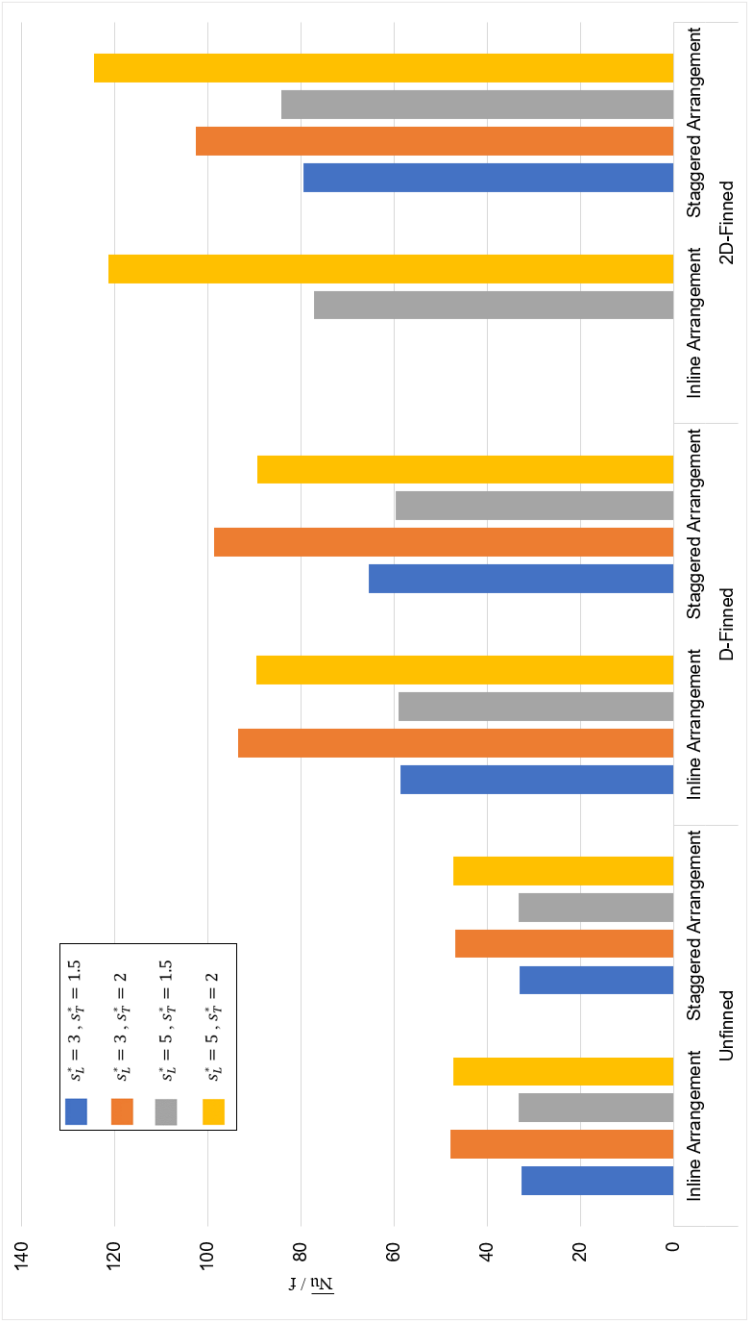


Figure 5.32. $\overline{Nu}/f$ values comparison for the studied cases (tables 5.1, 5.6) for both in-line and staggered arrangements where $Pr = 0.7$

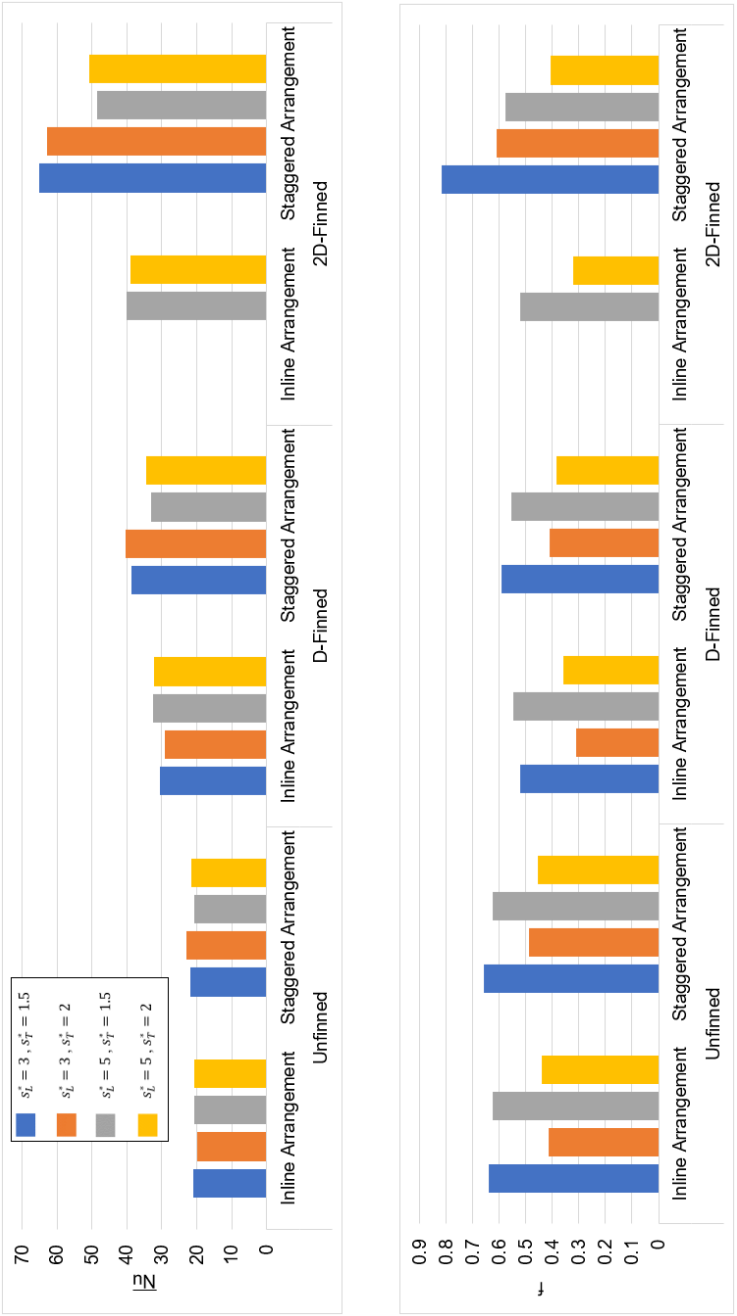


Figure 5.33. $\overline{\text{Nu}}$ where $\text{Pr} = 0.7$ and f comparisons for the studied cases (tables 5.1, 5.6) for both in-line and staggered arrangements

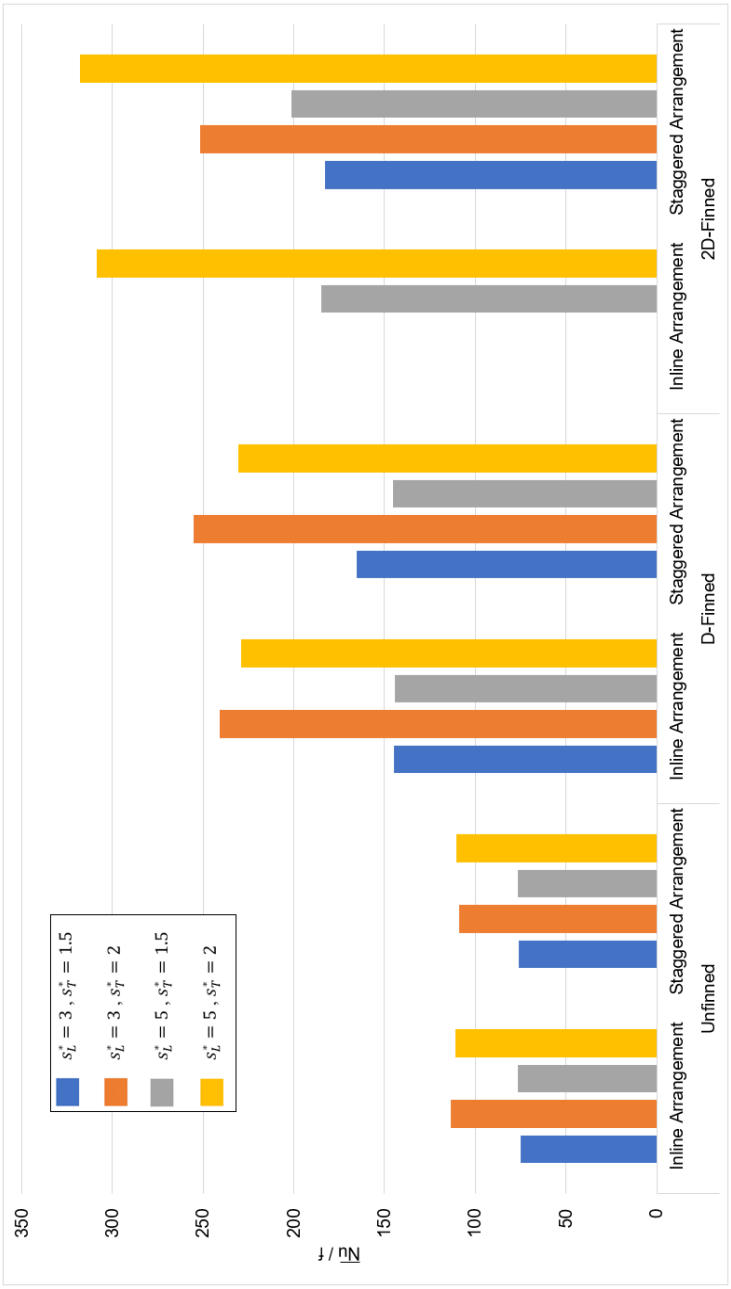


Figure 5.34. $\overline{Nu}$ / f values comparison for the studied cases (tables 5.1, 5.6) for both in-line and staggered arrangements where $Pr = 7$

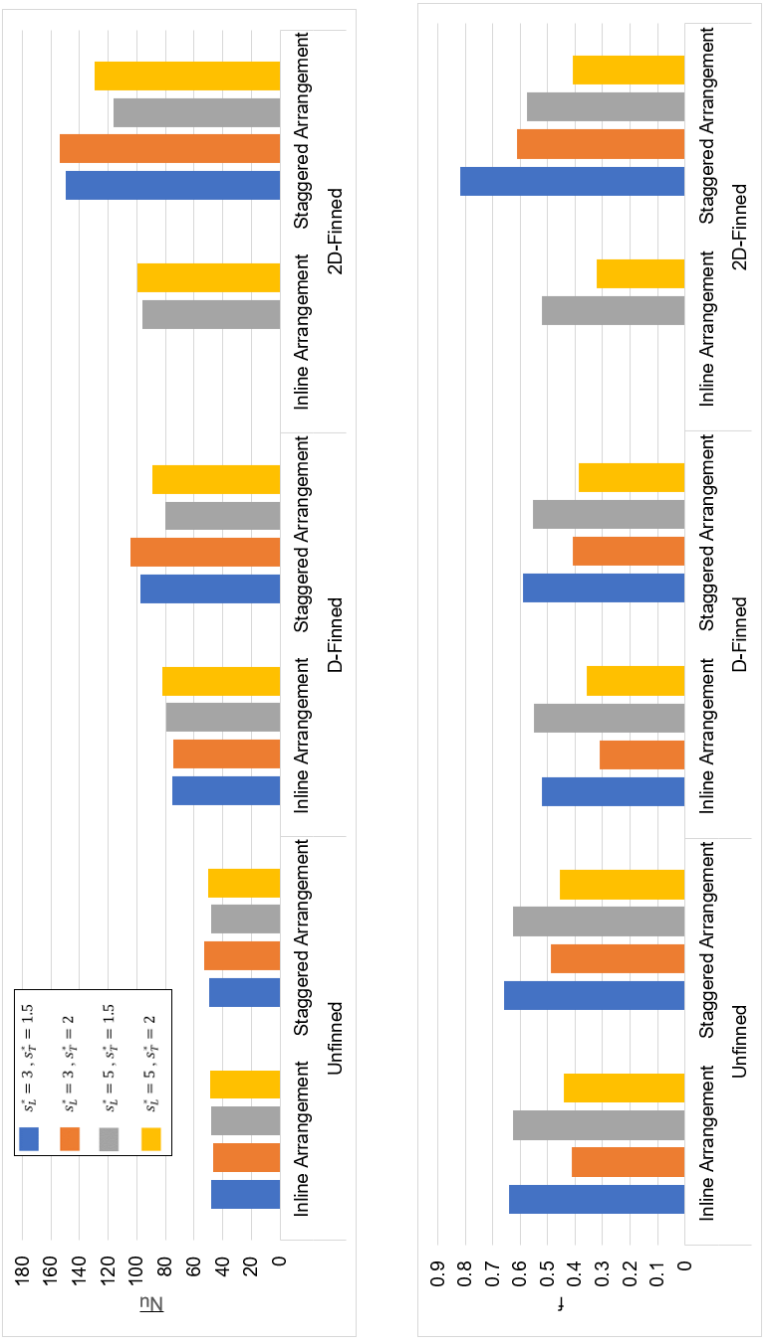


Figure 5.35. $\overline{\mathrm{Nu}}$ where $\mathrm{Pr} = 7$ and f comparisons for the studied cases (tables 5.1, 5.6) for both in-line and staggered arrangements

5.4. Optimization of Axially Finned Tube Banks

In this section, numerical optimization of heat and fluid flow over in-line and staggered tube banks are investigated for both unfinned and axially finned studies. The objective of the present optimization study is to obtain maximum heat transfer from tube bank with minimum volume of tube bank numerically for the given mass flow rate, allowable pressure drop and tube bank effectiveness which was formerly studied by Yilmaz and Yilmaz (2016) and Yilmaz et al. (2017).

Present optimization study has similar assumptions outlined in Yilmaz and Yilmaz (2016) and Yilmaz et al.'s (2017) works. Optimum in-line and staggered tube banks are obtained with the usage of their formulations. Thus, numerical calculation results are compared with their studies.

The fluid flow over tube bank is steady state, incompressible, turbulent and periodic fully developed. Inlet and wall temperatures are constant. Finite volume method solves the conservation equations. RNG k-ε model with enhanced wall treatment is selected for turbulent flow simulation. Multi-objective Genetic Algorithm II (MOGA-II) controls optimization studies.

Optimum designs are given in tables. Additionally, total heat transfer with total volume variations, transversal and longitudinal pitches' effects on objective functions are discussed with figures.

Both unfinned and axially finned optimization problems are solved for Prandtl number of 0.71, fixed mass flow rate over the tube bank of $\dot{m}_N = 0.5\ \mathrm{kg/s}$ and allowable pressure drop is given as $\Delta p_{allow} = 100\ \mathrm{Pa}$. Constant inlet temperature $T_i = 443.15\ \mathrm{K}$ and constant wall temperature $T_w = 383.15\ \mathrm{K}$ are given for the optimization studies. Tube diameter (D) equals to $10\ \mathrm{mm}$ and tube bank effectiveness (η) is 0.75. Air is used as a working fluid over tube bank and thermo-physical properties of air are given as:

$$\rho = 0.82\ \text{kg}/\text{m}^3 \quad ; \quad c_p = 1.017\ \text{kJ}/(\text{kg K}) \tag{5.4}$$
$$\upsilon = 2.93\ 10^{-5}\ \frac{\text{m}^2}{\text{s}} \quad ; \quad \text{Pr} = 0.71 \quad ; \quad k = 0.0344\ \text{W}/(\text{m K})$$

Optimization problems are run on a computer with an Intel I7 CPU 4720 GHz processor and 16 GB Ram on Microsoft Windows 10 operating system.

5.4.1. Unfinned and Axially Finned In-line Tube Bank Optimization Studies

5.4.1.1. Optimization Results of Unfinned In-line Tube Banks

The workflow of this optimization problem is given in figure 5.36. In figure 5.36, optimization algorithm (scheduler), design of experiments (DOEs), objective functions, constraint, output variables and optimization variables with their lower and upper values and increments (step sizes) are defined. Modefrontier program searches optimum values of optimization variables (s_L , s_T , N_L , N_T , B , t) within their limits for the given objective functions and constraint. Once the optimization algorithm run, the workflow starts from the beginning at every iteration with the changed values of optimization variables. Optimum designs are chosen as pareto designs by Modefrontier optimization driver. Pareto designs demonstrate optimum designs where one objective function gets better and the other objective function is worsened. Maximum obtainable heat transfer from tube bank can be calculated using equation 4.51 as $\dot{Q}_{max} = 30.51$ kW. A multi-objective design optimization problem given in equation 4.37 can be formulated for the given boundary conditions:

Objective Function	Maximize $\dot{Q}_N$, Minimize V_N	(5.5)
Constraint	$\dot{Q}_N \leq 22.88$ kW	
Optimization Variables with their limits and step sizes	$14.0 \leq s_L \leq 16.5$, step size = 0.1 mm, $14.0 \leq s_T \leq 16.5$, step size = 0.1 mm, $10 \leq N_L \leq 50$, step size = 1, $10 \leq N_T \leq 40$, step size = 1, $0.5 \leq B \leq 1.2$, step size = 0.1 m.	
Given Data	$\dot{m}_N = 0.5$ kg/s, $\Delta p_{allow} = 100$ Pa, $T_i = 443.15$ K, $T_w = 383.15$ K, $D = 10$ mm, $\eta = 0.75$	

The optimization workflow is run with 50 Design of Experiments (DOEs) which is created with Sobol sequence. Sobol sequence works well for the optimization variables in the range of 2 to 20 and the experiments distributed in the design space uniformly (Modefrontier User Manual). Multi-objective Genetic Algorithm II (MOGA-II) is used to obtain pareto designs. MOGA-II is designed for fast convergence to optimum designs and each optimization variable base has to be non-zero values (Modefrontier User Manual).

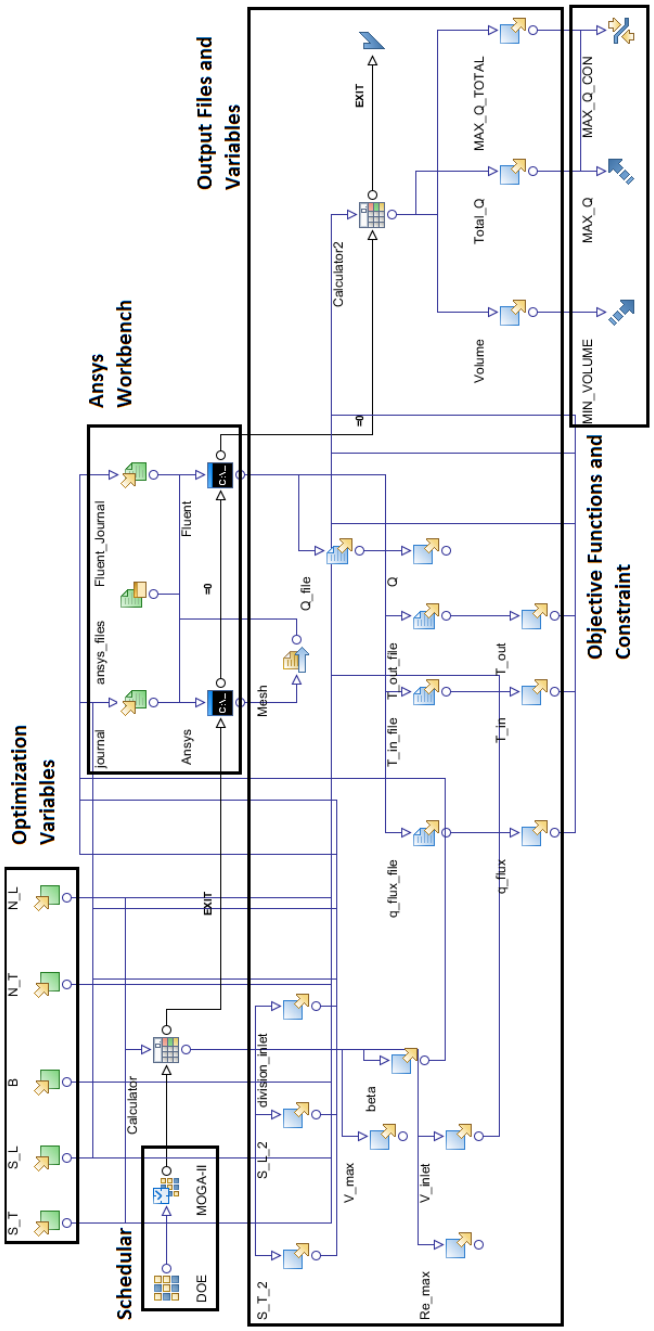


Figure 5.36. Optimization workflow for unfinned in-line tube bank

As a result, total number of 756 designs are generated to attain optimum values with Modefrontier, 625 feasible designs and 131 unfeasible designs are found. Finally, 132 designs are found as pareto designs in the optimization study and these pareto designs are tabulated in table 5.12. The optimum design is chosen from table 5.12 which corresponds to pareto design 9 because it has maximum heat transfer and minimum volume of the tube bank, while still provides constraint.

As it is mentioned before, this optimization study has similar assumptions with Yilmaz and Yilmaz's (2016) study and the optimum design results of Yilmaz and Yilmaz (2016) are presented in table 5.11 for the optimization problem given in equation 5.5. The difference of V_N of present optimum design with respect to Yilmaz and Yilmaz (2016) is about 3.25% where $\dot{Q}_N$ values are equal for both studies (22.88 kW). It should be noted that Yilmaz and Yilmaz (2016) consider an optimum pitch which must be equal to longitudinal and transversal pitches also, but in the present study transversal and longitudinal pitches are varied and optimum designs do not have to equal to each other as seen from table 5.12. So, differences are acceptable for the present optimum design (pareto design 9).

Table 5.11. Yilmaz and Yilmaz's (2016) optimum design results for the optimization problem given in equation 5.5

s_L (mm)	s_T (mm)	N_L	N_T	B (m)	$\dot{Q}_N$ (kW)	V_N (m^3)
16.30	16.30	15	12	1.028	22.88	4.92E-02

It took about 64 hours and 10 minutes to obtain optimum results.

Table 5.12. Pareto designs for unfinned in-line tube bank optimization study

Id	s_L (mm)	s_T (mm)	N_L	N_T	B (m)	$\dot{Q}_N$ (kW)	V_N (m^3)
1	14.00	14.00	10	10	0.50	8.86	9.80E-03
2	15.50	14.60	13	24	0.70	22.85	4.94E-02
3	14.00	14.00	10	16	0.50	12.89	1.57E-02
4	14.00	14.00	10	26	0.50	18.01	2.55E-02
5	14.00	14.00	10	10	0.60	10.30	1.18E-02
6	14.00	14.10	10	17	0.50	13.50	1.68E-02
7	14.10	14.00	10	10	0.50	8.86	9.87E-03
8	14.00	14.70	10	13	0.50	11.08	1.34E-02
9	15.60	14.90	13	24	0.70	22.88	5.08E-02
10	14.00	14.10	10	27	0.50	18.45	2.66E-02
11	14.00	14.10	10	10	0.60	10.31	1.18E-02
12	14.00	14.10	10	22	0.60	18.20	2.61E-02
13	14.00	14.80	10	10	0.50	8.96	1.04E-02
14	14.00	14.00	10	27	0.70	22.17	3.70E-02
15	14.00	14.00	10	17	0.50	13.48	1.67E-02
16	14.00	14.00	10	30	0.50	19.61	2.94E-02
17	14.30	14.20	10	12	0.50	10.33	1.22E-02
18	14.10	14.40	10	16	0.50	12.96	1.62E-02
19	14.00	14.10	10	22	0.50	16.19	2.17E-02
20	14.10	14.00	10	28	0.50	18.84	2.76E-02
21	14.00	14.00	10	28	0.50	18.83	2.74E-02
22	14.00	14.10	10	17	1.10	22.08	3.69E-02
23	14.00	14.10	10	10	0.70	11.66	1.38E-02
24	14.00	14.10	10	16	0.50	12.91	1.58E-02
25	14.00	14.00	10	26	0.70	21.76	3.57E-02
26	14.00	14.00	10	27	0.50	18.43	2.65E-02
27	14.00	14.70	10	10	0.60	10.39	1.23E-02

Table 5.12. continued …

Id	s_L (mm)	s_T (mm)	N_L	N_T	B (m)	$\dot{Q}_N$ (kW)	V_N (m^3)
28	14.10	14.00	10	10	0.70	11.64	1.38E-02
29	14.20	14.30	10	17	0.50	13.54	1.73E-02
30	14.00	14.10	10	17	0.60	15.38	2.01E-02
31	14.00	14.00	10	20	0.50	15.15	1.96E-02
32	14.00	14.20	10	16	1.20	22.38	3.82E-02
33	14.00	15.00	10	13	0.50	11.12	1.37E-02
34	14.00	14.40	10	19	0.60	16.63	2.30E-02
35	14.00	14.10	10	18	0.60	15.99	2.13E-02
36	14.00	14.10	10	15	0.60	14.08	1.78E-02
37	14.00	15.00	10	10	0.50	8.98	1.05E-02
38	14.00	14.10	10	26	0.50	18.03	2.57E-02
39	14.00	14.00	10	19	0.50	14.61	1.86E-02
40	14.00	14.00	10	24	0.50	17.12	2.35E-02
41	14.00	14.30	10	10	0.50	8.90	1.00E-02
42	14.00	14.00	10	36	0.50	21.64	3.53E-02
43	14.10	14.20	10	12	0.60	11.93	1.44E-02
44	14.10	14.00	10	34	0.50	21.01	3.36E-02
45	14.00	14.10	10	33	0.50	20.70	3.26E-02
46	14.00	14.10	10	14	0.60	13.39	1.66E-02
47	14.00	14.20	10	27	0.60	20.51	3.22E-02
48	14.00	14.40	10	10	0.50	8.91	1.01E-02
49	14.20	14.70	10	11	0.50	9.69	1.15E-02
50	14.00	14.20	10	21	0.50	15.70	2.09E-02
51	14.00	14.00	10	15	0.50	12.27	1.47E-02
52	14.10	14.20	10	10	0.70	11.67	1.40E-02
53	14.00	14.00	10	10	0.70	11.64	1.37E-02
54	14.00	14.00	10	19	0.60	16.55	2.23E-02

Table 5.12. continued …

Id	s_L (mm)	s_T (mm)	N_L	N_T	B (m)	$\dot{Q}_N$ (kW)	V_N (m^3)
55	14.00	14.10	10	24	0.60	19.18	2.84E-02
56	14.00	14.10	10	13	0.60	12.67	1.54E-02
57	14.00	14.70	10	12	0.50	10.39	1.23E-02
58	14.30	14.30	10	11	0.50	9.63	1.12E-02
59	14.00	14.00	10	21	0.70	19.38	2.88E-02
60	14.00	14.00	10	13	0.50	10.98	1.27E-02
61	14.30	14.20	10	17	0.50	13.52	1.73E-02
62	14.10	14.00	10	11	0.70	12.52	1.52E-02
63	14.00	14.10	10	26	0.60	20.08	3.08E-02
64	14.00	14.60	10	10	0.50	8.94	1.02E-02
65	14.00	14.00	10	18	0.60	15.97	2.12E-02
66	14.00	14.10	10	17	0.80	18.54	2.68E-02
67	14.00	14.00	10	11	0.50	9.59	1.08E-02
68	14.00	15.00	10	11	0.50	9.72	1.16E-02
69	14.00	14.80	10	13	0.50	11.09	1.35E-02
70	14.00	14.20	10	16	0.50	12.92	1.59E-02
71	14.00	14.10	10	28	0.60	20.90	3.32E-02
72	14.00	14.10	10	35	0.50	21.36	3.45E-02
73	14.00	14.00	10	18	0.50	14.06	1.76E-02
74	14.20	14.90	10	10	0.60	10.42	1.27E-02
75	14.00	14.10	10	19	0.80	19.79	3.00E-02
76	14.00	14.00	10	27	0.60	20.47	3.18E-02
77	14.00	14.40	10	26	0.60	20.13	3.14E-02
78	14.00	14.80	10	17	0.50	13.61	1.76E-02
79	14.00	14.70	10	11	0.50	9.68	1.13E-02
80	14.00	14.10	10	16	0.60	14.74	1.90E-02
81	14.00	14.00	10	24	0.60	19.15	2.82E-02

Table 5.12. continued …

Id	s_L (mm)	s_T (mm)	N_L	N_T	B (m)	$\dot{Q}_N$ (kW)	V_N (m^3)
82	14.00	14.70	10	10	0.50	8.95	1.03E-02
83	14.00	14.00	10	26	0.60	20.05	3.06E-02
84	14.10	14.20	10	16	0.60	14.76	1.92E-02
85	14.10	14.00	10	32	0.50	20.33	3.16E-02
86	14.00	14.10	10	21	0.60	17.68	2.49E-02
87	14.00	14.10	10	27	0.60	20.50	3.20E-02
88	14.10	14.30	10	10	0.80	12.94	1.61E-02
89	14.00	14.60	10	17	0.50	13.58	1.74E-02
90	14.00	14.10	10	20	0.60	17.14	2.37E-02
91	14.00	14.20	10	19	0.60	16.59	2.27E-02
92	14.00	14.60	10	10	0.60	10.38	1.23E-02
93	14.00	14.80	10	12	0.50	10.41	1.24E-02
94	14.10	14.20	10	17	0.60	15.40	2.04E-02
95	14.00	14.10	10	21	0.50	15.69	2.07E-02
96	14.10	14.00	10	36	0.50	21.64	3.55E-02
97	14.00	14.20	10	22	0.60	18.22	2.62E-02
98	14.00	14.10	10	29	0.50	19.26	2.86E-02
99	14.00	14.30	10	21	0.50	15.72	2.10E-02
100	14.00	14.10	10	17	0.70	17.05	2.35E-02
101	14.10	14.20	10	13	0.60	12.68	1.56E-02
102	14.00	14.00	10	13	0.70	14.17	1.78E-02
103	14.00	14.10	10	23	0.60	18.70	2.72E-02
104	14.10	14.00	10	15	0.70	15.67	2.07E-02
105	14.00	14.90	10	12	0.50	10.42	1.25E-02
106	14.00	14.00	10	16	0.70	16.36	2.20E-02
107	14.00	14.10	10	11	0.70	12.54	1.52E-02
108	14.00	14.20	10	19	0.50	14.65	1.89E-02

Table 5.12. continued …

Id	s_L (mm)	s_T (mm)	N_L	N_T	B (m)	$\dot{Q}_N$ (kW)	V_N (m^3)
109	14.10	15.00	10	10	0.50	8.98	1.06E-02
110	14.00	14.30	10	21	0.60	17.72	2.52E-02
111	14.00	14.20	10	15	0.50	12.31	1.49E-02
112	14.20	14.30	10	13	0.70	14.22	1.85E-02
113	14.00	14.00	10	40	0.50	22.78	3.92E-02
114	14.00	14.10	10	22	0.90	22.70	3.91E-02
115	14.00	14.10	10	13	0.70	14.19	1.80E-02
116	14.00	14.00	10	22	0.60	18.18	2.59E-02
117	14.10	14.10	10	40	0.50	22.80	3.98E-02
118	14.00	14.60	10	12	0.50	10.38	1.23E-02
119	14.10	15.10	10	10	0.50	9.00	1.06E-02
120	14.00	14.30	10	10	0.80	12.94	1.60E-02
121	14.20	14.40	10	13	0.70	14.24	1.86E-02
122	14.00	14.20	10	27	0.50	18.47	2.68E-02
123	14.00	14.40	10	40	0.50	22.85	4.03E-02
124	14.00	14.20	10	12	0.60	11.93	1.43E-02
125	14.00	14.10	10	25	0.60	19.64	2.96E-02
126	14.00	14.00	10	21	0.60	17.66	2.47E-02
127	14.10	14.10	10	37	0.50	21.96	3.68E-02
128	14.00	14.20	10	14	0.80	16.40	2.23E-02
129	14.00	14.60	10	19	0.60	16.67	2.33E-02
130	14.10	14.00	10	17	0.70	17.03	2.35E-02
131	14.10	14.00	10	40	0.50	22.78	3.95E-02
132	14.10	14.00	10	14	0.70	14.94	1.93E-02

In the following figures 5.37-5.41, feasible, unfeasible and pareto designs of the present multi-objective optimization study are illustrated, also Yilmaz and Yilmaz's (2016) optimum design values for the given optimization problem are demonstrated.

(a) Variation of objective function $\dot{Q}_N$ with objective function V_N

Figure 5.37 demonstrates the variation of $\dot{Q}_N$ with V_N. Maximum heat transfer values $\dot{Q}_N$ are obtained as 22.85 kW, 22.88 kW, 22.85 kW for the pareto designs of 2, 9, 123 as tabulated in table 5.12 and demonstrated in figure 5.37. Here, for the selected pareto designs 2, 9, 123 obtained volumes V_N are 4.94E-2 m^3, 5.08E-2 m^3, 4.03E-2 m^3, respectively. Pareto designs 2 and 123 have lower volumes than pareto design 9's volume but the drawback of pareto designs 2 and 123 is to have lower heat transfer values $\dot{Q}_N$ (22.85 kW) as compared to pareto design 9's heat transfer value which is 22.88 kW. Moreover, pareto designs 2 and 123 hold same heat transfer values but pareto design 123's volume is 18.42% lower than pareto design 2.

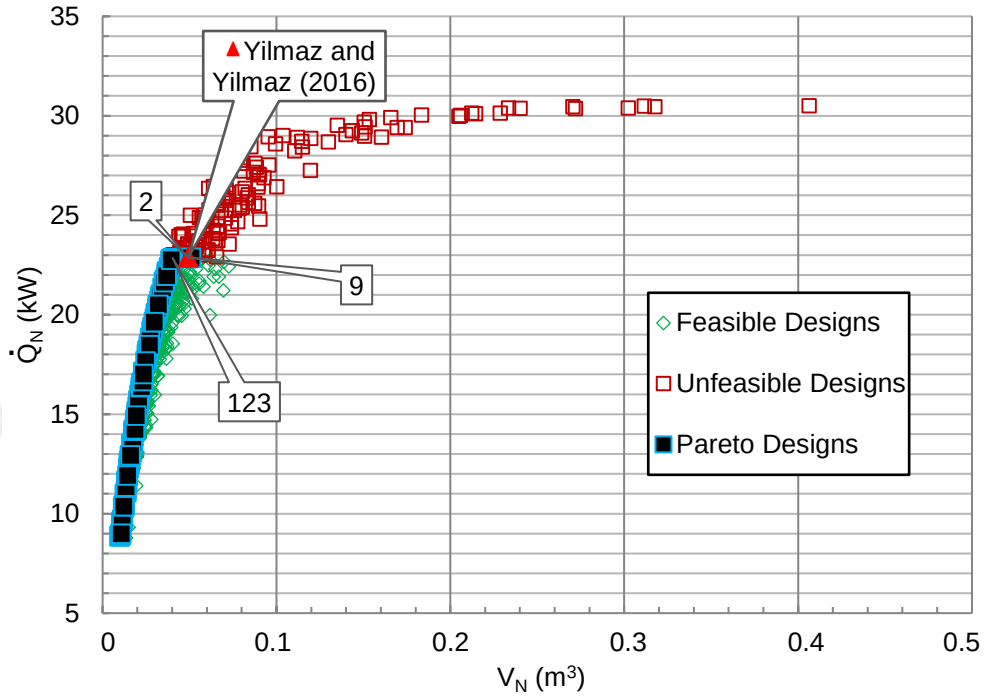


Figure 5.37. Variation of total heat transfer $\dot{Q}_N$ with total volume V_N for all designs of unfinned in-line tube bank

After the investigation of pareto designs in figure 5.37, it is found that a little reducing heat transfer result in considerable decrement in volume of the tube bank. As seen from figure 5.37, maximization of total heat transfer $\dot{Q}_N$ is improved while minimization of total volume V_N becomes worse for the pareto designs.

(b) Effect of pitches on objective functions $\dot{Q}_N$ and V_N

Variations of transversal and longitudinal pitches with respect to $\dot{Q}_N$ are demonstrated for all designs in figures 5.38 and 5.39, respectively. Moreover, variations of transversal and longitudinal pitches with V_N are shown in figures 5.40 and 5.41, respectively.

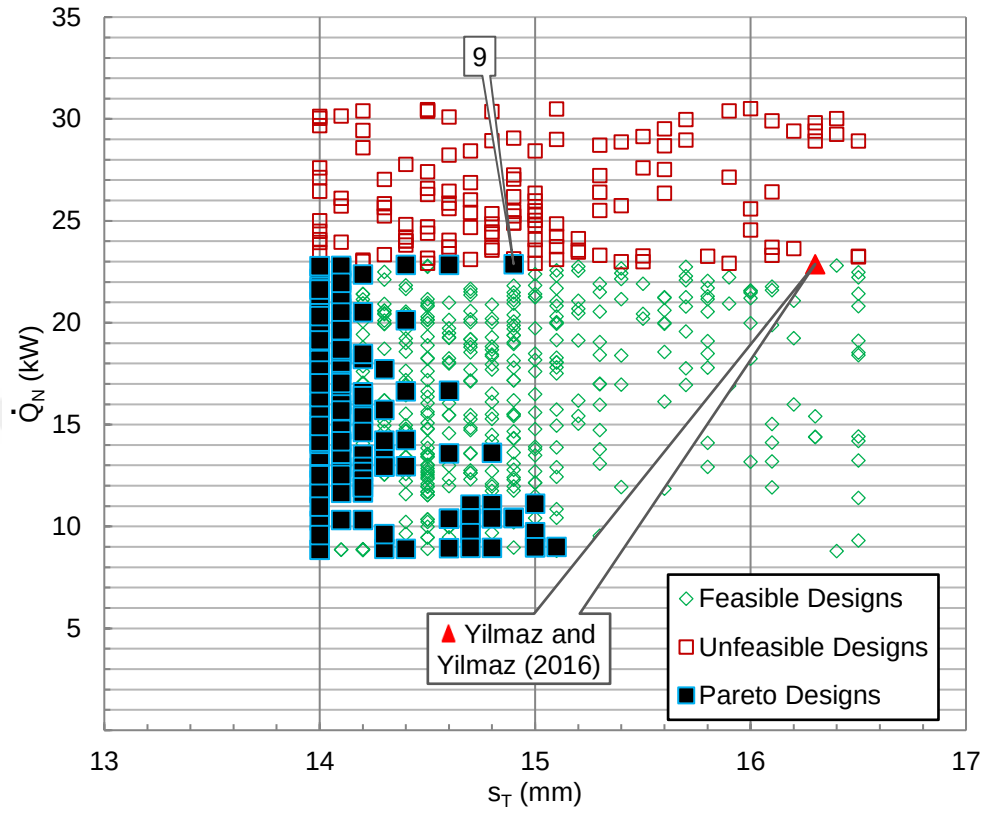


Figure 5.38. Variation of total heat transfer $\dot{Q}_N$ with transversal pitch s_T for all designs of unfinned in-line tube bank

For pareto design 9, transversal pitch is 14.90 mm and longitudinal pitch is 15.60 mm, Yilmaz and Yilmaz (2016) optimum design has equal pitches both in longitudinal and transversal directions which corresponds to 16.30 mm. The obtained results have different pitch values than Yilmaz and Yilmaz's (2016) optimum design pitches, whereas total heat transfer $\dot{Q}_N$ and total volume V_N values are nearly equal to each other as it is mentioned before.

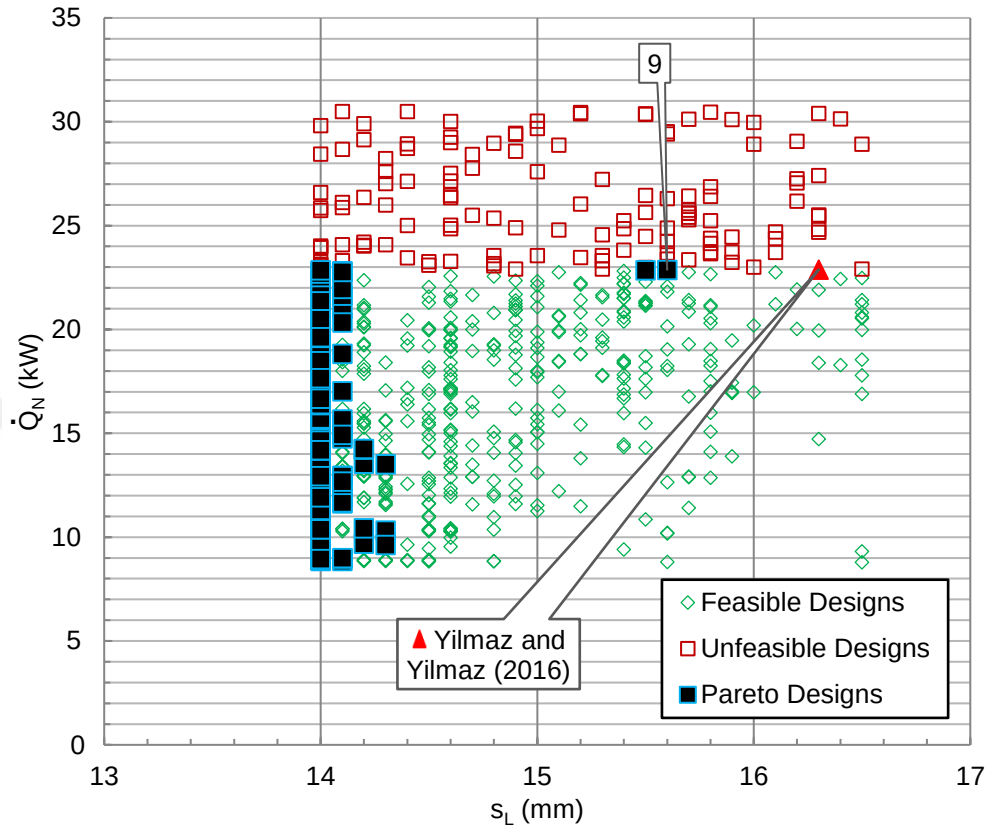


Figure 5.39. Variation of total heat transfer $\dot{Q}_N$ with longitudinal pitch s_L for all designs of unfinned in-line tube bank

Decreasing s_T lead to obtain more feasible designs, also any optimum design can be selected for different values of s_T (figure 5.38). From figure 5.39, it can be seen that pareto designs become dense in the lower values of s_L. As can be seen from figures 5.40 and 5.41, there is not any feasible design when the total volume V_N is greater than nearly 0.07 m^3.

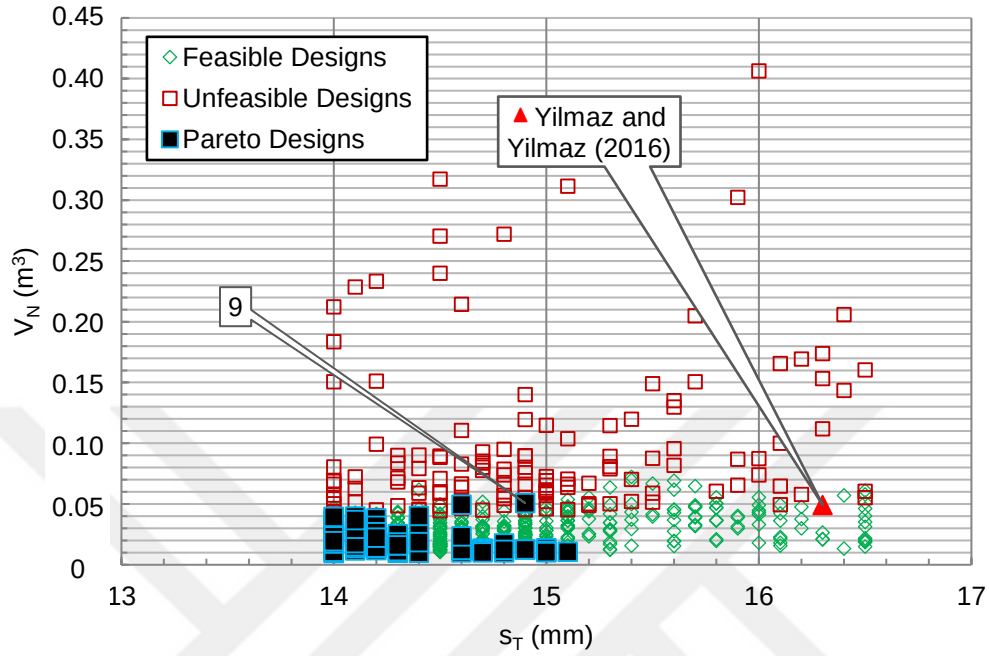


Figure 5.40. Variation of total volume V_N with transversal pitch s_T for all designs of in-line tube bank

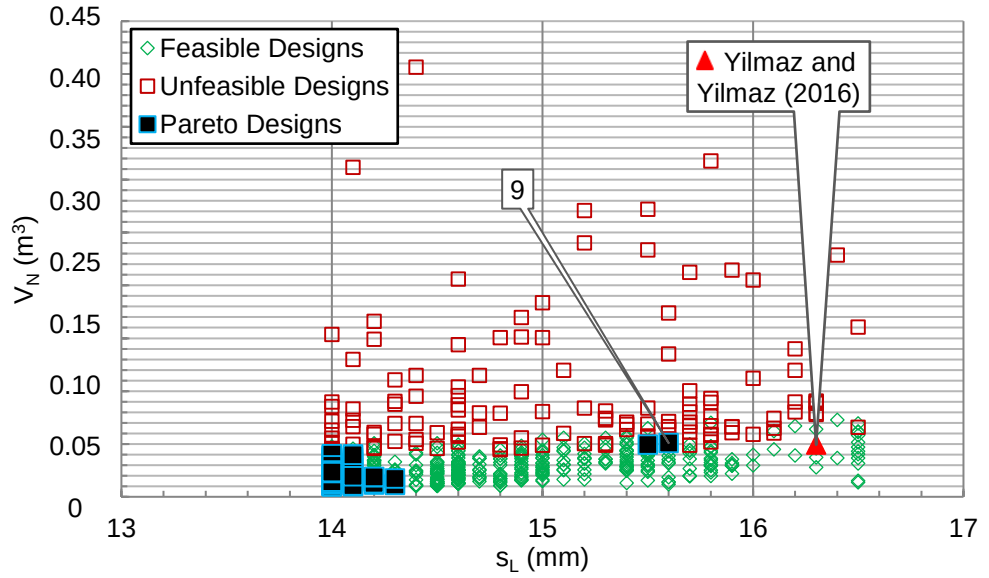


Figure 5.41. Variation of total volume V_N with longitudinal pitch s_L for all designs of in-line tube bank

5.4.1.2 Optimization Results of Axially Finned In-line Tube Banks

Similar optimization workflow is shown in figure 5.42. The difference between figures 5.36 and 5.42 is that fin thickness of axially finned in-line tube bank, t is specified as an input variable and also periodic model is adapted for axially finned in-line tube bank. Maximum obtainable heat transfer from axially finned in-line tube bank does not change and computed from equation 4.51 as $\dot{Q}_{max} = 30.51$ kW. A multi-objective design optimization problem given in equation 4.37 can be expressed for the given boundary conditions:

Objective Function	Maximize $\dot{Q}_N$, Minimize V_N	(5.6)
Constraint	$\dot{Q}_N \leq 22.88$ kW	
Optimization Variables with their limits and step sizes	$20.0 \leq s_L \leq 25$, step size = 0.1 mm, $(0.5D \leq L_f \leq 0.75D)$, $1.0 \leq t \leq 1.5$, step size = 0.1 mm, $14.0 \leq s_T \leq 16.5$, step size = 0.1 mm, $10 \leq N_L \leq 50$, step size = 1, $10 \leq N_T \leq 40$, step size = 1, $0.5 \leq B \leq 1.2$, step size = 0.1 m.	
Given Data	$\dot{m}_N = 0.5$ kg/s, $\Delta p_{allow} = 100$ Pa, $T_i = 443.15$ K, $T_w = 383.15$ K, $D = 10$ mm, $\eta = 0.75$	

50 DOEs are created with Sobol sequence and MOGA-II is used for the optimization study.

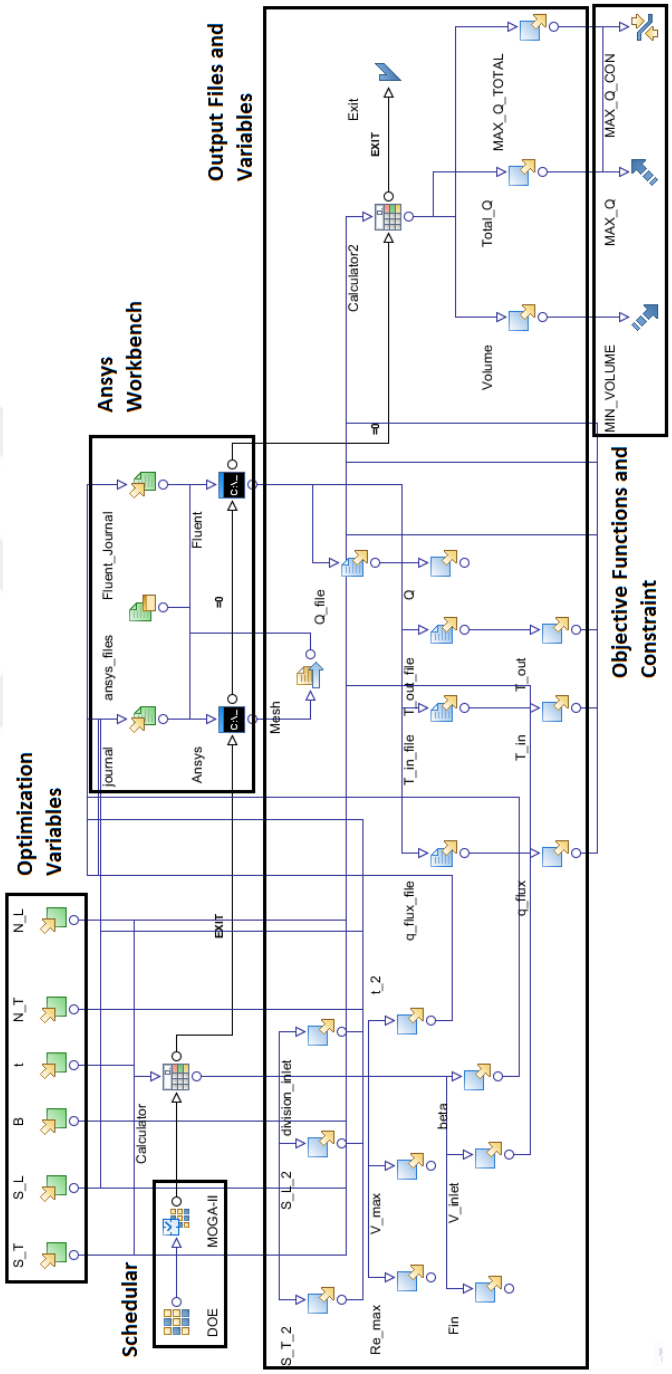


Figure 5.42. Optimization workflow for axially finned in-line tube bank

Consequently, total number of 844 designs are generated with Modefrontier, 752 feasible and 92 unfeasible designs are obtained. 103 designs are found as pareto designs and these pareto designs are presented in table 5.13. The optimum design is chosen from table 5.13 which is pareto design 9 because heat transfer is maximum and volume is minimum for the obtained heat transfer value and constraint is ensured.

The drawback of axial fins is to have higher volumes V_N while still satisfies equal heat transfer $\dot{Q}_N$ as compared to unfinned in-line tube bank optimization study. In the unfinned in-line optimization study, optimum design (pareto 9) is chosen from table 5.12 which has a volume of $V_N = 5.08E-2\ m^3$. V_N for unfinned in-line tube bank is lower about 52.08% than present optimum design (pareto 9) which has a volume of $V_N = 1.06E-1\ m^3$. After the investigation of pareto designs for both unfinned and axially finned studies in figure 5.43, it can be seen that axial fins perform worse when compared to unfinned optimization study. It should be noted here that optimum design (pareto 9) has a fin length of 0.65D and all other pareto designs have a fin length of nearly 0.5D. It can be concluded that increasing fin length increases volume of in-line tube bank, therefore, axial fins are not convenient for the given optimization study of in-line tube bank.

Optimum results are attained approximately 70 hours and 20 minutes.

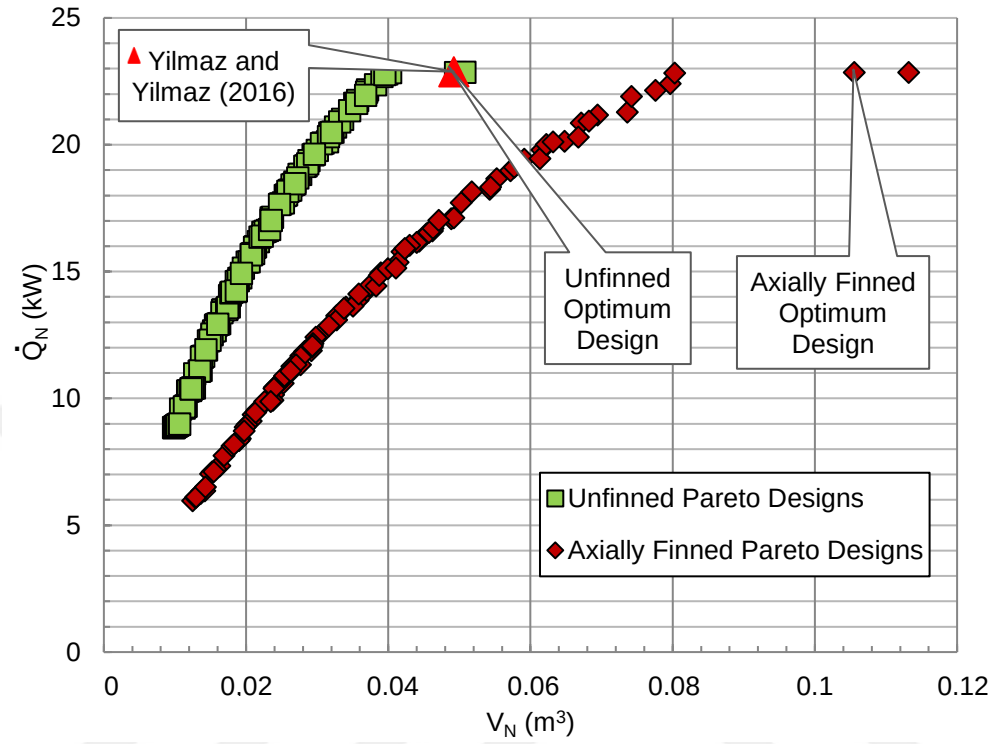


Figure 5.43. Variation of total heat transfer $\dot{Q}_N$ with total volume V_N for pareto designs of unfinned and axially finned in-line tube banks

Table 5.13. Pareto designs for axially finned in-line tube bank optimization study

Id	s_L (mm)	s_T (mm)	L_f (D)	t (mm)	N_L	N_T	B (m)	$\dot{Q}_N$ (kW)	V_N (m^3)
1	20.00	12.50	0.50	1.0	10	10	0.50	5.96	1.25E-02
2	20.20	14.00	0.51	1.5	29	23	0.60	22.86	1.13E-01
3	20.00	12.70	0.50	1.1	10	33	0.50	15.78	4.19E-02
4	20.00	12.50	0.50	1.1	10	16	0.60	10.44	2.40E-02
5	20.00	12.50	0.50	1.0	11	10	0.50	6.34	1.38E-02
6	20.00	13.50	0.50	1.2	10	10	0.50	6.24	1.35E-02
7	20.00	13.60	0.50	1.2	10	10	0.50	6.26	1.36E-02
8	20.00	12.50	0.50	1.1	10	14	0.60	9.36	2.10E-02
9	22.90	14.40	0.65	1.0	10	40	0.80	22.88	1.06E-01
10	20.00	12.70	0.50	1.1	10	17	0.50	9.55	2.16E-02
11	20.50	12.70	0.53	1.1	10	34	0.90	22.41	7.97E-02
12	20.00	12.50	0.50	1.1	11	24	0.70	16.60	4.62E-02
13	20.10	13.20	0.51	1.0	10	22	0.50	11.89	2.92E-02
14	20.10	13.20	0.51	1.0	10	19	0.50	10.59	2.52E-02
15	20.30	12.70	0.52	1.1	11	10	0.50	6.36	1.42E-02
16	20.10	12.90	0.51	1.2	10	25	0.70	16.49	4.54E-02
17	20.00	12.90	0.50	1.2	10	10	0.50	6.10	1.29E-02
18	20.00	13.60	0.50	1.2	10	12	0.50	7.35	1.63E-02
19	20.00	12.80	0.50	1.1	10	11	0.60	7.75	1.69E-02
20	20.00	13.00	0.50	1.2	10	10	0.50	6.12	1.30E-02
21	20.10	13.50	0.51	1.1	10	36	0.50	17.08	4.88E-02
22	20.00	12.70	0.50	1.1	10	10	0.60	7.10	1.52E-02
23	20.00	12.50	0.50	1.0	11	26	0.50	13.87	3.58E-02
24	20.00	12.60	0.50	1.1	10	26	0.50	13.27	3.28E-02
25	20.00	12.50	0.50	1.1	11	28	0.80	19.80	6.16E-02
26	20.10	12.50	0.51	1.0	11	20	0.50	11.33	2.76E-02
27	20.10	13.20	0.51	1.0	10	18	0.50	10.14	2.39E-02

Table 5.13. continued…

Id	s_L (mm)	s_T (mm)	L_f (D)	t (mm)	N_L	N_T	B (m)	$\dot{Q}_N$ (kW)	V_N (m^3)
28	20.10	12.90	0.51	1.0	10	16	0.50	9.10	2.07E-02
29	20.00	14.00	0.50	1.0	10	17	0.50	9.93	2.38E-02
30	20.10	13.60	0.51	1.1	10	20	0.90	17.12	4.92E-02
31	20.10	12.90	0.51	1.1	10	20	0.50	10.95	2.59E-02
32	20.00	12.80	0.50	1.1	10	19	0.70	13.60	3.40E-02
33	20.00	12.60	0.50	1.1	10	22	0.50	11.68	2.77E-02
34	20.00	13.10	0.50	1.0	10	25	0.50	13.10	3.28E-02
35	20.10	13.20	0.51	1.0	10	22	0.60	13.64	3.50E-02
36	20.10	12.90	0.51	1.0	10	19	0.90	16.21	4.43E-02
37	20.00	13.30	0.50	1.2	10	29	0.90	21.18	6.94E-02
38	20.50	13.50	0.53	1.2	10	38	0.70	21.29	7.36E-02
39	20.00	12.70	0.50	1.1	10	12	0.80	10.54	2.44E-02
40	20.00	12.70	0.50	1.1	10	17	0.70	12.47	3.02E-02
41	20.10	12.90	0.51	1.2	10	37	0.70	20.86	6.72E-02
42	20.00	12.90	0.50	1.1	10	13	0.60	8.97	2.01E-02
43	20.00	12.50	0.50	1.1	10	10	0.60	7.03	1.50E-02
44	20.00	13.40	0.50	1.1	10	23	0.60	14.24	3.70E-02
45	20.00	13.10	0.50	1.1	10	10	0.60	7.22	1.57E-02
46	20.00	12.60	0.50	1.1	10	16	0.70	11.85	2.82E-02
47	20.00	12.80	0.50	1.1	10	19	0.50	10.50	2.43E-02
48	20.10	12.90	0.51	1.1	10	38	0.60	19.43	5.91E-02
49	20.00	12.90	0.50	1.2	10	11	0.70	8.87	1.99E-02
50	20.30	13.30	0.52	1.1	10	40	0.60	20.13	6.48E-02
51	20.00	12.50	0.50	1.1	11	26	0.80	18.97	5.72E-02
52	20.10	12.60	0.51	1.1	10	20	0.50	10.81	2.53E-02
53	20.10	12.90	0.51	1.1	10	16	0.90	14.42	3.73E-02
54	20.10	12.80	0.51	1.1	10	10	0.70	8.12	1.80E-02

Table 5.13. continued…

Id	s_L (mm)	s_T (mm)	L_f (D)	t (mm)	N_L	N_T	B (m)	$\dot{Q}_N$ (kW)	V_N (m^3)
55	20.10	12.50	0.51	1.1	10	18	0.70	12.87	3.17E-02
56	20.10	13.00	0.51	1.2	10	25	0.70	16.54	4.57E-02
57	20.00	12.80	0.50	1.1	10	20	0.70	14.12	3.58E-02
58	20.10	12.50	0.51	1.1	10	40	0.50	17.72	5.03E-02
59	20.00	13.60	0.50	1.2	10	10	0.70	8.39	1.90E-02
60	20.10	12.80	0.51	1.0	10	19	0.90	16.15	4.40E-02
61	20.00	13.30	0.50	1.2	10	31	0.90	21.91	7.42E-02
62	20.00	12.70	0.50	1.1	10	12	0.70	9.45	2.13E-02
63	20.00	12.70	0.50	1.1	10	19	0.70	13.55	3.38E-02
64	20.00	13.00	0.50	1.2	11	10	0.50	6.51	1.43E-02
65	20.10	12.80	0.51	1.1	10	10	0.60	7.11	1.54E-02
66	20.10	12.50	0.51	1.1	10	31	0.50	14.96	3.89E-02
67	20.00	12.50	0.50	1.1	11	31	0.80	20.94	6.82E-02
68	20.10	13.60	0.51	1.1	10	20	0.70	14.43	3.83E-02
69	20.00	13.70	0.50	1.2	10	10	0.70	8.41	1.92E-02
70	20.10	13.20	0.51	1.0	10	26	0.60	15.37	4.14E-02
71	20.00	13.30	0.50	1.2	10	31	0.70	19.12	5.77E-02
72	20.10	12.50	0.51	1.1	10	16	0.70	11.76	2.81E-02
73	20.00	12.60	0.50	1.1	10	19	0.50	10.40	2.39E-02
74	20.20	12.60	0.51	1.3	10	31	0.70	18.66	5.52E-02
75	20.20	12.60	0.51	1.1	10	23	0.50	12.03	2.93E-02
76	20.00	12.80	0.50	1.1	10	21	0.80	16.03	4.30E-02
77	20.10	12.80	0.51	1.0	10	20	0.90	16.71	4.63E-02
78	20.10	13.50	0.51	1.3	10	40	0.50	18.25	5.43E-02
79	20.00	12.60	0.50	1.1	10	15	0.70	11.27	2.65E-02
80	20.00	12.70	0.50	1.1	10	20	0.50	10.89	2.54E-02
81	20.00	12.80	0.50	1.2	10	23	0.80	17.03	4.71E-02

Table 5.13. continued…

Id	s_L (mm)	s_T (mm)	L_f (D)	t (mm)	N_L	N_T	B (m)	$\dot{Q}_N$ (kW)	V_N (m^3)
82	20.00	12.60	0.50	1.1	10	21	0.80	15.91	4.23E-02
83	20.10	12.60	0.51	1.0	10	17	0.90	14.85	3.87E-02
84	20.10	13.50	0.51	1.2	10	10	0.70	8.34	1.90E-02
85	20.00	13.40	0.50	1.1	11	26	0.80	19.46	6.13E-02
86	20.00	13.60	0.50	1.2	10	40	0.50	18.33	5.44E-02
87	20.00	14.20	0.50	1.1	10	15	0.70	12.42	2.98E-02
88	20.00	12.90	0.50	1.1	10	19	0.60	12.16	2.94E-02
89	20.00	12.50	0.50	1.3	10	23	0.90	18.15	5.18E-02
90	20.10	13.10	0.51	1.1	10	15	0.50	8.72	1.97E-02
91	20.10	12.80	0.51	1.1	10	21	0.50	11.33	2.70E-02
92	20.10	12.90	0.51	1.2	10	22	0.70	15.12	3.99E-02
93	20.10	12.90	0.51	1.1	10	40	0.60	20.01	6.22E-02
94	20.30	13.70	0.52	1.1	10	40	0.60	20.30	6.67E-02
95	20.10	12.80	0.51	1.1	10	17	0.60	11.07	2.62E-02
96	20.10	12.90	0.51	1.1	11	18	0.80	15.14	4.11E-02
97	20.10	13.00	0.51	1.1	10	10	0.70	8.19	1.83E-02
98	20.10	12.50	0.51	1.1	10	18	0.50	9.88	2.26E-02
99	20.00	13.80	0.50	1.0	10	17	0.50	9.88	2.35E-02
100	20.10	13.10	0.51	1.1	10	40	0.60	20.11	6.32E-02
101	20.10	12.80	0.51	1.2	10	39	0.80	22.83	8.03E-02
102	20.10	12.80	0.51	1.1	10	19	0.60	12.08	2.93E-02
103	20.00	13.90	0.50	1.2	10	31	0.90	22.14	7.76E-02

5.4.2. Unfinned and Axially Finned Staggered Tube Bank Optimization Studies

5.4.2.1 Optimization Results of Unfinned Staggered Tube Banks

The workflow of this optimization problem is established similar to figure 5.36. Maximum obtainable heat transfer is found as $\dot{Q}_{max} = 30.51\,kW$ from equation 4.51. A multi-objective design optimization problem is formulated as below:

Objective Function	Maximize $\dot{Q}_N$, Minimize V_N	(5.7)
Constraint	$\dot{Q}_N \leq 22.88\,kW$	
Optimization Variables with their limits and step sizes	$12.5 \leq s_L \leq 16.5$, step size = 0.1 mm, $12.5 \leq s_T \leq 16.5$, step size = 0.1 mm, $7 \leq N_L \leq 45$, step size = 1, $10 \leq N_T \leq 40$, step size = 1, $0.3 \leq B \leq 1.2$, step size = 0.1 m.	
Given Data	$\dot{m}_N = 0.5\,kg/s$, $\Delta p_{allow} = 100\,Pa$, $T_i = 443.15\,K$, $T_w = 383.15\,K$, $D = 10\,mm$, $\eta = 0.75$	

Number of 40 DOEs are generated with Sobol sequence. MOGA-II is applied to find optimum designs. 731 designs are obtained in all where 657 and 74 designs are feasible and unfeasible, respectively. 178 designs are ultimately elected as pareto designs and listed in table 5.15. Pareto design 42 from table 5.15 is selected as an optimum design because tube bank has minimum volume for the maximum heat transfer value and constraint is satisfied.

As this optimization study is formulated similar to Yilmaz et al.'s (2017) assumptions, optimum design results of Yilmaz et al. (2017) are tabulated in table 5.14 for the optimization problem specified in equation 5.7. The obtained heat transfer values $\dot{Q}_N$ for Yilmaz et al. (2017) and present optimum design are equal while Yilmaz et al.'s (2017) volume value V_N is about 7.65% lower than present optimum design. Similar to Yilmaz and Yilmaz's (2016) study, Yilmaz et al. (2017) consider an optimum pitch which must satisfy $s_L^* = \frac{\sqrt{3}}{2} s_T^*$, but in the present study transversal and longitudinal pitches are varied regardless of the formula $s_L^* = \frac{\sqrt{3}}{2} s_T^*$ so designs do not have to obey above formula. Differences are agreeable for the present optimum design (pareto design 42).

Table 5.14. Yilmaz et al.'s (2017) optimum design results for the optimization problem given in equation 5.7

s_L (mm)	s_T (mm)	N_L	N_T	B (m)	$\dot{Q}_N$ (kW)	V_N (m^3)
13.00	15.00	6	14	1.03	22.88	3.38E-02

Optimum results are obtained in 85 hours and 20 minutes.

Table 5.15. Pareto designs for unfinned staggered tube bank optimization study

Id	s_L (mm)	s_T (mm)	N_L	N_T	B (m)	$\dot{Q}_N$ (kW)	V_N (m^3)
1	12.50	12.50	7	10	0.30	4.07	3.28E-03
2	12.50	12.50	7	14	0.30	5.54	4.59E-03
3	12.50	13.00	7	10	0.30	4.15	3.41E-03
4	12.50	12.50	7	23	0.30	8.55	7.55E-03
5	12.50	12.60	7	22	0.40	10.50	9.70E-03
6	12.50	12.80	7	10	0.30	4.12	3.36E-03
7	12.50	12.50	7	30	0.30	10.65	9.84E-03
8	12.50	12.50	7	21	0.40	10.07	9.19E-03
9	12.50	12.50	7	10	0.40	5.30	4.38E-03
10	12.50	12.50	7	16	0.50	9.68	8.75E-03
11	12.80	13.10	7	12	0.30	4.90	4.23E-03
12	12.50	12.50	7	31	0.30	10.93	1.02E-02
13	12.50	12.50	7	14	0.70	11.39	1.07E-02
14	12.50	12.50	7	12	0.30	4.81	3.94E-03
15	12.50	12.50	7	19	0.30	7.26	6.23E-03
16	12.50	12.50	7	31	0.40	13.62	1.36E-02
17	12.50	12.50	7	23	0.40	10.84	1.01E-02
18	12.50	12.50	7	15	0.30	5.89	4.92E-03
19	12.50	12.50	7	10	0.60	7.59	6.56E-03
20	12.50	12.70	7	17	0.30	6.64	5.67E-03
21	12.50	12.50	7	22	0.30	8.24	7.22E-03
22	12.50	12.50	7	21	0.30	7.92	6.89E-03
23	12.50	12.60	7	25	0.40	11.61	1.10E-02
24	12.50	12.60	7	19	0.40	9.31	8.38E-03
25	12.50	12.70	7	10	0.30	4.10	3.33E-03
26	13.20	12.70	7	30	0.90	22.06	3.17E-02
27	12.50	12.50	7	17	0.30	6.59	5.58E-03

Table 5.15. continued...

Id	s_L (mm)	s_T (mm)	N_L	N_T	B (m)	$\dot{Q}_N$ (kW)	V_N (m^3)
28	12.50	12.80	7	23	0.30	8.65	7.73E-03
29	12.50	12.60	7	10	0.40	5.32	4.41E-03
30	12.70	13.20	7	11	0.30	4.55	3.87E-03
31	12.50	12.50	7	11	0.40	5.77	4.81E-03
32	12.50	12.60	7	19	0.70	14.38	1.47E-02
33	12.50	12.50	7	25	0.50	13.70	1.37E-02
34	12.50	12.60	7	11	0.40	5.80	4.85E-03
35	12.50	12.50	7	18	0.40	8.87	7.88E-03
36	12.50	12.50	7	11	0.30	4.44	3.61E-03
37	13.30	12.90	7	40	0.70	22.52	3.36E-02
38	12.50	12.50	7	25	0.40	11.57	1.09E-02
39	12.50	12.50	7	15	0.60	10.65	9.84E-03
40	12.50	12.50	7	25	0.30	9.17	8.20E-03
41	12.50	12.50	7	11	0.60	8.24	7.22E-03
42	13.50	13.00	8	29	0.90	22.88	3.66E-02
43	12.50	12.50	7	18	1.00	17.58	1.97E-02
44	12.50	12.50	7	11	0.50	7.04	6.02E-03
45	12.50	12.60	7	19	0.50	11.16	1.05E-02
46	12.50	12.60	7	18	0.40	8.90	7.94E-03
47	12.50	12.50	7	19	1.00	18.18	2.08E-02
48	12.50	12.60	7	22	0.30	8.27	7.28E-03
49	12.50	12.50	7	27	0.40	12.28	1.18E-02
50	12.50	12.70	7	12	0.30	4.85	4.00E-03
51	12.50	12.90	7	15	0.30	5.98	5.08E-03
52	12.50	12.60	7	26	0.40	11.97	1.15E-02
53	12.50	12.50	7	12	0.40	6.24	5.25E-03
54	12.50	12.60	7	17	0.70	13.26	1.31E-02

Table 5.15. continued...

Id	s_L (mm)	s_T (mm)	N_L	N_T	B (m)	$\dot{Q}_N$ (kW)	V_N (m^3)
55	12.50	12.50	7	23	0.50	12.88	1.26E-02
56	12.50	12.70	7	16	0.30	6.29	5.33E-03
57	12.50	12.50	7	18	1.20	19.62	2.36E-02
58	12.50	12.60	7	18	0.30	6.95	5.95E-03
59	12.50	12.50	7	30	0.40	13.30	1.31E-02
60	12.50	13.20	7	17	0.30	6.75	5.89E-03
61	12.70	12.90	7	19	0.30	7.35	6.54E-03
62	12.50	12.60	7	12	0.70	10.11	9.26E-03
63	12.50	12.60	8	11	0.30	4.88	4.16E-03
64	12.50	12.50	7	16	0.70	12.63	1.23E-02
65	12.50	12.60	7	14	0.30	5.56	4.63E-03
66	12.50	12.50	7	33	0.40	14.25	1.44E-02
67	12.70	13.10	7	10	0.30	4.15	3.49E-03
68	12.50	12.80	7	11	0.50	7.12	6.16E-03
69	12.50	12.60	7	30	0.30	10.69	9.92E-03
70	12.50	12.60	7	30	0.60	17.63	1.98E-02
71	12.50	12.70	7	20	0.40	9.75	8.89E-03
72	12.50	12.50	7	21	0.90	18.12	2.07E-02
73	12.50	12.60	7	18	0.70	13.83	1.39E-02
74	12.50	12.60	7	20	0.30	7.62	6.62E-03
75	12.50	12.70	7	23	0.70	16.46	1.79E-02
76	12.50	12.60	7	21	0.50	12.06	1.16E-02
77	12.50	12.60	7	13	0.30	5.20	4.30E-03
78	12.50	12.70	7	12	0.50	7.65	6.67E-03
79	12.50	12.50	7	18	0.50	10.65	9.84E-03
80	12.50	12.60	7	11	0.90	11.52	1.09E-02
81	12.50	12.60	7	17	1.20	19.03	2.25E-02

Table 5.15. continued...

Id	s_L (mm)	s_T (mm)	N_L	N_T	B (m)	$\dot{Q}_N$ (kW)	V_N (m^3)
82	12.50	12.60	7	28	0.40	12.67	1.23E-02
83	12.50	12.60	7	17	0.50	10.21	9.37E-03
84	12.50	12.60	7	27	0.90	20.99	2.68E-02
85	12.50	13.10	7	15	0.30	6.02	5.16E-03
86	12.50	12.50	7	12	0.60	8.87	7.88E-03
87	12.50	12.60	7	18	0.60	12.32	1.19E-02
88	12.50	12.90	7	14	0.30	5.62	4.74E-03
89	12.70	13.30	7	10	0.30	4.18	3.55E-03
90	12.50	12.80	7	13	0.30	5.24	4.37E-03
91	12.50	12.60	7	16	0.70	12.67	1.23E-02
92	12.60	12.50	7	14	0.50	8.64	7.72E-03
93	12.50	12.50	7	18	0.90	16.42	1.77E-02
94	12.50	12.60	7	20	0.70	14.91	1.54E-02
95	12.50	12.60	8	10	0.30	4.47	3.78E-03
96	12.50	12.50	7	16	0.80	13.94	1.40E-02
97	12.50	12.70	7	10	0.50	6.53	5.56E-03
98	12.50	12.60	7	29	0.30	10.40	9.59E-03
99	12.50	12.60	7	32	0.50	16.34	1.76E-02
100	12.50	12.80	7	17	0.30	6.66	5.71E-03
101	12.50	12.60	7	24	0.40	11.25	1.06E-02
102	12.50	12.60	7	24	0.70	16.87	1.85E-02
103	12.60	12.80	7	12	0.50	7.67	6.77E-03
104	12.50	12.50	7	26	0.50	14.10	1.42E-02
105	12.50	12.60	7	19	0.60	12.84	1.26E-02
106	12.50	12.50	7	30	0.50	15.59	1.64E-02
107	12.50	12.50	7	37	0.40	15.45	1.62E-02
108	12.50	12.70	7	17	0.50	10.25	9.45E-03

Table 5.15. continued...

Id	s_L (mm)	s_T (mm)	N_L	N_T	B (m)	$\dot{Q}_N$ (kW)	V_N (m^3)
109	12.50	12.60	7	24	0.50	13.34	1.32E-02
110	12.50	12.60	7	11	1.00	12.50	1.21E-02
111	12.50	12.50	7	30	0.60	17.58	1.97E-02
112	12.50	12.70	7	22	0.40	10.54	9.78E-03
113	12.50	12.70	7	22	0.80	17.44	1.96E-02
114	12.50	12.80	7	14	0.50	8.76	7.84E-03
115	12.60	12.50	7	27	0.30	9.76	8.93E-03
116	12.50	12.60	7	17	1.10	18.06	2.06E-02
117	12.50	12.50	7	26	0.60	16.01	1.71E-02
118	12.50	12.60	7	31	0.30	10.97	1.03E-02
119	12.50	12.60	7	13	1.20	16.06	1.72E-02
120	12.50	12.60	7	23	0.40	10.88	1.01E-02
121	12.50	12.60	7	17	0.90	15.85	1.69E-02
122	12.50	12.70	7	22	1.00	19.93	2.44E-02
123	12.50	12.60	7	10	0.90	10.69	9.92E-03
124	12.50	12.60	7	19	1.20	20.28	2.51E-02
125	12.50	12.50	7	16	0.60	11.21	1.05E-02
126	12.50	12.50	7	17	0.40	8.45	7.44E-03
127	12.50	12.50	7	12	1.00	13.30	1.31E-02
128	12.50	12.50	7	19	0.80	15.73	1.66E-02
129	12.50	12.60	7	20	0.90	17.63	1.98E-02
130	12.50	12.50	7	29	0.30	10.36	9.52E-03
131	12.50	12.60	7	39	0.30	13.09	1.29E-02
132	12.50	12.50	7	21	0.70	15.38	1.61E-02
133	12.50	12.50	7	40	0.50	18.76	2.19E-02
134	12.50	12.50	7	10	0.50	6.47	5.47E-03
135	12.50	12.50	7	17	0.80	14.56	1.49E-02

Table 5.15. continued...

Id	s_L (mm)	s_T (mm)	N_L	N_T	B (m)	$\dot{Q}_N$ (kW)	V_N (m^3)
136	12.50	12.60	7	36	0.70	21.39	2.78E-02
137	12.50	13.00	7	19	0.40	9.44	8.65E-03
138	12.50	12.60	7	16	0.80	13.99	1.41E-02
139	12.50	12.50	7	16	0.90	15.16	1.58E-02
140	12.50	12.60	7	37	0.30	12.58	1.22E-02
141	12.50	12.50	7	33	0.30	11.48	1.08E-02
142	12.50	12.50	7	23	1.10	21.38	2.77E-02
143	12.50	12.60	7	17	0.40	8.48	7.50E-03
144	12.50	12.50	7	14	0.60	10.07	9.19E-03
145	12.50	12.60	7	25	0.60	15.64	1.65E-02
146	12.50	12.70	7	22	0.30	8.30	7.33E-03
147	12.50	12.50	7	17	1.00	16.95	1.86E-02
148	12.50	12.50	7	10	1.00	11.57	1.09E-02
149	12.50	12.80	7	22	0.90	18.79	2.22E-02
150	12.50	12.50	7	34	0.30	11.75	1.12E-02
151	12.50	12.60	7	16	0.40	8.06	7.06E-03
152	12.50	12.50	7	37	0.30	12.54	1.21E-02
153	12.50	12.70	7	35	0.50	17.37	1.94E-02
154	12.50	12.60	7	21	0.30	7.95	6.95E-03
155	12.50	12.60	7	25	0.30	9.21	8.27E-03
156	12.50	12.60	7	22	0.60	14.30	1.46E-02
157	12.50	12.50	7	29	0.70	18.92	2.22E-02
158	12.50	12.70	7	21	0.90	18.23	2.10E-02
159	12.50	12.60	7	10	0.80	9.71	8.82E-03
160	12.50	12.60	7	29	0.50	15.28	1.60E-02
161	12.50	12.50	7	20	1.10	19.83	2.41E-02
162	12.50	12.50	7	29	0.60	17.20	1.90E-02

Table 5.15. continued...

Id	s_L (mm)	s_T (mm)	N_L	N_T	B (m)	$\dot{Q}_N$ (kW)	V_N (m^3)
163	12.50	12.60	7	29	0.40	13.01	1.28E-02
164	12.50	12.50	7	24	0.70	16.82	1.84E-02
165	12.50	12.60	7	33	0.50	16.67	1.82E-02
166	12.50	12.60	7	14	0.60	10.11	9.26E-03
167	12.50	12.60	7	25	0.70	17.32	1.93E-02
168	12.50	12.50	8	10	0.30	4.45	3.75E-03
169	12.50	12.50	7	18	0.30	6.93	5.91E-03
170	12.50	12.60	7	26	0.50	14.14	1.43E-02
171	12.50	12.50	7	10	0.80	9.68	8.75E-03
172	12.50	12.60	7	22	1.10	20.94	2.67E-02
173	12.50	12.50	7	29	0.50	15.23	1.59E-02
174	12.50	12.60	7	38	0.40	15.78	1.68E-02
175	12.50	12.60	7	26	0.80	19.25	2.29E-02
176	12.50	12.60	7	14	0.70	11.43	1.08E-02
177	12.50	12.50	7	29	0.40	12.96	1.27E-02
178	12.50	12.70	7	37	0.30	12.63	1.23E-02

Figures 5.44-5.48 show present multi-objective optimization study results and all designs (feasible, unfeasible and pareto designs) are demonstrated separately. Optimum design of unfinned in-line tube bank (Section 5.4.1.1), Yilmaz and Yilmaz's (2016) optimum design for in-line configuration and Yilmaz et al.'s (2017) optimum design for staggered arrangement are also represented in the following figures.

(a) Variation of objective function $\dot{Q}_N$ with objective function V_N

The variation of $\dot{Q}_N$ with V_N is shown in figure 5.44. Pareto design 42 has higher volume value (3.66E-02 m^3) than Yilmaz et al.'s (2017) optimum design volume (3.38E-02 m^3) while obtained heat transfer values are same (22.88 kW).

Moreover, optimum design of unfinned in-line tube bank and Yilmaz and Yilmaz's (2016) optimum design are depicted in figure 5.44. Optimum design of unfinned in-line tube bank has a volume of 5.08E-02 m^3 and it is 38.80% higher volume value as compared to optimum design of unfinned staggered tube bank while they have nearly equal heat transfer values. Similarly, Yilmaz and Yilmaz's (2016) optimum design volume value (4.92E-02 m^3) is 45.56% higher than Yilmaz et al.'s (2017) optimum design.

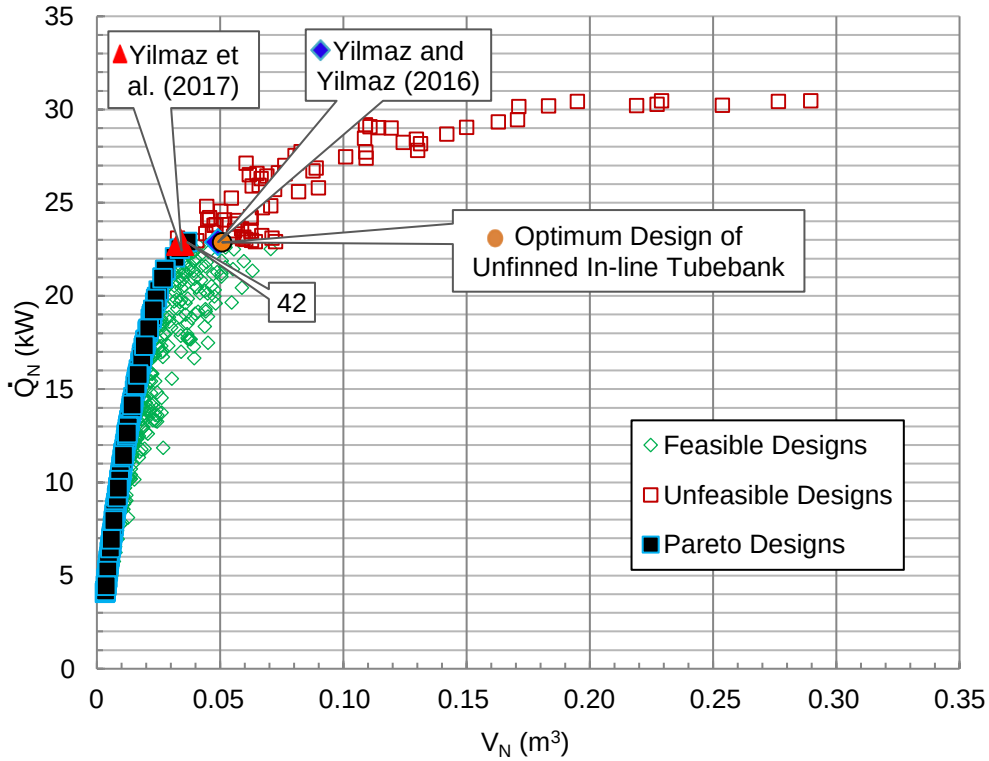


Figure 5.44. Variation of total heat transfer $\dot{Q}_N$ with total volume V_N for all designs of unfinned staggered tube bank

(b) Effect of pitches on objective functions $\dot{Q}_N$ and V_N

Transversal and longitudinal pitches variation vs. $\dot{Q}_N$ are illustrated for all designs in figures 5.45 and 5.46, respectively. Furthermore, transversal pitch vs. V_N is shown in figure 5.47 and longitudinal pitch with respect to V_N is presented in figure 5.48.

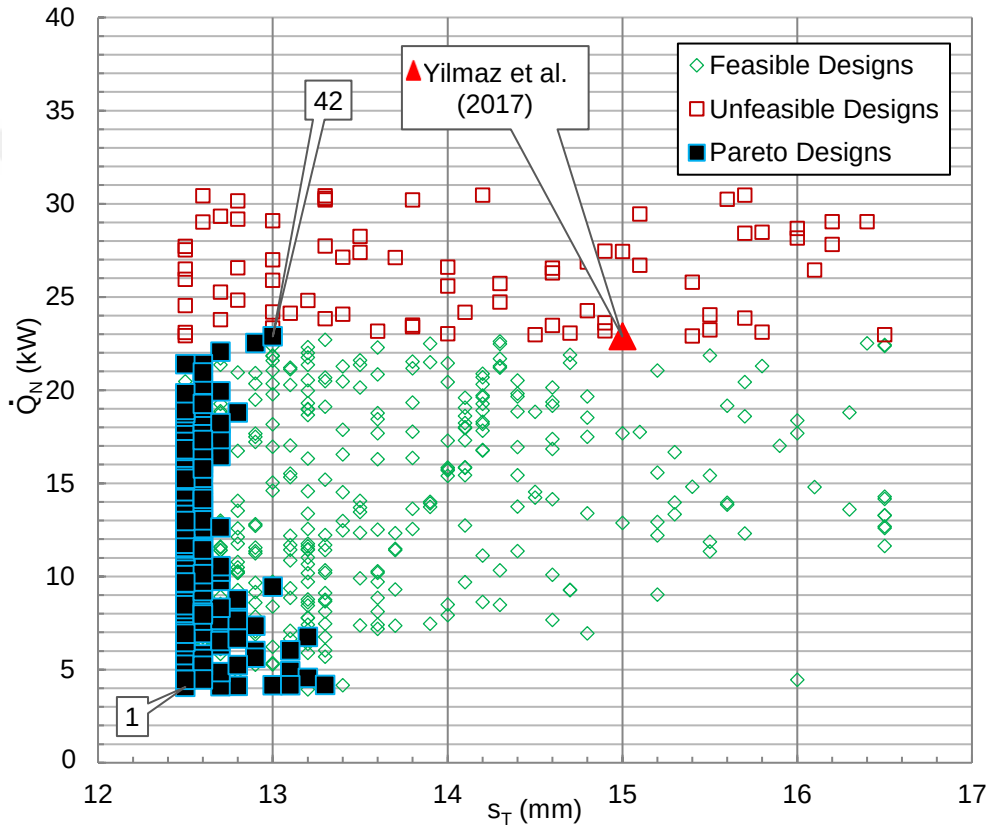


Figure 5.45. Variation of total heat transfer $\dot{Q}_N$ with transversal pitch s_T for all designs of unfinned staggered tube bank

For pareto design 42, longitudinal pitch is 13.50 mm and transversal pitch is 13.0 mm, Yilmaz et al.'s (2017) optimum design has to agree with $s_L^* = \frac{\sqrt{3}}{2} s_T^*$, pitches in longitudinal and transversal direction are given as 13 mm and 15 mm,

respectively (table 5.14). Yilmaz et al.'s (2017) optimum design pitches are different as compared to present unfinned staggered optimum design (pareto design 42) but total heat transfer $\dot{Q}_N$ and total volume V_N values have acceptable differences as it is stated previously.

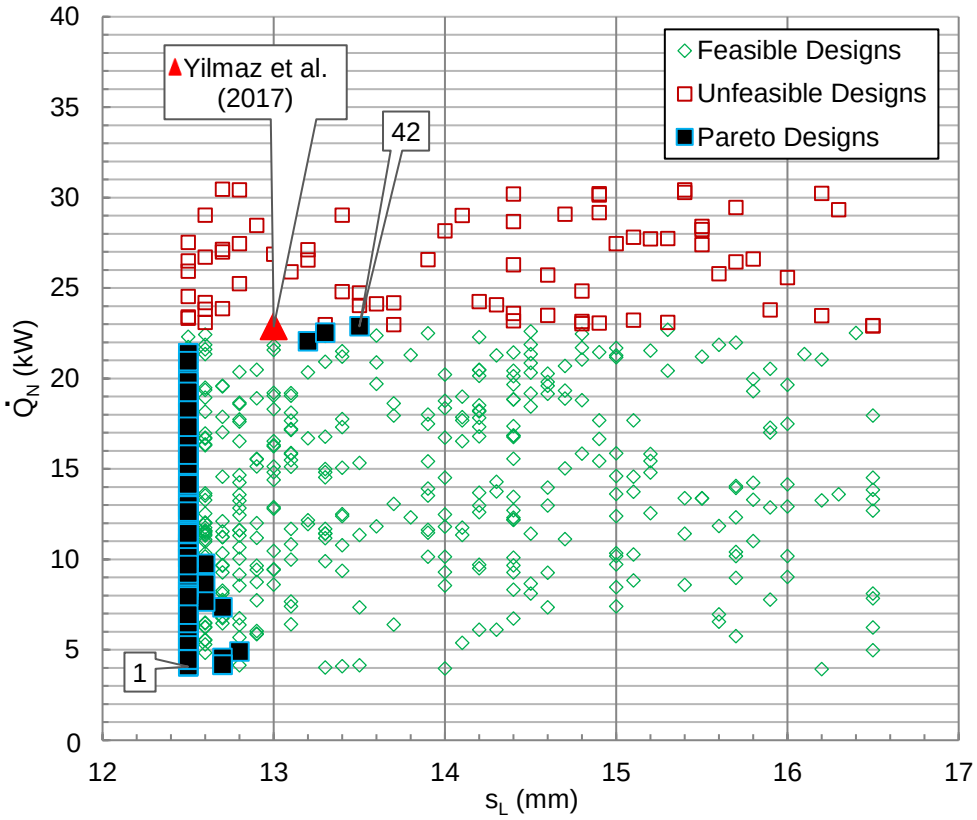


Figure 5.46. Variation of total heat transfer $\dot{Q}_N$ with longitudinal pitch s_L for all designs of unfinned staggered tube bank

The pareto designs are intense for the lower values of s_T and s_L, any pareto design can be chosen as an optimum design for the design purpose. For example, pareto design 1 has minimum volume (3.28E-03 m^3) while obtained heat transfer value (4.07 kW) is minimum as well. Similarly, longitudinal pitch and transversal

pitch values are same (12.5 mm) for pareto design 1. All designs are unfeasible when the total volume V_N is higher than closely 0.07 m^3 as it is shown in figures 5.47 and 5.48.

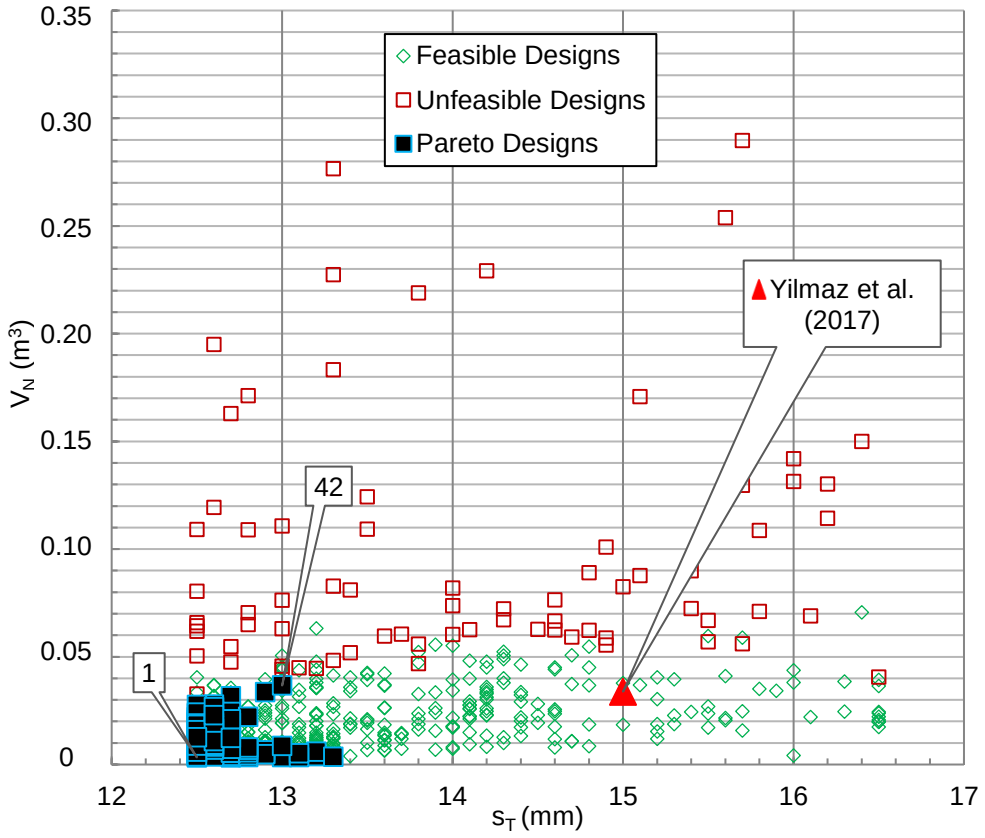


Figure 5.47. Variation of total volume V_N with transversal pitch s_T for all designs of unfinned staggered tube bank

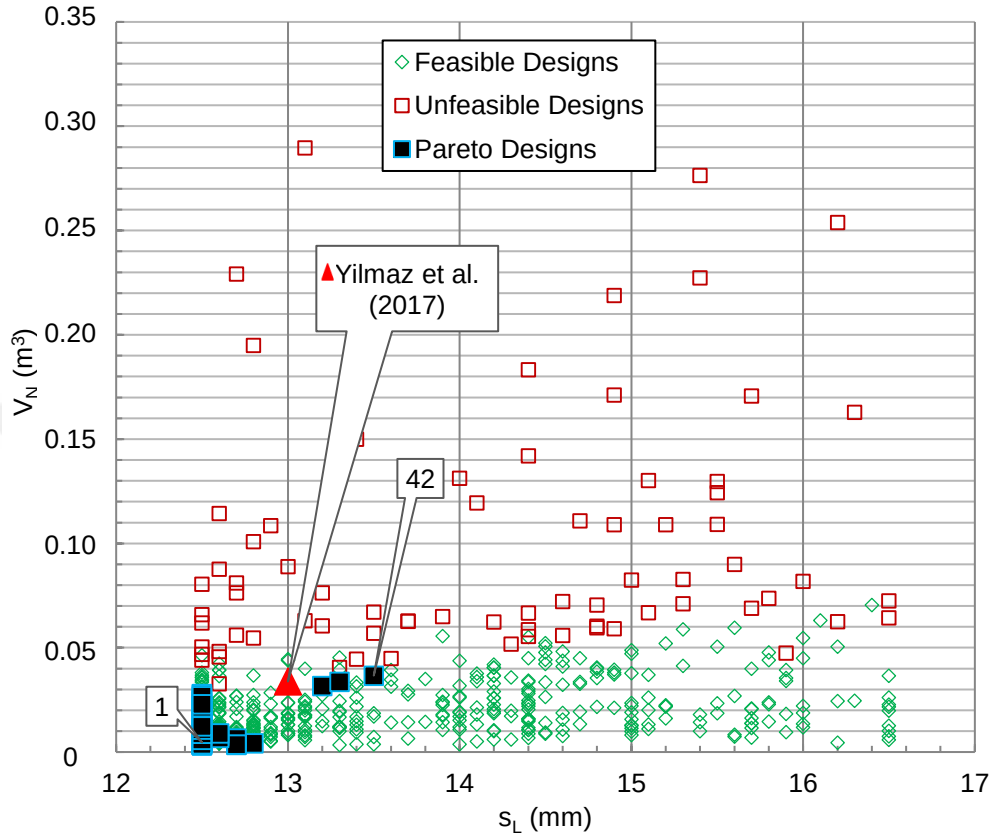


Figure 5.48. Variation of total volume V_N with longitudinal pitch s_L for all designs of unfinned staggered tube bank

5.4.2.2 Optimization Results of Axially Finned Staggered Tube Banks

Optimization workflow of axially finned staggered tube bank case is established similar to axially finned in-line tube bank optimization case which is given in figure 5.42. Fin thickness of axially finned staggered tube bank, t is given as an input variable again. Maximum obtainable heat transfer from axially finned staggered tube bank is $\dot{Q}_{max} = 30.51$ kW. The multi-objective design optimization problem is given as below:

Objective Function	Maximize $\dot{Q}_N$, Minimize V_N	(5.8)
Constraint	$\dot{Q}_N \leq 22.88$ kW	
Optimization Variables with their limits and step sizes	$12.5 \leq s_L \leq 20$, step size = 0.2 mm, $(0.75D \leq L_f \leq 1.5D)$, $1.0 \leq t \leq 1.5$, step size = 0.1 mm, $12.5 \leq s_T \leq 16.5$, step size = 0.1 mm, $10 \leq N_L \leq 50$, step size = 1, $10 \leq N_T \leq 40$, step size = 1, $0.5 \leq B \leq 1.2$, step size = 0.1 m.	
Given Data	$\dot{m}_N = 0.5$ kg/s, $\Delta p_{allow} = 100$ Pa, $T_i = 443.15$ K, $T_w = 383.15$ K, $D = 10$ mm, $\eta = 0.75$	

50 DOEs are formed with Sobol sequence, MOGA-II is selected to get pareto designs. Eventually, total number of 742 designs are found, 582 designs are feasible and 160 designs are unfeasible. 47 designs are selected as pareto design in this optimization study and these pareto designs are given in table 5.16. Pareto design 4 from table 5.16 is selected as an optimum design which has maximum heat transfer and minimum volume, also constraint of the optimization problem is satisfied.

Optimum designs of unfinned and axially finned staggered tube banks' volumes are $3.66E-2\ m^3$ and $2.10E-2\ m^3$. Axially finned staggered tube bank leads to 42.70% decrement in volume of staggered tube bank heat exchanger while obtained heat transfer values $\dot{Q}_N$ are same (22.88 kW). Moreover, fin length of

optimum axially finned staggered case is $L_f = 1.09D$ and fin thickness equals to 1.1 mm. So, axial fins for staggered configuration lead to obtain lower volume of tube bank while heat transfer values are equal for both unfinned and axially finned cases.

Optimum results are found nearly 74 hours and 15 minutes.

Table 5.16. Pareto designs for axially finned staggered tube bank optimization study

Id	s_L (mm)	s_T (mm)	L_f (D)	t (mm)	N_L	N_T	B (m)	$\dot{Q}_N$ (kW)	V_N (m^3)
1	12.50	12.50	0.75	1.1	10	10	0.50	12.25	7.81E-03
2	13.68	12.60	0.87	1.1	10	14	0.60	19.56	1.45E-02
3	14.47	12.50	0.95	1.1	10	10	0.50	14.07	9.05E-03
4	15.86	12.60	1.09	1.1	10	21	0.50	22.88	2.10E-02
5	14.28	12.50	0.93	1.1	10	10	0.70	18.04	1.25E-02
6	14.28	12.50	0.93	1.1	10	12	0.50	16.13	1.07E-02
7	13.49	12.50	0.85	1.1	10	10	0.70	17.42	1.18E-02
8	14.08	12.50	0.91	1.1	11	13	0.70	21.65	1.76E-02
9	14.08	12.50	0.91	1.1	10	13	0.50	17.03	1.14E-02
10	13.09	12.60	0.81	1.2	10	10	0.50	13.17	8.25E-03
11	13.68	12.50	0.87	1.1	10	13	0.50	16.80	1.11E-02
12	14.28	12.50	0.93	1.1	10	11	0.50	15.11	9.81E-03
13	12.89	12.50	0.79	1.1	10	10	0.90	19.64	1.45E-02
14	13.88	12.50	0.89	1.1	10	12	0.50	15.93	1.04E-02
15	14.28	12.50	0.93	1.1	10	13	0.50	17.11	1.16E-02
16	14.08	12.50	0.91	1.1	10	10	0.70	17.95	1.23E-02
17	14.08	12.50	0.91	1.1	10	13	0.60	19.34	1.37E-02
18	13.49	12.50	0.85	1.1	10	13	0.50	16.52	1.10E-02
19	14.08	12.50	0.91	1.1	10	10	0.60	16.06	1.06E-02
20	13.88	12.50	0.89	1.1	10	14	0.50	17.81	1.21E-02
21	13.09	12.50	0.81	1.1	10	10	0.50	13.10	8.18E-03
22	13.88	12.60	0.89	1.1	10	15	0.60	20.77	1.57E-02
23	13.88	12.50	0.89	1.1	10	12	0.60	18.17	1.25E-02
24	13.29	12.50	0.83	1.1	10	12	0.50	15.33	9.97E-03
25	13.88	12.60	0.89	1.1	10	16	0.60	21.63	1.68E-02
26	13.29	12.80	0.83	1.4	10	11	0.50	14.54	9.36E-03
27	14.28	12.50	0.93	1.1	10	10	0.50	14.04	8.92E-03

Table 5.16. continued …

Id	s_L (mm)	s_T (mm)	L_f (D)	t (mm)	N_L	N_T	B (m)	$\dot{Q}_N$ (kW)	V_N (m^3)
28	14.08	12.50	0.91	1.1	10	10	0.50	13.98	8.80E-03
29	14.08	12.70	0.91	1.3	10	11	0.50	15.16	9.83E-03
30	12.89	12.50	0.79	1.1	10	10	1.10	22.24	1.77E-02
31	13.88	12.50	0.89	1.1	10	10	0.50	13.86	8.68E-03
32	14.28	12.50	0.93	1.1	10	14	0.60	20.41	1.50E-02
33	13.68	12.70	0.87	1.3	10	11	0.50	14.88	9.56E-03
34	12.89	12.50	0.79	1.1	10	11	0.90	20.87	1.60E-02
35	13.88	12.70	0.89	1.3	10	11	0.50	14.99	9.70E-03
36	13.29	12.50	0.83	1.1	10	13	0.50	16.26	1.08E-02
37	13.88	12.50	0.89	1.1	10	13	0.60	19.19	1.35E-02
38	14.08	12.50	0.91	1.1	10	15	0.50	18.83	1.32E-02
39	13.88	12.60	0.89	1.1	10	15	0.70	22.85	1.84E-02
40	14.08	12.60	0.91	1.1	10	17	0.60	22.61	1.81E-02
41	14.47	12.50	0.95	1.1	10	13	0.60	19.47	1.41E-02
42	13.68	12.50	0.87	1.0	10	12	0.70	19.48	1.44E-02
43	13.29	12.50	0.83	1.1	10	11	0.50	14.35	9.14E-03
44	14.28	12.60	0.93	1.1	10	15	0.60	21.12	1.62E-02
45	13.29	12.50	0.83	1.1	10	10	0.50	13.32	8.31E-03
46	13.29	12.50	0.83	1.1	10	10	0.70	17.15	1.16E-02
47	14.08	12.60	0.91	1.1	10	15	0.60	20.91	1.60E-02

Feasible, unfeasible and pareto designs of the current multi-objective optimization study are shown in figures 5.49-5.53, unfinned staggered optimum design values (Section 5.4.2.1) are given in figures as well. It is possible to choose one of pareto designs arbitrarily as optimum design.

(a) Variation of objective function $\dot{Q}_N$ with objective function V_N

Figure 5.49 shows the variation of $\dot{Q}_N$ with V_N. In figure 5.49, optimum design of unfinned staggered tube bank values (pareto design 4) are given too. As it is stated previously, axially finned staggered tube bank's volume is 42.70% lower than unfinned one while same heat transfer values are found. Pareto designs of axially finned staggered tube bank reveal that decrement in volume result in heat transfer decrement as well.

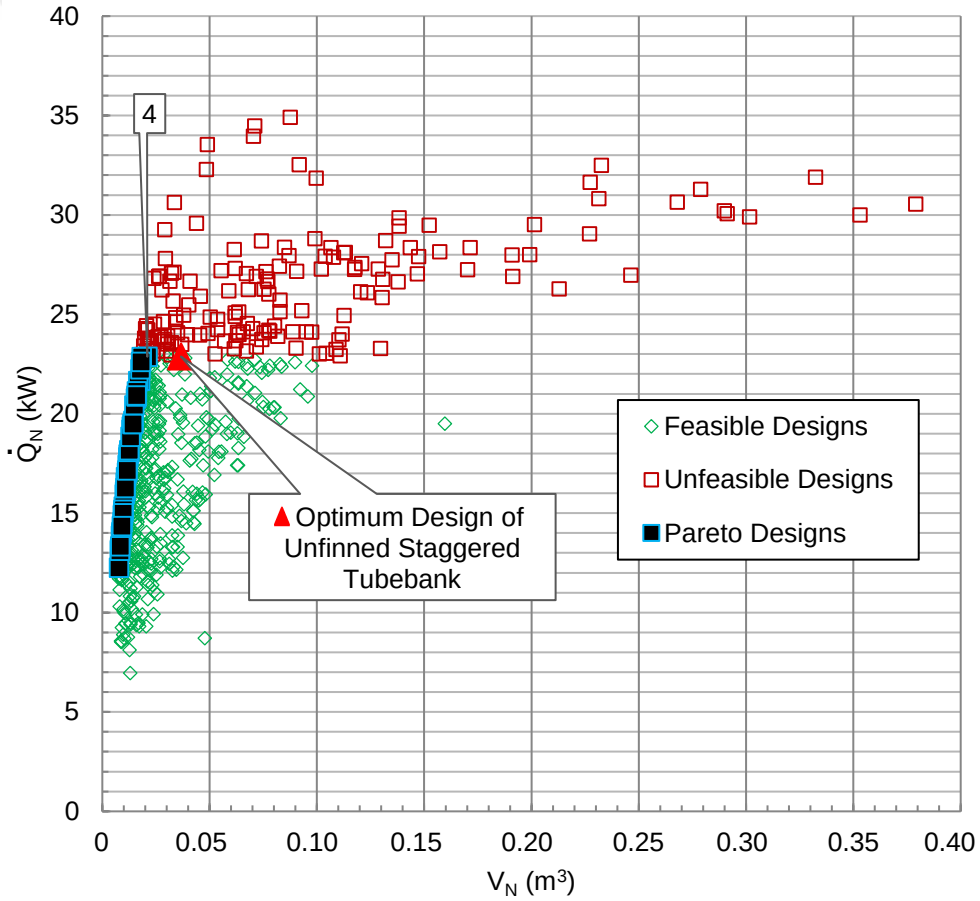


Figure 5.49. Variation of total heat transfer $\dot{Q}_N$ with total volume V_N for all designs of axially finned staggered tube bank

(b) Effect of pitches on objective functions $\dot{Q}_N$ and V_N

Variations of transversal and longitudinal pitches vs. $\dot{Q}_N$ are shown for all designs in figures 5.50 and 5.51, respectively. Besides, variations of transversal and longitudinal pitches with respect to V_N are given in figures 5.52 and 5.53, respectively.

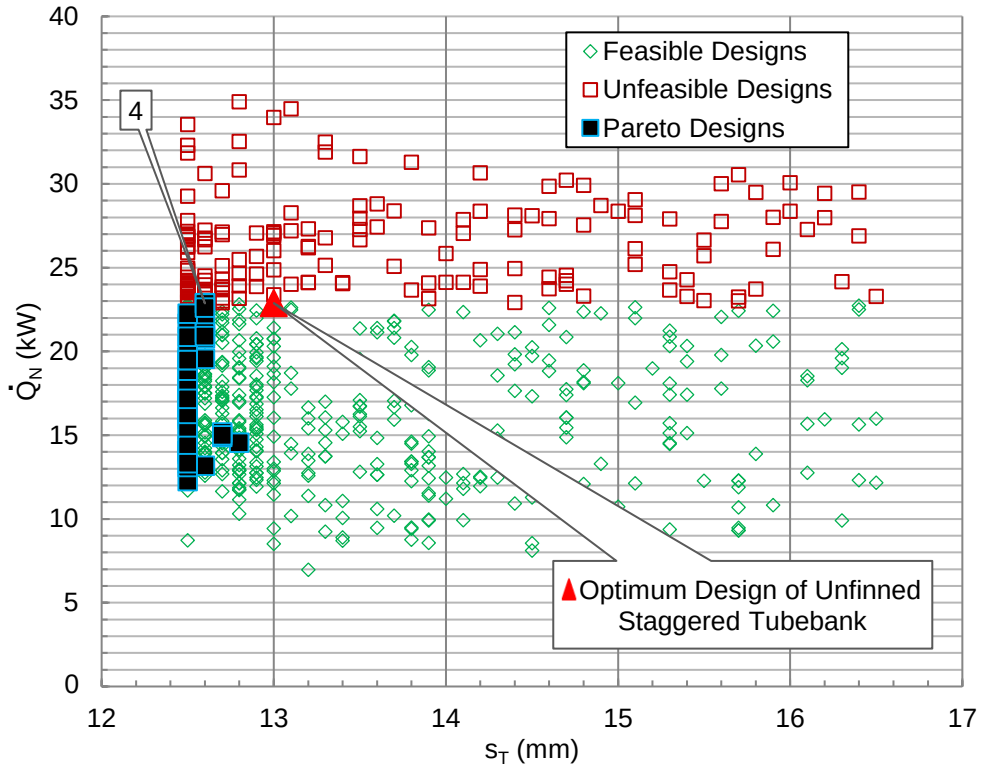


Figure 5.50. Variation of total heat transfer $\dot{Q}_N$ with transversal pitch s_T for all designs of axially finned staggered tube bank

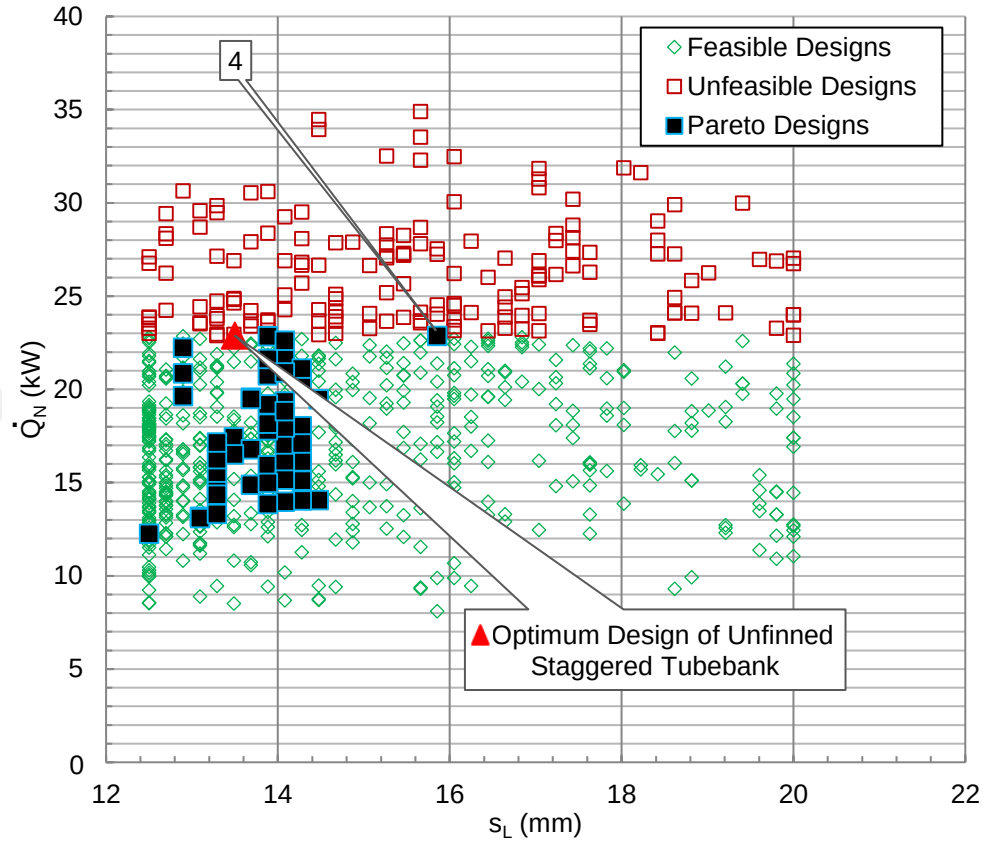


Figure 5.51. Variation of total heat transfer $\dot{Q}_N$ with longitudinal pitch s_L for all designs of axially finned staggered tube bank

Longitudinal pitch is 15.86 mm and transversal pitch is 12.60 mm for optimum design of axially finned staggered tube bank (pareto design 4), however unfinned staggered optimum design pitches in longitudinal and transversal direction are given as 13.5 mm and 13.0 mm respectively. The axially finned optimum design's pitches are different as compared to unfinned staggered optimum design. In the lower values of s_T and s_L, pareto designs are dense. When the total volume V_N is higher than nearly 0.16 m^3, designs are unfeasible as it is shown in figures 5.52 and 5.53.

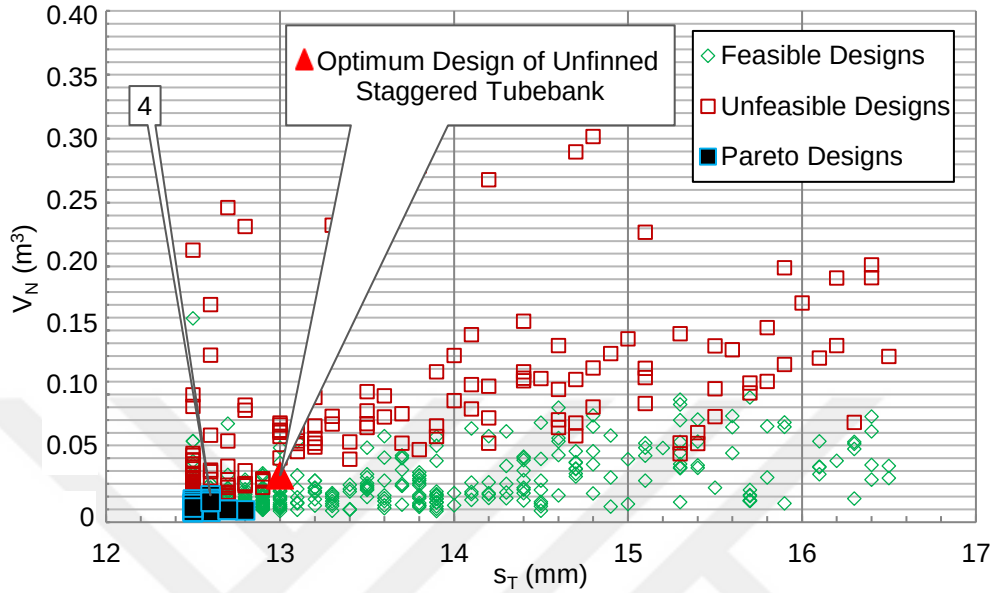


Figure 5.52. Variation of total volume V_N with transversal pitch s_T for all designs of axially finned staggered tube bank

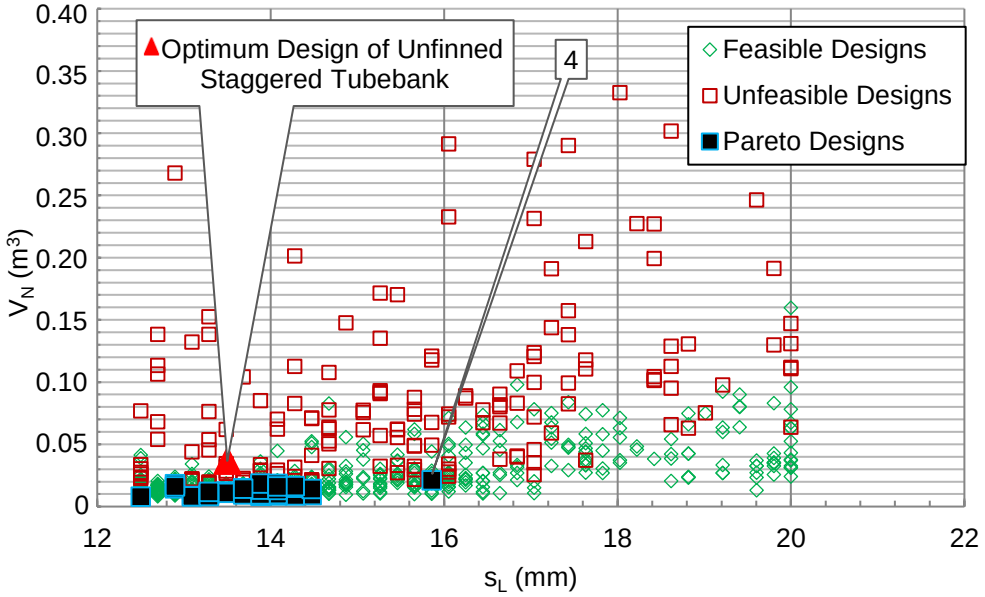


Figure 5.53. Variation of total volume V_N with longitudinal pitch s_L for all designs of axially finned staggered tube bank

6. CONCLUSIONS and FUTURE WORK

Numerical calculations of heat and fluid flow of in-line and staggered tube banks are studied for both unfinned and axially finned cases in this work. In the first part of study, heat transfer and pressure loss calculations for in-line and staggered axially finned tube banks in cross-flow is performed numerically and the effect of the fin lengths (D, 2D) for four cases (tables 5.1 and 5.6) are presented for two Prandtl numbers 0.7 and 7. Reynolds number values lie between 400 and 1500. Then, obtained results are compared each other. The following conclusions can be drawn.

For unfinned and axially finned in-line tube banks;

- The results indicate that the friction factor and average Nusselt number depend on the axial and transversal pitches, fin lengths, Reynolds numbers. Average Nusselt numbers are effected by Prandtl numbers also.
- Axial finning of in-line tube banks lead to significant increase in heat transfer. It is clear that the increment in Re number causes higher turbulence so that the enhancement of heat transfer is higher at higher Re values.
- For $s_L^* = 3$, $s_T^* = 1.5$, it can be seen from D-Finned computation results (table 5.2a) that heat transfer is maximum at Re = 1500 where 45.96% and 56.80% increment in average Nusselt number ($\overline{Nu}^+$) is observed for $Pr = 0.7$ and $Pr = 7$, respectively. Axial finning causes friction factor decrease as can be seen from figure 5.4. For Re = 400, D-Finned case has 23.73% decrement in friction factor (f^+).
- For $s_L^* = 3$, $s_T^* = 2$ and Pr = 7, average Nusselt number ($\overline{Nu}^+$) enhancement of 59.71% is obtained with respect to unfinned case at Re

= 1500. Also, friction factor is 24.91% (f^+) lower than unfinned case for Re = 1500.

- For $s_L^* = 5$, $s_T^* = 1.5$ and Pr = 0.7, D-Finned case leads to average Nusselt number ($\overline{Nu}^+$) enhancement of 55.90% while 2D-Finned case has average Nusselt number ($\overline{Nu}^{+,D}$) enhancement of 93.42% with respect to unfinned case at Re = 1500. Moreover, 2D-Finned case has average Nusselt number ($\overline{Nu}^{+,D}$) enhancement of 24.07% with respect to D-Finned case. Friction factor either decreases while fin length is increased from D-Finned to 2D-Finned.
- For $s_L^* = 5$, $s_T^* = 2$ and Pr = 7, D-Finned case leads to average Nusselt number ($\overline{Nu}^+$) enhancement of 68.08% with respect to unfinned case at Re = 1500, also 2D-Finned case has average Nusselt number ($\overline{Nu}^{+,D}$) enhancement of 102.92% with respect to unfinned case. Compared with the 127% and 254% of surface area increase, one can see that 58% and 40.5% of these values are arrived. However, friction factor is decreased (f^+) 18.72% for D-Finned case with respect to unfinned case while for 2D-Finned case 27.16% decrement (f_D^+) is observed as compared to unfinned case at Re = 1500.
- For a prescribed Reynolds number, increasing s_T^* from 1.5 to 2 contribute very little to the total heat transfer, but finning decreases friction factor.
- At Re = 1500 and Pr = 0.7, 2D-Finned case of $s_L^* = 5$ and $s_T^* = 2$ shows 34.50% $\overline{Nu}$ increment as compared to D-Finned case of $s_L^* = 3$ and $s_T^* = 2$. But f is increased from 0.30 to 0.32, so 3.55% f increment is observed for Re = 1500.

For unfinned and axially finned staggered tube banks;

- The results reveal that the axial and transversal pitches, fin lengths, Reynolds numbers influence average Nusselt number and friction factor. Moreover, Prandtl numbers affect average Nusselt numbers.
- Heat transfer increases substantially for longer fins and it can be seen that higher Re numbers have higher heat transfer values.
- 2D-Finned case of $s_L^* = 3,\ s_T^* = 1.5$ computation results (table 5.7a) reveal that heat transfer is maximum at Re = 1500 where 199.05% and 200.77% enhancement in average Nusselt number ($\overline{Nu}^+$) are obtained for $Pr = 0.7$ and $Pr = 7$, respectively. Axial finning causes friction factor decrement for D-Finned case and increment for 2D-Finned case according to unfinned case as can be seen from figure 5.20. For Re = 400, D-Finned case has 11.78% decrement to unfinned case and 2D-Finned case has 42.32% increment to D-Finned case.
- For 2D-Finned case of $s_L^* = 3,\ s_T^* = 2$ and Pr = 7, 190.33% increment in average Nusselt number ($\overline{Nu}^+$) is attained to unfinned case at Re = 1500. This value is fewer than 254% of the surface area increase by the reason of axial finning. Similarly, friction factor is 49.43% (f^+) higher than D-Finned case, for Re = 1500.
- D-Finned case of $s_L^* = 5,\ s_T^* = 1.5$ and Pr = 0.7 result in 58.19% increment in average Nusselt number ($\overline{Nu}^+$) while 2D-Finned case has 133.27% increment in average Nusselt number ($\overline{Nu}^{+,D}$) as compared to unfinned case at Re = 1500. Also, 2D-Finned case increases average Nusselt number ($\overline{Nu}^{+,D}$) 47.46% when compared to D-Finned case. Friction factor increases for 2D-Finned case as compared to D-Finned case (table 5.9b).

- For D-Finned case of $s_L^* = 5$, $s_T^* = 2$ and Pr = 7 leads to 76.81% enhancement in average Nusselt number ($\overline{Nu}^+$) as compared to unfinned case at Re = 1500, besides 2D-Finned case has 157.85% increment in average Nusselt number ($\overline{Nu}^{+,D}$) with respect to unfinned case. 60.5% and 62.1% of heat transfer increment values are obtained where 127% and 254% are surface area increment values. Friction factor decreases (f^+) 15.24% for D-Finned case to unfinned case while for 2D-Finned case 10.31% decrement (f_D^+) is obtained as compared to unfinned case at Re = 1500.
- Increasing s_T^* from 1.5 to 2.0 for studied cases does not cause a big change in average Nusselt numbers for both Prandtl values of 0.7 and 7. However, the values of f decrease with the use of $s_T^* = 2$. Almost the same heat transfer is obtained with a lower pressure drop at $s_T^* = 2$. The only disadvantage is that the heat exchanger size is larger for $s_T^* = 2$.
- Increasing s_T^* from 1.5 to 2.0 for all studied cases, average Nusselt number decreases only for 2D-Finned case of $s_L^* = 3$ where Re = 1500 and Pr = 0.7. However, f values decrease with the use of $s_T^* = 2$. Obtained heat transfer values are almost same with a lower pressure drop for $s_T^* = 2$, but heat exchanger has greater size.

In the second part of the study, optimization of heat and fluid flow over in-line and staggered tube banks for both unfinned and axially finned cases are examined numerically. Optimization problem has two goals: (1) maximization of total heat transfer from tube bank (2) minimization of tube bank volume, also obtainable heat transfer is given as a constraint. The objectives of the present numerical optimization studies are to get maximum heat transfer and minimum volume of tube bank for an allowable pressure drop and tube bank effectiveness

which was previously studied by Yilmaz and Yilmaz (2016) and Yilmaz et al. (2017). The following results are found:

- Pareto designs indicate optimum designs where one objective gets preferable and the other one is worsened. Pareto designs reveal that a little heat transfer reduction lead to significant decrement in volume of tube bank.
- Maximization of total heat transfer from tube bank $\dot{Q}_N$ is enhanced while minimization of tube bank volume V_N are worse for the pareto designs.
- For the present unfinned optimum in-line tube bank design, $\dot{Q}_N$ is same and V_N is lower 3.25% as compared to Yilmaz and Yilmaz's (2016) optimum design.
- The heat transfer values $\dot{Q}_N$ for Yilmaz et al. (2017) and present optimum unfinned staggered design are equal and V_N is 7.65% higher than Yilmaz et al.'s (2017) optimum design.
- Axial fins do not decrease volume for the given optimization study of in-line tube bank.
- Unfinned optimum in-line tube bank design has 38.80% higher volume than optimum unfinned staggered tube bank design while obtained heat transfer values are same.
- Optimum axially finned staggered design cause 42.70% volume decrement as compared to unfinned optimum staggered design for the same given data as obtained heat transfer values (22.88 kW) are same for each cases.
- Optimum axially finned staggered tube bank's fin length (L_f) and thickness (t) are 1.09D and 1.1 mm, respectively.
- Axial fins are practical with staggered tube banks because they provide lower volume and same heat transfer with respect to unfinned ones. But, for

in-line arrangements, increment in fin length increases volume of tube bank too and it is not convenient for the design purpose of this study.

For future works, it is recommended to use parallel algorithms for optimization studies to reduce computation times. Parallel algorithms can not be used with Modefrontier, so MOGA-II algorithm can be written in a programming language and the written code can be enabled for parallel programming. Morover, it is clear from numerical calculations that staggered tube banks with axial fins are very effective, so it can be validated with experimental studies in future.

REFERENCES

Abdel-Rehim, Z. S., 2012. A Numerical Study of Heat Transfer and Fluid Flow over an In-line Tube Bank. Energy Sources, Part A, 34, 2123–2136.

Akkoca, A., 2004. Computational Modeling of Turbulent Heat Transfer in Plate Fin and Tube Heat Exchangers. Çukurova University Institute of Natural and Applied Sciences, PhD. Thesis, Adana, 230p.

Aiba, S., Tsuchida, H. and Ota, T., 1982. Heat Transfer around Tubes in Staggered Tube Banks. Bulletin of the JSME, 25 (204), 927-933.

Ansys Fluent User's Guide.

Beale, S. B., 1992. Fluid Flow and Heat Transfer in Tube Banks. Imperial College, PhD. Thesis, London.

Beale, S. B. and Spalding, D. B., 1998. Numerical Study of Fluid Flow and Heat Transfer in Tube Banks with Stream-wise Periodic Boundary Conditions. Trans. CSME, 22(4A), 397-416.

Beale, S., 2008. Benchmark Studies for the Generalized Streamwise Periodic Heat Transfer Problem. Journal of Heat Transfer, 130, 114502-1/4.

Bejan, A., Fowler, A. J. and Stanescu, G., 1995. The Optimal Spacing between Horizontal Cylinders in a Fixed Volume Cooled by Natural Convection. Int. J. of Heat and Mass Transfer, 38 (11), 2047-2055.

Bergelin, O. P., Brown, G. A., Hull, H. L. and Sullivan, F. W., 1950. Heat Transfer and Fluid Friction during Viscous Flow across Banks of Tubes-III: A Study of Tube Spacing and Tube Size. Trans. A. Sot. Mech. Engrs., 72, 881-888.

Bergelin, O. P., Brown, G. A. and Doberstein, S. C., 1952. Heat Transfer and Fluid Friction during Flow across Banks of Tubes-IV: A Study of the Transition Zone between Viscous and Turbulent Row. Trans. A. Sot. Mech. Engrs., 74, 953-960.

Bordalo, S. N. and Saboya, F. E. M., 1995. Experimental Determination of Pressure Drop Coefficients in Circular and Elliptical Tubes and Plate Fin Heat Exchangers. Proc. 13th COBEM, Brazilian Conference on Mechanical Engineering, Belo Horizonte, Brazil.

Brauer, H., 1964. Compact Heat Exchangers. Chem. Process Eng., 8, 451-460.

Buyruk, E.,1999. Heat Transfer and Flow Structures around Circular Cylinders in Cross-flow. Tr. J. of Engineering and Environmental Science, 23, 299-315.

Buyruk, E., 2002. Numerical Study of Heat Transfer Characteristics on Tandem Cylinders, Inline and Staggered Tube Banks in Cross-flow of Air. Int. Comm. Heat Mass Transfer, 29(3), 355-366.

Chu, P., He, Y. L. and Tao, W. Q., 2009. Three-Dimensional Numerical Study of Flow and Heat Transfer Enhancement Using Vortex Generators in Fin-and-tube Heat Exchangers. Journal of Heat Transfer, 131, 091903-1/9.

Colburn, A. P., 1933. A Method of Correlating Forced Convection Heat Transfer Data and a Comparison with Fluid Friction. Trans. A. Inst. Chem. Eng., 29, 174-210.

Damavandi, M. D., Forouzanmehr, M. and Safikhani, H., 2017. Modeling and Pareto Based Multi-objective Optimization of Wavy Fin-and-elliptical Tube Heat Exchangers Using CFD and NSGA-II Algorithm. Applied Thermal Engineering, 111, 325–339.

Dhaubhadel, M. N., Reddy, J. N. and Telionis, D. P., 1987. Finite Element Analysis of Fluid Flow and Heat Transfer for Staggered Banks of Cylinders in Cross Flow. Int. J. Numer. Methods Fluids, 7, 1325-1342.

Du, X., Zeng, M., Wang, Q. and Dong, Z., 2014. Experimental Investigation of Heat Transfer and Resistance Characteristics of a Finned Oval-tube Heat Exchanger with Different Air Inlet Angles. Heat Transfer Engineering, 35, 703-710.

El-Shaboury, A. M. F. and Ormiston, S. J., 2005. Analysis of Laminar Forced Convection of Air Crossflow in In-line Tube Banks with Nonsquare Arrangements. Numerical Heat Transfer, Part A, 48, 99-126.

Engineering Sciences Data Unit, 1980. Pressure Loss during Crossflow of Fluids with Heat Transfer over Plain Tube Banks without Baffles. ESDU Data Item No. 74040, London.

Engineering Sciences Data Unit, 1973. Convective Heat Transfer During Crossflow of Fluids over Plain Tube Banks. ESDU Data Item No. 73031, London.

Faghri, M. and Rao, N., 1987. Numerical Computation of Flow and Heat Transfer in Finned and Unfinned Tube Banks. Int. J. Heat Mass Transfer, 30, 363-372.

Fowler, A. J., Ledezma, G. A. and Bejan, A., 1997. Optimal Geometric Arrangement of Staggered Plates in Forced Convection. Int. J. of Heat and Mass Transfer, 40 (8), 1795-1805.

Fujii, M. and Fujii, T., 1984. A Numerical Analysis of Laminar Flow and Heat Transfer of Air in an In-line Tube Bank. Numerical Heat Transfer, 7, 89-102.

Gaddis, E. S., 2010. Pressure Drop of Tube Bundles in Cross Flow. VDI Heat Atlas, Berlin, 1076-1091.

Gharbi, N. E., Kheiri, A., Ganaoui, M. E. and Blanchard, R., 2015. Numerical Optimization of Heat Exchangers with Circular and Non-circular Shapes. Case Studies in Thermal Engineering, 6, 194-203.

Gholami, A., Wahid, M. A. and Mohammed H. A., 2017. Thermal–hydraulic Performance of Fin-and-oval Tube Compact Heat Exchangers with Innovative Design of Corrugated Fin Patterns. Int. J. of Heat and Mass Transfer, 106, 573-592.

Gnielinski, V., 2010. Heat Transfer in Cross Flow around Single Rows of Tubes and Through Tube Bundles. VDI Heat Atlas, Berlin, 725-729.

Goldstein, L. G. and Sparrow, E. M., 1976. Experiments on the Transfer Characteristics of a Corrugated Fin and Tube Heat Exchanger Configuration. J. Heat Transfer, Trans ASME, February, 26-32.

Grannis, V. B. and Sparrow, E. M., 1991. Numerical Simulation of Fluid Flow Through an Array of Diamond-Shaped Pin Fins. Numerical Heat Transfer, Part A, 19, 38143.

Grimison, E. D., 1937. Correlation and Utilization of New Data on Flow Resistance and Heat Transfer for Cross Flow of Gases over Tube Banks. Trans. ASME, 59, 583-594.

Haitham, M. S. B., Anand, N. K. and Chen, H. C., 2005. A Numerical Study of Fluid Flow and Heat Transfer over a Bank of Flat Tubes. Numerical Heat Transfer, Part A, 48, 359-385.

Hilpert, R., 1933. Waermeabgabe Von Geheizten Rohren and Graehten. Forschung Auf Dem Gebiet Des Ingenieurwesens A, 4(5), 215–224.

Horvat, A., Leskovar, M. and Mavko, B., 2005. Comparison of Heat Transfer Conditions in Tube Bundle Cross-flow for Different Tube Shapes. Int. J. of Heat and Mass Transfer, 49, 1027-1038.

Huge, E. C., 1937. Experimental Investigation of Effects of Equipment Size on Convection Heat Transfer and Flow Resistance in Cross Flow of Gases over Tube Banks. Trans. ASME, 59, 573-581.

Ibrahim, E. and Moawed, M., 2009. Forced Convection and Entropy Generation from Elliptic Tubes with Longitudinal Fins. Energy Conversion and Management, 50, 1946-1954.

Igci, A. A. and Arici, M. E., 2016. A Comparative Study of Four Low-Reynolds-number k-ε Turbulence Models for Periodic Fully Developed Duct Flow and Heat Transfer. Numerical Heat Transfer, Part B, 69 (3), 234-248.

Lavasani, A. M. and Bayat, H., 2014. Experimental Study of Convective Heat Transfer From In-line Cam Shaped Tube Bank in Crossflow. Applied Thermal Engineering, 65, 85-93.

Lavasani, A. M. and Bayat, H., 2016. Numerical Study of Pressure Drop and Heat Transfer from Circular and Cam-shaped Tube Bank in Cross-flow of Nanofluid. Energy Conversion and Management, 129, 319-328.

Li, Y., Wu, J. and Wang, H., 2012. Fluid Flow and Heat Transfer Characteristics in Helical Tubes Cooperating with Spirally Corrugation. Energy Procedia, 17, 791-800.

Jaw, S. Y. and Chen, C. J., 1996. Present Status of k-ε Turbulence Models and their Achievements. Flow Modeling and Turbulence Measurements, Rotterdam, ISBN:9054108266.

Jayavel, S. and Tiwari, S., 2009. Numerical Study of Heat Transfer and Pressure Drop for Flow Past Inline and Staggered Tube Bundles. Int. J. Numer. Methods Heat Fluid Flow, 19 (8), 931-949.

Jeong, J. H., Ki, W. N., June, K. M., Kui, S. K. and Man, Y. H., 2011. The Effects of the Evaluation Method on the Average Heat Transfer Coefficient for a Mini-Channel Tube Bundle. Int. J. of Heat and Mass Transfer, 54, 5481-5490.

Jin, Y., Gui-Hua, T., Ya-Ling, H. and Wen-Quan, T., 2013. Parametric Study and Field Synergy Principle Analysis of H-Type Finned Tube Bank with 10 Rows. Int. J. of Heat and Mass Transfer, 60, 241-251.

Jin, Z., Chen, F., Gao, Z., Gao, X. and Qian, J., 2017. Effects of Pitch and Corrugation Depth on Heat Transfer Characteristics in Six-Start Spirally Corrugated Tube. Int. J. of Heat and Mass Transfer, 108, 1011-1025.

Joyner, U. T. and Palmer, C. B., 1943. An Experimental Survey of Flow Across Banks of Elliptical and Pointed Tubes. NACA-Report No: L-609.

Kays, W. M. and London, A. L., 1964. Compact Heat Exchangers. McGraw Hill, New York.

Khan, W. A., Culham, R. J., and Yovanovich, M. M., 2005. Fluid Flow around and Heat Transfer from Elliptical Cylinders: Analytical Approach. J. of Thermophysics and Heat Transfer, 19(2), 178-185.

Khan, W. A., Culham, J. R. and Yovanovich, M. M., 2006. Heat Transfer and Flow Structures around Circular Cylinders in Cross-Flow. International Journal of Heat and Mass Transfer, 49, 4831-4838.

Khan, W. A. and Khan, O. U., 2016. Analytical/Numerical Study of Fluid Flow and Heat Transfer across In-Line Cylinders. J. of Thermophysics and Heat Transfer, 30 (3), 490-498.

Kim, N., Lee, K., Han, J. and Choi, B., 2013. Thermal Performance of Sine Wave Fin-and-oval Tube Heat Exchangers. Int. J. of Air Conditioning and Refrigeration, 21(1).

Mandhani, V.K., Chhaabra, R. P. and Eswaran, V., 2002. Forced Convection Heat Transfer in Tube Banks in Cross Flow, Chem. Eng. Sci., 57, 379-391.

Mangrulkar, C. K., Dhoble, A. S., Deshmukh, A. R. and Mandavgane, S. A., 2017. Numerical Investigation of Heat Transfer and Friction Factor Characteristics from In-line Cam Shaped Tube Bank in Crossflow. Applied Thermal Engineering, 110, 521-538.

Mangrulkar, C. K., Dhoble, A. S., Chakrabarty, S. G. and Wankhede, U. S., 2017. Experimental and CFD Prediction of Heat Transfer and Friction Factor Characteristics in Cross Flow Tube Bank with Integral Splitter Plate. Int. J. of Heat and Mass Transfer, 104, 964-978.

Matos, R. S., Vargas, J. V. C., Laursen, T. A. and Saboya, F. E. M., 2001. Optimization Study and Heat Transfer Comparison of Staggered Circular and Elliptic Tubes in Forced Convection. Int. J. Heat and Mass Transfer, 44, 3953-3961.

Matos, R. S., Laursen, T. A., Vargas, J. V. C. and Bejan, A., 2004. Three Dimensional Optimization of Staggered Finned Circular and Elliptic Tubes in Forced Convection. Int. J. Therm. Sci., 43, 477-487.

Modefrontier User Manual.

Murray, D. B. and Fitzpatrick, J. A., 1988. Local Heat Transfer Coefficients for a Tube Array Using a Micro-Foil Heat Flow Sensor. Proc. 2nd U. K. Nat. Conf. on Heat Transfer, 2, 1635-1649.

Patankar, S. V., Liu, C. H. and Sparrow, E. M., 1977. Fully Developed Flow and Heat Transfer in Ducts Having Streamwise Periodic Variation of Cross-Sectional Area. J. of Heat Transfer, 99, 180-186.

Pierson, O. L., 1937. Experimental Investigation of the Influence of Tube Arrangement on Convection Heat Transfer and Flow Resistance in Cross Flow of Gases over Tube Banks. Trans. ASME, 59, 563-572.

Poskas, P. S. and Survila, V. J., 1983. Fluctuations of Velocity Cross-flow of Air in the Space between Tubes in Bundle. Heat Transfer Soviet Research, 15 (1), 75-86.

Rahmani, R., Mirzaee, I. and Shirvani, H., 2005. Computation of a Laminar Flow and Heat Transfer of Air for Staggered Tube Arrays in Cross-flow. Iranian Journal of Mechanical Engineering, 6(2).

Rainieri, S., Bozzoli, F. and Pagliarini, G., 2012a. Experimental Investigation on the Convective Heat Transfer in Straight and Coiled Corrugated Tubes for Highly Viscous Fluids: Preliminary Results. Int. J. of Heat and Mass Transfer, 55 (1), 498-504.

Rainieri, S., Bozzoli, F. and Cattani, L., 2012b. Experimental Investigation on the Convective Heat Transfer Enhancement for Highly Viscous Fluids in Helical Coiled Corrugated Tubes. Journal of Physics, Conference Series, 395(1), 012032.

Ranut, P., Janiga, G., Nobile, E. and Thévenin, D., 2014. Multi-objective Shape Optimization of a Tube Bundle in Cross-flow. Int. J. of Heat and Mass Transfer, 68, 585-598.

Rashidi, S., Bovand, M. and Esfahai, J. A., 2015. Heat Transfer Enhancement and Pressure Drop Penalty in Porous Solar Heat Exchangers: A Sensitivity Analysis. Energy Conversion and Management, 103, October, 726-738.

Rocha, L. A. O., Saboya, F. E. M., Vargas and J. V. C., 1997. A Comparative Study of Elliptical and Circular Sections in One- and Two-row Tubes and Plate Fin Heat Exchangers. Int. J. Heat and Fluid Flow, 18, 247-252.

Sayed Ahmed, S. E., Ibrahiem, E. Z., Mesalhy, O. M. and Abdelatief, M. A., 2014. Heat Transfer Characteristics of Staggered Wing-shaped Tubes Bundle at Different Angles of Attack. Heat Mass Transfer, 50, 1091-1102.

Sayed Ahmed, S. E., Mesalhy, O. M. and Abdelatief M. A., 2016. Heat Transfer Characteristics and Entropy Generation for Wing-shaped-tubes with Longitudinal External Fins in Cross-flow. Journal of Mechanical Science and Technology, 30 (6), 2849-2863.

Sparrow, E. M. and Kang, S. S., 1984. Longitudinally-finned Cross-flow Tube Banks and their Heat Transfer and Pressure Drop Characteristics. Int. J. Heat Mass Transfer, 28, 339-350.

Shi, Z. and Dong, T., 2015. Entropy Generation and Optimization of Laminar Convective Heat Transfer and Fluid Flow in a Microchannel with Staggered Arrays of Pin Fin Structure with Tip Clearance. Energy Conversion and Management, 94, 493-504.

Stanescu, G., Fowler, A. J. and Bejan, A., 1996. The Optimal Spacing of Cylinders in Free-stream Cross-flow Forced Convection. Int. J. of Heat and Mass Transfer, 39 (2), 311-317.

Tahseen, A., Ishak, M. and Rahman, M. M., 2013. Laminar Forced Convection Heat Transfer over Staggered Circular Tube Banks. Jourrnal of Mechanical Engineering and Sciences, 4, 418-430.

Tahseen, A., Ishak, M. and Rahman, M. M., 2015. An Overview on Thermal and Fluid Flow Characteristics in a Plain Plate Finned and Un-Finned Tube Banks Heat Exchanger. Renewable and Sustainable Energy Reviews, 43, 363-380.

Talaat, A. I. and Gomaa, A., 2009. Thermal Performance Criteria of Elliptic Tube Bundle in Crossflow. International Journal of Thermal Sciences, 48, 2148-2158.

Tang, L. H., Zeng, M. and Wang, Q. W., 2009. Experimental and Numerical Investigation on Air-side Performance of Fin-and-tube Heat Exchangers with Various Fin Patterns. Exp. Therm. Fluid Sci., 33, 818-27.

Tian, E., Ya-Ling, H. and Wen-Quan, T., 2015. Numerical Simulation of Finned Tube Bank across a Staggered Circular-pin-finned Tube Bundle. Numerical Heat Transfer, Part A, 68, 737-760.

Wang, C. C., Fu, W. L. and Chang, C. T., 1997. Heat Transfer and Friction Characteristics of Typical Wavy Fin-and-tube Heat Exchangers. Experimental Thermal and Fluid Science, 14, 174-186.

Wilson, A. S. and Bassiouny, M. K., 2000. Modeling of Heat Transfer for Flow across Tube Banks. Chem. Eng. Process, 39, 1-14.

Wung, T. S. and Chen, C. J., 1989. Finite Analytic Solution of Convective Heat Transfer for Tube Arrays in Crossflow. ASME J. Heat Transfer, 111, 641-648.

Yilmaz, A., Yilmaz, T. and Büyükalaca, O., 2000. Optimum Shape and Dimensions of Ducts for Convective Heat Transfer in Laminar Flow at Constant Wall Temperature. Int. J. of Heat and Mass Transfer, 43 (5), 767-775.

Yilmaz, A., 2008. Optimum Length of Tubes for Heat Transfer in Turbulent Flow at Constant Wall Temperature. Int. J. of Heat and Mass Transfer, 51 (13-14), 3478-3485.

Yilmaz, A., 2009. Minimum Entropy Generation for Laminar Flow at Constant Wall Temperature in a Circular Duct for Optimum Design. Heat and Mass Transfer, 45 (11), 1415-1421.

Yilmaz, A. and Yilmaz, T., 2016. Optimum Design of Cross-flow In-line Tube Banks at Constant Wall Temperature. Heat Transfer Engineering, 37(6), 523-534.

Yilmaz, A., Erdinç, M. T. and Yilmaz, T., 2017. Optimization of Crossflow Staggered Tube Banks for Prescribed Pressure Loss and Effectiveness, J. of Thermophysics and Heat Transfer, 1-11, doi: 10.2514/1.T5033.

Zhang, G., Tian, M., Zhou, N., Li, W. and Kukulka, D., 2014. Analysis of Flow and Heat Transfer Characteristics around an Oval-shaped Cylinder. Journal of Heat Transfer, 136, 044502-1.

Zukauskas, A., 1972. Heat Transfer from Tubes in Cross Flow. Ado. Heat Transfer, 8, 93-160.

Zukauskas, A. and Ulinskas, R., 1988. Heat Transfer in Tube Banks in Crossflow. Hemisphere, Washington, DC.

CURRICULUM VITAE

Muhammet Nasıf KURU was born in Tarsus in 1986. He enrolled Dokuz Eylul University mechanical engineering in 2003 and obtained BSc. degree in 2007. He completed his graduate study in computational science and engineering department at Istanbul Technical University. He began PhD education in Çukurova University at the department of mechanical engineering in 2011. Currently, he is a mechanical engineer in Hatay Provincial Directorate of Environment and Urbanization.

APPENDIX

Experimental Data, Empirical Correlations and Analytical Formulations for In-line and Staggered Tube Banks in Literature

Tube banks are investigated by a lot of researchers. In the followings, experimental data, empirical correlations and analytical formulations are given for in-line and staggered tube banks from literature. A great deal of publications about tube banks are concerned with experimental results and empirical formulations using these results. Also, analytical studies are very useful which includes wide range of parameters while making calculations.

A.1. Average Nusselt Number Calculations

In this section, average Nusselt number correlations for both in-line and staggered circular tube banks are presented detailly.

Colburn Correlation:

Firstly, Colburn (1933) presented an empirical correlation for staggered tube banks to calculate average Nusselt number as follows:

$$\overline{\mathrm{Nu}} = 0.33 \text{ x } \mathrm{Re}^{0.6} \text{ x } \mathrm{Pr}^{1/3} \qquad \text{(A.1)}$$

His empirical correlation is valid for 10 or more tubes ($N_L \geq 10$) in the longitudinal direction and for $10 < \mathrm{Re} < 4 \text{ x } 10^4$.

Grimison's Empirical Correlations:

Grimison (1937) gave a correlation in the following form for in-line and staggered tube banks in cross flow. Air is used for fluid flow over tube banks in the experiments.

$$\overline{\mathrm{Nu}} = C_1 \text{ x } \mathrm{Re}^{m} \qquad \text{(A.2)}$$

His empirical correlation was given for 10 or more tubes ($N_L \geq 10$) in the longitudinal direction and only valid for air. Thermo-physical properties must be taken at the average film temperature. Average Film temperature is defined as;

$$\overline{T}_f = \frac{(T_i + T_o)}{2} \tag{A.3}$$

C_1 and m constants in equation A.2 are evaluated for in-line and staggered tube banks from tables A.1a and A.1b respectively for prescribed dimensionless pitches s_L^* and s_T^*.

For number of tubes in the longitudinal direction fewer than 10 tubes ($N_L < 10$), Grimison's (1937) equation can be valid using Kays and London's (1964) C_2 correction factor, such that

$$\overline{Nu}|_{N_L<10} = C_2 \, x \, \overline{Nu}|_{N_L \geq 10} \tag{A.4}$$

The correction factor, C_2 is given for in-line and staggered tube banks in tables A.2a and A.2b, respectively.

Table A.1a. C_1 and m constants in equation A.2 for in-line tube banks where $N_L \geq 10$, Grimison (1937)

	s_T^*							
	1.25		1.5		2.0		3.0	
s_L^*	C_1	m	C_1	m	C_1	m	C_1	m
1.25	0.348	0.592	0.275	0.608	0.100	0.704	0.063	0.752
1.50	0.367	0.586	0.250	0.620	0.101	0.702	0.068	0.744
2.00	0.418	0.570	0.299	0.602	0.229	0.632	0.198	0.648
3.00	0.290	0.601	0.357	0.584	0.374	0.581	0.286	0.608

Table A.1b. C_1 and m constants in equation A.2 for staggered tube banks where $N_L \geq 10$, Grimison (1937)

s_L^*	s_T^*							
	1.25		1.5		2.0		3.0	
	C_1	m	C_1	m	C_1	m	C_1	m
0.600	-	-	-	-	-	-	0.213	0.636
0.900	-	-	-	-	0.446	0.571	0.401	0.581
1.000	-	-	0.497	0.558	-	-	-	-
1.125	-	-	-	-	0.478	0.565	0.518	0.560
1.250	0.518	0.556	0.505	0.554	0.519	0.556	0.522	0.562
1.500	0451	0.568	0.460	0.562	0.452	0.568	0.488	0.568
2.000	0.404	0.572	0.416	0.568	0.482	0.556	0.449	0.570
3.000	0.310	0.592	0.356	0.580	0.440	0.562	0.428	0.574

Table A.2a. Correction factor C_2 in equation A.4 for in-line tube banks where $N_L < 10$, Kays and London (1964)

N_L	1	2	3	4	5	6	7	8	9
C_2	0.64	0.80	0.87	0.90	0.92	0.94	0.96	0.98	0.99

Table A.2b. Correction factor C_2 in equation A.4 for staggered tube banks where $N_L < 10$, Kays and London (1964)

N_L	1	2	3	4	5	6	7	8	9
C_2	0.68	0.75	0.83	0.89	0.92	0.95	0.97	0.98	0.99

Moreover, Grimison (1937) gave an empirical correlation using experimental data of Pierson (1937) and Huge (1937)

$$\overline{Nu} = 0.32 \text{ x } F_a \text{ x } Re^{0.61} \text{ x } Pr^{0.31} \quad (A.5)$$

F_a was defined as arrangement factor and given by Grimison (1937) graphically for different values of Reynolds number and dimensionless pitches.

Hausen's Empirical Formulations:

Hausen (1983) presented empirical formulations for average Nusselt number $\overline{Nu}$ and arrangement factor F_a calculations using Grimison's (1937) studies for both in-line and staggered tube banks.

For in-line tube banks,

$$\overline{Nu} = 0.34 \text{ x } F_a \text{ x } Re^{0.61} \text{ x } Pr^{0.31} \tag{A.6}$$

and

$$F_a = 1 + \left(s_L^* + \frac{7.17}{s_L^*} - 6.52\right)\left[\frac{0.266}{(s_T^* - 0.8)^2} - 0.12\right]\sqrt{\frac{1000}{Re}} \tag{A.7}$$

for staggered tube banks,

$$\overline{Nu} = 0.35 \text{ x } F_a \text{ x } Re^{0.57} \text{ x } Pr^{0.31} \tag{A.8}$$

and

$$F_a = 1 + 0.1\, s_L^* + \frac{0.34}{s_T^*} \tag{A.9}$$

Zukauskas's Empirical Correlations:

Zukauskas (1972) presented empirical correlations in tables A.3a and A.3b for in-line and staggered tube banks respectively where number of tubes in the longitudinal direction is greater than 16 ($N_L > 16$).

Table A.3a. Average Nusselt Numbers, $\overline{Nu}$ for in-line tube banks where $N_L > 16$, Zukauskas (1972)

Average Nusselt Numbers, $\overline{Nu}$	Reynolds Number Range, Re
$\overline{Nu} = 0.9\ Re^{0.4}\ Pr^{0.36}\left(\frac{Pr}{Pr_w}\right)^{0.25}$	$10^0 - 10^2$
$\overline{Nu} = 0.52\ Re^{0.5}\ Pr^{0.36}\left(\frac{Pr}{Pr_w}\right)^{0.25}$	$10^2 - 10^3$
$\overline{Nu} = 0.27\ Re^{0.63}\ Pr^{0.36}\left(\frac{Pr}{Pr_w}\right)^{0.25}$	$10^3 - 2 \times 10^5$
$\overline{Nu} = 0.033\ Re^{0.8}\ Pr^{0.4}\left(\frac{Pr}{Pr_w}\right)^{0.25}$	$2 \times 10^5 - 2 \times 10^6$

Table A.3b. Average Nusselt Numbers, $\overline{Nu}$ for staggered tube banks where $N_L > 16$, Zukauskas (1972)

Average Nusselt Numbers, $\overline{Nu}$	Reynolds Number Range, Re
$\overline{Nu} = 1.04\ Re^{0.4}\ Pr^{0.36}\left(\frac{Pr}{Pr_w}\right)^{0.25}$	$10^0 - 500$
$\overline{Nu} = 0.71\ Re^{0.5}\ Pr^{0.36}\left(\frac{Pr}{Pr_w}\right)^{0.25}$	$500 - 10^3$
$\overline{Nu} = 0.35\ Re^{0.6}\ Pr^{0.36}\left(\frac{Pr}{Pr_w}\right)^{0.25}\left(\frac{S_T}{S_L}\right)^{0.2}$	$10^3 - 2 \times 10^5$
$\overline{Nu} = 0.031\ Re^{0.8}\ Pr^{0.4}\left(\frac{Pr}{Pr_w}\right)^{0.25}\left(\frac{S_T}{S_L}\right)^{0.2}$	$2 \times 10^5 - 2 \times 10^6$

Thermo-physical properties are taken at the average film temperature, but Prandtl number of wall Pr_w is evaluated at the wall temperature. We need to obtain thermo-physical properties $\overline{T}$ at the average film temperature rather than at the inlet temperature because larger fluid temperature difference $|T_i - T_o|$ lead to significant error.

When the number of tubes in the longitudinal direction is equal or smaller than 16 ($N_L \leq 16$), correction factor C_2 may be used such that (Zukauskas, 1972);

$$\overline{Nu}|_{N_L \leq 16} = C_2 \, x \, \overline{Nu}|_{N_L > 16} \qquad (A.10)$$

where the values of C_2 can be evaluated from tables A.4a and A.4b for in-line and staggered arrangements (For $N_L \geq 9$, C_2 can be taken as 1).

Table A.4a.Correction factor C_2 in equation A.10 for in-line tube banks where $Re \geq 1000$ and $N_L \leq 16$, Zukauskas (1972)

N_L	1	2	3	4	5	6	7	8	9
C_2	0.70	0.80	0.86	0.90	0.92	0.95	0.97	0.98	0.99

Table A.4b.Correction factor C_2 in equation A.10 for staggered tube banks where $Re \geq 1000$ and $N_L \leq 16$, Zukauskas (1972)

N_L	1	2	3	4	5	6	7	8	9
C_2	0.64	0.76	0.84	0.89	0.92	0.95	0.97	0.98	0.99

If $N_L > 16$, effect of N_L can be neglected for both in-line and staggered arrangements, as shown in figure A.1. The uncertainty of the average Nusselt number $\overline{Nu}$ values tabulated in tables A.3a and A.3b is in the range of $\mp 15\%$, (Zukauskas, 1972).

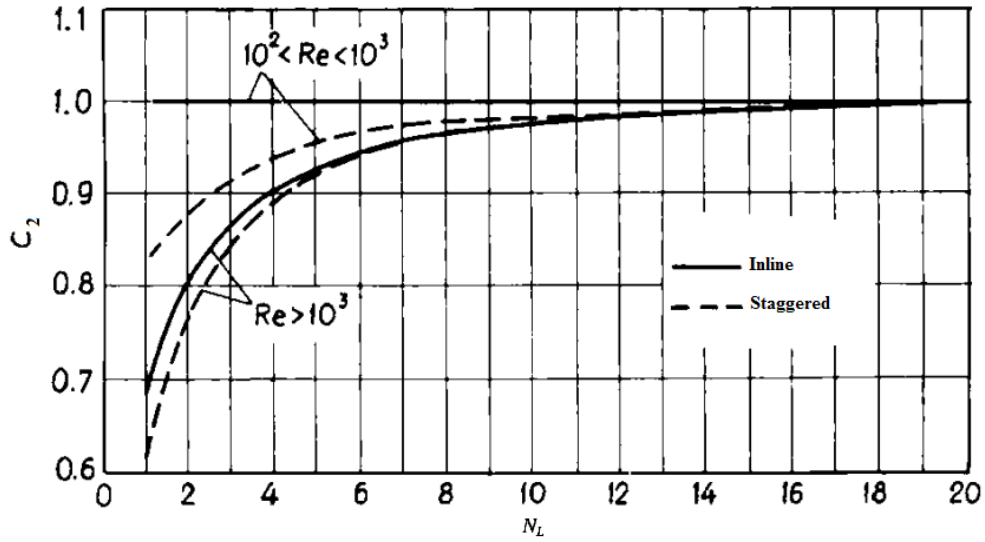


Figure A.1. Correction factor C_2 for the number of tube rows from tube banks, Zukauskas (1972)

Khan et al.'s Analytical Formulations:

Khan et al. (2006) presented analytical formulations including wide range of parameters for both in-line and staggered tube banks under steady, laminar and fully developed flow assumptions and isothermal boundary condition. For in-line and staggered tube banks,

$$\overline{Nu} = C_1 \text{ x } Re^{1/2} \text{ x } Pr^{1/3} \tag{A.11}$$

and for in-line tube banks, C_1 constant is given as:

$$C_1 = [0.25 + \exp(-0.55 * s_L^*)] \text{ x } (s_L^*)^{0.212} \text{ x } (s_T^*)^{0.285} \tag{A.12}$$

while for staggered tube banks,

$$C_1 = \frac{0.61\ (s_L^*)^{0.053}\ (s_T^*)^{0.091}}{[1 - 2\ \exp(-1.09\ s_L^*)]} \tag{A.13}$$

C_1 is valid for $1.05 \leq s_L \leq 3$ and $1.05 \leq s_T \leq 3$.

Gnielinski Correlations:

Gnielinski (2010) presented correlations for in-line and staggered tube banks to obtain average Nusselt number $\overline{Nu}$ for $N_L \geq 10$ and is given as below:

$$\overline{Nu} = Nu\ f_{A,N} \tag{A.14}$$

where Nu is the average Nusselt number which is independent from number of longitudinal tubes, N_L. $\overline{Nu}_L$ is determined using below formula:

$$\overline{Nu}_L = 0.3 + \left(Nu_{L,lam}^2 + Nu_{L,turb}^2\right)^{0.5} \tag{A.15}$$

where

$$Nu_{L,lam} = 0.664\ Re_{V,L}^{0.5}\ Pr^{1/3} \tag{A.16}$$

$$Nu_{L,turb} = \frac{0.037\ Re_{V,L}^{0.8}\ Pr}{1 + 2.443\ Re_{V,L}^{-0.1}(Pr^{2/3} - 1)} \tag{A.17}$$

Nu and $Re_{V,L}$ are given as follows:

$$\overline{Nu}_L = \frac{\pi}{2}\ Nu \tag{A.18}$$

$$\mathrm{Re}_{V,L} = \left[\frac{\pi}{2}\frac{(s_T^* - 1)}{\varepsilon\, s_T^*}\right]\mathrm{Re} \tag{A.19}$$

where

$$\varepsilon = \left(1 - \frac{\pi}{4s_T^*}\right) \tag{A.20}$$

$f_{A,N}$ is determined as below:

$$f_{A,N} = \frac{1 + (N_L - 1)f_A}{N_L} \tag{A.21}$$

where f_A for in-line arrangement is as follows:

$$f_A = 1 + \frac{0.7\left(\frac{s_L^*}{s_T^*} - 0.3\right)}{\left(1 - \frac{\pi}{4s_T^*}\right)^{1.5}\left(\frac{s_L^*}{s_T^*} + 0.7\right)^2} \tag{A.22}$$

and f_A for staggered arrangement is:

$$f_A = 1 + \frac{2}{3\, s_L^*} \tag{A.23}$$

The given equations from Gnielinski (2010) are valid for $10 \leq \mathrm{Re}_{V,L} \leq 10^5$.

Yilmaz and Yilmaz's Empirical Formulations:

The average Nusselt number correlations supplied by Zukauskas (1972) have large discontinuities and differences at $\mathrm{Re} = 100$ and $\mathrm{Re} = 1000$ for in-line

tube banks. Therefore, Yilmaz and Yilmaz (2016) derived equations based on Zukauskas's (1972) empirical data for in-line tube banks and it is determined using the below formula:

$$\overline{\mathrm{Nu}} = \mathrm{f_{N,N}}\, 0.9\, \mathrm{Re}^{0.4} \left[1 + \left(\frac{\mathrm{Re}}{290}\right)^{5}\right]^{0.05} \mathrm{Pr}^{0.36} \tag{A.24}$$

where

$$\mathrm{f_{N,N}} = 1 - 0.3 \exp[-0.42(\mathrm{N_L} - 1)^{0.87}] \tag{A.25}$$

$\mathrm{f_{N,N}}$ is the influence of longitudinal tube number $\mathrm{N_L}$ on the average Nusselt number, $\overline{\mathrm{Nu}}$ and it is derived from Zukauskas's (1972) data by Yilmaz and Yilmaz (2016). Equation A.24 is valid for $1 \leq \mathrm{Re} \leq 2\mathrm{x}10^{5}$.

Moreover, average Nusselt number correlations provided by Zukauskas (1972) have great discontinuities and variances at $\mathrm{Re} = 500$ and $\mathrm{Re} = 1000$ for staggered tube banks. Thus, Yilmaz et al. (2017) presented new equations based on Zukauskas's (1972) empirical data for staggered tube banks and it is given below:

$$\overline{\mathrm{Nu}} = \mathrm{f_{N,N}}\, 1.04\, \mathrm{Re}^{0.4} \left[1 + \left(\frac{\mathrm{Re}}{500}\right)^{1.84}\right]^{0.125} \mathrm{Pr}^{0.36} \tag{A.26}$$

where

$$\mathrm{f_{N,N}} = 1 - 0.36 \exp[-0.42(\mathrm{N_L} - 1)^{0.95}] \tag{A.27}$$

$f_{N,N}$ is the effect of longitudinal tube number N_L on the average Nusselt number $\overline{Nu}$ and it is obtained from Zukauskas's (1972) data by Yilmaz et al. (2017). Equation A.26 is valid for $10 \leq Re \leq 2x10^5$.

A.2. Friction Factor Calculations

Zukauskas's Graphical Forms:

For tube bank heat exchangers, it is important to increase overall heat transfer rate which is proportional to the pressure drop. Pressure drop across the tube bank is given by Zukauskas (1972) as follows:

$$\Delta p = N_L \chi \left(\frac{\rho U_{max}^2}{2}\right) f \tag{A.28}$$

In figure A.2, friction factor f is given for in-line tube banks where dimensionless longitudinal pitch ($P_L = s_L/D$) equals to dimensionless transversal pitch ($P_T = s_T/D$) which corresponds to square arrangement. In addition, correction factor χ is plotted in Figure A.2 so it is possible to obtain pressure drop for other in-line tube bank arrangements.

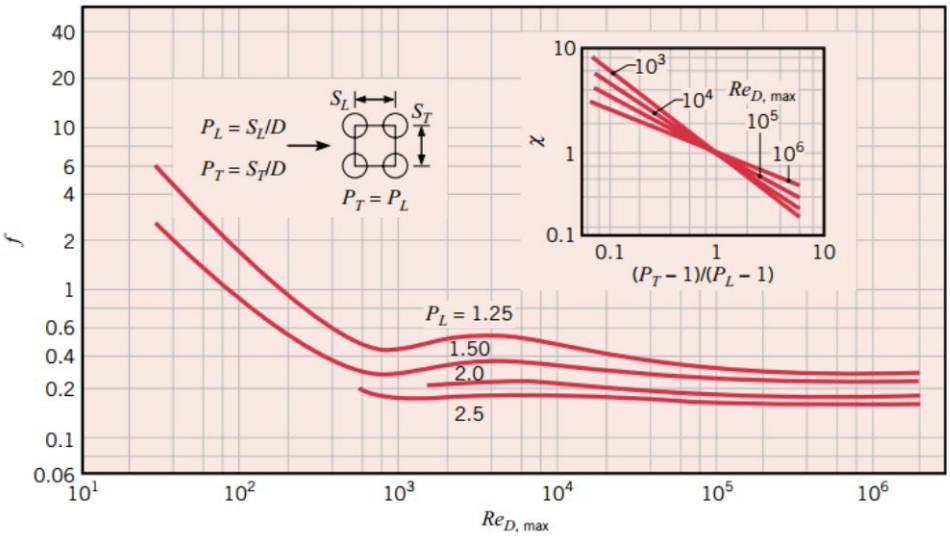


Figure A.2. Friction factor f and correction factor χ for in-line tube banks, Zukauskas (1972)

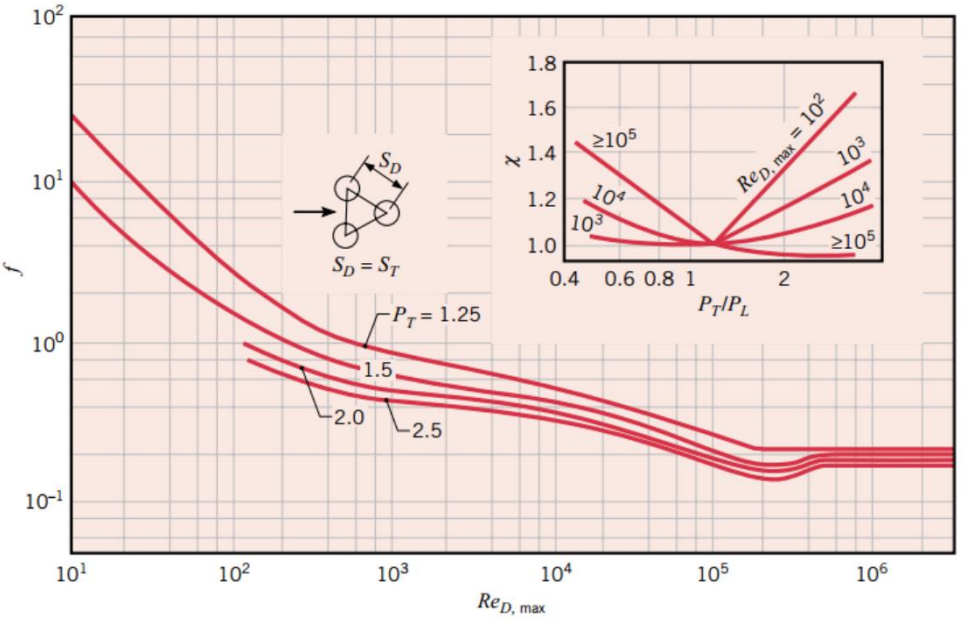


Figure A.3. Friction factor f and correction factor χ for staggered tube banks, Zukauskas (1972)

Similarly, friction factor f is plotted for staggered tube banks in figure A.3 where pitch between rows in the flow direction (s_D) equals to transversal pitch (s_T) which corresponds to equilateral triangle (ET) arrangement. Correction factor χ is also given in figure A.3 so pressure drop can be calculated for other staggered tube bank arrangements.

In figures A.2 and A.3, Reynolds number is obtained using maximum velocity U_{max} which occurs in the minimum cross-sectional area through the tube bank.

Gaddis Correlations:

Gaddis (2010) presented equations to calculate pressure drop for in-line and staggered tube banks and these equations are valid where the number of tubes in the longitudinal direction is equal or greater than 10 ($N_L \geq 10$). Gaddis's (2010) equations for friction factor f calculation are given below for in-line tube banks:

$$f = f_l + f_t \left[1 - \exp\left(-\frac{Re + 1000}{2000}\right)\right] \tag{A.29}$$

f_l and f_t are defined as follows:

$$f_l = \frac{280\,\pi\,\left[\left(s_L^{*\,0.5} - 0.6\right)^2 + 0.75\right]}{Re\,(\,4\,s_L^*\,s_T^* - \pi\,)s_T^{*\,1.6}} \tag{A.30}$$

$$f_t = \frac{\left[0.22 + 1.2\frac{\left(1-\frac{0.94}{s_L^*}\right)^{0.6}}{(s_T^*-0.85)^{1.3}}\right] 10^{0.47\left(\frac{s_L^*}{s_T^*}-1.5\right)}}{Re^{0.1\frac{s_L^*}{s_T^*}}} + \frac{0.03\,(s_T^*-1)\,(s_L^*-1)}{Re^{0.1\frac{s_L^*}{s_T^*}}} \quad \text{(A.31)}$$

For staggered tube banks, Gaddis (2010) presented following equations:

$$f = f_l + f_t\left[1-\exp\left(-\frac{Re\ +\ 200}{1000}\right)\right] \quad \text{(A.32)}$$

where

$$f_l = \frac{C_1}{Re} \quad \text{(A.33)}$$

C_1 can be determined from the equations below.

$$C_1 = \frac{280\pi\left[(s_L^{*0.5}-0.6)^2+0.75\right]}{(4s_L^*s_T^*-\pi)\,s_T^{*1.6}} \quad \text{(A.34)}$$

and f_t can be determined from:

$$f_t = \frac{2.5 + \frac{1.2}{(s_T^*-0.85)^{1.08}} + 0.4\left(\frac{s_L^*}{s_T^*}-1\right)^3 - 0.01\left(\frac{s_T^*}{s_L^*}-1\right)^3}{Re^{0.25}} \quad \text{(A.35)}$$

Gaddis (2010) also gave equations for in-line and staggered tube banks that takes the dependency of the number of tubes in the longitudinal direction only between 5 and 10 ($5 \leq N_L < 10$). Yilmaz and Yilmaz (2016) and Yilmaz et al. (2017) derived equations for in-line and staggered tube banks respectively using Zukauskas's (1972) data which considers the number of tubes N_L influence on the friction factor. For in-line tube banks, it is formulated as:

$$f_{N,f} = 1 + \frac{0.8}{N_L^{2.37}} \tag{A.36}$$

and for staggered tube banks, it is given as follows:

$$f_{N,f} = 1 + \frac{1.18}{N_L^{2.26}} \tag{A.37}$$

Friction factor which includes the influence of the number of tubes N_L can be calculated as:

$$f_N = f\, f_{N,f} \tag{A.38}$$

Yilmaz and Yilmaz and Yilmaz et al.'s Emprical Formulations:

Friction factors are given for equal dimensionless pitches ($s^* = s_L^* = s_T^*$) of 1.25, 1.50 and 2.0 in the graphics by Zukauskas (1972) as shown in figures A.2 for in-line tube banks. Yilmaz and Yilmaz (2016) derived friction factor equations for the same Reynolds number range given by Zukauskas (1972) and derived equations are given as follows:

$$s^* = 1.25 \;:\; f = \frac{217}{Re} + \frac{(Re/10^4)^2}{[1 + 48\,(Re/10^4)^5]^{0.5}} + 0.28 \tag{A.39}$$

$$s^* = 1.50 \;:\; f = \frac{70}{Re^{0.93}} + \frac{10\,(Re/10^4)^3}{[1 + 9.9\,(Re/10^4)^{2.14}]^{1.75}} + 0.23 \tag{A.40}$$

$$s^* = 2.00 \;:\; f = \frac{28}{Re^{0.91}} + \frac{0.25\,(Re/10^4)^2}{[1 + 0.77\,(Re/10^4)^{1.12}]^{3.57}} + 0.19 \tag{A.41}$$

The derived equations are valid for Reynolds numbers in the range of 6 and 10^6.

For staggered tube banks, friction factors are plotted for dimensionless transversal pitch (s_T^*) of 1.25, 1.50 and 2.0 in the graphics by Zukauskas (1972) where $s_L^* = s_T^* \sqrt{3} / 2$ as plotted in figure A.3. Yilmaz et al. (2017) obtained friction factor equations for the equivalent Reynolds number range given by Zukauskas (1972) and the equations are given below:

$$s^* = 1.25 \;:\; f = \frac{250}{Re} + \frac{1.81}{Re^{0.15}} \tag{A.42}$$

$$s^* = 1.50 \;:\; f = \frac{70}{Re^{0.93}} + \frac{2.45}{Re^{0.20}} \tag{A.43}$$

$$s^* = 2.00 \;:\; f = \frac{57}{Re}\left[1 + \left(\frac{Re}{40}\right)^{1.875}\right]^{0.4} \tag{A.44}$$

The equations are valid for Reynolds numbers ranging from 10 to 2 x 10^5.